Improvement of Cocoa Blends by

Enantiomeric and Melting Point Modification

Louise Sim

Submitted in accordance with the requirements for the degree of
Doctor of Philosophy

The University of Leeds

School of Food Science and Nutrition

August 2020

The candidate confirms that the work submitted is her own, except where work which has formed part of jointly authored publications has been included. The contribution of the candidate and the other authors to this work has been explicitly indicated below. The candidate confirms that appropriate credit has been given within the thesis where reference has been made to the work of others.

Reference for jointly authored publication:

> Guan, F., Kapur, N., Sim, L., Taylor, C.J., Wen, J., Zhang, X. and Blacker, A.J. A universal reactor platform for batch and flow: application to homogeneous and heterogeneous hydrogenation. *Reaction Chemistry & Engineering.* 2020.

The work on pressurised hydrogenolysis reported in this publication is presented in Chapter 5 of this thesis, which was performed by the candidate with the assistance of F. Guan.

Acknowledgements

My most sincere appreciation and gratitude must first go to my principal supervisor Prof. Megan Povey and co-supervisors Dr. Lisa Marshall and Prof. John Blacker. The continuous support, guidance and encouragement has been invaluable from both a personal and academic perspective; I cannot thank you enough for the conversations and time spent helping me along this journey. These thoughts are extended to Peng-Siong Chong, with whom many an enlightening discussion was held.

I would like to acknowledge Nestlé Product Technology Centre Confectionery, York, for the opportunity afforded to me and financial support, along with the Biotechnology and Biological Sciences Research Council (BBSRC) for funding the project.

In the School of Food Science and Nutrition I must thank all academics, staff and fellow postgraduate researchers. All of whom have played a role in my personal growth and development as a scientist; making my time there as an undergraduate and PGR an enjoyable and memorable experience. Special thanks to Dr. Marjorie Ladd Parada who always supported me as a colleague, but more importantly as a friend. Sincere gratitude goes to all the technical team, in particular Miles Ratcliffe, Sara Viney and Neil Rigby, who offered advice and practical support whenever it was needed. FS&N has been a significant part of my life and will forever have a place in my heart.

My thanks are extended to Dr. Mary Bayana and the PGRs from the iPRD in the School of Chemistry, particularly Nisha, Fanfu and Luke, for the welcome and advice you all gave so openly in your lab. My journey into organic synthesis would not have been possible without your support.

I will be forever appreciative to all that have helped me through this achievement, who had faith in my potential through many a time of self-doubt.

It is not possible to name everyone individually, but I consider each one as family and I am thankful for all that they do to show they care.

Finally, yet most certainly not least, I am truly grateful to my partner Jona, without whom I would not be where I am today. Your confidence in me helped me find a belief in myself. I appreciate all that you have done and continue to do; I thank you for your understanding, support, patience, but mostly for making me smile every day.

Abstract

Cocoa butter (CB) is the foremost ingredient in chocolate, holding responsibility for the products' functional and sensorial characteristics. Numerous studies have investigated the crystallisation and polymorphism of its component triacylglycerols (TAGs), yet no correlation has been made between their stereochemistry and crystalline behaviour; even though the predominant TAG, 1-palmitoyl-2-oleoyl-3-stearoyl-glycerol (POSt), is reportedly present in a racemic mixture. Moreover, several TAGs have higher melting points than human body temperature and their behaviour in the biophysical environment of the gastrointestinal tract is yet to be reported. In this multi-faceted project, three areas of research were investigated; enantiomeric ratio elucidation of CB POSt, the effect of high melting TAGs in the digestion process and organic synthesis measures for the formulation of enantiopure POSt. For the first parameter, two approaches were assessed using a *rac*-POSt standard for method development, chiral HPLC and derivatisation. Both were ineffectual for enantiomeric resolution, leaving unanswered questions on the enantiomeric composition of CB. For the second parameter, an *in vitro* analysis procedure was used successfully in an original study on the amount of free fatty acids (FFAs) released, comparing a range of initial melt temperatures (T_m), 37, 50 and 80 ^{o}C: temperatures intended to correlate with melting points of various constituent TAGs. Similarities in total FFA release were evident, indicating high melting components had no effect on the lipolysis of CB. Finally, transesterification and chemoenzymatic procedures were undertaken for the synthesis of enantiopure POSt. Difficulties in glycerol deprotection during the latter saw a novel approach introduced in the form of a small-scale reactor (fReactor), which proved consistent in removal of the benzyl protecting group. A near identical NMR spectra of the final product with that of *rac*-POSt allows determination that the synthesis of (*R*)-POSt was a success.

Table of Contents

List of Figures

List of Tables

Abbreviations

(*R*)-(+)	(R)-(+)-3-Benzyloxy-1,2-propanediol
(*S*)-(-)	(S)-(-)-3-Benzyloxy-1,2-propanediol
µm	Micrometre
ACN	Acetonitrile
ACW	Antral contract waves
APCI	Atmospheric-pressure chemical ionisation
AUC	Area under curve
BE	Bile extract
Bis-Tris	Bis(2-hydroxyethyl)amino-tris(hydroxymethyl)methane
BPR	Back pressure regulator
$CaCl_2$	Calcium chloride
$CaCl_2.2H_2O$	Calcium chloride dihydrate
CAL	Candida Antarctica lipase
CB	Cocoa butter
CBA	Cocoa butter alternative
CBE	Cocoa butter equivalent
CDA	Chiral derivatising agent
$CDCl_3$	Deuterated chloroform
CDMPC	Cellulose-tris (3,5-dimethylphenylcarbamate)
CH_2Cl_2	Dichloromethane
$CHCl_3$	Chloroform
CLSM	Confocal laser scanning microscopy
CoA	Certificate of analysis
CSP(s)	Chiral stationary phase(s)
DAD	Diode array detector
DAG	Diacylglycerol
DCM	Dichloromethane
DMAP	4-dimethylaminopyridine
DMSO	Dimethyl sulfoxide
DSD	Droplet size distribution

EDAC	*N*-(3-Dimethylaminopropyl)-*N′*-ethylcarbodiimide hydrochloride
Enantio	Enantiomeric
ESI	Electrospray ionisation
Et2O	Diethyl ether
EtMgBr	Ethyl magnesium bromide
EtOH	Ethanol
Et-Pa	Ethyl palmitate
Et-St	Ethyl stearate
FA	Fatty acid
FFA	Free fatty acid
FITC	Fluorescein 5(6)-isothiocyanate
FRC	Fraction collector
GIT	Gastrointestinal tract
H_2	Hydrogen
HCl	Hydrochloric acid
Hz	Hertz
IPA	Isopropanol
iPRD	Institute of Process Research and Development
KCl	Potassium chloride
KH_2PO_4	Potassium dihydrogen phosphate
M	Molar
m.p.	Melting point
MAG	Monoacylglycerol
MCT	Medium-chain triacylglycerol
MeOH	Methanol
$MgCl_2(H_2O)_6$	Magnesium chloride hexahydrate
MHz	Megahertz
MS	Mass spectrometry
MTBE	Methyl *tert*-butyl ether
MTPA-Cl	Methoxy-α-(trifluoromethyl)phenylacetyl chloride
MUFA	Monounsaturated fatty acid
M_w	Molecular weight

NaCl	Sodium chloride
NaOH	Sodium hydroxide
NARP-HPLC	Non-aqueous reverse-phase high-performance liquid chromatography
nm	Nanometres
NMR	Nuclear Magnetic Resonance
NR	Nile red
O	Oleic acid
OPP	2,3-dipalmitoyl-1-oleoyl-*sn*-glycerol
P	Palmitic acid
P'	Polarity index
PBR	Packed bed reactor
Pd/C	Palladium on carbon
PLU	Propyl laurate unit
POP	1,3-dipalmitoyl-2-oleoyl-glycerol
POSt	1-palmitoyl-2-oleoyl-3-stearoyl-glycerol
PPO	1,2-dipalmitoyl-3-oleoyl-*sn*-glycerol
ppm	Parts per million
PSD	Particle size distribution
PUFA	Polyunsaturated fatty acid
Py	Pyridine
rac	Racemic
RBF	Round bottom flask
RP-HPLC	Reverse-phase high-performance liquid chromatography
rpm	Revolutions per minute
r.t.	Room temperature
SFA(s)	Saturated fatty acid(s)
SFC	Solid fat content
SIF	Simulated intestinal fluid
sn	Stereospecific numbering
St	Stearic acid
ST(s)	Structured triacylglycerol(s)
StOSt	1,3-distearoyl-2-oleoyl-glycerol

StOP	1-stearoyl-2-oleoyl-3-palmitoyl-glycerol
T_c	Crystallisation temperature
THF	Tetrahydrofuran
T_m	Melt temperature
Tol	Toluene
t_r	Retention time
Tris	Tris(hydroxymethyl)aminomethane
USP	United States Pharmacopeia
v/v	Volume by volume
VP	Vinyl palmitate
VS	Vinyl stearate
w/v	Weight by volume
wt	Weight
wt%	Percent by weight
XRD	X-ray diffraction
ε	Dielectric constant

Chapter 1 Introduction

1.1 The origins of chocolate and modern-day demands

Chocolate consumption has been occurring for hundreds of years, with cocoa plantations dating back to Mayan civilisations, ca. 600 AD, when the cacao beans were processed into a form suitable for drinking[1]. However, with up to 50% of the cocoa bean consisting of the lipid component known as cocoa butter (CB), the appearance was depicted as unappealing as the fat droplets would float to the surface of the beverage[1, 2]. Many years later in 1828, a process that removed part of the fat element was discovered by the Dutch, which left a better-quality drinking chocolate but 'waste' in terms of the excess fat which had been pressed from small pieces of the bean kernels, the cocoa nibs: ca. 20 years after the Dutch invention, English confectioners saw potential in this by-product and used it to develop eating chocolate[1]. Up until this point, drinking chocolate was commonly consumed by those considered the elite of society but production of eating chocolate allowed it to become accessible to the public[2]. Over time, the manufacturing of solid chocolate bars became more significant than the production of cocoa powder, with advancements in technology allowing the addition of other ingredients to complement the flavour[3].

Occupying ca. 47% of the international candy and chocolate industry, chocolate confectionery is steadfast as the most popular sweet treat with the market expected to continue rising over imminent years[4, 5]. Due to increased disposable incomes, the greatest growth driver is Asia; which is predicted to become the second largest consumer of cocoa goods[6]. However, growth is set to continue in Europe, the largest chocolate consumers overall, with increased interest in higher quality and cocoa content in their products[7]. This rise in international consumer demand saw the use of ca. 1.8 million tonnes of cocoa beans in recent years by the top six chocolate producing companies alone[7]. However, meeting this demand may prove difficult for growers of *Theobroma cacao*, the cacao tree, considering the environmental impact of

climate change and the challenges this introduces[8, 9]. As global temperatures continue to rise, the prime growing region of West Africa, which produces ca. 75% of the worlds crop[10, 11], is forecast to see an increase of ca. 2 ^{o}C by 2050[9]. As a result, conditions for cultivation are expected to become sub-optimal with significant moisture loss from the soil and a lack of compensatory rainfall[9]: cacao trees require rainfall of 1500 – 2000 mm annually for optimal growth[12]. It is this lack of humidity that creates adverse conditions for the trees, not simply the temperature rise, as warmer growing regions are already succeeding in such heat; producing CB varieties of differing chemical composition and characteristics than those from cooler lands[13]. Growers must therefore adapt to the changing environment to find advantageous conditions, yet ecological adaptations may alter the chemical composition of the cacao bean; creating impediments for the chocolate manufacturer. Thus, research must continue to further understand the properties of cacao goods; particularly the nuances of CB, chocolates imperative ingredient, allowing chocolate production to persevere whilst creating innovative products to capitalise on the ever-expanding market.

1.2 A brief insight into chocolate making

Essentially, chocolate is a combination of CB, cacao nibs and sugar; the former being the only continuous phase, with its chemical and physical [9]properties affecting the overall characteristics of the product[1] (Figure 1.1).

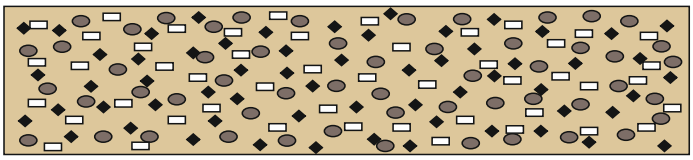

Figure 1.1 Illustration of the continuous fat phase (CB), represented by the coloured background, and other particles contained within a bar of milk chocolate; cocoa powder (ovals), sugar particles (diamonds) and milk powder (rectangles) (adapted from reference[14]).

Lecithin, a naturally derived phospholipid mixture[15], is also added as an aid to reduce friction between particles: phospholipids being compounds with a hydrophilic head group and hydrophobic ‘tails’. The head groups are attracted

to the surface of the sugar particles, with the ‘tails’ remaining in the CB and thus, assisting viscosity and flow properties in a commercial production environment[16].

The transformation from bean-to-bar is an extensive process that encompasses a variety of practices from harvesting of the cacao pod to developing the correct crystalline state in CB[1, 2]. The process diagram presented in Figure 1.2 demonstrates the numerous stages, each of which are essential to producing desirable qualities in chocolate. For an in-depth look into each processing step, the reader is referred to ‘The Science of Chocolate’ by Stephen T. Beckett[1].

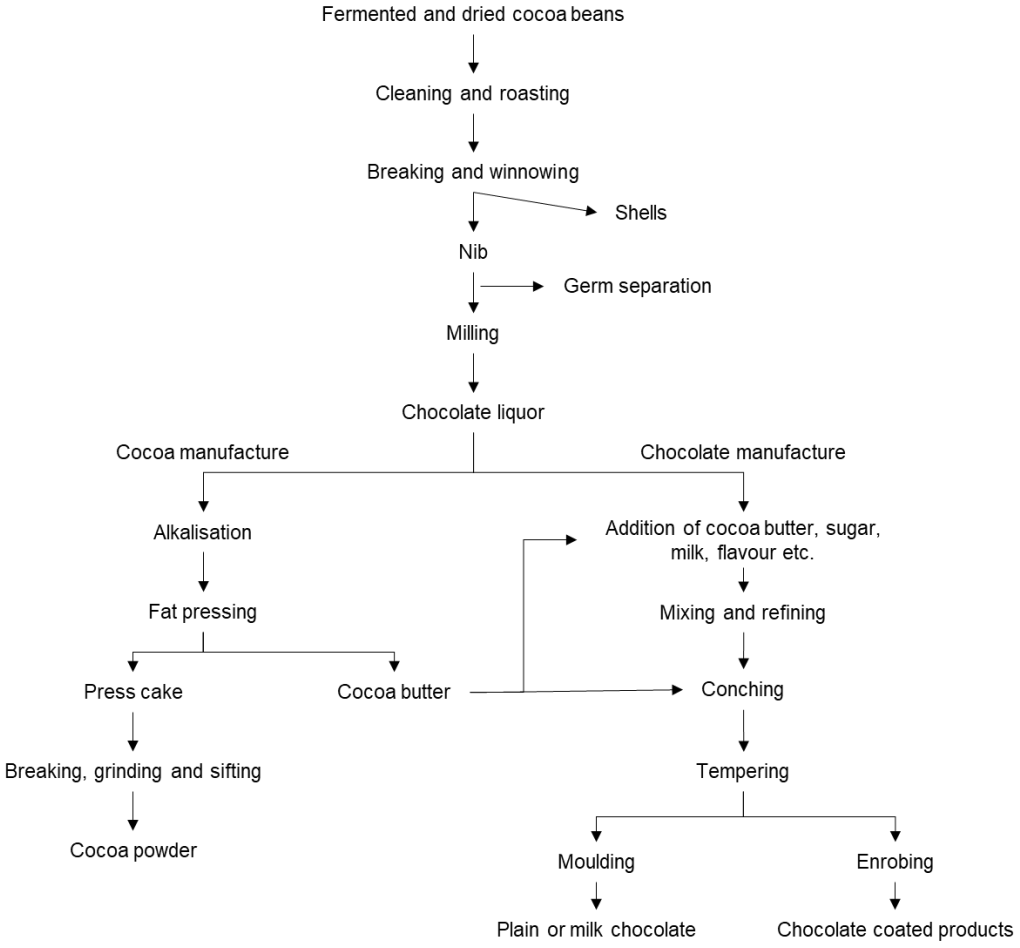

Figure 1.2 Flow chart illustrating the stages of chocolate production from cocoa bean processing through to the creation of cocoa powder, chocolate bars and enrobing of products[17].

Tempering should be highlighted as perhaps the main critical control point, which involves the use of shear and thermal manipulation to induce the chemical components of CB into seed crystals. These ‘seeds’ allow liquid chocolate to solidify in its most stable form[18], which is discussed in more depth in section 1.5. Failure to generate the appropriate crystal form creates an inferior product that presents demoulding difficulties and undesirable features such as fat bloom[18]; emphasising the importance of this step in chocolate production.

1.3 Chemical composition of cocoa butter

1.3.1 Fatty acids

Fatty acids (FAs) are the individual building blocks of CB that when combined create complicated structures with a multiplicity of functions[19]. Comprised of a hydrocarbon chain with a methyl group at one end and a carboxyl at the other, the organic acids play an important role in regulating the lipids’ overall performance and can be divided into two distinct groups, saturated and unsaturated. The latter comprising of at least one double bond along its carbon chain, which introduces a ‘u-shape’ into the molecule when the bond is one of *cis* configuration: neighbouring hydrogens attached to the carbons on the double bond repel each other, forcing the bend in the FA. An unsaturated FA with *trans* configuration displays a linear arrangement, similar to a saturated FA.

CB is relatively simplistic with seven known FAs but dominated by three, which account for ca. 95% of the composition; palmitic (P), oleic (O) and stearic (St). Each are of similar chain lengths, written as CN:DB (carbon number: double bond), but oleic acid (18:1) is a monounsaturated FA (MUFA), whereas stearic acid (18:0) and palmitic acid (16:0) are both saturated. They combine in a tripartite arrangement on a glycerol backbone to produce triacyclglycerols (TAGs); where the positional distribution greatly affects the stability, physical properties and nutritional performance of the TAG in which they belong[19, 20].

Monoacylglycerols (MAGs) and diacylglycerols (DAGs) can also be formed, but TAGs are the primary storage form in any lipid.

1.3.2 Triacylglycerols

Stearic, palmitic and oleic acid combine to create three TAG species in CB that account for 71 – 86 mol%[21], depending on the country of origin: 1,3-dipalmitoyl-2-oleoyl-glycerol (POP), 1,3-distearoyl-2-oleoyl-glycerol (StOSt) and 1-palmitoyl-2-oleoyl-3-stearoyl-glycerol (POSt). The numbers refer to the stereospecific numbering (*sn*) system, indicating the FA position on the glycerol; based on the orientation around the central carbon when observing a Fischer projection[22] (Figure 1.3). Where the acyl chain of the *sn*-2 carbon is positioned to the left of the glycerol, the upper carbon is defined as *sn*-1 and the lower as *sn*-3: numbering is reversed when the FA is positioned to the right[22].

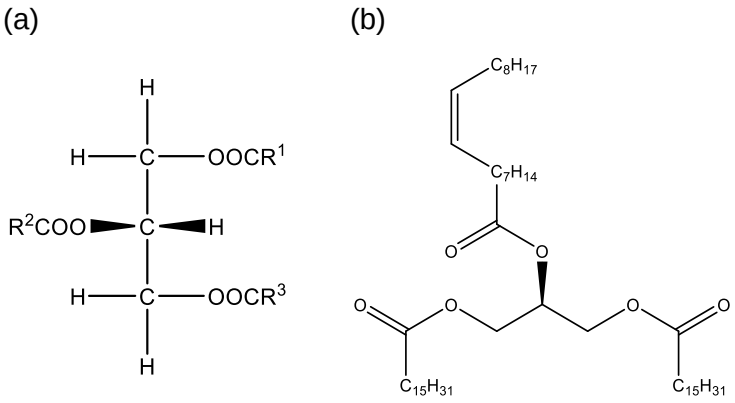

Figure 1.3 Chemical structures of TAGs showing (a) a Fischer projection indicating the FA positions; sn-1, sn-2 and sn-3 located at the top, centre and bottom of the structure respectively; (b) shorthand structure of POP.

Monounsaturated oleic acid resides in the *sn*-2 position for ca. 80% of all CB TAGs, with saturated fatty acids (SFAs), predominantly palmitic and stearic acid, at the *sn*-1,3 carbons, also known as the primary positions. This arrangement often sees them referred to as symmetrical and monounsaturated[1, 23]; known as SUS TAGs, where S represents saturated and U represents unsaturated.

Approximately 1 – 2% of CB TAGs are fully saturated and 5 – 20% are diunsaturated, giving it the property of being semi-liquid at room temperature[1]. Softer CBs are a result of higher levels of unsaturation, just as those of a firmer nature contain a larger ratio of saturated TAGs[13], which relates to the intermolecular packing of the FAs; discussed further in section 1.4.2. As such, the measure of solid mass at a given temperature, the solid fat content (SFC), can be related to saturation levels in the native fat[24]. For example, SFC at varying temperatures have been reported as (ºC): 82.1 (20), 78.7 (25), 58.3 (30) and 2.4 (37)[25]. Growing regions with consistent warmer climates produce CB with greater levels of SFAs and thus, a higher SFC and melting point (m.p.). Differences in TAG composition are exemplified in Table 1.1.

Table 1.1 Comparison of TAG composition by growing region (adapted from reference[26]).

TAG	Relative amounts (%)		
	Ivory Coast	**Malaysia**	**Brazil**
POP	18.3	17.8	17.0
POSt	41.7	40.7	38.7
StOSt	25.2	25.9	23.8
PPP	0.4	0.2	0.3
MOP	0.3	0.2	0.2
PPSt	0.7	0.8	0.6
PLP	1.8	1.8	2.2
PStSt	0.3	1.0	0.3
POO	2.4	2.4	5.0
PLSt	2.9	2.7	3.0
PLO	0.4	0.5	0.3
StStSt	0.2	0.6	0.2
StOO	2.9	2.8	6.0
StLSt + OOO	1.4	1.3	1.4
StOA	1.2	1.3	1.1

* M = myristic (14:0); L = linoleic (18:2 n-6); A = arachidic (20:0)

1.3.2.1 Biosynthesis of TAGs in plants

The formation of TAGs is an acyl-CoA dependent reaction known as the Kennedy pathway, involving sequential acylation to the glycerol backbone, beginning with *sn*-glycerol-3-phosphate (G3P), via three acyltransferases; glycerol-3-phosphate acyltransferase (GPAT), lysophosphatidic acid acyltransferase (LPAAT) and diacylglycerol acyltransferase (DGAT)[27, 28]. Hydrolysis of the phosphate group to produce *sn*-1,2-DAG is elicited by phosphatidic acid phosphatase (PAP), where DGAT completes the TAG synthesis via acylation at *sn*-3.

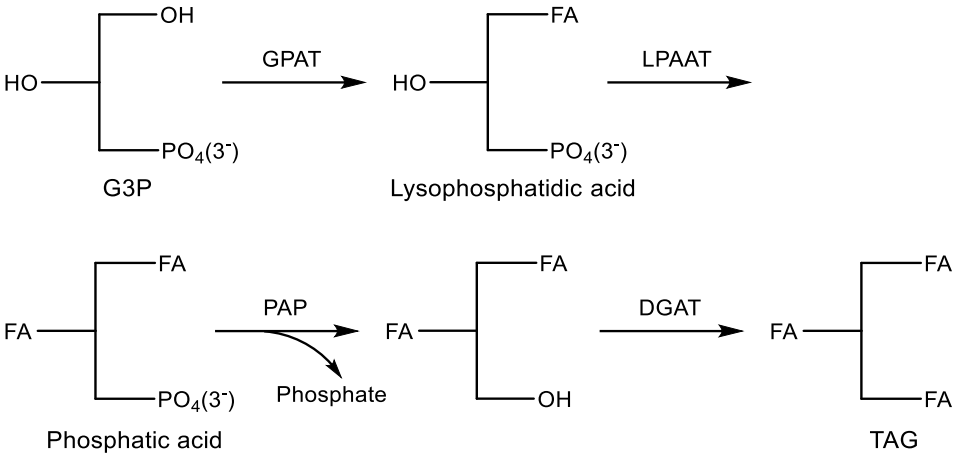

Figure 1.4 Simplified reaction scheme of the Kennedy pathway for TAG biosynthesis displaying the key acylation and hydrolysis stages. $PO_4(3^-)$ represents the phosphate group (adapted from reference[27]).

1.3.3 Stereochemistry

When dissimilar alkyl chains are at the *sn*-1,3 positions of a TAG, chirality is introduced into the system and presents the possibility of two enantiomeric, forms through the three-dimensional arrangement of the molecules[29, 30]. A chiral molecule is defined as non-superimposable on its mirror image: a classic representation is that of bromochlorofluoromethane, which is presented in Figure 1.5.

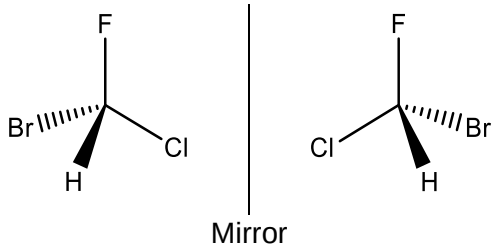

Figure 1.5 Depiction of bromochlorofluoromethane enantiomers as their mirror image, displaying the different spatial arrangements of the atoms around the central carbon[31].

Nomenclature conforms to the Cahn-Ingold-Prelog (CIP) priority rules, which assigns (*R*) and (*S*) to the different enantiomers in order to specify their individuality; (*R*) comes from the Latin for right, *rectus*, and (*S*) from the Latin for left, *sinister* [32, 33]. The CIP rules use atomic numbers to assign levels of priority to atoms attached to the chiral centre once determination of the

molecular structure has occurred. Higher priority is given to those with greater atomic numbers; 1 is assigned to the highest priority number and so forth[32]. The molecule is then viewed from the perspective of the atoms with the lowest priority and the direction in which the priorities increase will determine their classification; a clockwise or counter-clockwise direction dictates whether they are classified as (*R*) or (*S*) respectively (Figure 1.6).

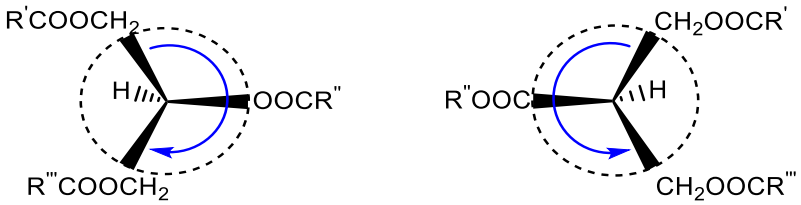

(R) *(S)*

Figure 1.6 Representation of the priority sequence for a TAG according to the CIP rules (adapted from literature[34]).

Determining enantiomers' (*R*) and (*S*) absolute configuration is often achieved through optical activity measurements, with each rotating the plane of polarisation in opposing directions[35]. However, enantiopure TAGs display immeasurable optical activity, to which the term 'cryptoactive' has been applied[34, 36, 37]. Identical physicochemical properties such as m.p. and retention time (t_r) present difficulties for separation and quantification, particularly when in a racemic (*rac*) mixture; which is a 1:1 ratio of the enantiomers.

CB contains nine chiral TAGs in variable proportions (Table 1.1), with the dominant POSt being one (Figure 1.7); where the primary FAs differ by virtue of two methylene units.

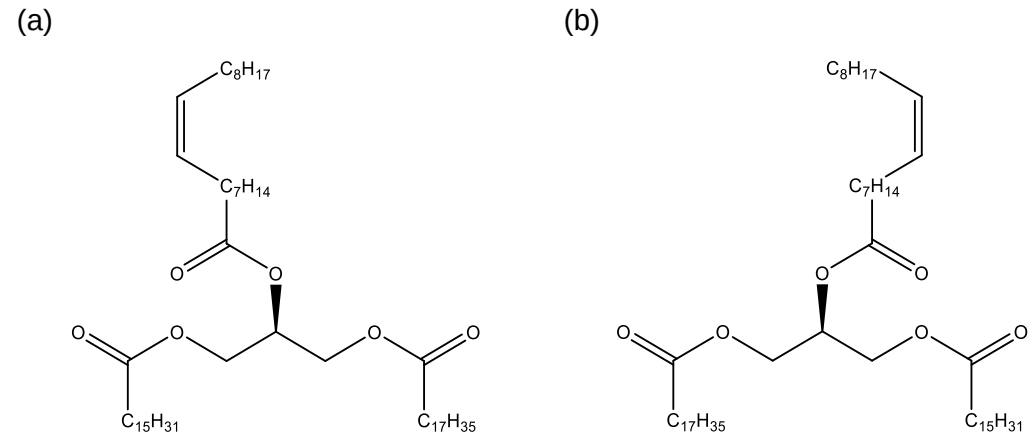

Figure 1.7: Enantiomers of POSt displayed as mirror images, where (a) is (R)-POSt and (b) is (S)-POSt.

1.3.4 Analytical approaches to molecular determination

High-performance liquid chromatography (HPLC) is frequently used in the identification of lipid TAGs through comparing the t_r of reference standards and the analyte. The instrument induces compound separation from a mixture through interactions with the stationary- (column) and mobile phase (solvent)[38]. Separation of TAG molecular species is commonly achieved through non-aqueous reversed phase HPLC (NARP-HPLC), where the column contains hydrocarbon chains immobilised to a silica base, largely octadecylsilyl (ODS; C18), and a polar solvent is used for the mobile phase[39]. The non-polar environment of the stationary phase offers a high level of TAG interaction through van der Waals forces[40]. Retention is based on the equivalent carbon number (ECN), defined as ECN = CN – 2DB, where CN is the number of carbons and DB is the number of double bonds; t_r increases with increasing ECN[41].

The basic components of a HPLC system include solvent pumps, an autosampler, a column oven and a detector. Numerous options are available for the latter such as UV-visible (UV-vis), photodiode array (PDA), refractive index, fluorescence, conductivity and evaporative light scattering detection (ELSD). However, with only a weak ester chromophore, lipids lack easily detectable functional groups and thus, options are limited for their analysis.

UV-vis can be used, but as there are a minimal amount of target molecules, only a small absorbance in the 180 – 200 nm range is observed[42]; whereas the ELSD is capable of detecting semi- and non-volatile analytes in volatile solvents following separation[43, 44]. Eluents are transported via carrier gas, nebulised, condensed and then removed as waste. The remaining analytes are subjected to focused light in the optical cell and the intensity of scattered light is detected, providing information on the analytes and their concentration[43, 45]. However, the ELSD response is non-linear, which makes quantitation difficult[46, 47]. Mass spectrometry (MS) coupled with NARP-HPLC resolves this, where electrospray ionisation mass spectrometry (ESI-MS) and atmospheric pressure chemical ionisation MS (APCI-MS) are often employed. The lack of electrostatic charge in TAGs determines they do not ionise readily in ESI-MS and require an electrolyte addition into the solvents, commonly ammonia salt to produce an ammonium adduct $[M+NH_4]^+$[48, 49]. Conversely, APCI-MS can readily ionise the TAGs to produce a gentle fragmentation pattern of protonated molecules $[M+H]^+$ and fragment ions $[M+H – RCOOH]^+$ that is not available with ESI-MS, yet advantageous for compound characterisation[41, 50]. The principle behind APCI-MS lies in ionisation of the gas phase following nebulisation and vaporisation of the solvent/analyte at high temperature. A highly charged electrode, the corona discharge needle, ionises solvent and analyte molecules; though excess of the former in comparison to the latter dictates it likely this will become the ionised component. Subsequently, recurrent collisions between solvent ions and analyte can displace a hydrogen atom, allowing the analyte to become charged via proton transfer[51].

For the resolution of chiral TAGs, stereospecific analysis procedures that are used for differentiating *sn* positions of FAs have been traditionally employed for converting the compounds into diastereomeric derivatives. These can then be separated through chromatographic means: diastereomers being defined as enantiomers that are not mirror images of each other and non-superimposable[52]. The derivatisation process involves several steps including partial hydrolysis using lipase or a Grignard reagent such as ethyl magnesium bromide (EtMgBr) to produce DAGs/MAGs, followed by reacting

with a derivatising agent such as (*R*)-(+)-1-(1-Napthyl)ethylamine or 3,5-dinitrophenyl isocyanate (3,5-DNPU)[53, 54]. Alternatively, a chiral shift reagent, such as α-methoxy-α-(trifluoromethyl)phenylacetyl chloride (Mosher's acid chloride; MTPA-Cl) can be added, which gives the diastereomeric esters distinct spectroscopic properties due to the presence of methoxy and trifluoromethyl groups[55]. Subsequently, these can be analysed using nuclear magnetic resonance (NMR). An example of the stereospecific analysis route and derivatisation procedure is presented in Figure 1.8.

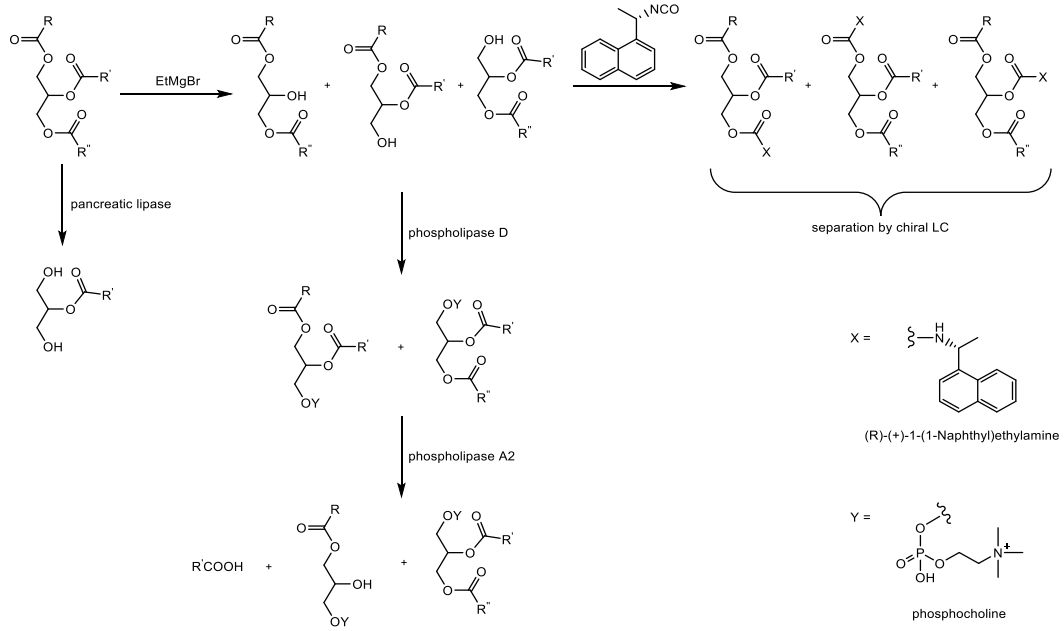

Figure 1.8 Stereospecific analysis of TAG structure via chemical and enzymatic means[56]. Phospholipase D catalyses a reaction between the free sn position and phosphocholine; phospholipase A2 is an sn-2 specific enzyme.

TAG breakdown via the phospholipase procedure allows structural determination through analysis of the free fatty acids (FFAs) and DAG products. The addition of a chiral derivatising agent (CDA) following the initial FA removal is perhaps the simpler route to resolution of chiral TAGs, which can subsequently be analysed by NARP- or chiral-HPLC as the resulting diastereomers have differing physicochemical properties. However, the procedure of stereospecific analysis/derivatisation is a laborious process that does not rule out the potential for acyl migration[29] and thus, APCI-MS in combination with chiral HPLC has become popular for quantification of

complete TAG enantiomers. In chiral-HPLC, separation is based on the enantiomers having different affinities for the chiral stationary phase (CSP), of which the selection is vast and suitability is highly dependent on the compound[57]. It is not possible to identify the appropriate conditions simply from success of previous literature; a thorough screening of CSPs and mobile phase combinations is required.

Many of the commercial columns consist of polysaccharide-based supports coated onto silica with chiral selectors attached for enantiorecognition, where resolution is based on the momentary formation of diastereomeric complexes[58, 59]. Recognition is based on the three-point interaction model, which dictates the spatial arrangement of the compound identifies with that of the CSP at three-points, where at least one must be stereoselective, to form intermolecular interactions such as π-π, hydrogen bonds, dipole-dipole, hydrophobic and steric[58-60]. Some of the most employed CSPs for enantiomeric TAG identification are presented in Figure 1.9.

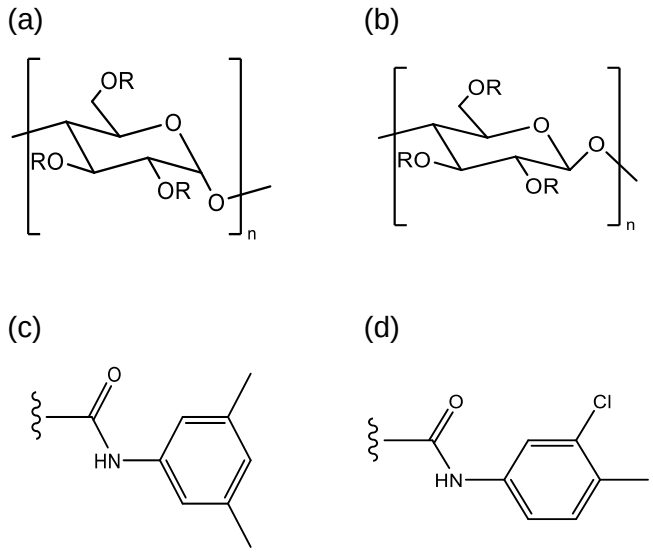

Figure 1.9 Examples of polysaccharide-based stationary phases used for enantiomeric TAG separation; (a) amylose and (b) cellulose where 'R' refers to chiral selectors; commonly used groups being (c) 3,5-dimethylphenylcarbamate or (d) 3-chloro-4-methylphenylcarbamate[61].

Using cellulose-tris as the stationary phase, Iwasaki et al.[62] investigated 3,5-dimethylphenylcarbamate (CDMPC) and 4-chlorophenylcarbamate (CCPC)

chiral selectors for separation of synthetic ECC/CCE and DCC/CCD, where E is eicosapentaenoic acid (20:5, n-3), D is docosahexaenoic acid (22:6, n-3) and C is caprylic acid (8:0). Enantioseparation for ECC/CCE was achieved with both columns, but DCC/CCD was only resolved using the CCPC column. The use of chlorine as a substituent on the chiral selector in place of methyl group(s) influences the electron density of the phenyl causing a slight increase in polarity, which was more attractive to DCC/CCD; the additional double bond and carbon atoms in docosahexaenoic acid defining the enantiopair as more polar than the eicosapentaenoic acid TAGs[61]. With regards to enantioseparation of ECC/CCE, the modified polarity in the CCPC column caused a reversal in order of elution. Analysis was conducted in normal-phase mode, where the mobile phase is non-polar.

The first report of successful enantiomeric TAG separation from a natural lipid without derivatisation was achieved using a CDMPC column in a recycle HPLC system[63]; where the enantiopair OOP/POO was isolated from palm oil and found to exist in a 3:2 ratio, known as a scalemic mixture[64]. The system allowed the analyte to repeatedly pass through the column and UV-vis detector via a recycle valve and pump until adequate resolution was achieved, at which point the valve direction was switched to transfer the flow to the APCI-MS for detection. Using isopropanol (IPA) as the solvent and methanol (MeOH) as the mobile phase at 0.5 mL min^{-1}, separation was not achieved until ca. 180 minutes when the peak for OOP appeared, followed by POO at ca. 184 minutes. It is not clear how many passes of the column were necessary to achieve separation, but the lengthy t_r is evidence of severe difficulties and that multiple CSP/analyte interactions are required to draw the enantiopair apart.

In a further study of natural lipids, Lísa and Holčapek[65] analysed the composition of hazelnut oil and human plasma without prior isolation of the TAGs. Using two CDMPC columns connected in series to increase the CSP/analyte interaction time, they identified several TAGs that were present as enantiopairs in both samples in scalemic ratios. Interestingly, PLO/OLP in hazelnut oil, where L is linolenic acid (18:2), is reported as being present in a near racemic ratio at 27:29 respectively. However, OLP eluted within a mixed

peak containing (POL+LOP+LPO)/OPL so it is possible that a miscalculation was made. However, this was the first study to analyse natural samples using this technique and demonstrated that separation is possible without derivatisation or fractionation.

1.4 Fundamentals of lipid crystallisation

1.4.1 Crystallisation

A solid crystal, or the term ‘crystalline’, can be described as a collection of symmetrical particles arranged in an orderly manner, contained within a space lattice[66, 67]. To understand the internal structure of the solid crystalline form, the four definitions as introduced by Marangoni and Wesdorp[66] are instrumental:

- Asymmetric unit: molecules, atoms or ions that are the foundation of which the crystal is constructed
- Space lattice: three-dimensional, repetitive arrangement of points that defines the basic structure of the crystal
- Crystal structure: arrangement of asymmetric units in a symmetrical manner within the space lattice
- Unit cell: the essential component of a crystal that contains all its symmetrical features. Through moving and repeating each point of the unit cell by the same amount in a direction, formation of the entire crystal will occur

Seven crystal systems have been identified through their symmetrical arrangement along with fourteen types of unit cells, which are able to stack in a manner that produces a particular space lattice[66]: a representation of a unit cell is presented in Figure 1.10.

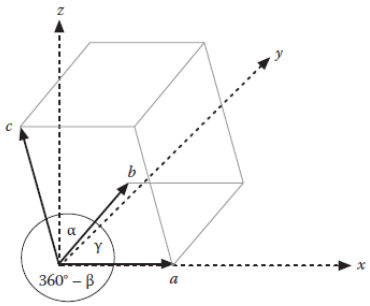

Figure 1.10 Representation of the three crystallographic axes a, b, c with their corresponding angles α, β, γ.

1.4.1.1 Nucleation

Nucleation of molten fat is the fundamental aspect for crystalline growth: a process driven by a decline in temperature of the melt to a point below the m.p. of the highest melting TAG, known as supercooling or undercooling, to create a supersaturated system[68, 69]. A moderate temperature reduction of the melt creates a metastable region, which can be defined as an intermediate phase where crystalline material does not develop[66]. Yet, in this zone amorphous aggregates (embryos) repetitively break down and reform[68, 69]. Through further undercooling, transformation from the embryonic stage into nuclei is a relatively gradual process as the molecules must overcome an energy barrier to rearrange themselves into lattice conformations where the optimum amount of atomic interaction can occur via physical or chemical bonds, allowing structures of critical size to form[70, 71].

Primary nucleation occurs without the presence of crystalline material, of which there are two forms, homogenous and heterogenous[67, 69, 72]. Homogenous nucleation is relevant to pure solutions and needs a great degree of undercooling, whereas heterogeneous nucleation requires the existence of a particle to promote crystal growth and is the most common form[69, 72]. These additional particles, which could relate to cocoa powder, sugar and milk powder in chocolate, organise molecules within the melt and act as prototypes from which further nuclei are able to develop. Secondary nucleation develops once primary has occurred, where the presence of crystals or their fragments elicits the growth of new nuclei on contact[69].

1.4.1.2 Crystal growth and aggregation

Crystal growth rates alongside their relative rates of nucleation have a distinct effect on product texture through the size of crystals that develop. By supercooling the liquid melt to a point where nucleation occurs faster than crystallisation, a greater amount of small crystals will be formed, and vice versa[73]: small crystal formation can be encouraged through mechanical force (shear), which fragments the growing nuclei thus producing further growth sites distributed throughout the system for crystallite development[1]. On consumption, the tongue is highly sensitive to particle detection and the presence of crystals larger than a few tens of microns creates a gritty rather than smooth sensation[11, 24, 70].

Once growth begins from the nuclei, the TAGs' chain length becomes significant, where those that are larger have slower crystal growth rates. It is suggested that this effect may be based on the period required to align the methyl planes[24]: here, plane being defined as the theoretical flat surface between methyl groups of individual TAGs, as indicated by the dotted lines in Figure 1.11. As the proportion of solid fat increases due to the touching of crystal interfaces, the growth rate slows significantly, resulting in an increased viscosity of the liquid melt[24, 73].

1.4.2 Polymorphism

Polymorphism is defined as the ability to exist in a number of forms that may exhibit some physical and chemical differences even though they contain identical molecules[74]. This is evident in the crystal arrangement (polymorphic form) of CB that determines the quality and sensory properties of chocolate due to the heat resistance of each polymorph, with each having a unique melting temperature (T_m); discussed further in section 1.5.

During fat crystallisation, TAGs develop into 'chair' or 'tuning fork' configurations (Figure 1.11), which are dictated by the arrangement of acyl chains on the glycerol[75]. The tuning fork occurs with symmetrical TAGs where the primary acyl groups position themselves side-by-side, allowing the *sn*-2

group to stand alone. Asymmetrical TAGs have a preference for developing into the chair configuration where the *sn*-1 acyl group stands alone (Figure 1.11)[24, 75]. Thin layers, often discussed as lamellar structures/ordering, are formed by the stacking of TAG crystals to create double and triple packed chain lengths (Figure 1.11 (i – iv)), known as 2L and 3L respectively[24, 76]; as measured by the distance between methyl planes, the long spacing.

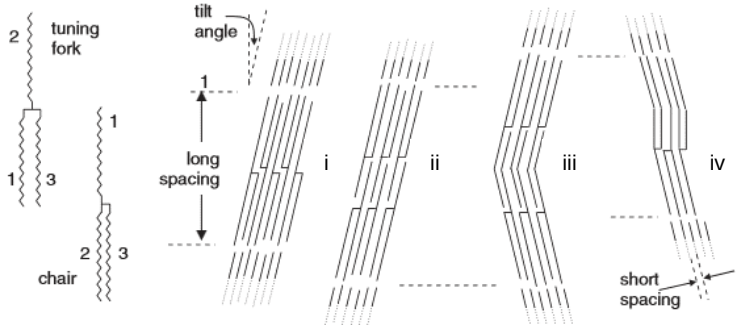

Figure 1.11 Representation of the polymorphic configurations (tuning fork and chair) and stacking (i – iv) that develop during TAG crystallisation, where the numbers 1 – 3 represent the sn positions on the glycerol. Images i and iv display 2L stacking, ii and iii show 3L structures. The long spacings reflect the distance between methyl planes (chain length packing) and the short spacings provide information on the subcell structure; indicating the packing of the FA chains and the distance between them[24, 66, 75, 77].

Double-chain packing occurs when the FA groups have similar properties, such as in a triacid TAG. Where differences with at least one of the acyl groups occurs, such as in POP, POSt and StOSt, triple-packing will take place; which is the most stable configuration for chocolate production[78]. The double bond in an unsaturated acyl group dictates the intermolecular packing by forcing alike chains to connect in matching conformations; as represented in Figure 1.11 iii and iv. As such, the ‘u-shape’ configuration of the *cis* chain packing determines the overall structure as less compact than those of a linear, saturated nature.

The three main polymorphs that develop, α, β' and β, can be seen in Figure 1.12, which are depicted in relation to their unit cells and level of order/stability.

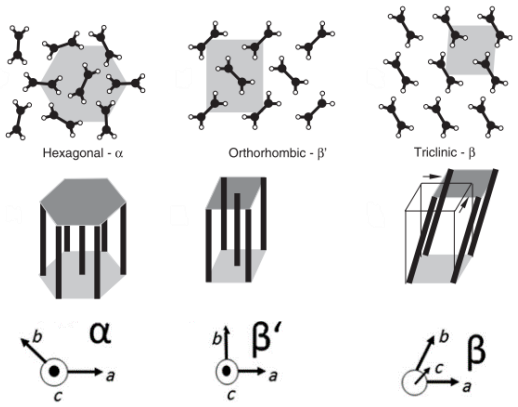

Figure 1.12 Depictions of the three primary polymorphic subcells in increasing order of stability, hexagonal (H; α form), orthorhombic ($O_{\perp}$; β' form), triclinic ($T_{//}$; β form) and their crystallographic axes within the unit cell (short spacing).

These crystalline arrangements are identified through X-ray diffraction (XRD), which provides information on the unit cell structure (short spacings) and distance between methyl planes (long spacings) by irradiating the sample with X-rays. The beam is diffracted as it comes into contact with atoms in the sample and the angle at which this occurs alongside its intensity can be used to calculate the distance between surfaces of lamellar ordering [24, 79]. The level of order is dependent on interactions between saturated and unsaturated acyl groups, which influences conformation of the glycerol.

1.4.3 Role of stereochemistry in crystallisation

Crystallisation of racemic mixtures presents complexities in the unit cell by introducing three possibilities that influence the melting behaviour. The most common and that which occurs in ca. 90 – 95% of all crystalline racemates is the racemic compound. In this arrangement, opposing enantiomers have a strong affinity with each other and order themselves in a 1:1 ratio within the unit cell. The second form is a conglomerate, which occurs when individual enantiomers are more strongly attracted to themselves, forming a mechanical mixture of pure (*R*) and (*S*) crystals. Lastly, randomisation of enantiomers within the crystalline unit gives rise to a solid solution, also known as a pseudo-racemate[80-82]. Each of these forms are portrayed in Figure 1.13.

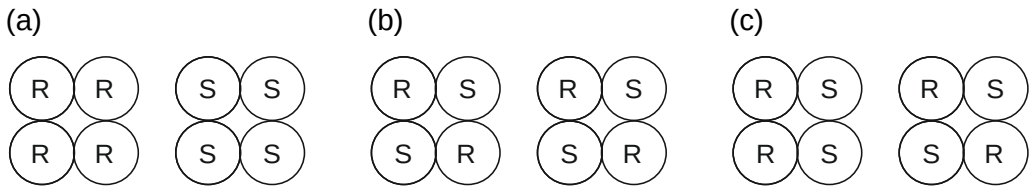

Figure 1.13 Depiction of crystalline structures formed by rac-TAGs; (a) conglomerate, (b) racemic compound and (c) pseudo-racemate (adapted from literature[80, 82]).

Their binary phase diagrams are presented in Figure 1.14, which shows marked differences in their melt behaviour. The conglomerate displays a eutectic where the pure enantiomers have increased thermal stability compared to a mixture of reduced enantiopurity, with racemate causing a significant reduction in m.p. In the racemic compound, a similar behaviour is observed where decreasing enantiopurity creates a eutectic point, however, when racemate is achieved the m.p. can increase, be equal to, or lower than the single enantiomers. An example of m.p. increase in racemate is seen with tartaric acid: the pure enantiomers have a m.p. of ca. 174 ^{o}C[83] whereas *rac*-tartaric acid melts at 206 ^{o}C[84]. The rarely seen solid solution has identical melting properties for the pure enantiomers and racemate[85].

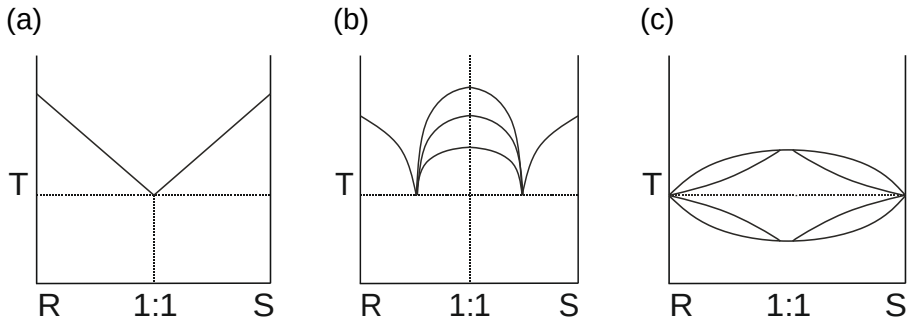

Figure 1.14 Binary phase diagrams for enantiomeric mixtures; (a) conglomerate, (b) racemic compound and (c) pseudo-racemate (adapted from reference[85]). R, S represents the respective enantiomers,1:1 is the racemic mixture and T denotes temperature.

Understanding the role of chirality in relation to *rac*-TAG crystallisation is noteworthy, yet few studies have been undertaken. Using m.p. determination and XRD techniques, Craven and Lencki[81] observed a racemic compound in the crystalline form of 1,2-bisdecanoyl-3-palmitoyl-*rac*-glycerol (*rac*-10:0-10:0-16:0), whereas the enantiopure TAG was β′ tending, suggesting the formation of a conglomerate. The latter is explained by the lack of antipode that would

complete the β unit cell[86]. The racemate showed a conglomerate in the β′ polymorph, signifying a rearrangement of enantiomers during phase transition to inhabit the unit cell in a 1:1 ratio. A trivial difference between the m.p. of enantiopure and racemate was observed with a reduction of 0.5 ^{o}C for the latter.

Using similar techniques, Mizobe et al.[87] observed the behaviour of binary mixtures of 1,2-dipalmitoyl-3-oleoyl-*sn*-glycerol/2,3-dipalmitoyl-1-oleoyl-*sn*-glycerol (PPO/OPP) where a eutectic was also detected, with a m.p. reduction of ca. 5 ^{o}C for the racemate compared to the pure enantiomers (Figure 1.15).

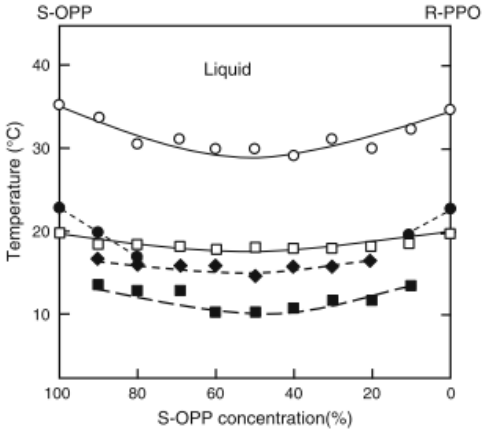

Figure 1.15 Binary phase behaviour of (S)-OPP and (R)-PPO mixtures. Experiments involved cooling and heating at a rate of 2 °C/min; filled circles T_c of β′-3, filled diamonds T_c of α-2, filled squares T_c of α-3, unfilled squares melt-mediated α-β′ transformation temperature, and unfilled circles T_m of β′-3[87].

Through the transformation of its least to most stable polymorph, which was found to be β', a racemic compound was observed in *rac*-PPO. The presence of a MUFA at *sn*-1(3) suggests crystallisation in the chair conformation, as described in section 1.4.2, yet as expressed by the authors, why β' is the favourable polymorph over β for that compound requires further investigation[87, 88].

1.5 Crystallisation and polymorphism in cocoa butter

To achieve the desirable properties of chocolate for which it is known such as the gloss, snap, heat resistance and fat bloom stability, several control elements must be in place[88]. Most notably, control of crystallisation is paramount to ensure the correct morphology of the crystal network; this aspect generates the structure in chocolate and is responsible for the characteristic mouthfeel during consumption[89].

In their pure forms, each of the main TAG species can develop into a number of polymorphs; POSt has four, StOSt has five and POP has six[90-92]. The interaction between these delivers a unique polymorphic capacity. Where CB differentiates itself from many other lipids is in its ability to develop six polymorphs, with each polymorphic arrangement having its own distinctive crystallisation temperature (T_c) and m.p.[88, 93].

Wille and Lutton[94] were the first to propose the polymorphs in CB after identifying them through an XRD study. They provided the nomenclature that is most commonly used in the manufacturing industry today, which uses Roman numerals as identifiers (I-VI) with ‘Form’ as their prefix and increasing order of m.p. (Table 1.2).

Table 1.2 Melting points and chain packing of the six associated polymorphs of cocoa butter (adapted from literature[95, 96]).

Form	Crystal Structure	Melting Point (ºC)	Chain Packing
I	Sub-α	~-5 - +5	Double
II	α	17 – 22	Double
III	β'_2	25.5	Double
IV	β'_1	27.5	Double
V	β_2	33.8	Triple
VI	β_1	36.3	Triple

Monotropic polymorphism is present, where Forms V and VI exhibit themselves as being the most thermodynamically stable, having gone through irreversible phase transformation from the metastable polymorphs[24, 97]. The transformation between Forms I and II happen relatively quickly but the instability of these are apparent when they continue the transformation into Forms III and IV, albeit at a slower rate[1]. Although Form VI is the most stable polymorph, Form V produces the characteristics required by confectioners to deliver pleasurable eating qualities to chocolate[98]. Form VI has a waxy and unpleasant mouthfeel due to its failure to melt in the mouth properly.

To achieve Form V, the process of tempering is essential which controls temperature fluctuations in liquid chocolate to develop the stable crystal structure[98]. ‘Seeding’ is the significant stage in this process. It involves the generation of Forms IV and V from the cooling of liquid chocolate combined with mixing and shearing to distribute the seed[1]. This is reheated to a temperature where Form IV no longer exists and Form V remains, which proceeds to seed the remaining product, providing a structure for the fat to solidify to[1, 98]. During this process, the Ostwald step rule is followed which defines that the least stable polymorphs are formed first[99]. However, it is possible to break this ‘rule’ by altering some of the factors involved such as pressure and seeding, which alters the process kinetics[78].

1.6 Enantiomeric composition of cocoa butter

There are only three studies that have analysed the enantiomeric TAG composition in CB, each of which focused on the predominant POSt[34, 53, 100]. Using different analytical procedures, each concluded the TAG as being present in a racemic mixture. The first reported incidence was in 1965 by Schlenk[34], who established this by comparing XRD patterns of synthetic enantiopure and *rac*-POSt with the isolated fraction from CB. The enantiopure POSt pattern was dissimilar to that of racemate by synthesis and the isolated fraction from CB, which appear almost identical. The formation of a racemic compound may have been discovered when the m.p. of (*S*)-POSt was found to be 33.9 – 34.5 ^{o}C and the racemate highlighted as 37.5 – 38 ^{o}C. It should be noted that thermal data for the latter was not analysed directly but taken from the work of another author. A later study analysing the polymorphic behaviour of POSt isolated from CB found the m.p. of its β form to be 35.5 ^{o}C[91], which correlates with the notion of a racemic compound but may also be too similar to the pure enantiomer to make an assertion.

Sampugna and Jensen[100] used stereospecific analysis techniques to break down the monounsaturated TAG fraction of CB containing POP, POSt and StOSt using *Geotrichum candidum,* an enzyme that targets cis-9 unsaturated FAs, such as oleic acid. The subsequent α-α- and α-β-DAGs were converted to DAG acetates and analysed by gas liquid chromatography (GLC): phospholipase A investigations of DAG phosphatidyl phenols were also conducted and the isomers of POSt calculated from the FFA and DAG components. Similarly, Takagi and Ando[53] used a combination of techniques to isolate the monounsaturated TAG fractions from the CB bulk, but they were able to isolate individual TAGs from the group using RP-HPLC. Stereospecific analysis procedures were followed to create 3,5-DNPU derivatives suitable for detection using chiral-phase HPLC and GLC.

Takagi and Ando[53] allude to the need for further research in order to establish *rac*-POSt as conclusive, but database searches for relevant studies failed to produce any results. However, a patent submitted by Chandler and

Quinlan[101] was identified that compared the crystallisation behaviour of an enantiopure (termed as chiral) and racemic cocoa butter equivalent (CBE), where the former was found to have a closer relationship with CB. The CBEs both contained identical ratios of POP (32%), POSt (55%) and StOSt (13%), but differed in enantiomeric content of POSt. Following seeding, observations were made during isothermal crystallisation at 20 and 25 ^{o}C, where the chiral CBE was found to maintain the same rate and polymorphic form as CB; whereas the racemic CBE crystallised in β' form at 20 ^{o}C and though in β form at 25 ^{o}C, the rate was much slower. Their conclusion being that the 'chiral' CBE would be suitable as a replacement for CB and not the racemic, which suggests a contradiction to the analytical studies.

1.7 Modification of lipid molecular structure

The synthetic rearrangement of FAs on a TAG molecule with the purpose of altering its physicochemical properties results in a compound deemed as a structured TAG (ST)[25, 102]. These can be tailored to requirement and are used in the food industry for improving the functionality and nutritional properties of products[102, 103]. Chemical or enzymatic means are used for the rearrangement, but the latter is preferred in food applications due to the milder conditions and ability to control the reaction using FA and regiospecific lipases[104-106]. This being useful for the manufacture of CBEs through the modification of low-cost vegetable oils as CB itself can be costly, as well as variable in quality[25, 107]. A directive set out by the European Union[108] defined six vegetable oils as being suitable for this purpose and the amount that can be added to chocolate products must not exceed 5%. However, even such a minimal amount can enhance CBs cost-effectiveness through dilution when the TAG profile is alike or allow the use of softer varieties by increasing the SFC through the addition of formulated products containing high StOSt[109].

1.7.1 Modes of enzymatic interesterification

Enzyme catalysed interesterification reactions occur between an ester and an alcohol (alcoholysis), an ester and an acid (acidolysis) or an ester and another ester (transesterification). These can be performed with or without solvent in batch or under continuous flow on a packed bed reactor (PBR)[110]: a PBR being a cylindrical vessel filled with a bed of immobilised catalyst[111]. Under laboratory conditions, batch is commonly used for ease of control and reduced enzyme load; however, a disadvantage is the extended reaction times required that can lead to randomisation of products through acyl migration, which is a relocation of acyl chain(s) between *sn* positions of the glycerol. With a PBR, the high enzyme to substrate ratio increases the interaction and subsequent rate of product formation, whilst maintaining regiospecificity[112]. Several control parameters must be taken into consideration for enzyme catalysed reactions such as substrate molar ratio, enzyme load, enzyme support, temperature, reaction time and water content[107]. These are specific to the system in place and difficult to estimate, thus, much of the research is based on elucidating the optimum conditions for maximum yield of the target TAG.

A multitude of lipases with varying specificities for the *sn* positions are available; developed from bacterial, yeast and fungal sources, such as *Candida Rugosa, Aspergillus niger* and *Rhizomucor miehei*[113, 114]. These can be free or immobilised, though the latter is generally favoured for their thermostability, reusability and ease in which they can be separated from the reactants and products[115, 116].

1.7.1.1 Alcoholysis

Alcoholysis is common in the manufacture of biodiesel, there referred to as transesterification, where a reaction between a monohydric alcohol and TAG(s) from vegetable oil sources is initiated to produce alkyl esters and glycerol[117] (Figure 1.16). The reaction is analogous to hydrolysis, where the alcohol takes on the role of the nucleophile as the system is largely anhydrous[118].

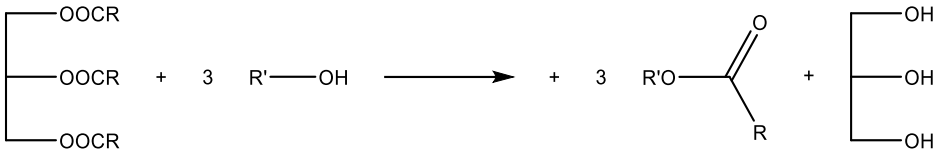

Figure 1.16 General scheme of alcoholysis reaction[117].

The technique is not widespread in the formulation of structured lipids, particularly in CB related products, but it has shown to be effective as a precursor to esterification for emulating a USU TAG present in human milk. As demonstrated by Schmid et al.[119], regiospecific lipases can be used to control the exchange of ester groups with the alkoxy fraction(s) of a TAG[117]. An *sn*-1,3 lipase was used in a two-stage reaction, alcoholysis followed by esterification, under batch conditions to synthesise 1,3-dioleoyl-2-palmitoyl-glycerol (OPO) (Figure 1.17).

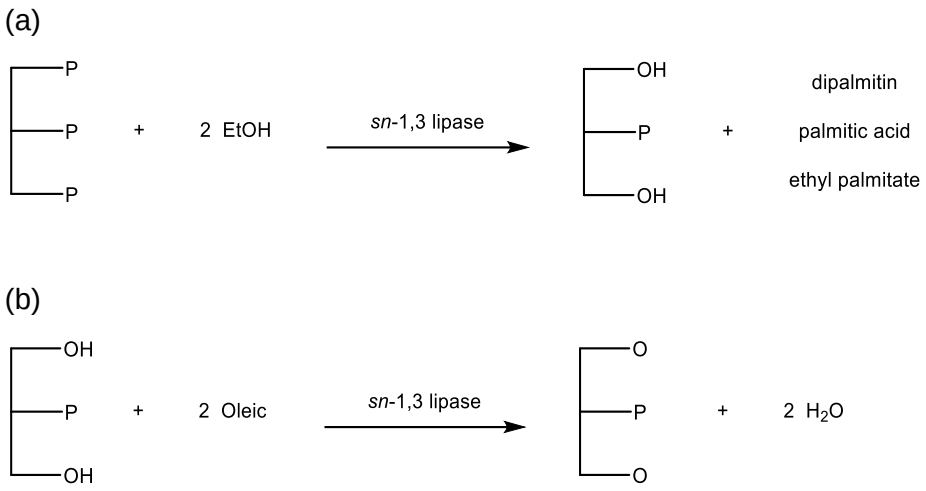

Figure 1.17 Reaction scheme for the synthesis of OPO, where O represents oleic acid and P is palmitic acid, using a regiospecific lipase where (a) shows the 2-MAG formation through alcoholysis and (b) esterification of oleic (adapted from literature[119]).

The benefit of this system is the ability to run at extremely low water content as no hydrolysis is required; it is merely an exchange of ester groups and thus, no diacylglycerol (DAG) intermediates are formed.

1.7.1.2 Acidolysis

During this process, an exchange is made between the FA(s) of the TAG substrate and an acid. Regiospecific lipases are used to hydrolyse the acyl groups, allowing esterification of the acid to take place[120] (Figure 1.18).

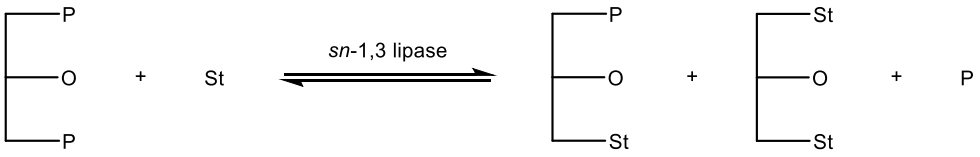

Figure 1.18 Acidolysis reaction scheme between POP TAG and stearic acid (St) ; producing POSt and StOSt TAGs, with palmitic acid (P) as a by-product [112].

One of the difficulties of this technique is the need for water to be present for enzymatic catalysis. To achieve desirable conversion of substrate to product, esterification must dominate over hydrolysis, yet failure to control this can result in an excess of undesirable side products such as FFAs and DAGs[116]. The latter are unavoidable, thermodynamically unstable intermediates

produced during the reaction that have the potential to elicit inter- and intramolecular acyl migration, leading to undesirable TAGs being formed[121, 122]. Equilibration of the immobilised enzyme to a low water level has shown to be effective for minimising this and achieving high yields, with the optimal amount being particular to the reaction system in use[107, 123].

A variety of oils can be used as the TAG substrate, but the presence of oleic acid at *sn*-2 aids in the creation of a product with a similar profile to CB; thus, *sn*-1,3 lipases can be used to incorporate palmitic and stearic acids to the primary acyl groups. Under these conditions, the choice of substrate molar ratio is of importance to achieve optimal conversion, which forms an integral part of the research in each study. Optimal substrate ratio, where the first figure refers to the TAG component and the latter the FA mixture, has been reported between the ranges of 1:2 to 1:7[107, 121, 123-125]. Systems with unsaturated FAs at the *sn*-1/3 positions of the TAG substrate, such as POO or OOO, require higher ratios of FA substrate to allow maximum incorporation[112]. Using OOO plus palmitic and stearic acids as substrates, Çiftçi et al.[126] found that mole ratios greater than 1:3:3 (OOO:P:St) caused the reaction rate to decrease, which was explained by the excess FAs either acidifying the enzyme through free or ionised carboxyl groups, or reducing its activity by desorption of water from the interface. Conversely, Kadivar et al.[107] found a 1:7 ratio of high oleic sunflower oil (HOSO) to a FA mixture as optimal for maximum yield with low acyl migration. Differences are evident in the experimental parameters (Table 1.3).

Table 1.3 Comparison of optimum conditions for acidolysis reaction using sn-1,3 specific lipases.

Reference	Reaction time (h)	Temperature (ºC)	Enzyme load (%)	Water content (%)
Çiftçi et al.[126]	10	45	20	5
Kadivar et al.[107]	6	65	10	1

This is the most widely reported technique in the production of CBEs due to the use of natural products and minimal solvent interaction. However, the number of potential by-products catalysed through hydrolysis and/or acyl migration are a drawback when the compound of interest is a singular TAG and not a mixture.

1.7.1.3 Transesterification

Transesterification is the reaction between the ester groups of two different TAGs (Figure 1.19), or between TAGs and methyl/ethyl esters where regiospecific lipases are used to interchange the groups[112, 119].

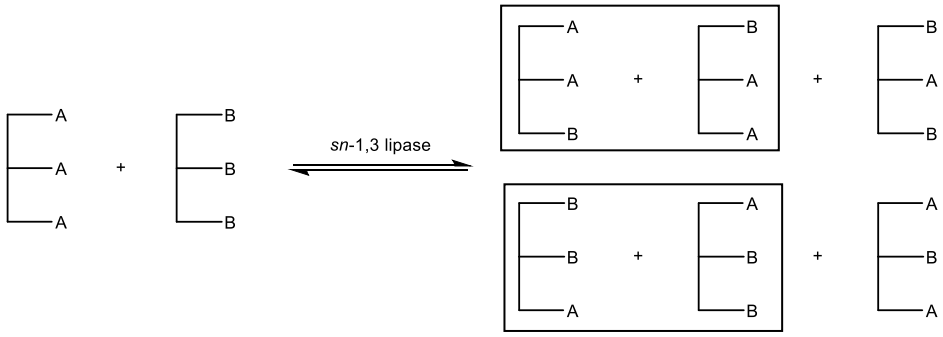

Figure 1.19 Schematic representation of monoacid TAG-TAG transesterification; boxed reaction products display enantiomeric pairs (adapted from literature[112]).

The potential for acyl migration is reduced when using FA methyl/ethyl esters as the reaction can be performed at lower temperatures with minimal water content. Methanol and ethanol are both permissible for use in the processing of food components[127] so their FA esters would be acceptable for ST

formulation. Iwasaki et al.[62] used this method for the synthesis of ECC/CCE enantiopair as discussed in section 1.3.4. Using CCC and ethyleicosapentaenoate (Et-EPA) in a solvent free batch system, control of the reaction to esterify only one of the primary positions was achieved by using the TAG substrate in molar excess at 3:1 (CCC:Et-EPA). Ethyl caprylate (Et-Ca), formed as a by-product, was removed under vacuum to facilitate an equilibrium shift towards the formation of ECC/CCE. The reaction was conducted at 40 ^{o}C for 24 hours, with a reduction in pressure after sixteen to assist the conversion, allowing 71% of the Et-EPA to be consumed. However, only 22.3 mol% of the target TAG was achieved.

The efficiency of a high enzyme/substrate ratio in a continuous PBR was demonstrated by Kim et al.[128], who used an 8.5 molar ratio of HOSO to a 2:3 (mol/mol) mixture of ethyl palmitate (Et-Pa) and ethyl stearate (Et-St) to achieve ca. 49% (w/w) conversion to the target TAGs (POP, POSt and StOSt) in 28.5 minutes. The optimised conditions delivered a high proportion of POSt, comparable to the ratio observed in CB. Though effective, the conditions were not immune to acyl migration with a small portion of regioisomers generated (6.1%, w/w), alongside DAGs and FFAs. A notable amount of Et-Pa and Et-St starting materials remained after the reaction, together with ethyl oleate (Et-O) that was formed as a by-product; all of which would have to be removed for the product to be of use as a CBE. Akin to acidolysis, side products are unavoidable, but the reduced acyl migration is a distinct advantage to this technique for improved regiospecific control.

1.7.2 Chemoenzymatic synthesis

Chemoenzymatic synthesis allows complete regioselective control of the ST and can range from a simple two-step process to produce ABA type TAGs, to a four to six-step procedure for enantiomeric compounds of the AAB or ABC type. An example of the former was efficiently demonstrated by Halldorsson, Magnusson and Haraldsson[129] who used an immobilised *sn*-1,3 lipase in the first step to esterify vinyl esters of medium chain FAs (MCFAs) to the primary positions of a glycerol skeleton. In contrast to the previously discussed

methods for TAG synthesis where acids or methyl/ethyl esters are used, vinyl esters offer an irreversible reaction through rapid tautomerization of the vinyl alcohol by-product to its aldehyde, and thus shifting the equilibrium towards the desired product[130]. As a further control parameter, the reaction was performed in an anhydrous environment using low temperatures to ensure acyl migration opportunities were eradicated. This proved to be highly efficient with yields of 90 – 92% 1,3-DAG after recrystallisation. In the second stage, polyunsaturated FAs (PUFAs) were introduced to *sn*-2 through a coupling reaction, using 1-(3-dimethylaminopropyl)-3-ethylcarbodiimide hydrochloride (EDAC) as the coupling agent and 4-dimethylaminopyridine (DMAP) as a base and catalyst; achieving yields of 90 – 95%. Both compounds used for the coupling are polar, therefore easily separated from the non-polar final product. Often this is achieved through column chromatography where EDAC and DMAP will bind to the polar silica gel, allowing the reaction product to elute in a non-polar solvent. The method is easily transferable to FAs of varying chain lengths and saturation and has shown success with long-chain FAs in an alternative approach to the synthesis of OPO[131]. The final product achieved higher purity and yield compared to alcoholysis and esterification of the same compound[119].

Synthesis of enantiopure ABC-type TAGs cannot be achieved without protection-deprotection of the glycerol[129]; allowing the systematic introduction of FAs to optically active starting materials without acyl migration occurring[117, 129]. Several steps are required, which introduces the potential for multiple complications; nonetheless, high yields are reported in literature[129, 132, 133]. An example reaction scheme is presented in Figure 1.20.

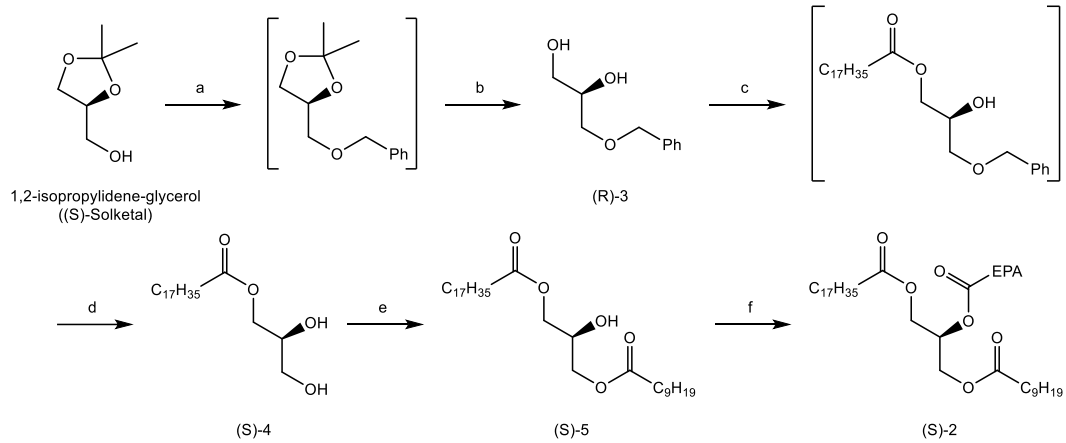

Figure 1.20 Reaction scheme presented in literature for the synthesis of enantiopure ABC type TAG[(133)]. Reagents and conditions: (a) NaH, THF, then BnBr; (b) 1 M HCl, H_2O-EtOH, reflux 30 min, 87% (2 steps); (c) vinyl stearate, CAL, CH_2Cl_2, r.t.; (d) H_2, 10% Pd/C, THF-hexane, 85% (2 steps); (e) vinyl capriate, CAL, THF, r.t., 85%; (f) EPA, EDAC, DMAP, CH_2Cl_2, r.t., 91%.

Synthesis using 1,2- or 2,3-isopropylidene glycerol has been widely reported in literature, however, enantiomerically pure (*R*) and (*S*) starting materials with benzyl protective groups, represented as (*R*)-3 in Figure 1.20, are commercially available, thus circumventing at least two steps of the process. Starting with 3-O- or 1-O-benzyl-*sn*-glycerol reduces the error potential, such as isomerisation during deprotection of the isopropylidene glycerol[(62)].

The chemical processing necessary for this approach to TAG synthesis is a drawback and would not be useful for food applications. However, for the preparation of enantiopure TAGs as analytical standards, the process is essential as they are not readily accessible through manufacturers.

1.8 Lipid behaviour in the gastrointestinal tract

Lipid digestion is a complex biomechanical process that begins in the mouth and continues throughout the gastrointestinal tract (GIT) to the small intestine, where up to 90% of the breakdown occurs[134]. It relies on the adsorption of lipolytic enzymes to the interfacial layer between the lipid droplet and aqueous intestinal fluid[135]. Many dietary lipids are emulsified within a food matrix on consumption, but those that are not must be emulsified within the GIT to aid the interfacial breakdown of the TAG. Mastication is able to elicit a crude lipid mixture and antral contract waves (ACW) in the stomach create elongational flow that breaks the lipid into smaller particles, thus creating a greater surface area[135]. However, it is not until they reach the small intestine that a stabilising factor is introduced in the form of bile salts (BS); predominantly cholic acid, deoxycholic acid and chenodeoxycholic acid[136]. These are planar biosurfactants synthesised from cholesterol in the liver that are released from the gall bladder on hormonal stimulation to the presence of food. They exist in a steroidal structure with opposing hydrophobic and hydrophilic faces and are conjugated with taurine or glycine, thus increasing their water solubility and amphiphilic nature[136, 137] (Figure 1.21).

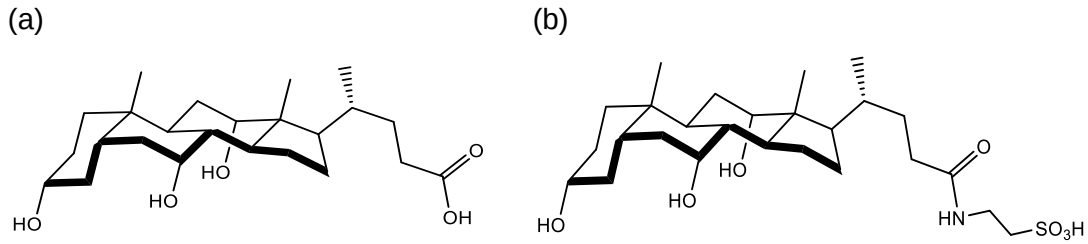

Figure 1.21 Chemical structure of (a) cholic acid and (b) taurocholic acid; displaying the concave/convex perspectives, relating to the hydrophilic and hydrophobic faces[136].

In the aqueous environment of the small intestine, bile salts self-assemble to form micelles whereby intermolecular hydrogen bonds are formed through hydroxyl and acidic group interaction[138]. Under physiological conditions they are present above their critical micelle concentration (CMC), which allows them to saturate the oil/water interface reducing interfacial tension, thus aiding in emulsification and stabilising the droplets against aggregation[137, 139]. *In vitro* analysis has shown excess BS facilitates lipid digestion through the

micellization of hindering lipolytic by-products[134]. However, their structure does not allow them to pack closely, resulting in larger droplets above the CMC than what would be observed for a typical surfactant[136].

Following BS stabilisation, the encased TAGs must undergo lipolysis to allow the FAs to be absorbed. This is an interfacial reaction facilitated by *sn*-1,3 specific pancreatic lipase; however, the high surface activity of BS has been shown to prevent the enzyme from adsorbing through electrostatic repulsion[139, 140]. To overcome this, pancreatic lipase forms a complex with co-lipase, an amphiphilic protein co-factor of a tertiary structure: lipase binds to the hydrophilic face, where the hydrophobic surface successively binds to the BS/droplet interface. The central parameter controlling this event is the available surface area, which is relative to the size of the emulsion droplets[141]. As discussed, this could be due to the initial formulation or the induced conformation following biophysical processing.

1.8.1 Physical state of lipids during digestion

The m.p. of a fat is noteworthy in relation to its ability to be emulsified; those with crystalline components at body temperature are resistant to micellization, which is required for the co-lipase/lipase complex to bind[142]. Bonnaire et al.[143] demonstrated this when comparing two emulsions prepared from tripalmitin using an anionic surfactant; one containing liquid lipid particles and another with solid lipid particles that exhibited a m.p. of ca. 61 ^{o}C. The latter displayed minimal change in electrical charge (ζ-potential) on addition of bile, indicating that it was unable to efficiently displace the surfactant and bind to the interface. As a result, analysis using an *in vitro* digestion model saw the solid lipid particles achieve ca. 35% total FFA release, compared to ca. 55% for the liquid lipid particles. In a similar study, Golding et al.[141] found differences in the GIT performance of emulsions prepared with liquid oil and that which contained 25% SFC content at 37 ^{o}C. In the acidic environment of the stomach, both displayed significant coalescence, but the 25% SFC aggregated to create visible masses. This was attributed to the crystalline material creating a bridged network between the droplets, preventing them

from relaxing into their spherical shapes. *In vitro* lipolysis showed a significantly lower rate of FFA release for the solid containing droplets compared to the liquid; correlating with *in vivo* absorption data that showed fewer TAGs were present in the blood samples. Both results indicating the 25% SFC containing emulsion was not digested as quickly or as efficiently as the liquid droplets.

CB is molten at ca. 36 ^{o}C but, depending on the variety, contains ca. 1% SFC at body temperature, which relates to the high-melting component TAGs (Table 1.4).

Table 1.4 Selection of TAGs present in Ivory Coast CB, their relative percentages and associated melting points.

TAG*	**CB[26] (%)**	**Melting point[142]** ** **(°C)**
POP	18.3	35.2
POSt	41.7	37.5 – 38
StOSt	25.2	41.6
PPP	0.4	66.4
PPSt	0.7	62.7
PStSt	0.3	65.2
POO	2.4	18.2
StStSt	0.2	73.1
StOO	2.9	24.0
StLSt + OOO	1.4	OOO = 5.5

** see Table 1.1 for complete TAG composition; ** note the information for TAG melting point is taken from one study and slight differences may be observed according to the method used for determination.*

Although the SFC is minimal, it is possible that the 26.8% of the TAG composition with a m.p. greater than human body temperature, may hold microcrystalline structures that form bridge networks, thus hindering

emulsification. Consequently, this would affect the extent of lipolysis, which is known to be relative to the droplet size[140].

1.9 Justification and aims of this thesis

The TAG composition of CB has been studied for many years, yet there are only three studies that have investigated its chirality[34, 53, 100]. The XRD and stereospecific analysis investigations appear to show conclusively that *rac*-POSt is present in CB, though the patent work on crystallisation suggests otherwise (see section 1.6). Enzyme systems responsible for the synthesis of natural compounds are chiral in themselves[144], so the presence of a racemic mixture in lipids, as also alluded to for PLO/OLP, is intriguing as it is expected this would require contrasting enzymes. Evidence of homochirality in natural systems is seen in proteins and carbohydrates, where the former are only present as L-amino acids and the latter formulated from D-saccharides[145]. Of the studies that defined CB POSt as racemic, only one clarified the geographical source of the lipid, with no study defining the species; therefore if the apparent natural occurrence of racemate is accurate, it could be questioned whether it is relative to specific growing conditions or if it transpires throughout all genus. As the ratio of component TAGs differs between growing regions, it may also be possible to observe a difference in enantiomeric composition. As no further studies on CB enantiomers have been identified, a gap is highlighted for research to be conducted using modern instrumentation that can elucidate the composition without prior derivatisation. Furthermore, quantification may provide additional insight into CB crystallisation. The studies that have found differences in polymorphic behaviour for enantiopure and *rac*-TAGs are scarce[81, 87], yet offer an interesting concept to explore. The affinity of enantiopairs to couple in a unit cell in the most stable polymorph may be a notable parameter to exploit for enhancing the crystallisation and functionality of CB. It could be postulated that this attraction would allow the production of non-tempered, ‘self-healing’ chocolate: just as the strands of a DNA helix are destined to connect to one another, so are the enantiomeric TAG pairs. As the enantiopairs are separated under force, such as melting, they are attracted to each other as before, thereby developing their most stable

structure; that being the β polymorph for POSt, which is the desirable form for chocolate production. However, it has been observed that enantiomeric excess (ee) can increase the m.p. when compared to racemate[87] and thus, the notion was borne that there may be an optimum ratio to enhance the crystallisation behaviour of a mixed TAG system such as CB. Quantifying this may establish reformulation parameters that can be used in a commercial environment to improve functionality without increasing saturation.

With regards to CB digestibility, *in vivo* studies have determined it as being comparable to corn oil, which is classified as a well digested lipid[146]. However, this was based on data of faecal FAs and the process undertaken within the intestines is unknown in relation to its crystalline structures. Iwahashi and Kasahara[147] cite Larsson, who found that TAGs maintain a pseudo-lamellar structure in the melt that remained at 20 – 40 ^{o}C above the m.p., promoting the idea of the melt memory effect in relation to crystallisation. This raised the notion that perhaps these structures endured throughout the GIT and impact on the ability of the lipid to be efficiently emulsified: as discussed, liquid crystalline structures can affect droplets' behaviour. Moreover, understanding the lipids' behaviour is a prominent consideration for any reformulation, such as enantiomeric modification, where the new product must have a comparable digestion profile to the natural form.

1.9.1 Aims

- Identify the optimum ratio of TAG enantiomers that will promote superior crystallisation properties and thermal stability to CB.
- Understand if high-melting TAGs influence the emulsification ability of CB and if enantiomeric modification changes the lipids' behaviour during digestion.

1.9.2 Objectives

- Characterise and isolate the enantio-TAG species from CB using multidimensional HPLC procedures in order to quantify enantiomeric excess (ee) or racemate.
- Evaluate the polymorphic behaviour of CB following manipulation of its native enantio-TAG composition through the addition of enantiopure materials.
- Determine if high-melting TAGs retain microcrystalline structures at body temperature that affects bile emulsification.
- Evaluate the digestibility of enantiomerically modified CB using *in vitro* analysis techniques.

Chapter 2 Materials and methods

2.1 Materials

2.1.1 General

2.1.1.1 Autosampler vials and closures

Amber glass crimp top borosilicate glass vial (2 mL) and aluminium crimp cap (11 mm) with red rubber septum were from Fisher Scientific (Loughborough, England). Clear snap vials (2 mL) and polyethylene caps with PTFE septum were purchased from Thermo Fisher Scientific (Cheshire, England). Both variants were used for samples analysed under HPLC conditions.

2.1.1.2 Syringe filter

Chromacol PTFE syringe filters of 0.2 or 0.45 µm pore size (17 mm) (Fisher Scientific, Loughborough, England) were used prior to HPLC analysis; samples were passed through via 1 - 2 mL polypropylene syringes into an autosampler vial.

2.1.1.3 Filter paper

Whatman® Grade 1 circle filter paper, 110 and 150 mm diameter, was used to separate the palladium catalyst from reaction mixture in the synthesis of enantiopure TAGs (2.2.11).

2.1.1.4 Centrifuge tubes

Conical polypropylene centrifuge tubes in volume sizes of 15 and 50 mL (Fisher Scientific, Loughborough, England) and clear polypropylene microcentrifuge tubes with hinged lid in 1.5 and 2 mL volume (Star Lab, Milton Keynes, England) were used for sample preparation and storage of solutions.

2.1.1.5 Solvents

The following range of solvents were used in experiments across the project: HPLC grade dichloromethane (DCM), acetonitrile (ACN), isopropanol (IPA); anhydrous toluene, deuterated chloroform ($CDCl_3$) and dimethyl sulfoxide (DMSO) were purchased from Sigma-Aldrich Company Ltd. (Dorset, England). Hexane, methanol (MeOH) and ethanol (EtOH) were acquired from Fisher Scientific (Loughborough, England).

A Millipore purification system (Milli-Q®) was used for ultrapure water with a resistivity of 18.2 MΩ.cm at 25 ^{o}C.

Anhydrous tetrahydrofuran (THF) and DCM were acquired from the solvent purification system based in the School of Chemistry, University of Leeds; a dispensing unit that produces ultra-dry solvents by flowing them through a number of moisture removing filtration columns to reduce levels down to ppm[148].

2.1.2 Lipids and associated standards

CB samples of African origin and cocoa butter alternatives (CBAs) were provided by Nestlé Product Technology Centre Confectionery (York, England). TAG standards acquired for reference: 1,3-dipalmitoyl-2-oleoylglycerol (POP; 833.40 g mol^{-1}) was obtained from Sigma-Aldrich Company Ltd. (Dorset, England); 1,3-distearoyl-2-oleoylglycerol (StOSt; 889.50 g mol^{-1}) and 1-palmitoyl-2-oleoyl-3-stearoyl-*rac*-glycerol (*rac*-POSt; 861.40 g mol^{-1}) were purchased from Larodan (Solna, Sweden).

2.1.3 Fluorophores for confocal laser scanning microscopy

Nile Red Bioreagent ≥98% (318.37 g mol^{-1}), Fluorescein 5(6)-isothiocyanate Bioreagent ≥90% (FITC; 389.38 g mol^{-1}), and Rhodamine B (479.01 g mol^{-1}) were purchased from Sigma-Aldrich Company Ltd. (Dorset, England).

2.1.4 Products used for enzymatic transesterification

Medium-chain triacylglycerol (MCT) oil (504.22 g mol^{-1}) was acquired from AAK (Aarhus, Denmark). Glyceryl trioleate ~65% (885.43 g mol^{-1}), ethyl palmitate ≥99% (Et-Pa; 284.48 g mol^{-1}) and ethyl stearate (Et-St; 312.53 g mol^{-1}) for synthesis was purchased from Sigma-Aldrich Company Ltd. (Dorset, England). Lipozyme® 435 lipase (Candida Antarctica lipase B (CAL B); 10,000 PLU/g) was from Novozymes (Bagsvaerd, Denmark).

2.1.5 Chemicals for the derivatisation of racemic TAG

(*R*)-(−)-α-Methoxy-α-(trifluoromethyl)phenylacetyl chloride ≥99.0% ((*R*)-(−)-MTPA-Cl), Mosher's acid chloride; 252.62 g mol^{-1}), porcine pancreatic lipase type II (100 – 500 units/mg protein (using olive oil (30 min incubation)), 30 – 90 units/mg protein (using triacetin)) and bovine bile (dried, unfractionated; 500 g $mol^{-1(149)}$) were purchased from Sigma-Aldrich Company Ltd. (Dorset, England). Anhydrous calcium chloride ($CaCl_2$; 110.98 g mol^{-1}), Tris(hydroxymethyl)aminomethane, 99% (Tris; 121.14 g mol^{-1}) and Tris buffer solution (1 M; pH 7.9 – 8.1 at 25 ^{o}C) were acquired from VWR International Ltd (Lutterworth, England).

2.1.6 Compounds for enantiopure TAG synthesis

(*R*)-(+)-3-Benzyloxy-1,2-propanediol 99% ((*R*)-(+); 182.22 g mol^{-1}), vinyl stearate ≥95% (310.51 g mol^{-1}), oleic acid ≥99% (reagent grade; 282.46 g mol^{-1}), *N*-(3-Dimethylaminopropyl)-*N′*-ethylcarbodiimide hydrochloride (EDAC; 191.70 g mol^{-1}) and 4-dimethylaminopyridine (DMAP; 122.17 g mol^{-1}) were purchased from Sigma-Aldrich (Dorset, England). Vinyl palmitate >96% (282.47 g mol^{-1}) was purchased from Tokyo Chemical Industry UK Ltd. (Oxford, England). CAL B as described in 2.1.4.

Various forms of Palladium on carbon (Pd/C) were used for catalytic hydrogenation: 10 wt.% loading (powder); 5 and 10 wt.% loading (wet; ~50% water) were purchased from Sigma-Aldrich Company Ltd. (Dorset, England).

2.1.7 Chemicals for simulated intestinal fluid preparation

Potassium dihydrogen phosphate (KH_2PO_4; 136.09 g mol^{-1}), sodium chloride (NaCl; 58.44 g mol^{-1}), calcium chloride dihydrate ($CaCl_2.2H_2O$; 147.01 g mol^{-1}) and bis(2-hydroxyethyl)amino-tris(hydroxymethyl)methane BioUltra ≥99.0% (Bis-Tris; 209.24 g mol^{-1}), dipotassium phosphate (K_2HPO_4; 174.18 g mol^{-1}) were purchased from Sigma-Aldrich Company Ltd. (Dorset, England). Potassium chloride (KCl; 74.55 g mol^{-1}) and magnesium chloride hexahydrate ($MgCl_2(H_2O)_6$; 203.30 g mol^{-1}) was acquired from Merck Millipore (Darmstadt, Germany).

Porcine bile extract and porcine pancreatin (8x USP) was purchased from Sigma-Aldrich Company Ltd. (Dorset, England); bovine bile as described in 2.1.5.

Sodium hydroxide (1 M NaOH; 40.00 g mol^{-1}) was purchased from VWR International Ltd. (Leicestershire, England): the solution was used neat for pH adjustment and diluted to 0.1 M using Milli-Q® water for use as the titrant in pH stat analysis.

2.2 Methods

2.2.1 Protocol for RP-HPLC analysis

A method developed by Kadivar et al.[121] forms the foundation of procedures, with modifications where necessary, such as change of flow rate. TAG analysis was conducted on a Shimadzu Prominence HPLC system (Kyoto, Japan); composed of a DGU-20A5 degasser, two LC-20AD XR solvent delivery systems, an SIL-20AC auto-sampler, a CTO-20AC column oven, an FRC-10A fraction collector and an ELSD-LT II detector. A Supelco Ascentis(R) C18 (150 mm x 2.1 mm, 3 µm) column purchased from Sigma-Aldrich Co. Ltd. (Dorset, England) was used. Data acquisition was via Shimadzu LC solutions software.

Lipid samples were melted at 50 ^{o}C and then dissolved in a concentration of 0.01 – 5 mg mL^{-1} in DCM/ACN (30:70, v/v) in a 50 mL centrifuge tube and homogenised using a vortex mixer. An aliquot of the solution (2 mL) was transferred into a 2 mL crimp top borosilicate glass vial using a 2 mL polypropylene syringe via either a 0.2 or 0.45 µm syringe filter and sealed using an aluminium cap with red rubber septum. Sample vials were held in the auto sampler at 40 ^{o}C. The mobile phase was delivered at variable flow rates depending on the analysis; a flow rate of 1 mL min^{-1} was required during TAG isolation using the fraction collector whereas 0.35 – 0.5 mL min^{-1} was enough for general analysis of compounds. A varied injection volume was used; 20 µL for TAG identification and 40 µL for TAG isolation to accommodate the split in flow from the ELSD to the fraction collector. The column temperature was held at 20 ^{o}C and the ELSD conditions were as follows: signal, 0.00; gain, 1; pressure of 335 KPa and drift tube temperature of 38 ^{o}C. The carrier gas used was air. The mobile phase was delivered as a linear gradient over a period of 33 min where A = DCM, B = ACN. The gradient conditions were as follows: initial conditions began with 30% A and 70% B, concentration of B was reduced to 49% at 25 min, 30% B at 26 min, maintain 30% B at 27 min then returning to 70% B at 28 min and held for 5 min.

2.2.1.1 Method validation

TAG standards (POP, POSt and StOSt) were used to produce eight-point calibration curves with known concentration plotted against peak area. Concentrations ranging from 0.01 – 1 mg mL^{-1} were injected into the instrument (20 µL) and analysis performed under conditions described in 2.2.1. Retention times were used to identify the associated peaks in all lipid samples.

The limit of detection (LOD) and limit of quantification (LOQ) were calculated from the regression line equation of the calibration curves[121]. The LOD and LOQ formulas are as follows:

$$LOD = 3.3D/S \quad (1)$$

$$LOQ = 10D/S \quad (2)$$

where *D* is the standard error of the intercept of the regression line and *S* is the slope of the calibration curve.

2.2.2 Isolation of TAG fractions

The HPLC system and methods defined in 2.2.1 were used for isolating the POSt TAG fraction of CB for further analysis to ascertain its enantiomeric composition: the FRC-10A fraction collector being the integral instrument for the separations.

A T-fitting (Figure 2.1) was attached to the flow line connecting a Supelco Ascentis(R) C18 (150 mm x 2.1 mm, 3 µm) column to the ELSD in order to split the flow between the detector and the FRC.

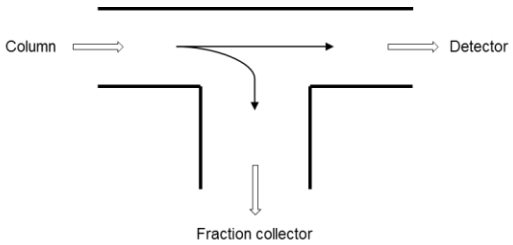

Figure 2.1 Schematic representation of a T-fitting and the direction of mobile phase flow due to its splitting action from the column flow line.

A CB sample in the concentration of 5 mg mL^{-1} was analysed to identify the t_r of POSt and the systems' software programmed to begin isolation at the relevant time point by opening the FRC valve; closing the valve stopped collection. Using Shimadzu LC Solutions software, the FRC was programmed with the following conditions: width 20 s; slope 100 uV/s; level 10000; vial volume 2 mL; response 0.5 s.

Glass test tubes (3.5 – 4.5 mL) were placed in the FRC trays for collection of the isolated TAGs/mobile phase. Solvent was removed under nitrogen using a Techne sample concentrator with the Dri-Block heater (DB 100/3) set at 70 ^{o}C for ca. 30 min. The remaining sample was dissolved in 2 mL of DCM/ACN (30:70, v/v) and analysed under the same HPLC conditions as previously described in 2.2.1

2.2.3 Chiral column screening conditions

To determine the most suitable column(s) for TAG enantiomer separation, a chiral screening service provided by Phenomenex was undertaken in-house, using the instrument as described in 2.2.1.

Several columns/stationary phases were analysed for suitability in both normal-phase (NP) and reverse-phase (RP) modes over two visits (Table 2.1).

Table 2.1 Phenomenex chiral columns used and their stationary phases; all varieties used in the column screening service at the University of Leeds.

Column	Stationary phase
Lux i-Cellulose-5	Cellulose tris (3, 5-dichlorophenylcarbamate)
Lux Amylose-1	Amylose tris (3, 5-dimethylphenylcarbamate)
Lux Amylose-2	Amylose tris (5-chloro-2-methylphenylcarbamate)
Lux Cellulose-1	Cellulose tris (3, 5-dimethylphenylcarbamate)
Lux Cellulose-2	Cellulose tris (3-chloro-4-methylphenylcarbamate)
Lux Cellulose-3	Cellulose tris (4-methylbenzoate)
Lux Cellulose-4	Cellulose tris (4-chloro-3-methylphenylcarbamate)

The *rac*-POSt standard was dissolved in a concentration of 2 mg mL^{-1} in a 50 mL centrifuge tube and homogenised using a vortex mixer; solvents being 100% hexane for NP, MeOH/IPA (63:37, v/v) for RP. Vial preparation, column oven and ELSD conditions as in 2.2.1. The sample vial was held in the auto-sampler at ambient temperature and the injection volume was 20 µL. The

mobile phase was delivered at a flow rate of 1 mL min^{-1}, with its composition being dependent on the column in use; discussed in 3.1.2.

2.2.4 Atmospheric pressure chemical ionisation-mass spectrometry

Reproduction of the Lísa and Holčapek[65] method was trialled at the University of Bradford Analytical Centre using atmospheric pressure chemical ionisation-mass spectrometry (APCI-MS); a Waters 2695 separations module coupled to a Quattro Ultima Triple Quadrupole Mass Spectrometer. Two chiral columns (Chiralcel® OD; 250 mm x 4.6 mm, 10 µm) were used for analysis alongside a Chiralpak® AD (250 mm x 4.6 mm, 10 µm) column. The *rac*-POSt standard was dissolved in a concentration of 2 mg mL^{-1} in hexane, in a 50 mL centrifuge tube and homogenised using a vortex mixer: the sample vial was prepared under the conditions described in 2.2.1. The vial was held in the auto-sampler at ambient temperature and the injection volume was 20 µL. The column oven was held at 35 ^{o}C and the mobile phase delivered at 1 mL min^{-1}, both isocratically and as a gradient, containing hexane/IPA in various concentrations see results section (3.1.3) for associated conditions and relative amounts. The variation being due to trials of alternative methods but in brief, the mobile phase gradient as in literature[65] was as follows: initial conditions began with 90% A and 10% B followed by an increase in concentration of B to 40% over 180 min; where A is hexane and B is hexane/IPA (99:1, v/v). Three runs were performed under these conditions with 30 min column equilibration time between each.

2.2.5 External column screening

Samples of the *rac*-POSt standard were sent to Phenologix (California, USA) and Daicel (Ilkirch, France) for column screening at their in-house laboratories. It was requested that both companies trial the chiral TAG method reported in literature[65] as this is the preferred technique. A full evaluation of their column range was also undertaken for suitability assessment; these are discussed in 3.1.2.

2.2.6 Analytical method development: transesterification substrates

Preliminary samples were dissolved in MeOH in 1.5 mL microcentrifuge tubes and homogenised using a vortex mixer. Three dilutions of MCT oil were tested to ascertain which would provide an adequate signal in the detector; 1:10, 1:100 and 1:1000 (MCT:MeOH). An aliquot of each solution (500 µL) was transferred into 2 mL snap cap vials using a 1 mL polypropylene syringe via a 0.2 µm syringe filter.

Stage one

Analysis was conducted on an Agilent 1100 series HPLC (Santa Clara, USA); composed of a G1322A degasser, G1312A binary pump solvent delivery system, G1313A auto-sampler, G1316A COLCOLM column compartment and a G1315A diode array detector (DAD). The column was a Waters Symmetry C18 (4.6 mm X 250 mm, 5 µm); the mobile phase was delivered at a flow rate of 1 mL min^{-1} and the injection volume was 5 µL. The column compartment was held at 25 ^{o}C and the DAD set to 205 nm. The mobile phase was delivered as a linear gradient over a period of 30 min where A = MeOH, B = IPA:hexane (5:4, v/v). The gradient conditions were as follows: initial conditions began with 100% A and 0% B, concentration of B was increased to 50% at 25 min, maintain 50% B at 26 min then returning to 0% B at 30 min. The 1:10 dilution was analysed under these conditions.

Stage two

Analysis time was reduced to 15 min and each of the dilutions were examined during this stage. Delivery of the mobile phase was relative to the change in run time, with the gradient as follows: initial conditions began with 100% A and 0% B, concentration of B was increased to 25% at 12.5 min, maintain 25% B at 13 min then returning to 0% B at 15 min. All other conditions remained the same.

A 1:10 dilution of Et-Pa in MeOH was prepared under the same conditions as MCT oil and analysed to determine the peak t_r.

Stage three

Et-Pa and MCT oil were combined to ensure each were resolved. Samples were prepared in 1.5 mL microcentrifuge tubes as: 110 µL Et-Pa in 900 µL MeOH and 200 µL MCT in 900 µL MeOH, then 1 mL of each was transferred to a 2 mL microcentrifuge tube and homogenised using a vortex mixer. 1 mL was transferred into a 2 mL snap cap vial using a 1 mL polypropylene syringe via a 0.2 µm syringe filter.

Stage four

The method as described in Stage two was used for analysis of MCT oil (1:10 dilution) with a change in column and HPLC system; the column was a Supelco Ascentis(R) C18 (150 mm x 2.1 mm, 3 µm) (Sigma-Aldrich, Dorset, England) and the system was a Shimadzu Prominence as described in 2.2.1. The Waters symmetry column was also used for comparison. Injection volume was 5 µL and the column compartment was held at 25 ^{o}C. The DAD was set to 205 nm. Conditions for the mobile phase are described in Stage two

2.2.7 Enzymatic transesterification: stirred batch and continuous flow

A stirred batch reaction involves combining the substrates and enzyme into one reaction vessel and stirring under magnetic dispersion until the reaction is deemed complete. Greater complexity arises with the continuous flow method, yet the principle remains the same. Simulating conditions analogous with HPLC, the enzyme is packed into a column, which becomes the stationary phase and the substrates pumped through as the mobile phase. As the substrates interact with the column bed the reaction occurs and the product collected in a vessel from the end of the column exit line, which is recycled through the system until the reaction is complete.

2.2.7.1 Stirred batch experimental protocol

CAL B was packed into an Omnifit® chromatography column (100 mm x 25 mm) to fill ca. two thirds of its capacity and the amount of enzyme used was measured by weight (1.06 g). Approximately half of this amount was used for the stirred batch experiment; 517.9 mg of CAL B (5179 PLU) was added to a 25 mL round bottom flask (RBF). MCT oil (5 mL; 9.39 mmol) and Et-Pa (5 mL; 15.06 mmol) were added along with a small magnetic stirrer. The RBF was sat in a Drysyn block filled with low iron sand to enable even heat distribution and this was placed on a heated stirrer plate set at 30 ^{o}C, stirrer speed 600 rpm. The reaction scheme for transesterification of an MCT oil TAG (tricaprylic) with Et-Pa is displayed in Figure 2.2.

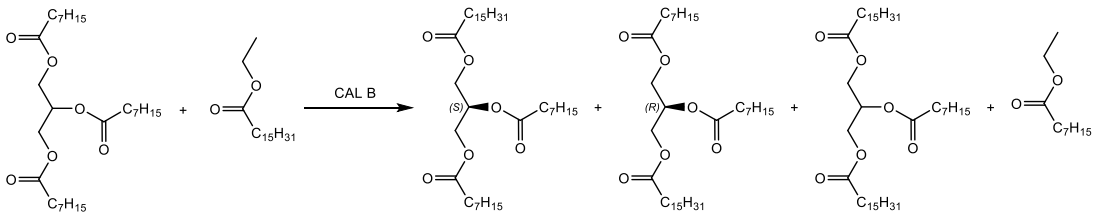

Figure 2.2 Reaction scheme for transesterification of Et-Pa and a tricaprylic TAG of MCT oil. CAL B is an immobilised sn-1/3 lipase with an active site containing a serine residue, featuring a 1º hydroxyl group.

2.2.7.2 Continuous flow experimental protocol

A 250 mm stainless steel HPLC column was packed with ca. 1.44 g CAL B (14,418 PLU) and placed in an aluminium heating block. The column was equilibrated by drawing pure MCT oil from a beaker at 1 mL min^{-1}: once oil was visible in the exit line, the flow was reduced to 0.5 mL min^{-1} and the volume expelled over 2 min observed to confirm accuracy of flow rate. The heating block was set to 50 ^{o}C and allowed to equilibrate: a digital controller maintains the temperature via a thermocouple placed in the heating block and thermal cut-out system. Setting the HPLC pump to 0.5 mL min^{-1} produced a flow rate of 0.25 mL min^{-1}, which was the desired rate. MCT oil (11 mL; 20.66 mmol) plus Et-Pa (11 mL; 33.13 mmol) was added to a 50 mL continuous stirred tank reactor (CSTR) with thermostatic jacket. An in-line filter connected to the outlet and inlet lines of the CSTR was placed in the vessel to hold any solidified product whilst the mother liquors are recirculated. Temperature was regulated via a Haake silicon oil temperature controller for the latter of two reactions; the first was at ambient. The system was primed by drawing 1 mL of MCT/Et-Pa solution through each of two check valves, leaving 20 mL of reactants. The experimental set up is shown in Figure 2.3.

(a) *(b)*

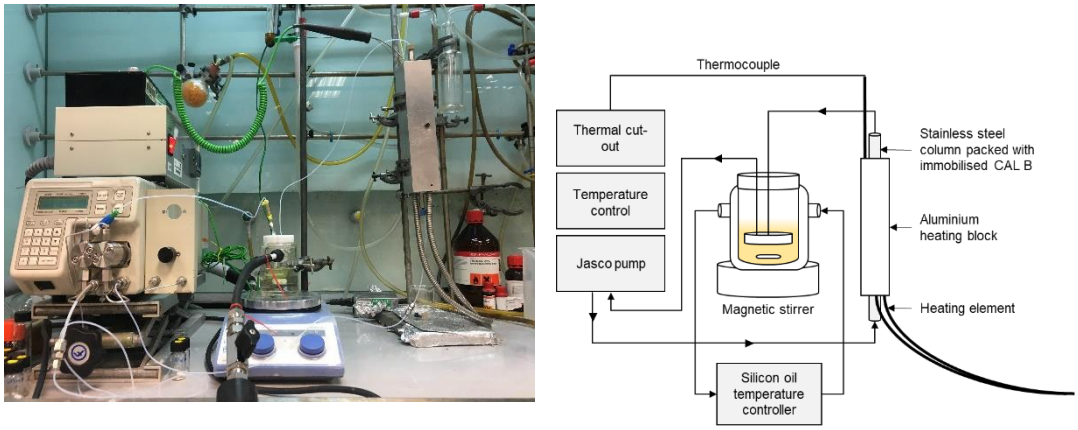

Figure 2.3 Experimental set up for in-flow transesterification; (a) photographic image and (b) schematic. The CSTR sits atop the magnetic stirrer with stirrer bar and in-line filter placed inside. Column temperature was maintained at 50 °C through the heating block for both experiments. Note that the silicon oil temperature controller was not present for the primary; thereby this was performed at ambient. CSTR temperature was maintained at 37 °C for the secondary.

2.2.8 Analytical protocol for transesterification reaction products

The chosen method for analysis for the stirred batch and continuous flow reaction products differed to those trialled during development (2.2.6). Samples were diluted to 1:10 using DCM/ACN (3:7, v/v) as the solvent and peaks identified using the Waters Symmetry column. The HPLC conditions in 2.2.1 were used, inclusive of the described mobile phase and gradient, but with 5 μL sample injection.

2.2.9 Derivatisation of enantiomeric TAG

In a 1 L beaker, 500 mL of Tris buffer (1 M) was prepared by dissolving 60.57 g of Tris in 400 mL of Milli-Q® water; this was brought up to the experiment working temperature (40 ^{o}C) in a shaking water bath and pH measured using a Mettler Toledo (S220) pH meter. The buffer was adjusted to pH 8 by adding 6 M HCl and relevant amount of Milli-Q® to reach the desired volume of 500 mL. A bile salt solution (0.05%, w/v) was prepared by dissolving 10.1 mg of bovine bile in 20.2 mL Milli-Q® water; $CaCl_2$ solution (2.2%, w/v) was prepared by dissolving 44 mg in 2 mL of Milli-Q®. Both solutions were prepared in 15 mL centrifuge tubes and homogenised using a vortex mixer.

The *rac*-POSt standard (9.8 mg; 1.14 x 10^{-2} mmol) was added to a test tube followed by 20 mg pancreatic lipase, 1 mL Tris buffer (prepared or as purchased), 0.25 mL bile solution and 0.1 mL $CaCl_2$: all solutions were equilibrated to 40 ^{o}C prior to use. The reaction mixture was incubated in a shaking water bath at 40 ^{o}C for ca. 3 min at 35 rpm, removed, then 10 mL EtOH and 1 mL of anhydrous toluene added to stop the reaction.

All liquids/solvent were removed under nitrogen using a Techne sample concentrator with the Dri-Block heater (DB 100/3) set at 70 ^{o}C. (*R*)-(−)-MTPA-Cl (4.34 µL; 2.32 x 10^{-2} mmol) was dissolved in 1 mL anhydrous toluene and added to the test tube, then stirred at room temperature for 1 hour on a magnetic stirrer at speed 2.5: the solvent was removed under nitrogen. Anhydrous toluene (3 mL) was added, solution mixed under vortex, and solvent removed under nitrogen to eliminate any remaining moisture in the sample: this was repeated. The products of the first two experiments were diluted with 0.6 mL of $CDCl_3$ and analysis tubes prepared as in 2.2.10. However, insolubility issues arose, which led to multiple solvent trials: these are discussed in 3.1.4**.** The reaction scheme for enantiomeric conversion is presented in Figure 2.4.

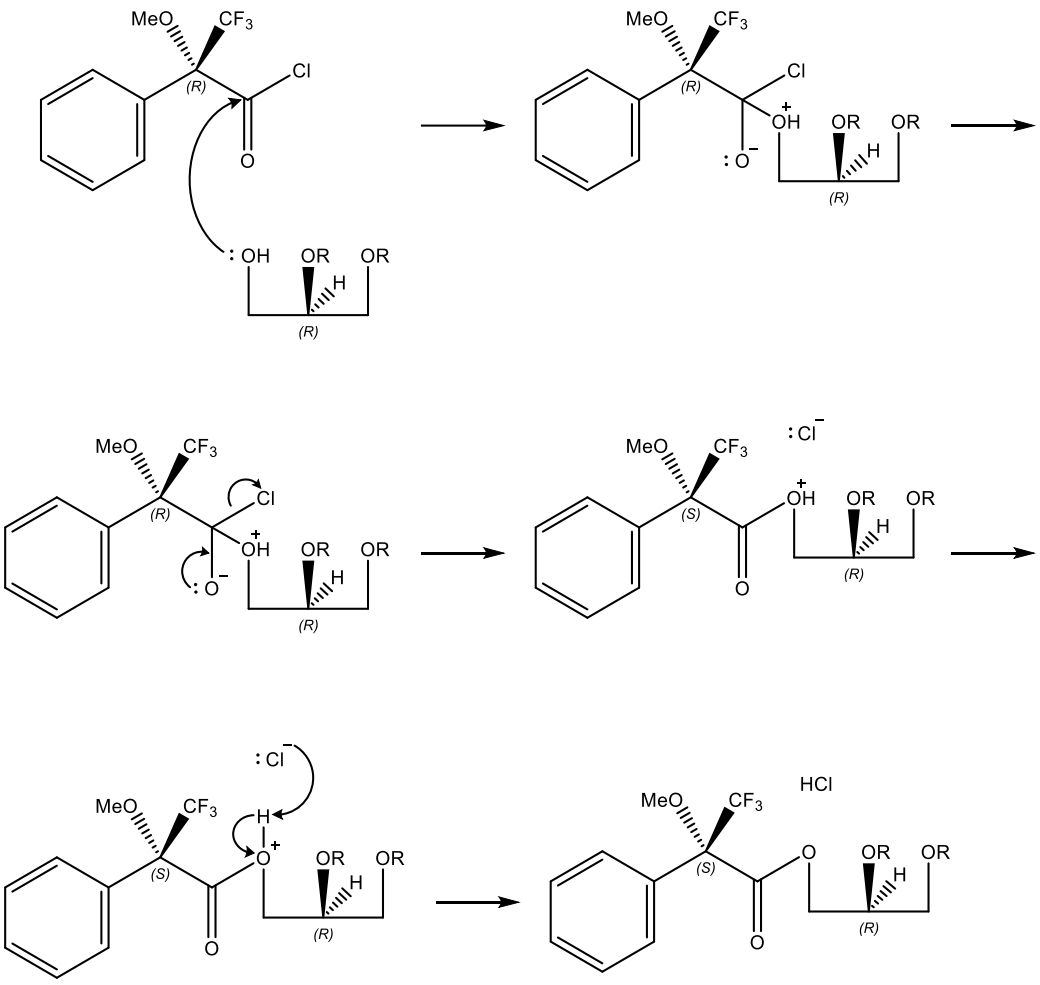

Figure 2.4 Reaction scheme between (R)-(-)-MTPA-Cl and (R)-DAG enantiomer derived from its native TAG through partial hydrolysis. The reaction produces an (SR) type compound, whereby the opposing TAG/DAG enantiomer creates a product of the (SS) type: the (SS) and (SR) compounds can be distinguished.

HPLC analysis of the reaction product was conducted on the instrument described in 2.2.1 and NMR as described in 2.2.10; ^{19}F NMR being the principal technique used here.

2.2.10 NMR sample preparation and data analysis

Liquid samples (60 µL) were transferred to 1.5 mL microcentrifuge tubes via an automated pipette and solid samples were weighed directly into the tubes: $CDCl_3$ (0.6 mL) was added as the solvent and the solution mixed under vortex. Solutions were transferred into Norell XR55 NMR tubes via 150 mm glass pipettes with rubber bulb and sealed with an NMR tube cap. Analysis was conducted on a Bruker ADVANCE III HD-400 MHz spectrometer; producing ^{1}H, ^{13}C, ^{19}F and COSY NMR spectra. All data was processed using TopSpin 4.0.7 software.

2.2.11 Synthesis of enantiopure TAG

Modifications to substrate volumes are discussed in Chapter 5. Volumes as specified in literature[132, 133] were used during method development for steps a and b (Figure 2.5) and shall be detailed here. Solutions of (*R*)-(+)-3-benzyloxy-1,2-propanediol (505 mg, 2.77 mmol) and vinyl palmitate (1028 mg, 3.64 mmol) were combined with anhydrous DCM (5 mL) and immobilised CAL B (60 mg); the reaction mixture was stirred for ca. 90 min at room temperature under a stream of nitrogen. CAL B was removed via filtration and the solvent removed in vacuo on a Buchi R-210 rotary evaporator. Removal of the benzyl protective group was performed in a Parr reactor under the conditions described in 2.2.11.1 and/or 2.2.11.2. Purification was achieved by dissolving in dry THF (20 – 100 µL) and a four-fold volume of hexane (80 – 400 µL) added: solvent volumes dependent on sample size. Into a 10 mL RBF, 1-palmitoyl-sn-glycerol (115.5 mg, 0.35 mmol) and vinyl stearate (168 mg, 0.32 mmol) were added, dissolved in anhydrous THF (2 mL) and CAL B (45 mg) added. The mixture was stirred at room temperature for ca. 3 hours under a stream of nitrogen. Lipase was removed via filtration and solvent in vacuo using a rotary evaporator. Sample purification was achieved through recrystallisation from MeOH. In a 10 mL RBF, 1-palmitoyl-3-stearoyl-*sn*-glycerol (100 mg, 0.17 mmol) and oleic acid (43 mg, 0.15 mmol) were dissolved in DCM (2 mL); followed by the addition of DMAP (3.34 mg, 30 µmol) and EDAC (29 mg, 0.15 mmol). The resulting solution was stirred at room

temperature on a magnetic stirrer for ca. 17 hours. The reaction was stopped by removing the solvent in vacuo. The extraction of any remaining DMAP and EDAC was achieved through the use of a separatory funnel, using a saturated brine solution and hexane. The hexane layer was drained into a 100 mL RBF, separatory funnel rinsed, and the solvent removed in vacuo.

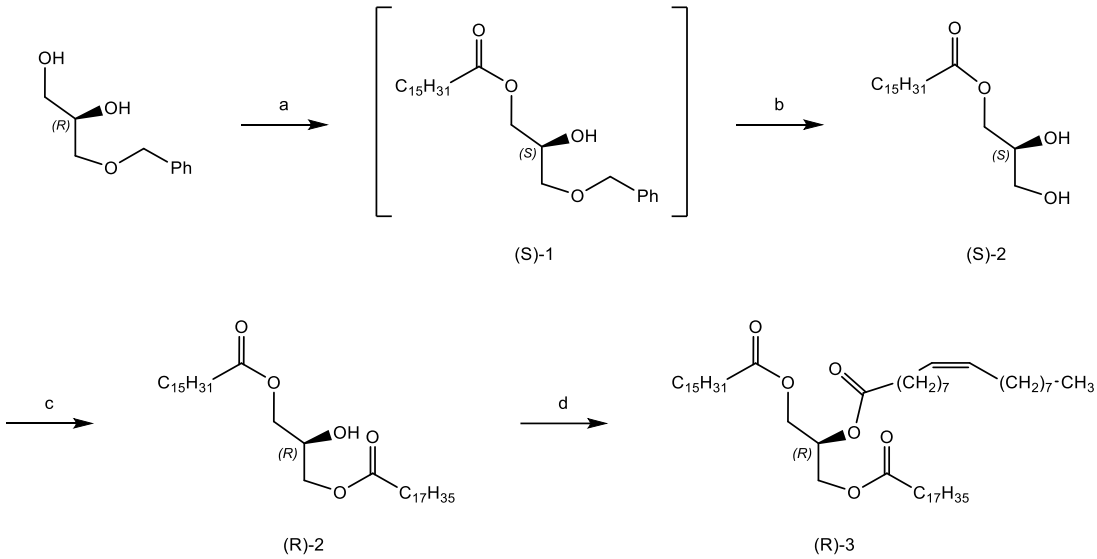

Figure 2.5 Chemoenzymatic synthesis of enantiopure (R)-POSt. Reagents and conditions: (a) vinyl palmitate, CAL B, DCM, r.t.; (b) H_2, Pd/C (5 or 10% loading; wet or dry), THF/hexane or DCM; (c) vinyl stearate, CAL B, THF, r.t.; (d) oleic acid, EDAC, DMAP, DCM, r.t.

Stages of the reaction were monitored via ^{1}H, ^{13}C and COSY NMR as described in 2.2.10., and infrared (IR) spectroscopy.

2.2.11.1 Parr reactor protocol

Catalytic hydrogenolysis was performed in a Parr Stirred Reactor (Illinois, USA) equipped with pressure gauge, liquid sampling valve, gas inlet valve, gas release valve, thermocouple, internal stirring system consisting of a motor drive magnetically coupled to an internal stirrer shaft with attached turbine-type impeller and Thermowell heating mantle[150].

In a 250 mL RBF, the product of the first acylation step (Figure 2.5, (*S*)-1) was dissolved in 30 mL dry THF and 170 mL hexane added. Pd/C catalyst (30 – 60 mg; 5% wet) was added to a 600 mL stainless-steel high-pressure reactor

vessel and the reaction mixture introduced. The vessel was connected and secured to the system using a split-ring closure with 8 compression bolts and the heating mantle positioned. Air was removed from the reactor by purging five times with nitrogen, followed by five times with hydrogen. Hydrogen was charged into the reactor vessel to a pressure of 5 bar and the stirrer speed increased incrementally from 200 – 1000 rpm, at which point the reaction was deemed to have begun. Repeats of the experiment used 10% powder and 10% wet Pd/C, discussed further in section 5.1.4.

Reaction times ranged from 2 – 20 hours. On completion, the vessel was depressurised and purged five times with nitrogen before opening to the atmosphere. The catalyst was removed via filtration into a 250 mL conical flask and the vessel rinsed with hexane, which was passed through the filter. The reaction mixture was transferred to a 250 mL RBF and solvent removed using a rotary evaporator. An aliquot of the product was transferred to a 1.5 mL microcentrifuge tube and the sample/NMR tube prepared as in 2.2.10: ^{1}H, ^{13}C and COSY NMR was performed to determine completion of reaction.

2.2.11.2 fReactor protocol

Small-scale hydrogenolysis was performed using a 2 mL fReactor; a CSTR designed at the Institute for Process Research and Development (iPRD) at the University of Leeds. The instrument as described in 2.2.11.1 was used with a 2 mL single batch fReactor (Figure 2.6 (b)), attached via a length of 1/16 PEEK tubing.

Variable amounts of (*S*)-1 (Figure 2.5), discussed in 5.1.4, was dissolved in 0.7 – 1 mL of dry DCM. Pd/C (5.5 – 20 mg, 10% wet) was added to the fReactor, the (*S*)-1/DCM mixture charged by syringe to the module, and a cross-shaped magnetic stirrer bar placed inside. A circular piece of toughened glass cushioned with a Viton O-ring was used to seal the mixture inside, held in place with the top section and secured by way of three screw points. The module was positioned atop a magnetic stirrer and a 250 psi back pressure

regulator (BPR) attached via flangeless ferrules and 1/8 PEEK tubing. Set-up as displayed in Figure 2.6.

(a) (b)

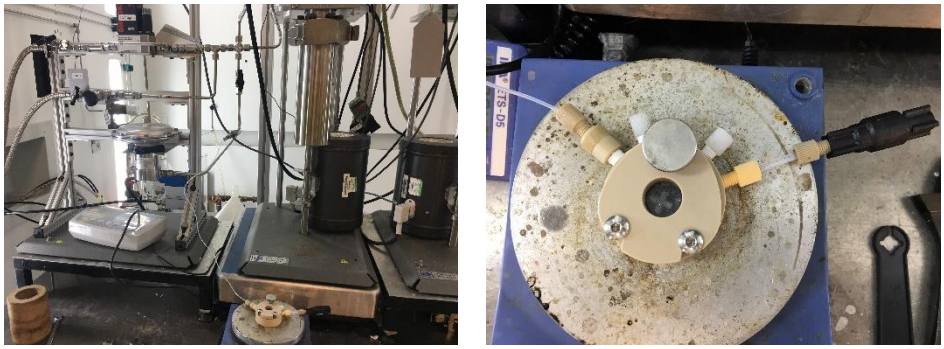

Figure 2.6 Image of (a) fReactor attached to the Parr instrument via PEEK tubing and (b) a close up of the reaction vessel. The four entry ports visible at the top of the fReactor, from left to right, shows the inlet tube from the Parr connected to a one-way check valve receiving H_2, two central blanking nuts and a ferrule connected to a 250 psi BPR.

Air was removed from the fReactor by purging five times with nitrogen, followed by five times with hydrogen. H_2 was charged into the reactor to a pressure of 9 bar, BPR sealed with a blanking nut and the stirrer speed set to 400 rpm: this being the reaction start point. The BPR was fitted as a precautionary measure during pressurisation but sealed once pressure was met to prevent solvent evaporation.

After 1 – 1.5 hours, stirring was stopped and the H_2 valve sealed to halt the reaction. The fReactor was depressurised and purged five times with nitrogen. Removal of the catalyst and solvent was as described in 2.2.11.1 using RBFs of 10 – 25 mL volume in place of the conical flask; analysis conditions using NMR also remained the same.

2.2.12 Melting point determination using DSC

Differential scanning calorimetry (DSC) was predominantly used to understand the polymorphic behaviour and melting point (m.p.) of CB following a temperability procedure, which involves cooling and heating of the sample under precise conditions to encourage formation of the β_v polymorph; determined by its m.p.

Samples of molten CB and CBA (1.3 – 2 mg) were placed into 30 µL aluminium pans and sealed with an aluminium cover. The prepared pan was placed inside a Perkin Elmer Diamond DSC 8000 (Massachusetts, USA) and analysed using a proprietary temperability programme.

2.2.13 Static emulsification protocol

Duodenal, $CaCl_2$ and bile salt solutions were prepared according to a protocol provided by Dr Anwesha Sarkar at the University of Leeds. The duodenal solution was prepared by adding K_2HPO_4 (6.8 g; 39.0 mM L^{-1}), KCl (0.2536 g; 3.4 mM L^{-1}), NaCl (1.1232 g; 19.2 mM L^{-1}) and 190 mL of 0.1 M NaOH solution to a 1 L volumetric flask, mixing under magnetic dispersion until clear, adjust to pH 6.8 with 1 M HCl then made up to volume with Milli-Q® water. Both $CaCl_2$ (0.44 g) and porcine bile salts (2.33 g) were prepared under the same conditions: added to 90 mL of the duodenal solution in a 100 mL volumetric flask, mixed under magnetic dispersion, pH adjusted to pH 6.8 with 0.1 M NaOH then made up to volume with Milli-Q® water.

The solutions for analysis were prepared by adding 10 mL of each to 50 mL volumetric flasks; $CaCl_2$, bile, bile (7.5 mL) plus $CaCl_2$ (2.5 mL) and distilled water. These were placed in a shaking water bath at 37 ^oC and allowed to equilibrate. CB was incubated overnight at 37 ^oC: ca. 10 mg was added to each of the equilibrated solutions, which were returned to the shaking water bath for 1.5 hours at 80 rpm.

2.2.14 pH stat titration for measurement of FFA release

pH stat titration monitors shifts in proton concentration of a sample and the subsequent changes from neutral pH to acidic/basic or vice versa are returned to the desired constant via the addition of acid or alkali solutions[151]. In the case of this project, the degree of FAs released from the glycerol backbone of TAGs are monitored and the consequential decline in sample pH neutralised through titration of a basic solution. This static *in vitro* digestion model was used to evaluate the percentage of free fatty acids released from CB and a CBA first melted at the different temperatures: 37, 50 and 80 °C then intestinal hydrolysis performed at 37 °C.

Figure 2.7 Metrohm pH stat titration system consisting of two dosing units, pH sensor with temperature monitoring and a 60 mL jacketed reaction vessel connected to a heated water bath circulator sat on the stirrer unit.

2.2.14.1 Stock electrolyte solutions for pH stat titrations

Concentrated electrolyte solutions were prepared following the INFOGEST protocol for standardised *in vitro* digestion[152](Table 2.2), with a slight modification to the solution formula; substituting sodium bicarbonate ($NaHCO_3$) with Bis-Tris in equivalent molarity. The rationale is discussed in section 3.2.

Table 2.2 Stock electrolyte solutions for use in simulated intestinal fluid.

Constituent	**Stock conc.**	
	g 250 mL^{-1}	**mol L^{-1}**
KCl	9.32	0.50
KH_2PO_4	17.01	0.50
Bis-Tris	104.62	1.00
NaCl	29.22	2.00
$MgCl_2(H_2O)_6$	7.62	0.15
$CaCl_2.2H_2O$	11.03	0.30

Each of the stock electrolytes were dissolved in 250 mL of Milli-Q® water and mixed under magnetic dispersion. The resulting solutions were distributed between 50 mL centrifuge tubes and stored at -20 ^oC until required. To return the solutions to their liquid state, they were either placed in a refrigerator at 4 ^oC overnight or in a water bath at ca. 40 ^oC if required that day.

2.2.14.2 Simulated intestinal fluid stock preparation

The stock electrolytes (2.2.14.1) were used to produce a 1.25x concentrate simulated intestinal fluid (SIF) solution (Table 2.3).

Table 2.3 Simulated intestinal fluid constituents as recommended in the INFOGEST protocol.

Constituent	**Vol. of stock**	**Conc. in SIF**
	mL	**mM L^{-1}**
KCl	6.8	6.8
KH_2PO_4	0.8	0.8
Bis-Tris	42.5	85
NaCl	9.6	38.4
$MgCl_2(H_2O)_6$	1.1	0.33

The appropriate volume of each stock constituent was transferred to a 500 mL beaker using an automated pipette. The solution was made up to 400 mL with Milli-Q® water and mixed under magnetic dispersion for ca. 10 minutes. The SIF concentrate was distributed, stored and thawed as in 2.2.14.1.

2.2.14.3 Experimental SIF

SIF stock concentrate was diluted to reach accurate electrolyte concentrations according to the INFOGEST protocol; the total volume of SIF stock was equivalent to four parts of the final solution volume.

The volume of bile solution prepared was sufficient for three experiments. A typical preparation adhered to the following: 82.5 mL of SIF stock was added to a 250 mL beaker followed by 0.75 g bovine bile extract and mixed under magnetic dispersion at 37 ^{o}C (400 rpm) for ca. 30 min. Milli-Q® water (14.85 mL) was added and the solution allowed to equilibrate. pH was measured and adjusted to pH 7 using 1 M HCl. Total volume after addition of HCl was calculated and the solution made up to 112.35 mL with Milli-Q® water. The bile solution was distributed between three 50 mL centrifuge tubes (37.45 mL each) and allowed to stand at ambient until required. A total of 150 μL $CaCl_2$ is added over the experiments, bringing the total volume of prepared solution to 112.5 mL.

SIF stock was distributed between three 15 mL centrifuge tubes, each containing 12.5 mL solution, and stored at 37 ^{o}C until required: awaiting pancreatin addition. Pancreatin (ca. 0.77 g) was weighed into a 15 mL centrifuge tube and stored at -20 ^{o}C until required; this was repeated twice.

2.2.15 pH stat protocol

CB or CBA was melted at 37, 50 or 80 ^{o}C for at least one hour in a water bath and held at the relevant temperature until required. Each T_m was analysed in triplicate.

A total volume of 50 mL experimental SIF (2.2.14.3) was used for each experiment. For a 2% fat solution, the following conditions were undertaken: 37.45 mL of bile solution was added to a 60 mL conical titration vessel with thermostatic jacket held at ca. 37 ^{o}C and brought up to temperature. Once equilibrated, the pH was measured and adjusted to pH 7 with 1 M HCl. Molten CB or CBA (1 mL) was added to the solution and allowed to emulsify for 3 min under magnetic dispersion at stirrer speed 12. During this time, 0.77 g of pancreatin was removed from the freezer, added to 12.5 mL of SIF stock, vortexed and returned to 37 ^{o}C storage until required (ca. 1 min). Following 3 min of bile/lipid emulsification, 50 μL of 0.3 M $CaCl_2.2H_2O$ was added and the experiment initiated. After ca. 30 s, the pancreatin solution was added to the reaction mixture. Minimum titration rate was set to 20 μL min^{-1} until 400 s then reduced to 9 μL min^{-1}; maximum titration was set to 0.75 μL min^{-1} throughout. pH was maintained at pH 7 via the Metrohm 902 Titrando unit using tiamo^{TM} 2.0 control software: 0.1 M NaOH solution was used and the titration lasted for 2 hours.

$CaCl_2$ and bovine bile extract reached concentrations of 0.3 mM and 10 mM respectively in the final reaction mixture.

2.2.15.1 Processing of lipolysis reaction data

tiamo^{TM} 2.0 software was used to monitor the reaction and gather data on the rate and volume of titration. Results were extracted to Excel, means over the three replicates calculated and the volume of NaOH titrated plotted against time.

Using Eq.(3)[134], the percentage of FFA release was calculated from the number of moles of 0.1 M NaOH required to neutralise the FFAs produced from the TAGs if they were all digested (assuming two FFAs per TAG through the action of lipase).

$$\%FFA = 100 \times \left(\frac{V_{NaOH} \times M_{NaOH} \times M_{w\ lipid}}{2 \times W_{lipid}} \right) \quad (3)$$

where V_{NaOH} is the volume (mL) of NaOH released during the titration, M_{NaOH} is the molarity of NaOH titration solution used (0.1 M), $M_{w\ lipid}$ is the molecular weight of CB (0.85793 kg mol^{-1})[1] and W_{lipid} is the weight of lipid initially present in the reaction vessel[2].

2.2.16 Confocal laser scanning microscopy

Fluorophore stock solutions were prepared and placed in 2 mL microcentrifuge tubes for storage in a freezer at -20 ^{o}C until required. Each was prepared in a 1 mg mL^{-1} concentration, 3 mg in total; FITC was prepared in Milli-Q® water/EtOH (1:1, v/v), Rhodamine B in Milli-Q® water and Nile red in DMSO.

Stock solutions were diluted using the analytes to the following concentrations: 1:50, 1:75, 1:100 and 1:150 (e.g. 1 part dye to 50 parts analyte). The analytes were CB, bile, $CaCl_2$ and bile plus $CaCl_2$; as prepared under the conditions described in 2.2.13. The final volume of the dilutions was 1.5 mL. Rhodamine B and FITC was used to stain the bile solution, $CaCl_2$ and the bile plus $CaCl_2$; Nile Red was used to stain CB. The CB was melted at 60 ^{o}C prior to staining and was in liquid form on addition of the dye.

The applicable amount of each analyte was placed in a 2 mL microcentrifuge tube, the respective amount of dye added, and the tube shaken for ca. 1 min until the sample appeared homogenous. Aliquots of the samples (300 µL) were transferred into the sections of 8-well glass bottom µ-slides (Figure 2.8) using an automated pipette. The remaining solutions were placed into a 4 ^{o}C refrigerator for storage. The lid was placed on top of the µ-slide and sealed in place with Parafilm around the perimeter.

[1] Calculated from the CoA for IRMM 801 certified reference material

[2] Lipid density at the relative melt temperature

(a)

(b)

Rhodamine B in bile

1:50	1:75	1:100	1:150
1:50	1:75	1:100	1:150

FITC in bile

Figure 2.8 Image of (a) an 8-well µ-slide and (b) a representation of a prepared slide containing bile solution mixed with either Rhodamine B or FITC and their dilutions.

A Zeiss LSM 880 inverted confocal microscope with Airyscan (Carl Zeiss MicroImaging GmbH, Jena, Germany) was used for analysis. A drop of immersion oil was placed onto the objective lens (10 – 40x magnification) and the µ-slide fixed in place on the microscope stage. Imaging was achieved from below, through the glass bottom of the slide. Nile red was excited at 488 nm, Rhodamine B at 568 nm and FITC at 516 nm.

2.2.17 Acoustic attenuation spectroscopy

The Ultrasizer MSV is an acoustic attenuation spectroscopy instrument, capable of analysing liquids and emulsions in their pure form; eliminating the need for sample dilution. The technique was used to determine changes in droplet size distribution (DSD) of CB suspended in a bile solution. Soundwaves are transported through the sample at low and high frequency between two transducers, where the detector generates a response in the form of a voltage signal[153]. This response is a measure of attenuation in the sample, indicated by diffraction/scatter of the emitted soundwave, which can be attributed to particles in the solution in the form of solids or emulsions. The level of attenuation allows the determination of particle size and concentration. The propagation distance is automatically adjusted throughout the measurement period giving an accurate measure of the sample.

Bovine bile (2.5 g) was added to 400 mL of SIF stock and 0.5 mL of $CaCl_2.2H_2O$ as prepared under the conditions described in 2.2.14.2. The solution was made to pH 7 using 1 M NaOH, total volume calculated then made up to 500 mL using Milli-Q® water and mixed under magnetic dispersion for 2 hours at 45 ^oC. CB was incubated at 37 ^oC overnight.

For analysis, 500 mL total solution was prepared by placing 450 mL of the SIF/bile mixture into the instruments' chamber followed by 50 mL of molten CB. Chamber temperature was maintained at 37 ^oC via a Huber circulating water bath. Mixing of the sample was achieved via an overhead stirrer set to 250 – 500 rpm. Fifty data points were collected over a 38-minute period between 1.5 and 115 MHz and levels of attenuation measured. The analysis was repeated consecutively to achieve a minimum experimental period of 2 hours.

Chapter 3 Determining the enantiomeric ratio of cocoa butter triacylglycerols

Chirality is introduced into a TAG when the primary positions are esterified by different FAs, allowing two enantiomeric forms to exist. Nature tends to favour the biosynthesis of one enantiomer, D-sugars and L-amino acids for instance, yet this preference does not appear to be the case during TAG formation. The objective of this research was to clarify the reported 1:1 ratio of (*R*)- and (*S*)-POSt enantiomers in CB, known as a racemic mixture or racemate. A method for isolating the POSt fraction from CB was developed using NARP-HPLC connected to a fraction collector (FRC) with the aim of transferring the protocol to isolation of enantiomers once suitable chiral HPLC conditions were identified. A comprehensive column screening service was performed in-house and externally using a *rac*-POSt standard to ascertain an appropriate chiral selector for the ABC type TAG. An indirect approach to chiral analysis was also conducted, whereby the *rac*-POSt standard was converted into diastereomeric derivatives using a chiral derivatising agent (CDA), (*R*)-(-)-MTPA-Cl (Mosher's acid chloride). The procedure involved partial hydrolysis of the TAG using *sn*-1,3 specific porcine pancreatic lipase, followed by acylation of the CDA to afford Mosher esters. Subsequently, these were analysed using ^{19}F and ^{1}H NMR to identify changes in chemical shift for the determination of enantiomeric ratio. Additional analysis of the derivatisation product was conducted using HPLC as supporting information to the NMR data.

3.1 Results

3.1.1 Identification of triacylglycerols in cocoa butter

The three predominant TAGs in CB were identified by comparison of retention times (t_r) with reference standards using the Shimadzu Prominence HPLC with

ELSD detection (see section 2.2.1). The peak areas were used to calculate relative percentages (Table 3.1), indicating a comparative ratio with those presented in literature[26].

Table 3.1 Relative percentages of the predominant TAGs in a West African CB used in this thesis compared to those of varying geographical regions[26].

TAG	Current work	Ivory Coast	Malaysia	Brazil
POP	20	21	21	21
POSt	47	49	48	49
StOSt	33	30	31	30

The TAG standards were used to produce eight-point calibration curves from 0.01 – 1 mg mL^{-1} concentration (see appendix A.1) as described in the methodology section and used to calculate the LOD and LOQ (Table 3.2).

Table 3.2 LOD, LOQ and calibration curve data for the predominant TAGs in CB.

TAG	LOD (mg/mL)	LOQ (mg/mL)	Calibration curve equation	Correlation coefficient
POP	0.06	0.18	$y = 1 \times 10^6x - 39669$	0.9932
POSt	0.12	0.36	$y = 587065x - 10645$	0.9604
StOSt	0.09	0.27	$y = 1 \times 10^6x - 63114$	0.9845

The non-linear response of the ELSD as reported in literature[46, 47, 154] was evident at concentrations ≤0.35 mg mL^{-1}. Such low range strengths were chosen to challenge the sensitivity of the detector ahead of enantiomeric analysis as the concentrations in that respect are expected to be weak. POP and StOSt displayed similar results, however, the POSt figures were disparate, showing a reduced response for data points of 0.2 mg mL^{-1} and above. Concentrations of 0.2 and 0.35 mg mL^{-1} were outliers, thus, contributors to the lower correlation coefficient. It is not clear why this effect occurred, but it could be postulated that the pseudo-symmetrical configuration of the TAG may influence the scattering of the detector. Literature corroborating this notion has

not been identified, however, differences in ELSD response for monoacid TAGs has been observed[154], which supports the variable results in this thesis. Response factors, calculated as peak area divided by peak concentration, were reported as 0.01 – 1.16 relative to trioleate (OOO), which was set to 1.00[154]; thus displaying the breadth of detector response for TAGs dependent on their acyl chains.

3.1.1.1 Isolation of POSt fraction from CB using in-line fraction collector

An in-line fraction collector (FRC) connected to the previously described HPLC (see section 3.1.1) was used to isolate the POSt fraction from CB. Following two runs, the collated fractions were analysed under the conditions described in the methodology section (2.2.2): a small peak is observed, which is confirmed to be POSt from the overlay of its reference standard (Figure 3.1).

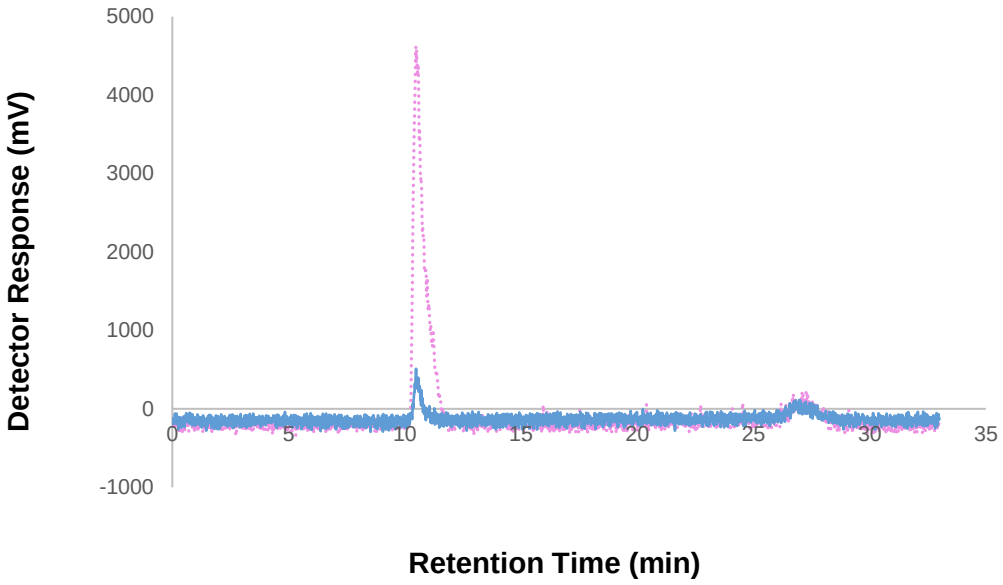

Figure 3.1 Overlay of collected POSt fraction from CB (blue solid line) and reference standard at 1 mg mL^{-1} concentration (pink dotted line).

Using the calibration curve, the amount of collected POSt was estimated to be 0.04 mg. Numerous runs of the protocol were subsequently performed to amass product for further analytical procedures; enantiomeric determination and isolation of individual enantiomers.

3.1.2 Chiral column screening for separation of triacylglycerol enantiomers

Several columns were screened in-house using the Shimadzu Prominence HPLC with ELSD detection (2.2.1) in order to determine the appropriate chiral stationary phase (CSP) for enantiomeric TAG separation, using *rac*-POSt as the analyte. Of the seven columns that were trialled (see section 2.2.3), no separation of the *rac*-POSt enantiomers was evident. An example is presented in Figure 3.2, the Lux i-Cellulose-5 result.

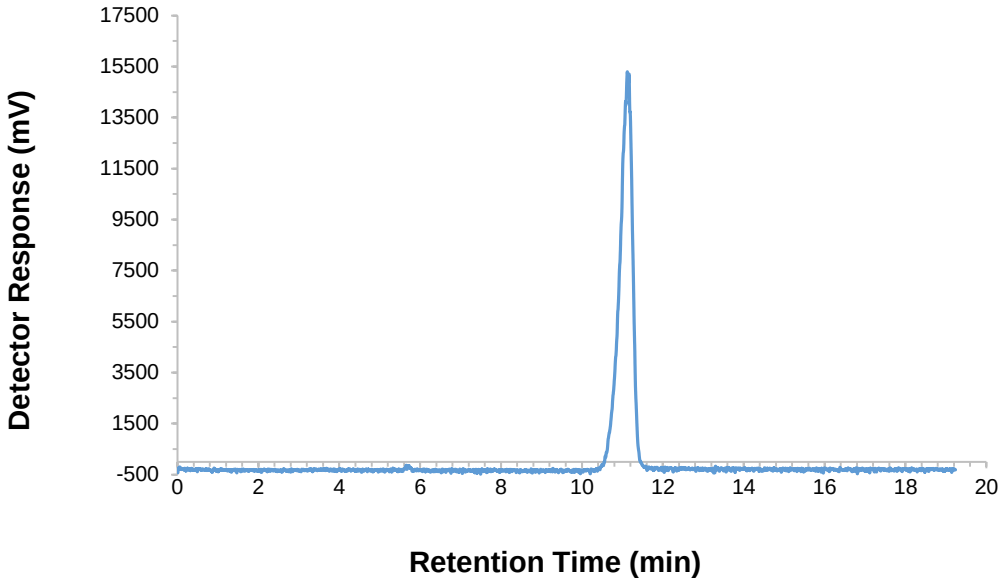

Figure 3.2 Chromatogram of a rac-POSt standard analysed using the Lux i-Cellulose 5 chiral column from Phenomenex. Sample was dissolved in DCM/ACN (3:7, v/v) and analysed isocratically using ACN as the mobile phase.

Successful separation would be identifiable by two peaks of similar height and shape directly after one another. Under different conditions, the Lux Cellulose-3 column produced a split peak with an onset time of ca. 2 min (Figure 3.3).

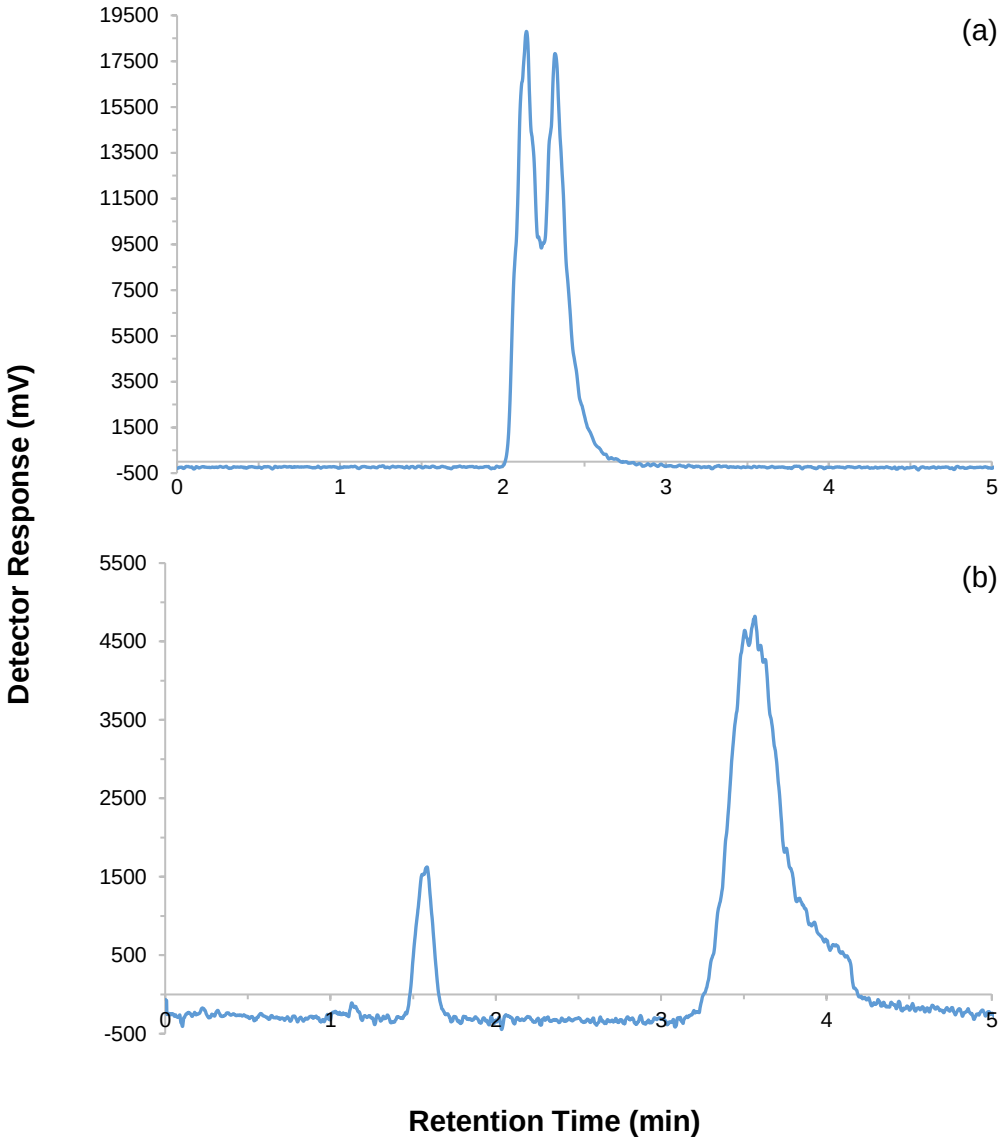

Figure 3.3 Analysis of rac-POSt using a Lux Cellulose-3 chiral column. TAG was dissolved in MeOH/IPA (63:37, v/v) and analysed isocratically using a mobile phase of (a) ACN/IPA (95:5, v/v); (b) ACN/H_2O (9:1, v/v).

Early elution in Figure 3.3 (a) suggests that the two peaks are not the enantiomers, as lengthy retention times in enantiomeric TAG separation appear to be routine[29, 36, 63, 65]. Altering the mobile phase allowed for two peaks to emerge (Figure 3.3 (b)). The first at ca. 2 minutes is expected to be the solvent front, thus, only one peak represents the sample; indicating a lack of enantioseparation. This suggests that the split peak in Figure 3.3 (a) is co-elution of solvent and compound. Results observed in the presented chromatograms are representative of all other columns/conditions in the trial.

The external column screening service provided by Phenologix (California, USA) and Daicel (Ilkirch, France) also failed to separate the two enantiomers. As requested, they first replicated the Lísa and Holčapek[65] method, which was recognised for their successful separation of enantiomeric TAGs from natural sources. The Phenologix result is presented in Figure 3.4. Chromatographic data for this method was not provided by Daicel, but the most significant results from their screen are displayed in Figure 3.5. Between the companies, twenty-three columns were trialled (Table 3.3) under various conditions, but enantiomer separation was not achieved.

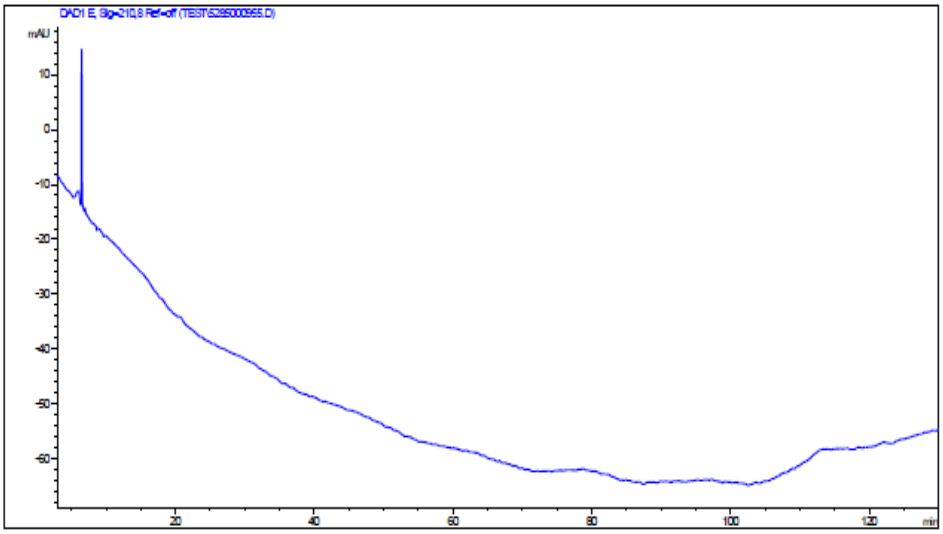

Figure 3.4 Chromatogram taken from the Phenologix report showing analysis of the rac-POSt standard using the journal method[65] (1 mL min^{-1} flow rate; 35 ^{o}C column temperature; mobile phase gradient: 0 min 90% A + 10% B, 180 min 60% A + 40% B, where A is hexane and B is hexane:2-propanol (99:1, v/v)). Column series was a Lux 5 µm Cellulose-1 (250 mm x 4.6 mm) connected to a Lux 3 µm Cellulose-1 (250 mm x 4.6 mm); detector was a diode array.

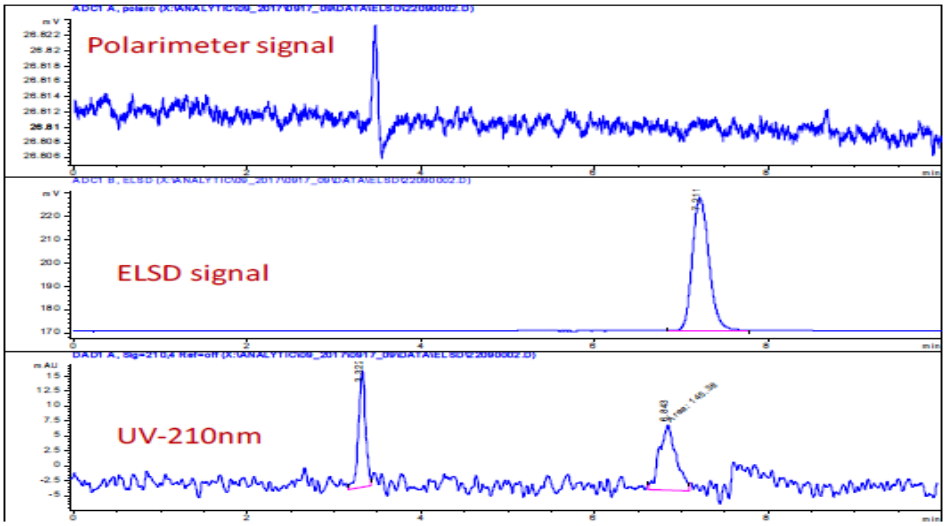

Figure 3.5 Image taken from the Daicel report showing the most relevant data for the rac-POSt standard. Each method of detection failed to resolve the enantiomers: these results were achieved using an alternative method to that of Lísa and Holčapek[65]. Conditions were as follows: column was a Chiralpak® IC (250 x 4.6 mm, 5 µm), eluent was heptane/MTBE (7:3, v/v), flow rate of 1 mL min^{-1} and an oven temperature of 25 ^{o}C.

Table 3.3 Chiral columns/stationary phases trialled in the screening service and the providers.

	Stationary phase	Column	Screening service provider
Amylose *tris*	3, 5-dimethylphenylcarbamate	Lux Amylose-1*	Phenologix, USA
		Lux i-Amylose-1	
		Chiralpak IA	Daicel, France
		Chiralcel AD-H	
	3, 5-dichlorophenylcarbamate	Chiralpak IE	Daicel, France
	5-chloro-2-methylphenylcarbamate	Chiralpak AY-H	Daicel, France
	3-chloro-4-methylphenylcarbamate	Chiralpak AZ-H	Daicel, France
		Chiralpak IF	
	3-chloro-5-methylphenylcarbamate	Chiralpak IG	Daicel, France
	(S)-α-methylbenzylcarbamate	Chiralpak AS-H	Daicel, France
Cellulose *tris*	3, 5-dimethylphenylcarbamate	Lux Cellulose-1*	Phenologix, USA
		Chiralpak IB	Daicel, France
		Chiralpak IB-N	
		Chiralcel OD-H	
	3-chloro-4-methylphenylcarbamate	Lux Cellulose-2*	Phenologix, USA
		Chiralcel OZ-H	Daicel, France
	4-methylbenzoate	Lux Cellulose-3*	Phenologix, USA
		Chiralcel OJ-H	Daicel, France
	4-chloro-3-methylphenylcarbamate	Lux Cellulose-4*	Phenologix, USA
		Chiralcel OX-H	
	3, 5-dichlorophenylcarbamate	Lux i-Cellulose-5*	Phenologix, USA
		Chiralpak IC	Daicel, France
	3-chlorophenylcarbamate	Chiralpak ID	Daicel, France

*Columns were also used in the Phenomenex screening service delivered in-house at the University of Leeds, with the addition of Lux Amylose-2

All of the Phenologix columns in Table 3.3 were screened using each of the conditions listed in Table 3.4. Overall, forty-nine conditions were tested with no successful separation.

Table 3.4 Summary of the separation modes trialled by Phenologix in the chiral screening service under isocratic conditions; eluent was hexane:IPA (1:1, v/v).

Mode	Mobile phase	%A/B	Additives
Normal phase	A = Hexane, B = EtOH	95:5	0.1% Diethylamine
	A = Hexane, B = EtOH	95:5	0.1% Trifluoroacetic acid
Reverse phase	A = 20 mM Ammonium bicarbonate, B = ACN	60:40	0.1% Diethylamine
Polar organic	A = MeOH, B = IPA	90:10	0.1% Diethylamine
	A = MeOH, B = IPA	90:10	0.1% Trifluoroacetic acid
	A = ACN, B = IPA	95:5	0.1% Diethylamine
	A = ACN, B = IPA	95:5	0.1% Trifluoroacetic acid

Similarly, Daicel performed a comprehensive service, using multiple columns and mobile phases, as summarised in Table 3.5. It is not clear what mobile phases were used when alkane, alcohols, polar organic and HILIC are referred to as it is not stated in the report, nor are conditions such as solvent ratios, flow rate or oven temperature. Nonetheless, enantioseparation was not possible in the thirty-five conditions trialled. Very limited retention was reported for alkane/alcohol, even when the proportion of the latter was only 2%, similar to the observations in Figure 3.3.

Table 3.5 Summary of conditions used by Daicel during the chiral column screening.

Column	Mobile phase			
	Alkane/Alcohols	**Alkane/MTBE***	**Polar organic**	**HILIC****
IA	x	x	x	x
IB	x	x		x
IB-N	x	x	x	x
IC	x	x	x	x
ID	x	x	x	x
IE	x	x	x	x
IF	x	x	x	x
AD-H	x			
AS-H	x			
AY-H	x			
AZ-H	x			
OD-H	x			
OJ-H	x			
OX-H	x			
OZ-H	x			

*Methyl *tert*-butyl ether **Hydrophilic interaction liquid chromatography

3.1.3 Atmospheric pressure chemical ionisation mass-spectrometry for enantiomeric separation of a racemic TAG

Resolution of *rac*-POSt and subsequent quantitation of the enantiomers was attempted using chiral-HPLC with an atmospheric pressure chemical ionisation mass-spectrometer (APCI-MS) as the detector. Using a method previously described for regioisomer and enantioseparation of TAGs in underivatized natural lipid samples[65] (see section 2.2.4), two chiral columns were connected in series to increase the length of the stationary phase; extending the interaction time between analyte and CSP. A *rac*-POSt standard

was dissolved in hexane at a concentration of 2 mg mL^{-1} and analysed under gradient conditions over a period of 180 minutes. However, with only one peak observed, the conditions were not suitable to elicit chiral resolution (Figure 3.6).

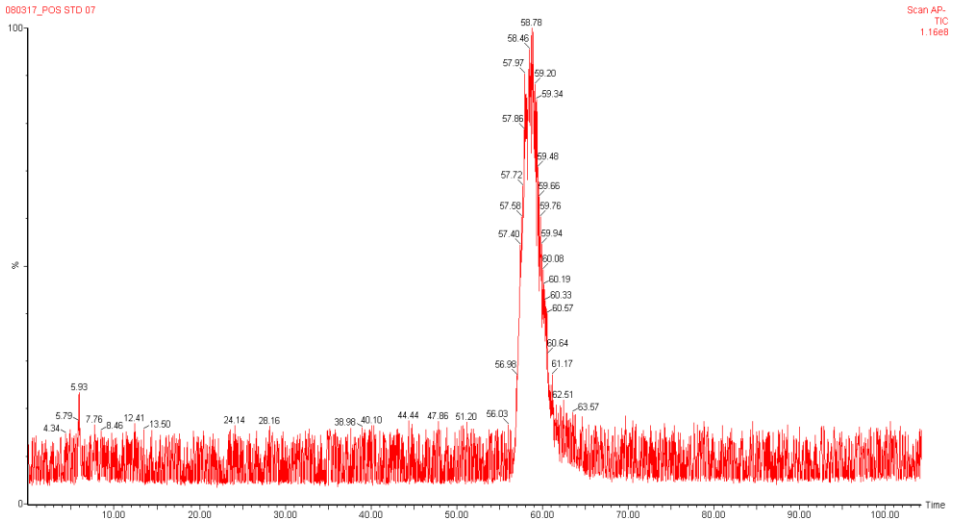

Figure 3.6 Enantioseparation attempt of rac-POSt standard using two Chiralcel® OD columns (250 mm x 4.6 mm, 10 µm) connected in series. Conditions were as described in 2.2.4.

Differences in column packing to that used in previous research[65] may be a contributing factor to the lack of separation. The stationary phases were of the same material, cellulose-tris 3,5-dimethylphenylcarbamate (CDMPC), but the particle size was here greater at 10 µm in comparison to 3 µm used in literature. Access to the identical type was not possible, and beyond our skill to make. Thus, the most suitable and accessible replacement was used. The smaller particle size of the 3 µm column contains a higher number of theoretical plates and consequently, greater chromatographic efficiency: the 'plates' being fictional sections within the column where sample equilibration occurs as the analyte(s) partition between phases prior to moving to the next via transport in the eluent[155].

Two further attempts under differing conditions were trialled (Figure 3.7). Each was stopped earlier than planned following the observation of a sole peak, with no indication of any more after at least 10 minutes: evidence that the

enantiomers had not separated. Reasons behind these failures are deliberated in the discussion below (section 3.2).

(a)

(b)

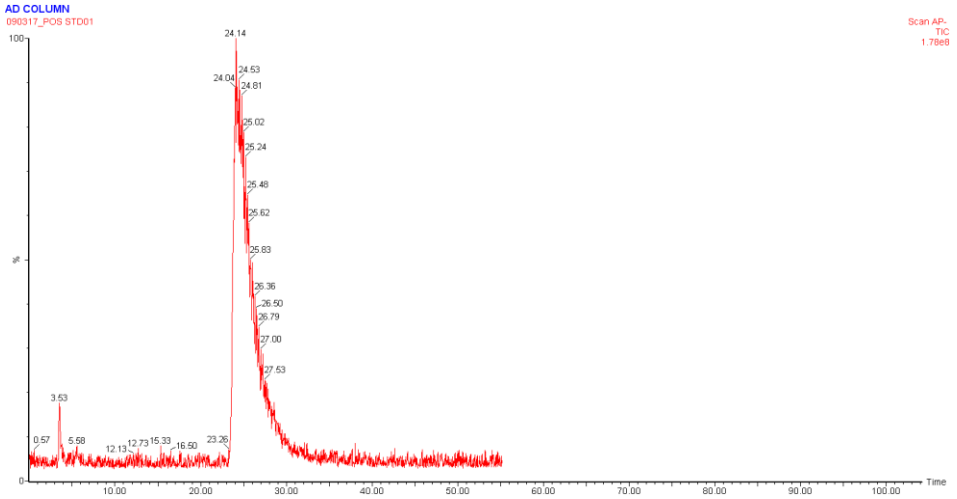

Figure 3.7 Alternative methods trialled for the determination of rac-POSt enantiomers; (a) two Chiralcel® OD columns (250 mm x 4.6 mm, 10 µm) connected in series with hexane/IPA (99:1, v/v) mobile phase delivered isocratically; (b) a Chiralpak® AD (amylose-tris 3, 5-dimethylphenylcarbamate) column (250 mm x 4.6 mm, 10 µm) using a gradient mobile phase described in 2.2.4, where A is hexane and B is hexane/IPA (99:1, v/v). For both conditions, the flow rate was 1 mL min^{-1} and the oven temperature 35 ^{o}C.

3.1.4 Diastereomeric TAG formation from a racemic antecedent using a chiral derivatising agent

Partial hydrolysis of *rac*-POSt followed by the addition of (*R*) Mosher's acid chloride ((*R*)-(-)-MTPA-Cl) was undertaken using conditions described in the methodology section (2.2.9) to create diastereomeric derivatives of the (*R*) and (*S*) enantiomers. Introduction of the chiral derivatising agent (CDA), also discussed as a chiral shift agent, alters the δ ppm for each of the diastereomeric pairs: the lone trifluoromethyl group of the CDA can be identified using ^{19}F NMR and proton shifts with ^{1}H NMR.

^{19}F NMR data from the primary experiment shows several peaks at -71.24 ppm that differ from the CDA starting material (Figure 3.8); indicating a reaction had occurred with the available *sn*-1(3) position(s) of the DAG/MAG following enzymatic hydrolysis of palmitic and/or stearic acid using pancreatic lipase.

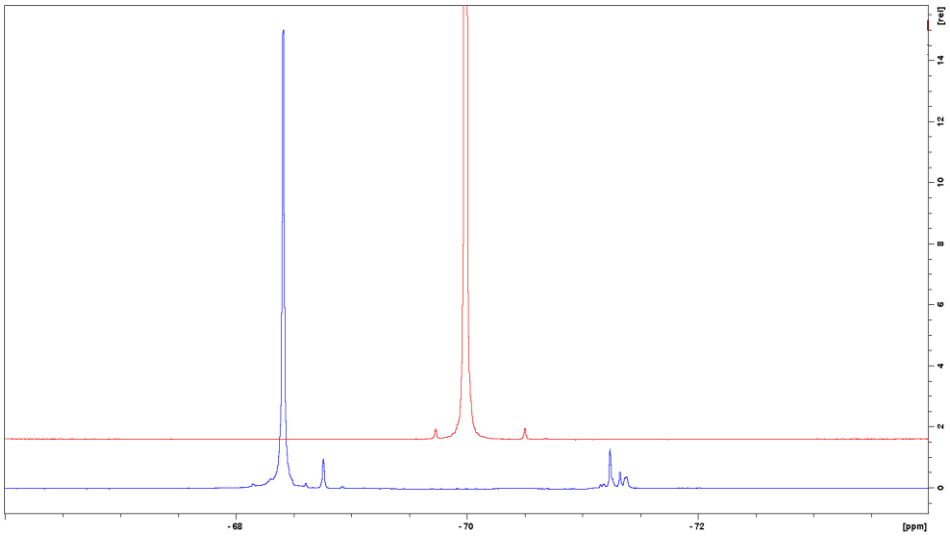

Figure 3.8 ^{19}F NMR spectra for the derivatisation product of a rac-POSt standard showing peaks at -71.24 and -68.41 ppm (bottom, blue spectra) and (R)-(−)-MTPA-Cl CDA (3.7 µL in 0.6 mL $CDCl_3$) starting material (top, red spectra) showing a peak at -69.99 ppm, corresponding with the CF_3 group of the compound.

Observation of the Mosher's ester derivatised sample in the NMR tube, which corresponds with the bottom spectra in Figure 3.8, showed the reaction product had not dissolved in the solvent. Phase separation was evident, with the product sitting atop the $CDCl_3$ (Figure 3.9).

Figure 3.9 NMR tube containing the product of rac-POSt derivatisation using (R)-(−)-MTPA-Cl CDA, evidencing the products insolubility in $CDCl_3$ with the phase separation.

It is possible that residual water from the hydrolysis stage was present in the sample, which may have affected the solubility; therefore, supplementary steps were added into the protocol to extract this using toluene. The procedure was completed again with the additional stages. The second attempt was more successful, with a larger number of peaks in the spectra (Figure 3.10). Though different to Figure 3.8 (bottom spectra), the peaks appear around a similar ppm, an indication that both procedures were efficacious in some part.

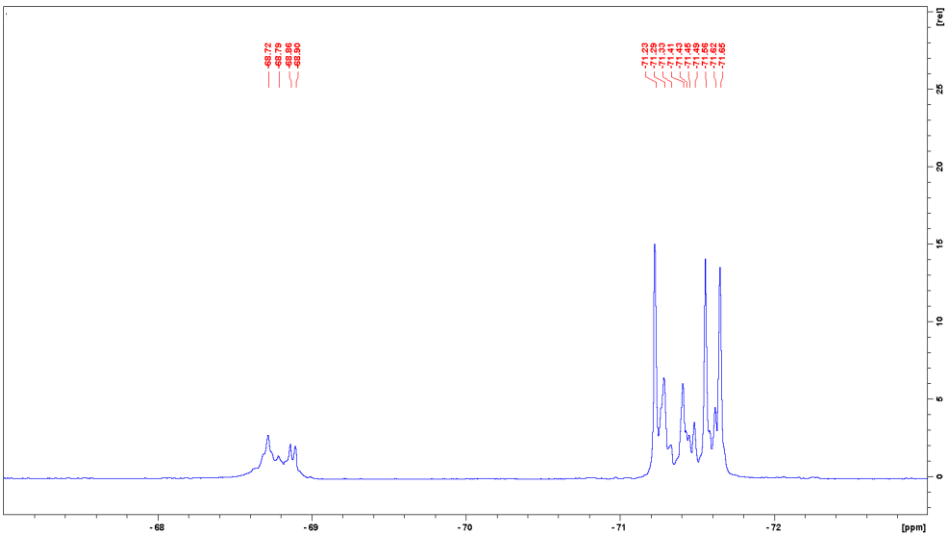

Figure 3.10 ^{19}F NMR spectra of the second derivatisation attempt of a rac-POSt standard using (R)-(−)-MTPA-Cl CDA.

Conversely, the same issue occurred as with the first attempt, whereby the sample had not fully dissolved and so it is not apparent as to what the peaks in the spectra correspond, thus, their assignment has not been possible. The

trifluoromethyl group in the structure of (*R*)-(-)-MTPA-Cl determines one peak would be expected for each diastereomer: including a compound where the CDA has attached at both primary positions, seven potential derivatives are predicted (see Appendix; Figure A.2). In an attempt to clarify the peak assignment, several solvent/solvent mixture trials were performed to ascertain a clearer spectra (Table 3.6).

Table 3.6 Solvents/solvent mixtures trialled for the derivative products of rac-POSt.

Solvent/solvent mixture	**Ratio (v/v)**	**Dielectric constant (20 °C)[156] (ε)**
Hexane	-	1.89
Toluene	-	2.38 (23)
DCM	-	8.93 (25)
$CHCl_3$/MeOH	2:1	14.21
MeOH/DCM	2:1	24.98
ACN	-	36.64
DMSO	-	47.24
H_2O/MeOH	2:1	64.40
H_2O	-	80.10

* ε for $CHCl_3$ = 4.81; MeOH = 33.0

The dielectric constant of the solvent mixtures was calculated using Eq.(4)

$$f_A\varepsilon_A + f_B\varepsilon_B \quad (4)$$

where *f* is the volume fraction of the solvent and ε is the dielectric constant[157].

The sample in H_2O/MeOH (2:1, v/v) appeared sufficiently dilute to be analysed using the HPLC, as described in 3.1.1. Yet, the chromatogram failed to show any data to indicate that the derivatisation had been successful (Figure 3.11). The analytical procedure followed a method used in literature with the (*R*)-(-)-

MTPA-Cl CDA and solvent mixture[158], though the substrate there analysed was different (amphetamine). Briefly, the conditions were as follows: MeOH/H_2O (6:4, v/v) mobile phase; isocratic for 20 minutes, linear gradient to 100% MeOH at 40 minutes; all other conditions were as described in 2.2.1.

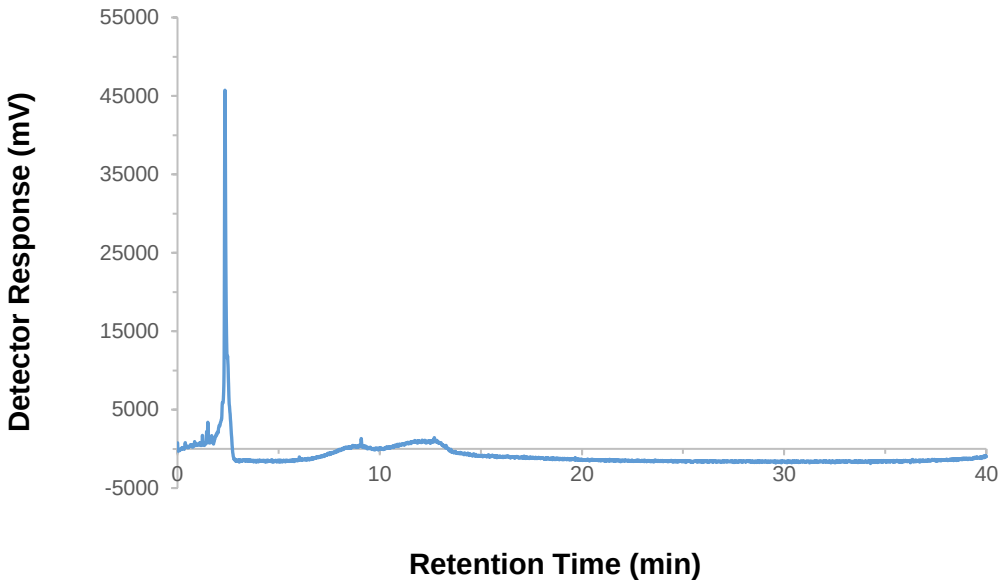

Figure 3.11 Chromatogram of rac-POSt derivative using the method of Miller et al.[158]. Column was a Waters Symmetry C18 (4.6 x 250mm, 5 µm); flow rate 1 mL min^{-1}.

Although two slight mounds appear at ca. 9 and 13 min, they are not evidence of the two diastereomers, which was confirmed by repetition whilst increasing the detectors' sensitivity (data not shown). A further analysis was conducted at 0.25 mL min^{-1} flow rate to allow the derivatisation product(s) longer interaction time with the column, producing a singular peak at 12.4 minutes (Figure 3.12).

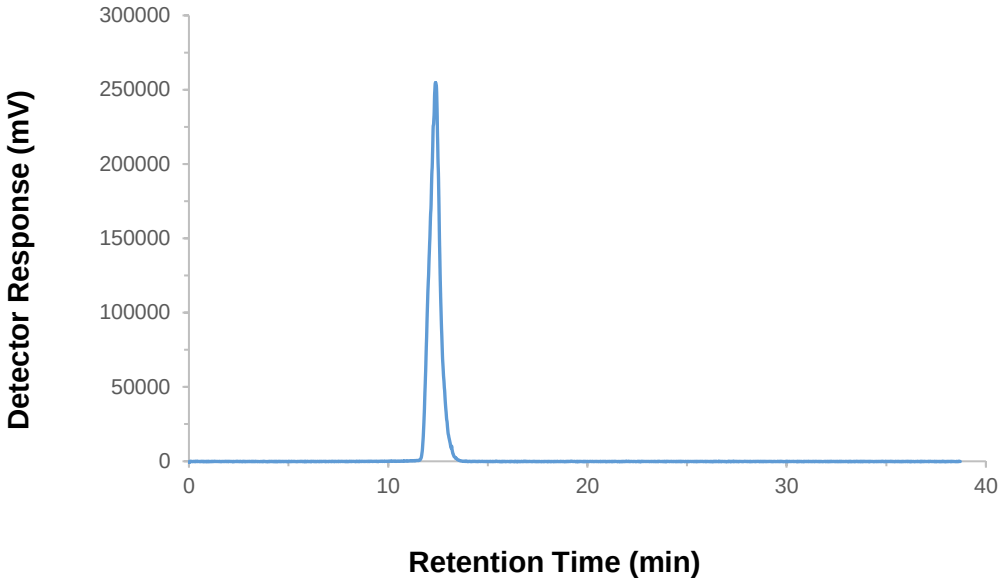

Figure 3.12 Derivatisation product analysed under the conditions of Miller et al.[158] using a flow rate of 0.25 mL min^{-1}.

A t_r difference was expected through using a reduced flow rate, but reasons behind the dissimilar chromatogram pattern are unclear. Nonetheless, analysis of the same sample failed to show more than one peak.

Removing the H_2O/MeOH solvent and attempting to dissolve in toluene once more gave a different result to the first effort, where the sample appeared to fully disperse (Figure 3.13 (a)). A further derivatisation was conducted, however, when it came to prepare the mixture for NMR analysis, toluene was ineffective (Figure 3.13 (b)).

(a) (b)

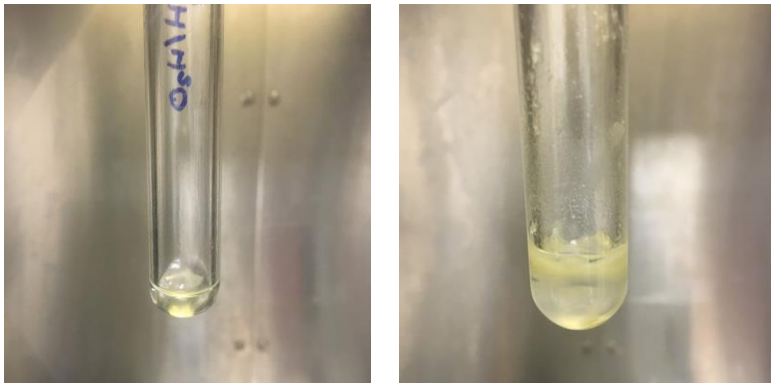

Figure 3.13 Reaction mixtures of the rac-POSt derivatisation. Both tubes show the product in 0.6 mL toluene; (a) product was found to dissolve after several attempts using other solvents and (b) following the full procedure in one day, the sample was insoluble.

Comparing the two, it is thought that with each addition and removal of solvent during the trials the sample was purified, and molarity greatly reduced; thus, when adding toluene a second time, solubilisation occurred. Both samples were analysed using ^{19}F, ^{1}H and ^{13}C NMR: see appendix A.3.1 and A.3.2 for results.

The ^{19}F NMR spectra for Figure 3.13 (a) (Figure A.2 (a)) was incomprehensible, with an erratic baseline and a wide peak at -173 ppm. It is possible that the instrument was not functioning during this analysis only as the ^{1}H and ^{13}C collected directly afterwards were stable; however, these spectra suggest only a trace amount of sample remained and the observed effect is that of the solvent. The data for Figure 3.13 (b) is comparable with previous results (Figure 3.10), but the additional ^{1}H and ^{13}C spectra did not help with peak assignment; being complicated to interpret. These results reinforced the idea that the mixture contained a variety of diastereomers intertwined with products of the partial hydrolysis.

3.2 Discussion

Identifying the elution order for the predominant TAGs in CB proved consistent, with numerous analyses of the lipid sample and standards demonstrating the instruments capability. However, moderate shifts in t_r

occurred which presented difficulties when it came to isolate POSt using the FRC. The software was programmed to open the FRC valve slightly earlier than the expected t_r for POSt to allow time for the solvent stream to split from the ELSD flow line towards the collection vials via the T-fitting: a preliminary analysis of CB was executed each morning of TAG isolation so an assessment of how the instrument was performing could be made. This was generally effective for programming the collection timepoint, however, t_r fluctuations throughout the day nullified some of the isolations. During several runs it was observed that the peak height amplified as the FRC valve opened for collection, giving a false area reading and subsequently, an unknown concentration of POSt deposited in the vials. Attempts were made to estimate this by subtracting the POSt area under curve (AUC) of a CB sample analysed previously, but this was erroneous: the peaks were not clearly defined for the FRC runs, determining co-elution and thus an inaccurate AUC figure. Nonetheless, an amount was collected which was to be analysed for its enantiomeric ratio, once a suitable protocol was sourced.

The results from multiple CSP screenings confirmed that chiral separations of such pseudo-symmetrical materials are difficult to resolve. Guarantee of CSP suitability based simply on the structure of the bonded phase and its interaction with TAGs is not possible; predictions can be made, but not assurances[159]. Achieving resolution with one TAG does not mean that it will work in a comparable manner for another of similar structure[160], which is clear from the extensive chiral screen. For example, two research groups attempted to separate *sn*-PEE and *sn*-EEP, where E is eicosapentaenoic acid (20:5, n-3), using 3,5-dimethylphenylcarbamate bonded phases and only one was successful[36, 63]. Differences lay in the CSP support material, cellulose-tris on silica was unsuccessful whereas a modified β-cyclodextrin achieved resolution[36]. It is expected that the hydrophobic cavity within β-cyclodextrin may have assisted through non-stereoselective adsorption[159].

Our screening of chiral columns were aimed initially at replicating the method of Řezanka and Sigler[36]. However, an attempt to dissolve *rac*-POSt in the MeOH solvent system understandably failed due to differences in polarity: the

resolved enantio-TAGs in their study contained at least one FA with five double bonds and thus, moderately more polar than POSt. IPA (ε = 20.18) was added as a modifier in aliquots until visually the compound had dissolved, hence the unusual ratio (Figure 3.3). The ε value for the binary mixture (ε = 28.26) was comparable with DCM/ACN (3:7, v/v; ε = 28.34), which has been used successfully as a solvent for *rac*-POSt, along with a number of other TAG standards and CB, so it is likely that the MeOH/IPA combination was in the acceptable polarity range. The apparent solubility may have been due to low relative molarity of the compound through an overall increase in solvent volume.

Of the twenty-four screening conditions that were performed, twenty used MeOH/IPA (63:37, v/v) as the solvent, with the other four being DCM/ACN (3:7, v/v): an example of the latter is presented in Figure 3.2. The best suggestion of enantioseparation was using the Lux Cellulose-3 column with MeOH/IPA solvent and pure ACN or ACN/IPA (95:5, v/v; ε = 35.82) mobile phases under isocratic conditions (Figure 3.3 (a)). Yet, minimal retention did not deliver confidence that the beginnings of a peak splitting were relative to the enantiomers; with the effect likely being co-elution of solvent and compound. The only difference with the conditions in Figure 3.3 (b) that identified a solo peak is the marginal share of the mobile phase; with Figure 3.3 (a) containing 5% IPA and (b) 1% water. The polar water acting as a repellent to the TAG, driving it towards the surface layer of the solution and allowing it to interact with the CSP; whereas interactions with IPA will have kept the compound in the bulk, away from the surface, drawing it straight through the column. Ultimately, it was not possible to find the appropriate column and/or mobile phase combination under the conditions available.

Correlations between alkyl chain length at the *sn*-1/3 positions and separation capacity of enantiomeric TAGs was apparent in the work of Kalpio et al.[29], with longer hydrocarbons displaying earlier elution. *rac*-18:1-18:1-14:0 showed weak signs of enantiomer separation at ca. 95 minutes, whereas a similar pattern for *rac*-18:1-16:0-16:0 was evident earlier at ca. 60 minutes. With the primary groups of *rac*-POSt (16:0-18:1-18:0) being similar in length

to the latter it could be estimated that a similar pattern would be observed, but this was not the case. Analytical trials at Bradford using APCI-MS produced only a single peak at ca. 60 minutes using the protocol of Lísa and Holčapek[65], which was at a flow rate of 1 mL min^{-1} with no recycle system, whereas Kalpio et al.[29] used 0.5 mL min^{-1} with a recycler. With the latter, the compounds passed through the first column, were detected via UV and then exposed to a second column; continuous recycling ensued until complete resolution was achieved. Unlike the singular peak achieved during analysis at Bradford (Figure 3.6), Kalpio et al.[29] were able to produce an array across the chromatogram through repeated exposure to the detector. Of those, two peaks appear prior to the initial signs of enantioseparation, with the first at ca. 5 minutes and the second at ca. 30 minutes, indicating that it took ca. 25 minutes for the recycler to send the compounds through both columns and back to the detector. Complete separation was at ca. 255 minutes for *rac*-18:1-16:0-16:0. In the attempt to separate *rac*-POSt using two columns connected in series for this thesis, there were no peaks evident at either of those time points (5 or 30 minutes); or earlier as would be expected using a faster flow rate. Extending CSP exposure time through a recycling system was not a viable option.

Previous research has shown that separation of enantiomer pairs in natural samples without prior derivatisation is somewhat achievable[36, 65], such as POO/OOP at ca. 87.5 and 88.5 minutes[65]. However, the resolution is not definitive with only a split peak as evidence. A peak identified as StOP+StOSt is apparent in the chromatogram of hazelnut oil[65] at 83.5 minutes, where a co-elution of enantiomers within that was declared. It is reasonable to assume that the authors are referring to StOP/POSt, which would correlate with the results in this thesis in that separating said enantiomers using CDMPC columns appears to be unattainable. However, as they could not resolve the suggested enantiomeric pair, it cannot be verified that both were present: it may have been pure StOP or POSt.

Phenologix replicated the method presented in literature[65] using almost identical conditions, but without APCI-MS as the detector. They were unsuccessful in the enantioseparation of *rac*-POSt and managed to acquire

very different data to the journal article and method trial performed at Bradford for this work. Aside from the early peak at ca. 7 minutes (Figure 3.4), no others are evident. The research paper[65] did not analyse the same compound, but their results fail to report any peaks prior to ca. 72 minutes, racemate or otherwise, and the outcome of our APCI-MS trial using similar conditions did not see a peak until ca. 58 minutes (Figure 3.6). Thus, it is not clear why Phenologix achieved such dissimilar data with all their peaks eluting in less than 10 minutes.

The degree of work conducted by the external companies is evident (Table 3.4 and Table 3.5), with eighty-four separation modes trialled between them. When combined with the twenty-four performed in-house, a total of 108 different modes were unsuccessful in achieving enantioseparation.

One consideration with regards to the efficiency of the commercial columns for this compound is the amount of coating on each of the CSPs tested: a fact that is not clear in the column specifications. Wei et al.[161] found there to be an optimal amount of CDMPC for separation of enantiomeric pairs: it should be noted that none of these were TAGs, nonetheless, the concept may be of relevance. Their evaluation was conducted by preparing variable concentrations of CDMPC (0.05, 0.1, 0.15, 0.2 and 0.25 g) in THF and coating porous silica gel one, two, three, four or five times to achieve the desired loading. They discovered that an optimal coating amount of 18.37% (0.15 g x three coatings) gave the best resolution factor for four of the seven enantiomers analysed. Interestingly, they revealed that the amount of CDMPC on the columns was not the only factor in determining their separation efficiency. Though the total load percentage may be identical, the number of silica coatings was a major contributor. For example, at 6.98% their compound D achieved resolution of 0.28 when the silica was loaded three times (0.05 g x 3), yet the enantiomers failed to separate when it had been loaded once (0.15 g x 1). This was the only compound out of the seven and the only conditions where this occurred, but the result may be relative to the difficulties seen in this thesis. Perhaps the principles can be considered when attempting to understand why none of the commercial CSPs worked for *rac*-POSt: it is

feasible that the column loading was too low and/or the number of coatings was not adequate.

When a request for information on the CSP loading of their columns was made to Phenomenex, they were unable to provide specifics as preparation differs to their usual manufacturing process, in that the phases are coated on the silica rather than bonded as would be the case for reverse phase columns. As Wei et al.[161] produced columns on a small scale they were able to monitor the specific load, whereas Phenomenex who produce them on mass cannot. Without knowledge of how much chiral phase is on their columns, it is not possible to say definitively that the amount was insufficient for *rac*-POSt, but it is something that should be taken into consideration: this is also relative to Daicel columns.

In further consideration as to why none of the CSPs trialled were successful, it is likely that the three-point interaction mechanism, introduced in section 1.3.4, was unable to distinguish between the alkyl chains at *sn*-1 and *sn*-3[162]. Much of the research that has achieved satisfactory enantioseparation has done so with TAGs of non-identical alkyl groups at the *sn*-1/3 positions, with one being a SFA and the other a MUFA/PUFA[29, 36, 63, 65, 162]. Enantiomeric TAGs with similar length *sn*-1/3 groups have been separated, but these have been PUFAs with dissimilar numbers of double bonds; clearly being sufficient for differentiation[36]. With a difference of merely two methylene units between the chain lengths of palmitic and stearic acid, the similarity appears inadequate for the CSPs to distinguish between them and thus, the enantiomers of POSt. The precise retention mechanism for polysaccharide based CSPs and enantio-TAGs is not apparent , but it is considered that where the racemate are of the SUU/UUS type, the initial attraction is a π-π interaction between the double bond(s) of the *sn*-1(3) chain and the phenyl group; similar to the π-π stacking effect amongst aromatic groups. Consequently, the remaining compound fits amongst the chiral groove and is drawn towards the axis of the polysaccharide helix where the polar carbamate group can form a hydrogen bond with the carbonyl of the TAG around *sn*-2[163, 164]. A CDMPC CSP is represented in Figure 3.14.

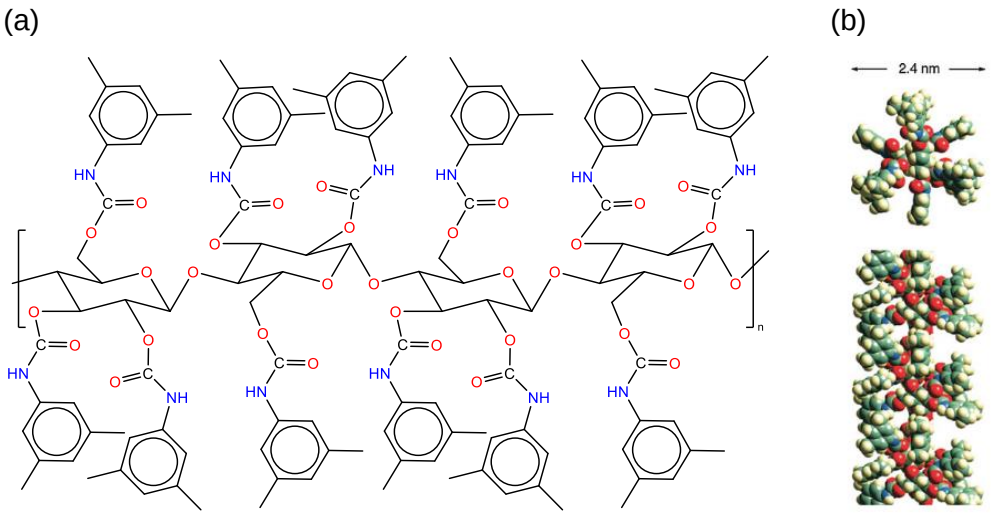

Figure 3.14 Schematic representation of (a) cellulose tris (3,5-dimethylphenylcarbamate) CSP and (b) a three dimensional depiction displaying the perpendicular view to the axis (top) and along the helix (bottom)[163].

The third point of interaction is not clear but could be attributed to steric effects or van der Waal forces[164]. The described mechanism would explain why the t_r is longer for compounds with a greater number of double bonds; more π-π interaction points with the CSP phenyl group. Also, potentially some clarification as to why the CSPs showed little to no attraction with the linear primary alkyl groups of *rac*-POSt.

Future investigations into a suitable CSP should include trials of cyclodextrin-based columns. It is predicted that the apolar cavity within the cyclic polysaccharide would be attractive to the acyl chains through London dispersion forces[165], forming an inclusion complex[58, 159, 166]: surface interactions ensuing with the partial charge of the ester bonds around the glycerol[167]. Thus, it is feasible to assume that (*R*) or (*S*)-POSt would show greater affinity due to the arrangement around *sn*-2, allowing for separation of the pair.

One of the primary aims of utilising chiral HPLC was so that it could be used alongside the FRC in a preparative manner to isolate the enantiomer(s) of interest, without affecting the natural conformation of the TAG. Once it was evident that this technique would not function for the intended purpose, it was essential to find an alternative for resolution. As mentioned in section 1.6, two

of the publications that have determined POSt as racemic in CB use stereospecific analysis for understanding which FAs are present at each *sn* position[53, 100]. Although established as an investigative method, an alternative was desired that would, in theory, allow for an easier analytical procedure by reducing the number of stages. The use of a CDA was established to create diastereomeric derivatives suitable for analysis via NMR; to acquire structural information without dissecting the compound into its component parts. Similar to literature[168, 169], a partial hydrolysis step was used to remove the primary acyl groups, but following this (*R*)-(-)-MTPA-Cl was added to produce (*RR*) and (*RS*) diastereomeric derivatives of the *rac*-POSt standard. However, the derivatised product(s) failed to dissolve in the common solvent for NMR analysis ($CDCl_3$) and thus a range were trialled for suitability. Hexane was used previously for *rac*-POSt during the APCI-MS trial at Bradford therefore this was the next choice, however, this too failed to dissolve the derivatised sample. The derivatives' lack of solubility in hexane was unforeseen, as its overall polarity was not expected to change significantly with attachment of the CDA. Solvent recommendations for use with (*R*)-(-)-MTPA-Cl and its derivatives were acquired from Merck[170] where toluene, chloroform, dimethyl sulfoxide (DMSO), methyl *tert*-butyl ether (MTBE), dioxane, tetrahydrofuran (THF), or N,N-dimethylformamide (DMF) were advised. The first three were trialled (Table 3.6) but the others excluded due to time constraints and availability. Ideally, solubility trials of the starting material(s) would have been conducted, but limited amounts of product restricted this through trepidation of loss and/or altering the structure(s) prior to derivatisation.

Although there were solvent difficulties, ^{19}F, ^{1}H and ^{13}C NMR data was acquired, but the accuracy of each cannot be verified as analogous studies have not been identified. The complicated ^{1}H NMR spectra does not allow for all peak assignments to be made, but the methods' potential is indicated by similarities between two of the ^{19}F NMR spectra that differ from the (*R*)-(-)-MTPA-Cl starting material. The reaction mixture/sample is believed to be a mixture of diastereomers, DAGs and MAGs; a partial explanation to the complex ^{1}H NMR. Future replication of the method should include additional steps to remove unwanted by-products of the hydrolysis and isolation of

DAGs. Centrifugation would be recommended for lipase removal and preparative TLC for isolating the DAGs/MAGs, which can subsequently be converted to Mosher ester derivatives: solvent purification could also be used as an alternative to TLC. FFAs would thus be removed from the mixture, making determination of the ^{1}H and ^{13}C NMR spectra less complex. Tentative evidence of this effect can be observed in the ^{1}H NMR spectra for the reaction product following solvent trials (see Appendix A.3.1), where the various polarities will have extracted the range of hydrolytic compounds. Solvent removal was performed using the Dri-block solvent evaporator: being an open system, it is assumed the compound and by-products were evaporated along with the solvent. Subsequently, the concentration of the remaining product is decidedly reduced through the multiple addition and removal of solvents, leaving characteristic peaks for the anticipated compound near undetectable; such as the glycerol protons, which would be expected in the range of 4 – 5 ppm. Weak evidence of these can be observed when the spectra is enhanced (data not shown), but it appears that little of the overall sample remains; hence the tentative interpretation of 'purification', as characterisation of the remaining compound cannot be made. Comparing the ^{1}H NMR spectra with that of a sample derivatised and analysed on the same day (see Appendix A.3.2), similarities are observed with three strong peaks between 7.1 – 7.0 ppm and a pentuplet around 2.1 ppm. However, these correlate with the solvent, toluene, and cannot be interpreted as evidence of a diastereomeric compound.

From the ^{1}H NMR spectra alone it is not apparent that a reaction occurred between the CDA and the available *sn* positions of the glycerol following partial hydrolysis; however, a marked difference is observed between the ^{19}F NMR spectra of the freshly prepared sample (Figure 3.10) and pure (*R*)-(-)-MTPA-Cl (Figure 3.8; top spectra), indicating a reaction had proceeded. It should however be noted that interpretation of the spectra is cautious as the product was not fully dissolved.

Mosher ester analysis where the CDA is substituted in the secondary alcohol position has shown the chemical shift of the (*R*) compound to be more upfield

than its corresponding (*S*) enantiomer; achieved through the shielding/deshielding effect of the phenyl[171] (Figure 3.15).

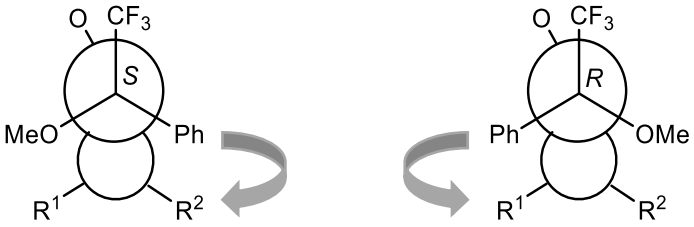

Figure 3.15 Representation of the diastereomeric conformations of Mosher esters where the CDA is attached to the secondary alcohol. The CDA aligns in a planar arrangement, where the phenyl group creates a shielding effect on other substituents of the compound; signified by the grey arrows (adapted from reference[171]).

A similar effect was anticipated for the *rac*-POSt diastereomeric esters. There appears to be an upfield shift for the glycerol protons (see insert of Figure A.5), though this may belong to the by-products and/or impurities. Moreover, three sets of triplets can be observed around 1.0 – 0.9 ppm where the methyl group signal is expected, which could be postulated as evidence of unreacted *rac*-POSt plus (*RR*) and (*RS*) diastereomers. However, without enantiopure standards for reference, peak assignment to the relative (*R*) or (*S*) cannot be achieved. Mori[172] synthesised 1(3)-monopalmitin and used Mosher ester analysis for determination of the (*R*) and (*S*) forms; acylating (*S*)-(+)-MTPA-Cl to the *sn*-1,2 and *sn*-2,3 positions to produce bis-(*R*)-MTPA esters for analysis by ^{1}H NMR. The spectra for racemate shows several signal pairs due to the presence of both diastereomeric esters, with a difference of ca. 0.1 ppm between them, yet it is not clear as to which they belong until they were analysed individually. Similar to previous literature[173], differences in chemical shift for the diastereotopic protons on the primary carbons are noted, thus the observations seen in this thesis may be apt, even if the enantiomeric forms cannot be determined.

On reflection, it would have been beneficial to replicate an established method for stereospecific analysis of TAGs prior to attempting MTPA ester analysis to allow for comparison of results. Specifically, the protocol of Takagi and Ando[53]

who are one of the few groups to have determined CB POSt as racemic (Figure 3.16).

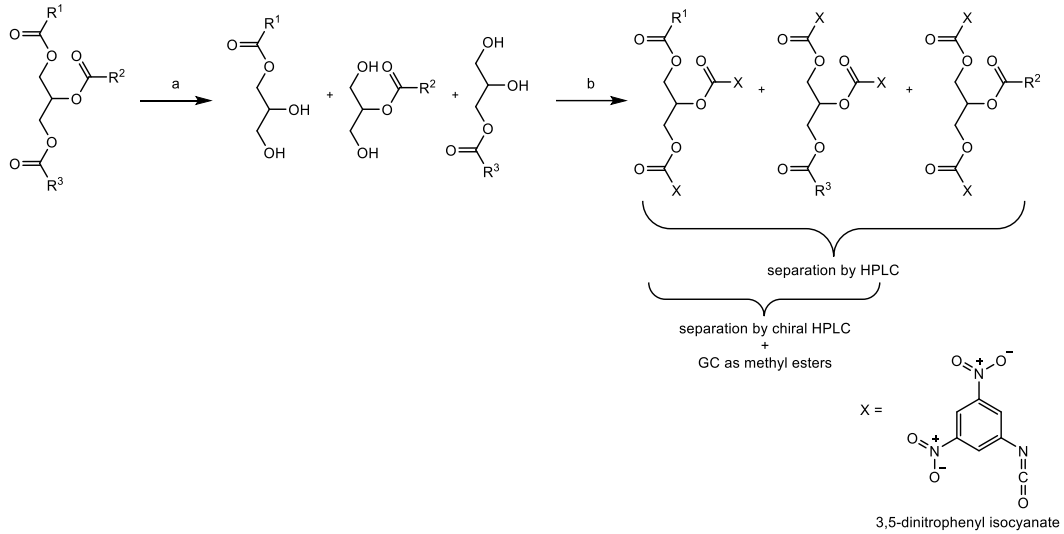

Figure 3.16 Reaction scheme presented in literature for the stereospecific analysis of TAGs[53]. Reagents and conditions: (a) Et2O, EtMgBr; (b) Tol, Py, 3,5- dinitrophenyl isocyanate, r.t. (2 steps).

As discussed in the introduction (1.3.4), such a laborious procedure does not rule out the potential for acyl migration which can give incorrect results, hence the desire to acquire enantiomeric composition by alternative means. Yet, with no direct comparison for results of the Mosher ester analysis, a replication of the stereospecific procedure just discussed would have given a framework of which to assess the accuracy of the work.

3.3 Conclusions

Enantiomeric separation of *rac*-POSt proved to be a substantially difficult task that was unattainable. The inability to source a suitable chiral column led the demand for alternative ways to identify and quantify the enantiomers; a route which was not desirable as it required altering the TAGs' natural conformation. A protocol was established for derivatisation using Mosher ester analysis, but this was inconclusive, though potentially promising following modifications such as the removal of hydrolytic by-products prior to reacting with MTPA-Cl. In purifying the sample, the peaks of the glycerol protons in the NMR spectra

may be more aligned with what has been previously observed[171, 172], allowing easier interpretation of the diastereomeric pairs. A side issue arising from failed CSP trials was the incapacity to isolate pure POSt enantiomer(s) from CB; subsequently to be used for manipulating the natural proportions. As a result, the synthesis of enantiopure POSt became a priority, which is discussed in Chapter 5.

Ultimately, this area of investigation was not able to elucidate the racemate phenomenon in CB through refutation or corroboration of previous research[34, 53, 100]. Consequently, the curiosity is one that remains unresolved.

Chapter 4 *In vitro* analysis techniques for the determination of lipid digestibility

As with most dietary lipids the composition of CB is dominated by TAGs, several of which have a melting point (m.p.) greater than body temperature (37 ^{o}C). Pseudo-lamellar structures have been reported for TAGs up to 40 ^{o}C above their m.p., which may hinder their ability to be digested through the formation of bridge networks that impede emulsification. In order to comprehend the effect of high melting TAGs in the intestinal environment, two approaches were undertaken. The first aimed to investigate the effectiveness of bile as an emulsifier by measuring the progress of lipid droplet sizes in a duodenal solution. Initially, work was conducted using a shaking water bath or vortex mixing of a molten CB and duodenal solution at 37 ^{o}C to emulsify the lipid; where droplet dimensions were to be monitored via confocal laser scanning microscopy (CLSM). Following this, acoustic attenuation spectroscopy using simulated intestinal fluid (SIF) and molten CB was attempted with the purpose of acquiring insight into emulsion development in real time. The second set of experiments used pH stat titration to determine the amount of FFAs released during *in vitro* intestinal lipolysis. CB was melted at 37, 50 and 80 ^{o}C prior to SIF and lipase exposure: temperatures intended to correlate with melting points of various component TAGs. The titration proceeded for 2 hours and the amount of sodium hydroxide released to basify the reaction mixture was used for calculations of FFA release. A fat of similar TAG composition to CB yet with an elevated level of saturation, a cocoa butter alternative (CBA), was analysed under the same conditions and the pH stat profile used for comparison.

4.1 Results

4.1.1 Emulsification of CB in duodenal solutions

A set of experiments were performed to observe the capacity of various solutions to emulsify molten CB; those being $CaCl_2$, bile, bile plus $CaCl_2$ and distilled water. Each were treated under the conditions described in the methods section (2.2.13) and as expected due to large differences in polarity, the water and $CaCl_2$ solutions exhibited distinct phase separation (data not shown): the two bile solutions are presented in Figure 4.1.

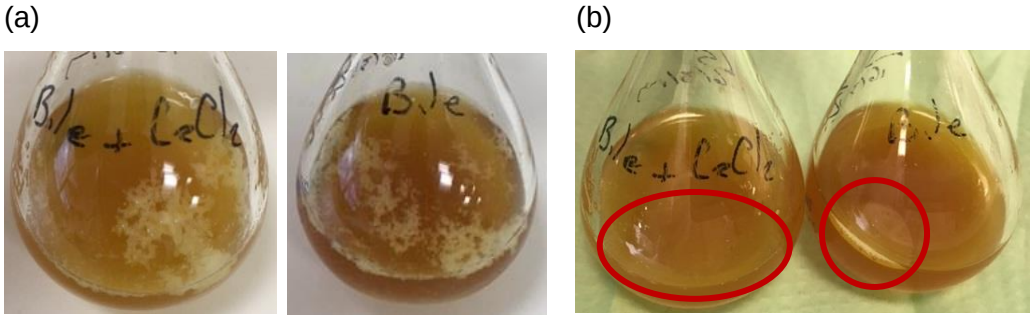

Figure 4.1 Comparison of two CB samples in various bile solutions; bile plus $CaCl_2$ or bile alone. CB was melted at 37 ^oC overnight prior to use and (a) ca. 10 mg added to each flask; (b) samples following 1.5 hours in a 37 ^oC shaking water bath at 80 rpm. Samples on the left-hand side of (a) and (b) contain 7.5 mL bile buffer plus 2.5 mL $CaCl_2$; right-hand samples contain 10 mL bile buffer. Circles highlight the coalescence of CB in the solutions.

Lipid coalescence is evident (Figure 4.1 (b)) and thus, both solutions were ineffective in their ability to emulsify under these conditions. On removal from the water bath, the bile plus $CaCl_2$ solution appeared to have created an emulsion, but as evidenced in the image taken within ca. 5 minutes, this was unstable. The rapid coalescence proved to be significant as the next stage was aimed at measuring progression in droplet size(s) following emulsification under these conditions. However, the shaking water bath used for mixing the phases was inefficient at formulating an emulsion and thus, an alternative procedure was explored where changes in droplet size could be measured in situ, acoustic attenuation spectroscopy.

4.1.2 CLSM measurements for droplet size distribution

Development of a confocal microscopy protocol was undertaken in parallel with static emulsification trials for the purpose of gathering qualitative data on CB in bile suspensions. A crude emulsifier (soap) was used for preliminary analysis of Nile red (NR) stained CB (Figure 4.2). Here it can be recognised that with an adequate surfactant, stained CB droplets can be clearly distinguished from the suspending phase.

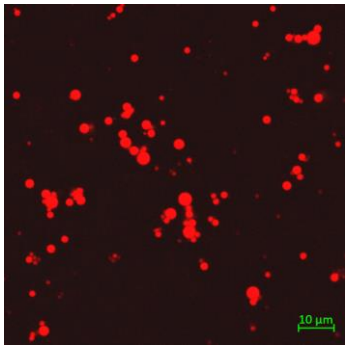

Figure 4.2 CB in water emulsion using washing detergent as the emulsifier. CB was stained using Nile red as evident in the droplets; water was left in its natural state, which is displayed as the black background.

The droplets showed no sign of coalescence for the duration of preparation and analysis. The exact period was not recorded but it is estimated to be over 30 minutes due to the time taken for transferring the sample to the imaging dish then microscope stage, followed by optimisation of the instrument settings for image acquisition.

Fluorescein 5(6)-isothiocyanate (FITC) stained $CaCl_2$ solutions without CB display blanket fluorescence, broken up by rod-like structures in both images (Figure 4.3), which are expected to be $CaCl_2$ crystals.

(a) (b)

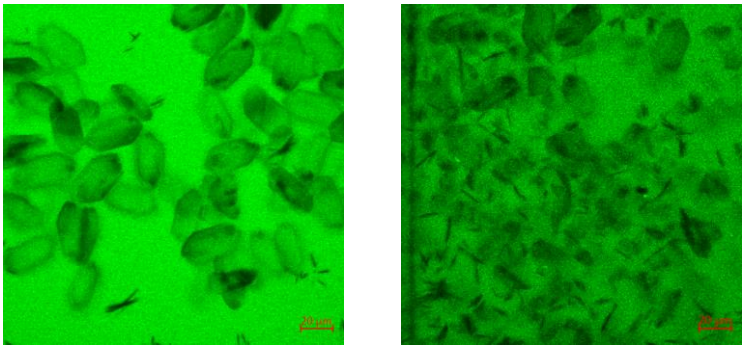

Figure 4.3 Confocal images of the intestinal digesta components stained with FITC (1 mg mL^{-1} in Milli-Q®); (a) $CaCl_2$ as a 1:75 (FITC:$CaCl_2$) dilution and (b) bile plus $CaCl_2$ as a 1:50 (FITC:bile+$CaCl_2$) dilution.

The images appear somewhat identical, aside from a darker hue to that which contains bile solution (Figure 4.3 (b)). The $CaCl_2$ crystals consume more of the frame, which will have prevented light from penetrating as clearly as in Figure 4.3 (a) but it is likely to relate to the bile solution creating an opaque effect.

Trials for the NR stained CB (Figure 4.4) indicate the higher dye concentration (Figure 4.4 (b)) was better for clearer imaging of the lipid. The potential droplet size distribution (DSD) of an emulsion may include minute droplets, as seen in Figure 4.2, and thus it was expected that the 1:100 (NR:CB) dilution would not deliver enough contrast when within a suspending phase. Alternative concentrations were also trialled, 1:50 and 1:150 (images not shown), but the former oversaturated the lipid and the latter had a similar issue of insufficient contrast. The dark areas are assumed to be solidified portions of CB as the imaging was performed at room temperature, estimated to be ca. 20 ^{o}C, and there were no other components present with the ability to produce this effect.

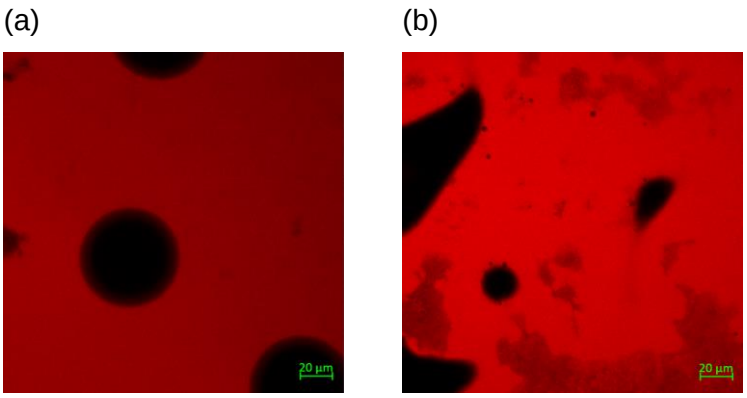

Figure 4.4 Confocal images of the Nile red (1 mg mL^{-1} in DMSO) stained CB at differing dye concentrations; (a) 1:100 and (b) 1:75 (NR:CB) dilution. The visible dark areas are assumed to be partial/fully solidified CB.

The 1:75 v/v (NR:CB) stained CB was used to perform a static emulsification with the aim of imaging the resulting droplet size(s). Using a different approach to earlier attempts at the static emulsification (see section 4.1.1), mixing was performed under vortex on a magnetic stirrer at 37 ^{o}C, rather than a shaking water bath, and using SIF as prepared under the conditions described in 2.2.14.3 (Figure 4.5).

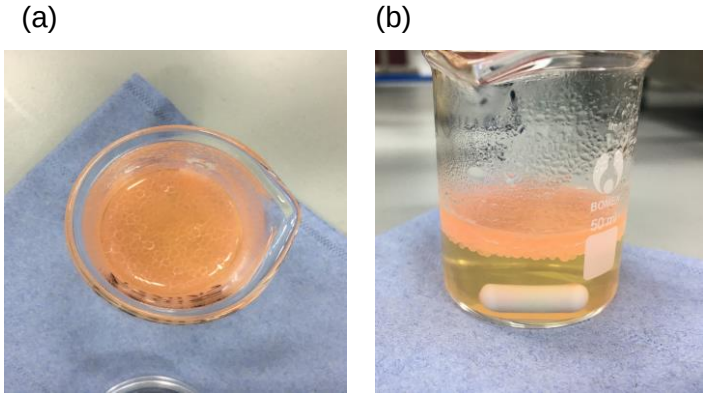

Figure 4.5 Nile red stained CB (1:75; NR:CB) following emulsification in bile solution from an (a) aerial and (b) side view. CB droplets appear to have formed, yet phase separation is evident in the side view.

Although the CB appears to have formed droplets, these proved to be unstable. After transferring the 'emulsion' to a cell culture dish for imaging in the CLSM, the lipid coalesced within ca. 5 minutes, just as in Figure 4.1 (b). Therefore, imaging did not occur.

4.1.3 Acoustic attenuation spectroscopy measurements for droplet size distribution measurements

Following observations that CB droplets formed in bile solution were unstable and incapable of maintaining their shape for long periods, the Malvern Ultrasizer was employed as a means of measuring changes occurring in real time. The instrument has shown previous success in analysing the particle size distribution (PSD) of milk fat droplets[174] and so it was anticipated that it would be capable of the same for CB in bile. A typical appearance of the sample before, during and after analysis is displayed in Figure 4.6.

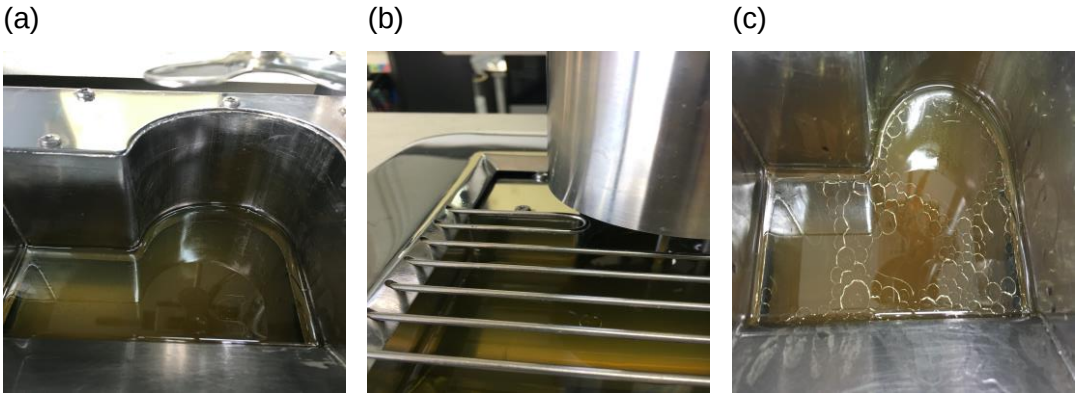

Figure 4.6 Images show CB and bile solution at various stages of analysis in the chamber of the Malvern Ultrasizer; (a) CB melted at 50 °C prior to experiment onset sitting atop the bile solution, (b) CB during analysis with the transducers at minimum range and overhead stirring, (c) CB in bile solution following ca. 3 hours of agitation, with noticeable droplet formation.

The image in Figure 4.6 (c) displays droplets of variable sizes, however, just as in the static emulsification, they were unstable and coalesced shortly afterwards. This experiment was repeated several times with a similar outcome for each.

Information was collected over fifty data points ranging from low to high frequency: Figure 4.7 shows the progression of a CB in bile solution over a 38-minute time frame.

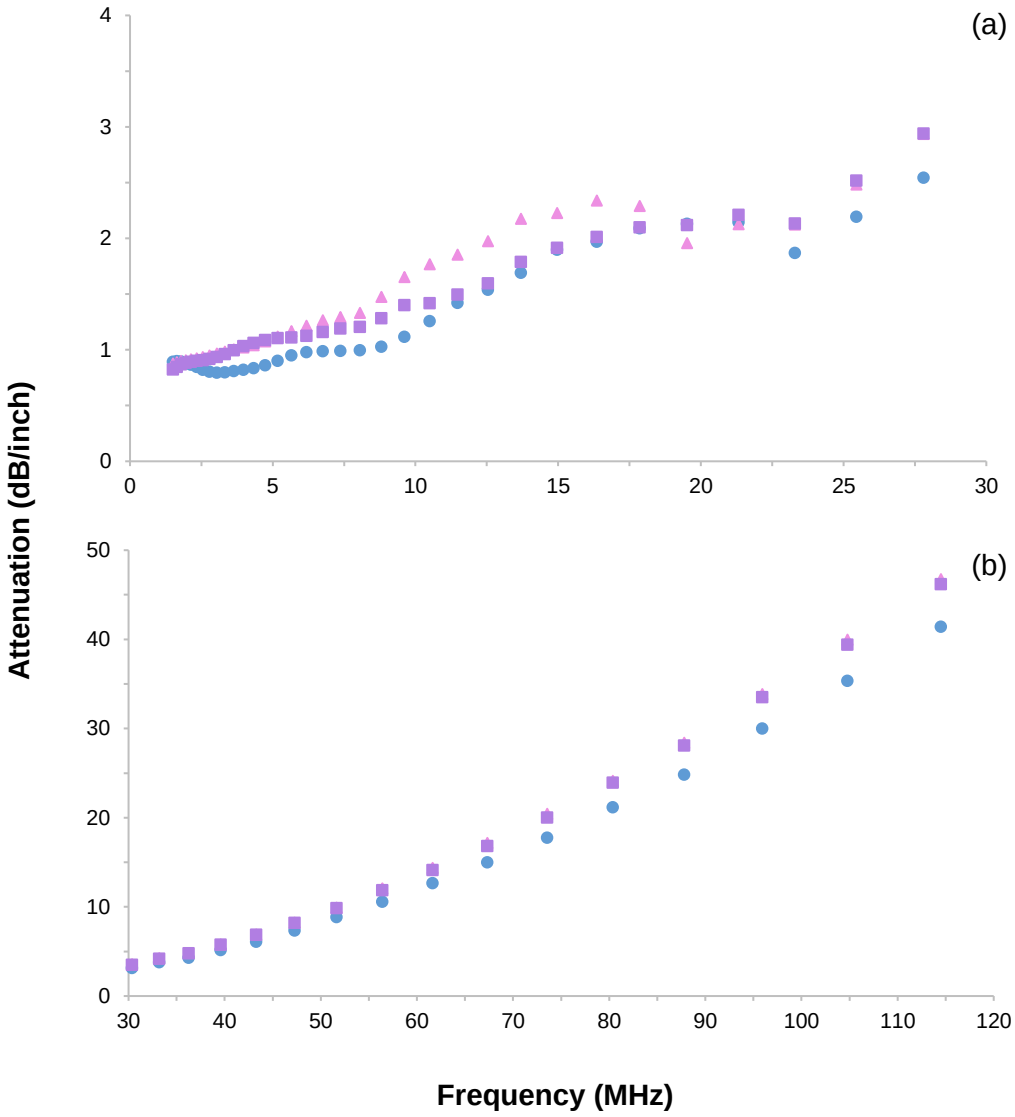

Figure 4.7 Plots of attenuation against frequency for CB in bile solution showing evolution of the sample through (a) low to (b) mid-high frequency. Data represents three sets of analysis out of five collected over a 38-minute period; the primary run (blue circles), median (pink triangles) and closing run (purple squares).

Absence of successful emulsification is indicated by the low levels of attenuation: an enhanced interfacial area would have increased acoustic scattering. There is no evidence of DSD progression between the first and last sample, with each data set being almost identical. The apparent hump between ca. 9 and 23 MHz (Figure 4.7 (a)), is assumed to be a wave of the lipid passing through the transducers' path or perhaps air being drawn into the system. For comparison, Figure 4.8 shows the same plot for Milli-Q® water; the material used to calibrate the instrument due to its high purity. Aside from the marginally elevated attenuation and hump at low frequency for CB (Figure

4.7 (a)), the plot is comparable to Milli-Q®, which contains no measurable particles.

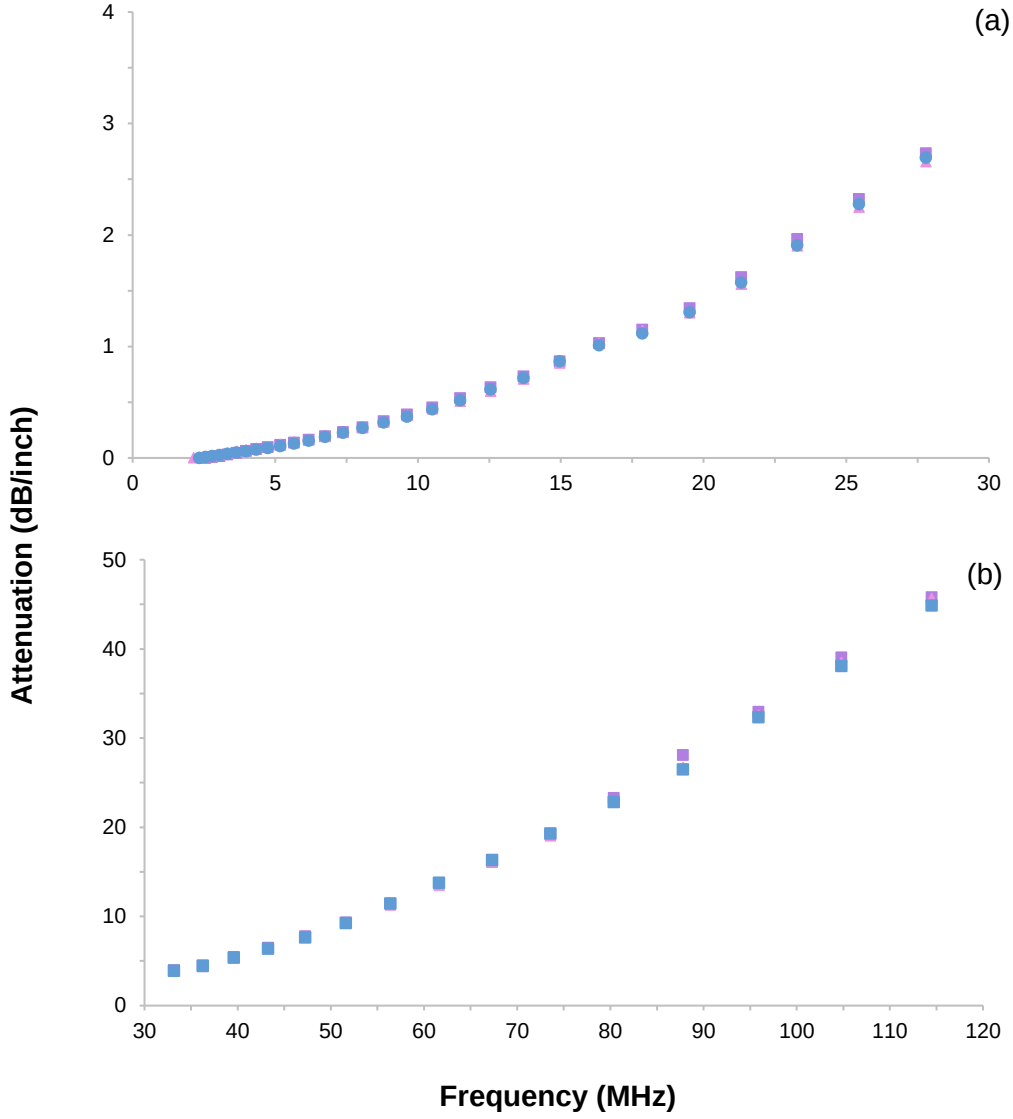

Figure 4.8 Attenuation against frequency plots for calibration material (Milli-Q® water) going from (a) low to (b) mid-high frequency. Both charts contain three data sets represented by blue circles, pink triangles and purple squares: results being near identical.

The inability to collect sufficient DSD measurements, aside from the lack of a stable emulsion, could be due to the differing densities between the aqueous bile solution and CB, causing an upward creaming effect followed by coalescence. Any droplets that may have formed would migrate above the wavelength emitted by the transducers. At 37 ºC, water has a density of 0.9933

g mL^{-1} [175] whereas CB was measured as 0.8947 g mL^{-1}: without sufficient emulsification, phase separation was inevitable.

4.1.4 Lipolysis of CB and CBA using pH stat

Using various initial melt temperatures (T_m) of 37, 50 and 80 °C, CB was analysed using pH stat to determine if the high-melting TAGs had any effect on its ability to undergo lipolysis. The results presented in Figure 4.9 were achieved following the INFOGEST[152] protocol for intestinal conditions.

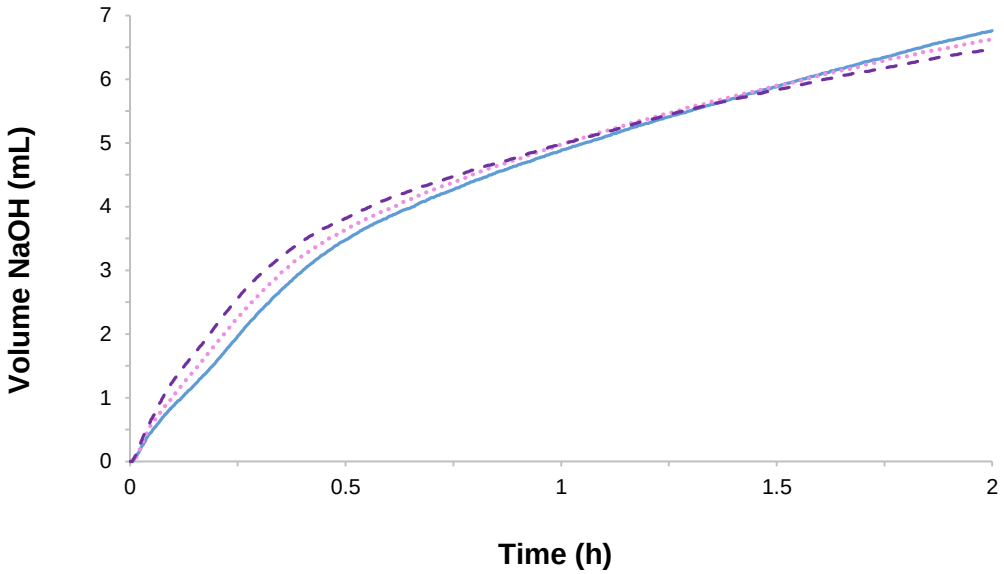

Figure 4.9 pH stat profiles for CB melted at various temperatures; 37 °C (blue solid), 50 °C (pink dotted) and 80 °C (purple dashed) (n = 3).

The moderately slower initial rate of titration for the 37 °C melt may be due to the high-melting TAGs having more solidity in structure, less freedom of movement, and thus the lipase took longer to reach and hydrolyse the ester bond. Differences in the samples can be observed in the images of molten CB (Figure 4.10): the 'solid' portions possibly being StOSt and TAGs with a higher m.p. such as StStSt.

(a) (b)

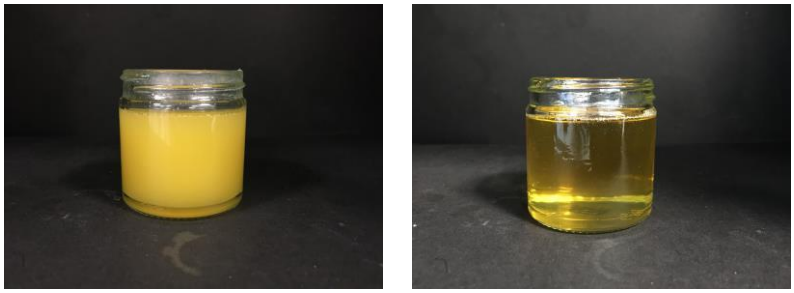

Figure 4.10 Images of CB melted for ca. 3 hours in a water bath at (a) 37 °C and (b) 50 °C. Both samples were fluid but the higher opacity of 37 °C indicates some solid particles remained within the molten fat. CB melted at 80 °C had a similar appearance to 50 °C (image unavailable).

Melting CB at the temperatures specified produced oils of differing viscosities, which likely contributes to their emulsification capacity and thus, the available surface area for lipase activity. An inverse correlation is evident, whereby as the temperature increases, the viscosity lowers and as such, is easier to emulsify the CB. Evidence of this is present in Figure 4.9, where the initial rates of titration increase with temperature.

CB density at 37, 50 and 80 °C was measured using an Anton Paar DMA 4500 M Density Meter (Hertfordshire, England); the results were 0.895, 0.889 and 0.867 g mL^{-1} respectively. pH stat data collected over three replicates for each T_m was used to calculate the percentage of FFA released from the TAGs: the results are displayed in Figure 4.11.

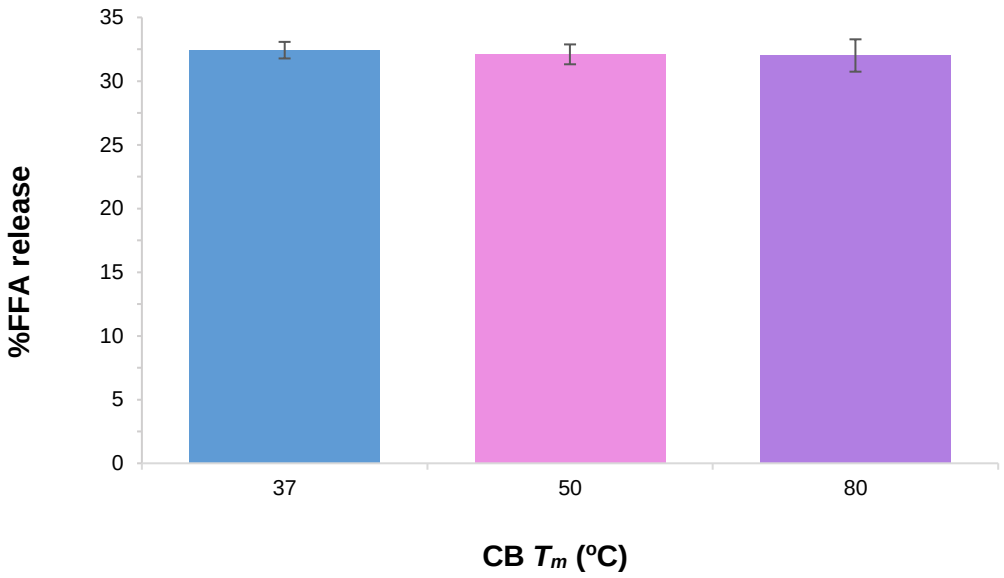

Figure 4.11 Percentage of FFA release for the range of CB melt temperatures after 2 hours under simulated intestinal conditions (n = 3).

The results show similarities between the samples that was unexpected as both the rate of titration and percentage of FFA release were predicted to rise with increasing T_m as a result of high-melting TAGs losing their crystallinity. This is examined further in the discussion.

A CBA was subject to the same lipolysis conditions. The fat consisting of the same component TAGs as CB but a higher proportion of StOSt, along with slightly lower POP and POSt (Figure 4.12). This was determined through HPLC analysis using the method described in 2.2.1.

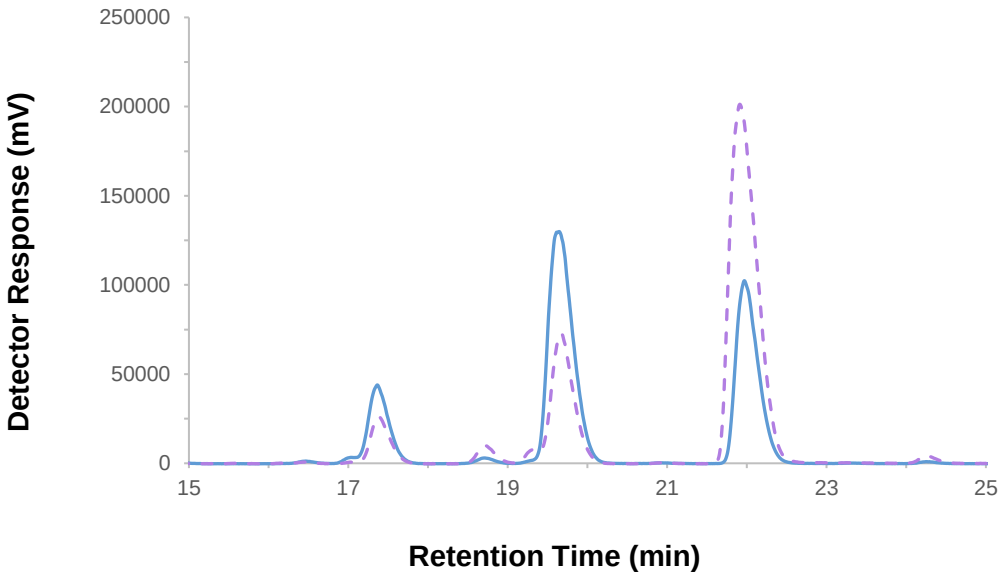

Figure 4.12 HPLC chromatogram comparing the TAG compositions of CB (blue solid) and CBA (purple dashed). Both samples were prepared as 1 mg mL^{-1} in DCM/ACN (3:7, v/v); 20 μL injection. From left to right, the three main peaks correspond with POP, POSt and StOSt. Note, the X axis has been concentrated to improve visualisation of the relevant data; no further peaks were identified prior or after this.

Data acquired in the HPLC analysis was used to calculate the concentration of TAGs in each lipid (Table 4.1): differences between POSt and StOSt being elucidated.

Table 4.1 Concentration of the predominant TAGs in CB and CBA, calculated from the calibration curves.

Lipid	**Concentration (mg/mL)**		
	POP	**POSt**	**StOSt**
CB	0.06	0.23	0.13
CBA	0.05	0.13	0.21

The high StOSt level of the CBA was significant for the lower T_m lipolysis experiment. Following overnight storage in an Incushake at 37 ^{o}C, the fat was semi-solid rather than liquid (Figure 4.13). Considering the m.p. was established as 31 ^{o}C using DSC (see Appendix B.1), this was unforeseen.

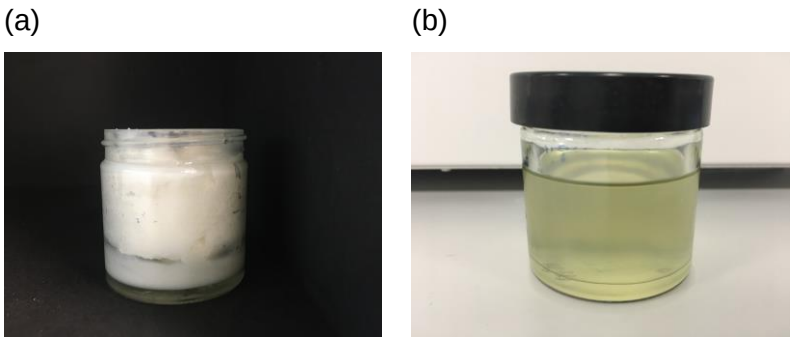

Figure 4.13 CBA melted (a) overnight at 37 °C in an Incushake in comparison to (b) a water bath at 50 °C for ca. 3 hours.

Consequently, it was not possible to pipette 1 mL as with all other samples: weighing was necessary. Three samples were placed into a weigh boat and returned to the Incushake for equilibration. In order of analysis, the weights were 0.243, 0.431 and 0.459 g. Volumes of NaOH titrated were 3.273, 2.425 and 4.598 mL respectively, indicating that the sample weight had no effect on lipolysis for this lipid. A correlation would see the volume of NaOH titration increase with increasing mass due to higher amounts of TAG being present. As expected, the titration rate was significantly lower for the 37 °C T_m due to its inability to be emulsified (Figure 4.14), but the 50 and 80 °C show a similar profile to CB.

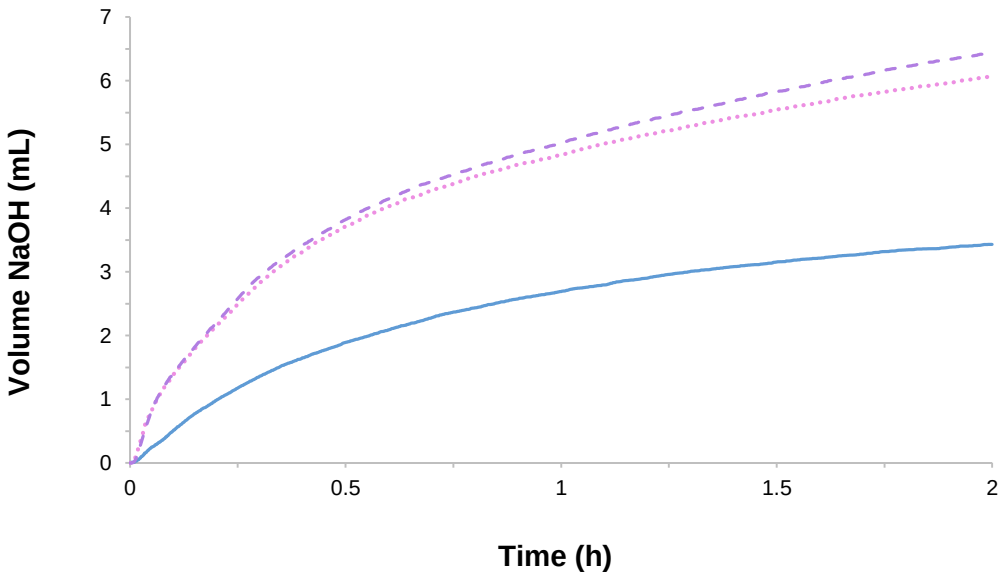

Figure 4.14 pH stat profiles for a CBA melted at 37 °C (blue solid), 50 °C (pink dot) and 80 °C (purple dashed) (n = 3).

When comparing the total NaOH titration between samples (Figure 4.15), the effect of increased saturation can be observed. Although in a similar range to CB, the moderately lower titration volume for the CBA at 50 ^{o}C T_m, may be a result of the StOSt content. It is possible that the TAG developed microcrystalline structures as the lipid equilibrated to the experimental temperature, thus preventing lipase from hydrolysing the *sn*-1/3 stearic.

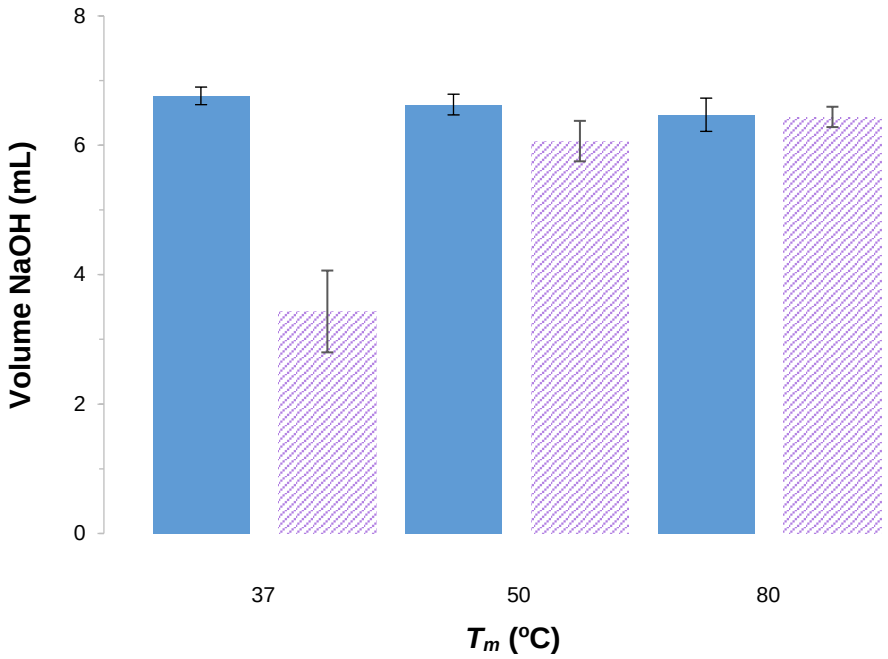

Figure 4.15 Comparison of total NaOH titration between CB (blue solid) and CBA (purple striped) and their various melt temperatures. Each bar represents n = 3 for that condition.

Interestingly, the volumes for 80 ^{o}C T_m are alike, which is expected to relate to all TAG components being fully molten at that temperature and thus, able to be hydrolysed at the same rate.

4.2 Discussion

Measuring droplet sizes as a precursor to the efficient digestibility of CB was founded on research where it was determined the smaller the droplets, the greater level of lipolysis was achieved[176-178]. The controlled formation of emulsions was not desired for this work as understanding the effectiveness of bile at increasing the surface area of CB under *in vitro* conditions was sought;

with the hypothesis that microcrystalline TAGs may be present that would negatively impact small droplet formulation. Lipids are generally consumed in an emulsified form, if not, the forces generated in the environment of the gastrointestinal tract (GIT) encourage this effect to occur. Intentions were to monitor the droplet sizes over time by periodically extracting aliquots for analysis, however, measuring this proved to be an unattainable task. With coalescence occurring after each stirring attempt, it was evident that bile was not acting as a stabiliser under such conditions. Differences in bile solution between those that were mixed in a shaking water bath and those under vortex or overhead stirring made no difference to the outcome. Changing the SIF composition was due to identifying the INFOGEST[152] method: a protocol designed to standardise *in vitro* procedures and thus, deemed to be most appropriate. Sarkar et al.[134] managed to produce bile extract stabilised emulsions that were capable of withstanding centrifugation using soy oil as the lipid component. However, differences are acknowledged in the manner which their emulsions were formulated and those attempted in this work. Their combination of high-speed mixing at 6500 rpm for 3 minutes followed by two-stage homogenisation at 250 bar (stage one) and 50 bar (stage two) to force the oil and bile solution into an emulsion, evidently being successful.

CLSM was to be employed as a means of gathering supportive information on droplet size progression, but the inability of bile to act as a surfactant rendered this technique unnecessary. Therefore, it did not proceed past the initial development stage. The parameters were defined so that had emulsification been successful, differentiation between duodenal components and CB would have been possible using NR to stain the lipid; exemplified by the fluorescence shown in the detergent stabilised sample (Figure 4.2). Dark patches presented in the CB images (Figure 4.4) through solidification at ambient (ca. 20 ^{o}C), appear as though they may have affected the results, but the temperature-control function within the incubation chamber would have been engaged to maintain it at 37 ^{o}C, overcoming this limitation.

Clearly bile is effective as a form of emulsifier or it would not be possible for lipids to be digested *in vivo*, so the inability to form stable droplets in this work

must have arisen from the manner in which the experiments were attempted. Considering the success of Sarkar et al.[134], their combination of high speed mixing and homogenisation clearly has greater efficiency at disturbing the large lipid droplets through turbulence and shear flow[179] than the stirring methods used here. Forces in the biological environment of the GIT appear much reduced in comparison to synthetic emulsification and thus the intention of the experiments in this thesis was not to apply artificial strengths, but attempt to maintain naturality: the duodenum only produces a maximum frequency of eleven contractions per minute[180] which are unlikely to equate to high speeds or pressure. The techniques here used were a shaking water bath at 80 rpm, a magnetic stirrer at 400 – 600 rpm and for the Malvern Ultrasizer, an overhead mixer at 250 – 500 rpm: though unmatched in terms of rpm, only the style of the latter is analogous with the primary mixing stage of Sarkar et al. However, the Ultrasizer results (Figure 4.7) fail to show evidence of emulsification, which could be due to stirring inefficiency and/or relative to the large solution volume in the sample chamber. When merely 10% of the 500 mL total volume consisted of CB, it is possible that any droplets that were formed failed to be captured by the transducers. The instrument has proven its capability in the detection of particle size distribution (PSD)[174], but here it is expected that the relative low density of CB caused an upwards migration of the droplets out of the transducers' path, rendering them undetected. For comparison of attenuation, Meyer et al.[174] discovered the particles in whole milk produced ca. 650 dB/inch at 100 MHz, whereas here it was ca. 95 dB/inch at the same frequency. It is expected that a larger distribution of droplets through effective emulsification would have brought the amount of scattering closer to levels discussed in literature[174]. The data collected through these experiments were insufficient to fit the Epstein Carhart Allegra and Hawley (ECAH) predictive model for droplet concentration that is generally used with ultrasonic attenuation. Several thermophysical parameters are required, which were not available for the phases.

In consideration of the overhead stirring, it was expected that the pitched blade design of the impeller (Figure 4.16 (a)) responsible for creating axial flow, would have been ample to draw CB into the bile suspension due to the strong

vertical current[181] (Figure 4.16 (b)). Conversely, the stirrers' position may have been sub-optimal for effective mixing of this particular blend, contributing to the unfavourable results. Rather than being centralised in the chamber, the impeller is positioned in the crescent shaped area towards the side (Figure 4.6 (a) and (c)), which may be impractical for creating a flow sufficient to mix the entirety of a solution with two phases of differing densities.

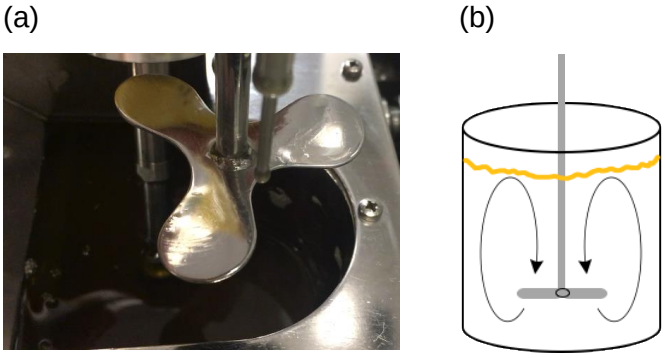

Figure 4.16 Image shows (a) the pitched blade propeller on the Malvern Ultrasizer impeller head and (b) a schematic displaying the axial flow of solution created by the stirrer (adapted from reference[182]).

Regardless of stirring method, it is recognised that imitation of peristaltic mixing and propulsion that occurs in the stomach should be the objective; followed by the effect of forcing the bolus through the pylorus. Early intentions were to use a model stomach as developed by Chen et al.[183] to emulate the retropulsive forces preceding transport from stomach to intestines; however, literature discussing ACW in the stomach[179] states that it is not particularly effective for emulsification and that the forces required to reduce lipids to fine droplet sizes are not capable of being produced. Conversely, the combination of mechanical action and surface active compounds naturally present or released through interaction with human gastric lipase (HGL) is documented as facilitating emulsification in conjunction with transport through the pylorus[135, 140]. As such, it is acknowledged that these phases of the digestive process would have been a beneficial inclusion, but due to the focus on bile salt activity, their significance was underestimated at the time. Through the use of a homogeniser, Sarkar et al.[134] was able to emulate the forces produced via transport across the pylorus passage and provides an account

as to how they were able to create an emulsion stabilised by bile extract. Dispersion through the homogeniser propelled the lipid into fine droplets, successively saturated by bile salts that prevented coalescence through electrostatic repulsion[134].

It was believed the high-melting TAGs in CB could hold their microcrystalline structures at 37 ^{o}C, affecting the fats ability to be efficiently emulsified and subsequently, not fully digested. A concept that has not been established through this work. Recognising the difficulties in DSD analysis, lipid hydrolysis under static *in vitro* conditions was undertaken as an alternative line of investigation. The perception being similar to emulsion analysis in that the 'solid' TAGs at lower temperatures would prevent lipase from cleaving the ester bonds, thus limiting overall digestibility. Though CB has a m.p. of ca. 35 ^{o}C[184] and research states there is no SFC at this temperature[185], it was unclear if the high-melting TAGs would affect lipolysis: the theory being that pseudo-lamellar structures in the melt[147] would restrict their inclusion into the active site of lipase. Literature discusses heating CB to 60 ^{o}C to ensure it is fully molten[185], so some crystalline remnants would be expected below that. Temperatures of 37, 50 and 80 ^{o}C were used to ensure the component TAGs were molten in variable proportions; thinking specifically of StOSt and StStSt. The extreme of 80 ^{o}C being ample to ensure StStSt, the highest melting TAG in CB at 72.5 ^{o}C, is fully molten in its stable β form[184].

As mentioned in the materials and methods (2.2.14.1), $NaHCO_3$ was substituted with Bis-Tris, which acts as a buffer[186], to avoid basification of the SIF solution[187]. When $NaHCO_3$ makes contact with an acid, such as when FAs are released from the glycerol, carbon dioxide (CO_2) is formed which has the potential to react with water to produce carbonic acid (H_2CO_3). For example, palmitic acid with a pKa value of 4.75 reacting with $NaHCO_3$ (pKa 6.3) would liberate it from its salt[188] (Eq.(5)); followed by an equilibrium reaction with CO_2 and H_2O[189] (Eq.(6)).

$$CH_3(CH_2)_{14}CO_2H + NaHCO_3 \longrightarrow CH_3(CH_2)_{14}NaCO_2 + CO_2 + H_2O \quad (5)$$

$$CO_2 + H_2O \rightleftharpoons H_2CO_3 \rightleftharpoons HCO_3^- + H^+ \quad (6)$$

The generation of H_2CO_3 is unfavourable as the subsequent dissociation to hydrogen (H^+) and bicarbonate (HCO_3^-) ions is possible, causing an increase in solution pH[190]: the more CO_2 that is produced, the greater the effect. In a method that is based on responding to sensitive changes to the ionic environment, inaccurate results would ensue through reduced NaOH titration, hence the buffer substitution.

Observations of pH stat profiles (Figure 4.9) and percentage of FFA release (Figure 4.11) show similar patterns for each T_m. It was believed the higher T_m would achieve a greater value, but with each of the three states releasing ca. 32% FFAs, a high portion of TAGs remain intact after two hours under intestinal conditions for all. With an area percentage of ca. 27.9[191] and 44 °C m.p., StOSt was expected to show greater influence on total lipolysis between 37 and 50 °C than it did. This could be due to its minimal presence in comparison to the overall volume. In 51 mL of solution (50 mL SIF; 1 mL CB), no more than ca. 280 μL would have contained StOSt, and thus likely that it dissolved amongst the liquid solution[192]. It is worth noting that this is a basic calculation based on the 1 mL volume of CB: the minor components also present will accommodate a portion of that and so the actual volume of StOSt will be less, but not substantially.

Initial titration rates increase with T_m; however, this is not expected to be linked with melting of particular TAG species, but likely viscosity reduction in relation to increasing temperature[193]. The lipids' lower viscosity at 80 °C allows for enhanced incorporation into SIF under vortex mixing than 37 and 50 °C: being quicker at forming a temporary emulsion. Consequently, bile can act upon the droplets sooner, thus facilitating the anchoring of lipase/co-lipase. It is not apparent as to why the 50 and 80 °C slowed to a similar rate of FFA release as 37 °C, but an inverse relationship between T_m and total TAG is observed, which is assumed to bear a correlation. The molarity for each T_m was calculated to be 1.043, 1.033 and 1.011 mmol for 37, 50 and 80 °C

respectively. As CB equilibrated to the experimental temperature, the viscosity is expected to have become comparable between samples, producing similar emulsification abilities. Subsequently , the amount of available TAG became of greater relevance rather than the emulsification capacity: with reduced molarity in the higher T_m, there is less opportunity for lipolysis to occur. It must be acknowledged that the M_w calculation for CB was based on the CoA for IRMM-801 reference material[191]. The variety used in the experiments is likely to have a different value, but it is not expected to be significant.

It is considered that the presence of lipolytic by-products such as MAGs and FFAs may be a contributory factor to the low FFA released and perhaps the eventual similarities in rate of basification. Their inclination to adsorb to the droplet surface creates competition for lipase; a difficult situation to overcome with diminished bile activity. The incorporation of FFAs and MAGs into mixed micelles creates a depletion in available bile and as a result, the displacement of components from the interface lessens, affecting the rate of emulsification and/or lipolysis[194]. Furthermore, the development of insoluble Ca soaps from liberated palmitic and stearic acids act as an additional obstruction[195]. Their arrangement into crystalline structures create a resistance to micellar uptake and as such, may have become an impediment to the displacement activity of bile. Under *in vivo* conditions these products would be removed through transport across the intestinal wall (micelles) or via peristaltic action along the intestinal tract (soaps)[196].

Day-to-day consumption of CB would be within a food matrix, likely to be chocolate, though not exclusively. As discussed in the introduction, CB is the continuous phase in chocolate whereby particles such as sugar and cocoa powder are suspended with the aid of an emulsifier such as lecithin[1, 14]. Considering this in conjunction with the mechanical and biophysical interactions occurring throughout the digestive process, along with the findings of this work, it can be concluded that high-melting TAGs have no effect on the ability of CB to be adequately digested *in vivo*, corroborating previous research[146]. However, when looking at the CBA with StOSt as its largest TAG fraction and thus semi-solid at body temperature, its crystalline form restricted

lipolysis at 37 ^{o}C. The mass was unable to be emulsified/broken down into micelles, which is a key stage to lipolysis[142]. When the T_m was increased sufficiently to ensure the StOSt fraction was molten, lipolysis proceeded analogously with CB.

Prior to these experiments, the level of StOSt in the CBA was not expected to present melting and subsequent lipolysis difficulties at 37 ^{o}C. DSC analysis (see Appendix B.1) was conducted to determine m.p. following a temperability protocol, where the lipid was encouraged into the stable β_V polymorph. Sample sizes of 1.326 and 2.000 mg gave m.p. values of 31 and 33 ^{o}C respectively. Here the effect of sample weight can be observed where that which is larger requires more heat to disrupt the crystalline form and induce phase transition from solid to liquid. For comparison, 1.357 and 1.500 mg of CB had respective values of 27 and 30 ^{o}C, similar to those achieved by van Malssen et al.[96] (29.4 and 30.5 ^{o}C). Considering this, it can be estimated that the higher m.p. established for both fats are more accurate, which should have determined the CBA as being fully molten for all pH stat conditions. Crystallisation was not controlled or monitored prior to the experiments, but it is reasonable to assume that the β_V form was achieved through the Ostwald ripening process and that each T_m sample will have been in the same polymorphic form as they were stored under identical conditions. A caveat to this theory would be their storage under ambient conditions: seasonal variations in temperature are likely to have caused portions of the lipids to melt and recrystallise. Consequently, a variety of polymorphic forms may have been present. However, it is speculated that transition into β_{VI} form occurred as the lipids were resting for a prolonged period. With a reported β_{VI} m.p. of 36 ^{o}C[94] for CB, this would not affect its ability to melt at body temperature as seen here, but for the CBA this m.p. is not known and may be causation for the low T_m results.

4.3 Conclusions

For bile salts to be effective emulsifiers/surfactants, the manner in which they are used must be representative of the processes that occur *in* vivo. Each stage of digestion from mastication through to duodenal peristalsis contributes to the breakdown of lipids and should not be neglected in experimental procedures. Attempting a 'simple emulsification' using raw lipid and SIF does not consider the complex mechanical and biophysical interplay that occurs and as such, saw the attempted measurements of changing DSD as ineffective.

Similarities were observed for the total FFA released for CB at various melt temperatures, indicating no effect of microcrystalline structures on lipolysis. However, the reduced amount of TAG as melt temperatures increase is likely a factor in the apparent similarity. It would therefore be interesting to repeat the analysis by CB weight, rather than volume, to achieve a similar amount of TAG in each sample; e.g. 1 g of CB for all conditions. Enantiomer determination and synthesis had to take precedence in this thesis, which limited focus that could be placed on the digestion aspect of the work. Nonetheless, this appears to be the first study to have investigated variable melt temperatures on total lipolysis and rate of FFA release. Further studies are suggested to compare the effect of saturation and crystallinity by using alternative lipids such as sunflower oil and various CBAs.

Chapter 5 Synthesis of triacylglycerol enantiomers: transesterification and chemoenzymatic methods

For studies on enantiomeric composition, enantiopure reference standards are required, yet such specialist compounds are not readily available to purchase commercially. The demand for which in this project was three-fold; for use as standards in chiral HPLC, the definition of crystallisation and polymorphic behaviour of binary blends using m.p. determination and lastly, for modification of the natural ratio in CB. Enzymatic synthesis protocols were undertaken by way of transesterification and chemoenzymatic means. Transesterification was performed under two conditions; in batch and using a continuously recirculating instrument with solid supported lipase in a packed bed reactor. Aliquots of the reaction material were gathered at several time points where the progress of new compounds was monitored via HPLC. A more tailored approach to the formulation of enantiopure (*R*)-POSt was a multi-step chemoenzymatic procedure involving protection/deprotection of the glycerol moiety for systematic introduction of acyl groups. Using (*R*)-(+)-3-benzyloxy-1,2-propanediol as starting material, the three-dimensional arrangement of molecules around *sn*-2 is pre-defined, thus ensuring synthesis of the target chiral compound. In an anhydrous environment, vinyl esters were esterified to the starting material using an *sn*-1/3 specific lipase; ensuring an irreversible reaction due to rapid tautomerization of the vinyl alcohol by-product to its aldehyde[130]. Removal of the benzyl protecting group was performed under pressure using catalytic hydrogenolysis in a small-scale reactor (fReactor) for the first time, thus introducing a novel technique for dealing with practical volumes of reaction material during method development. The reaction stages were monitored via ^{1}H, ^{13}C and COSY NMR.

5.1 Results

5.1.1 Analytical method development for recognition of transesterification products

Defining an analytical procedure for the products of transesterification was necessary for monitoring reaction success. Substrates chosen for this purpose, MCT oil and Et-Pa, were used to determine a HPLC method. This was completed in several stages to clarify the optimum conditions for separation of components; beginning with variable dilutions of MCT oil to ascertain the instruments behaviour towards the compound. Each of the chromatograms discussed for the development can be seen in Appendix C. Of the three dilutions trialled, the strongest (1:10) achieved the best signal and defined the required intensity for analysis of the compounds. Negative dips in the baselines were evident for the 1:100 and 1:1000, which did not stabilise until ca. 6 – 8 minutes, followed by barely visible peaks in the latter (data not shown). Peak front tailing is present in the 1:10 and 1:100 dilutions, of which the reasons are unclear. Sample concentration is known to be a factor in this occurrence[197], but those used here are not expected to have an influence. It was assumed to be an issue with the column, but as the peaks show adequate separation, the flaw was deemed acceptable.

Detection of four peaks in MCT oil during stage one occurred in less than half of the programmed run time. Subsequently, stage two proceeded as endorsement that reducing the run time would produce the same level of detection. Analysis time was halved, yet peak detection remained: Et-Pa analysis under these conditions was also efficient. Combining the substrates (MCT 0.38 mmol; Et-Pa 0.33 mmol) for stage three established no peak overlap; confirmation that changes to any of the substrates during transesterification would be detectable.

Moving analysis to an alternative system (stage four) for reasons of practicality and accessibility, required further trials to establish if the protocol would be adequate with the instrument and ELSD as the detector. Insufficient peak

separation was evident with the Supelco Ascentis column (Figure 5.1 (a)), but adequate with the Waters Symmetry (Figure 5.1 (b)) due to the longer length allowing the compounds more interaction time with the stationary phase.

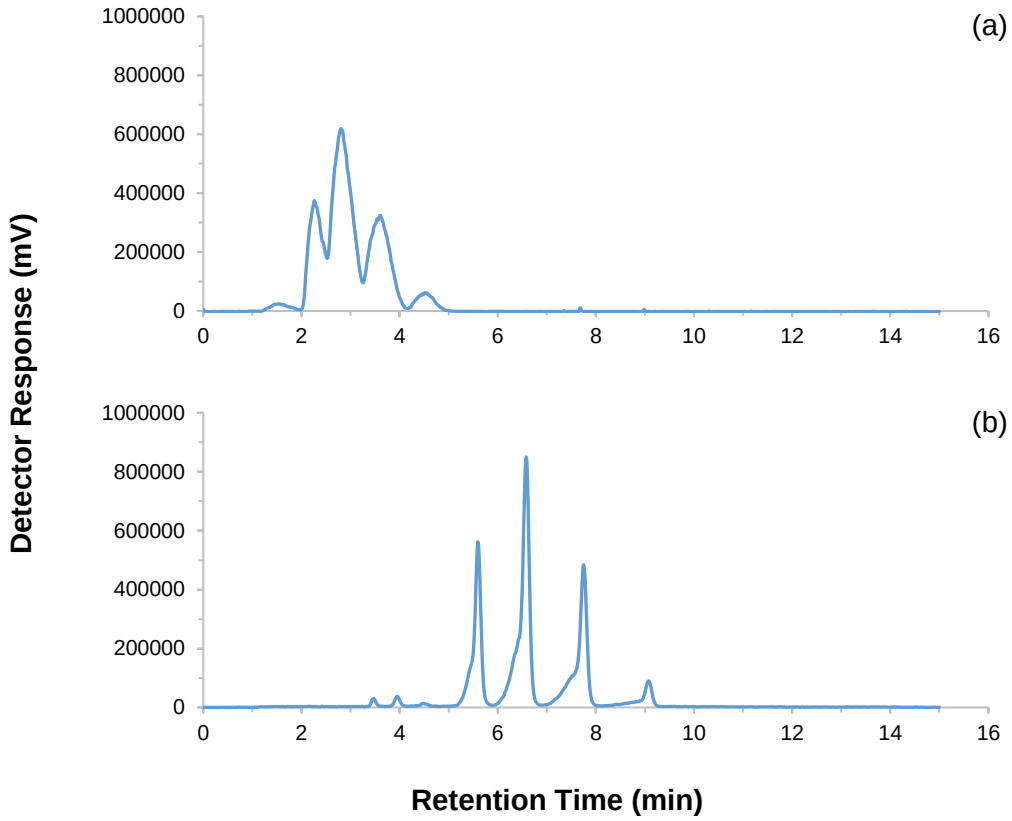

Figure 5.1 HPLC analysis of MCT oil by means of ELSD detection on a Shimadzu Prominence system using (a) the Supelco Ascentis column with 0.5 mL min^{-1} flow rate and (b) Waters Symmetry column with 1 mL min^{-1} flow rate. Conditions as described in 2.2.6 (stage two).

5.1.2 Transesterification: stirred batch experiment

The reaction product of 24 hours under SBE conditions failed to dissolve in MeOH, the solvent used throughout development. On returning to the original substrate vials following storage at 4 ^{o}C, it became apparent that this was the case (Figure 5.2).

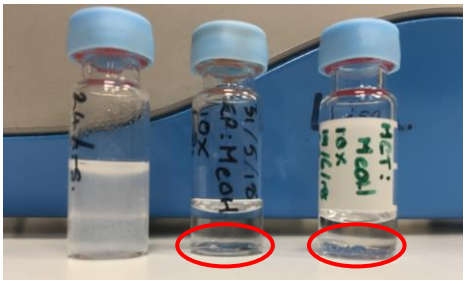

Figure 5.2 Image shows the 24 h SBE product with evident phase separation (left), Et-Pa (centre) and MCT oil (right); all prepared in MeOH as 1:10 dilutions. Droplets are visible in the circled portions, evidence of substrate insolubility.

This effect had not been previously identified; thus, it is possible that the substrates precipitated out of solution at low temperature. Irrespective of this, the reaction product was not dissolving, and an alternative solvent was required. Both the product and substrates were successfully dissolved in DCM/ACN (3:7, v/v) and analysed using the Kadivar et al.[121] method as described in section 2.2.1: Figure 5.3 shows analysis of the substrates, with the method being largely successful.

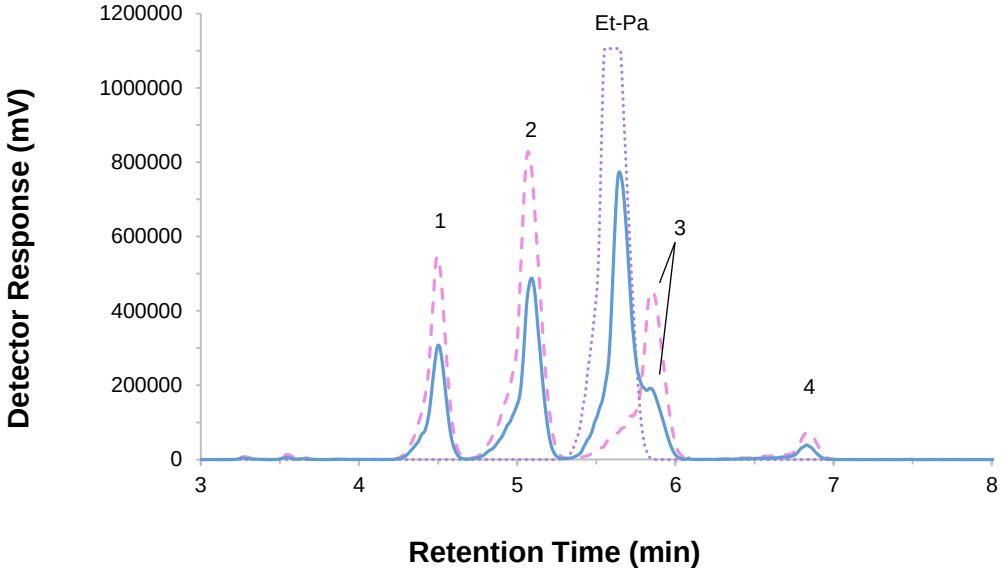

Figure 5.3 Peak identification of the starting materials (MCT oil and Et-Pa) and a combination of both. MCT oil (pink dashed; peaks 1-4) and Et-Pa (purple dotted) were prepared as 1:10 dilutions; MCT oil plus Et-Pa (blue solid) present as 1:10 dilution. DCM/ACN (3:7, v/v) was used as the solvent and analysed using the Shimadzu Prominence HPLC system with ELSD; column was the Waters Symmetry C18. Analysis was performed over 33 min, but the baseline remained stable after 7 min, hence the condensed X axis for improved graphic of the peaks.

Some co-elution of MCT and Et-Pa in the mixed sample is observed (blue solid), but the data overlay allows the third peak of MCT/Et-Pa to be determined as Et-Pa and the 'shoulder' as the third peak of MCT oil. This is confirmed through the specific t_r of each peak (Table 5.1).

Table 5.1 Peak retention times for the transesterification substrates analysed individually and the combined sample (n = 3).

Sample	**Peak number and t_r**				
	1	**2**	**Et-Pa**	**3**	**4**
MCT	4.49 ± 0.01	5.06 ± 0.02		5.84 ± 0.02	6.84 ± 0.02
Et-Pa			5.61 ± 0.02		
MCT/Et-Pa	4.50 ± 0.01	5.08 ± 0.01	5.64 ± 0.01	5.81 ± 0.03	6.83 ± 0.02

TAG configurations of the MCT oil have been estimated using the manufacturers' specification sheet[198]. Full details of their composition were not stated and unable to be determined analytically: liquid chromatography mass spectrometry (LCMS) using electrospray ionisation was attempted but hindered by the inability of TAGs to readily ionise[48] (data not shown). The TAGs were reported as caprylic/capric (C8:0/C10:0), with FAs in the proportion of C8:0 59.5% and C10:0 40.4%: minor FAs representing <0.1% of the total composition were also described. With uncertainty in the full composition, the oils' M_w could only be estimated; achieved by calculating tricaprylic as 59.5% of the lipid and tricapric as 40.4%. However, four possible TAG combinations have been predicted (Table 5.2), which correlate with peaks 1 – 4 in Figure 5.3 and Table 5.1. Estimations do not take the minor FAs into consideration.

Table 5.2 Estimated TAG composition of MCT oil calculated from the specification sheet data. TAGs are listed in order of molecular weight, which is expected to correspond with their order of elution.

TAG	Molecular Formula	Molecular Weight ($g\ mol^{-1}$)
Tricaprylic	$C_{27}H_{50}O_6$	470.69
1,2-dicaprylic-3-capric	$C_{29}H_{54}O_6$	498.75
1,2-dicapric-3-caprylic	$C_{31}H_{58}O_6$	526.80
Tricapric	$C_{33}H_{62}O_6$	554.85

The increasing chain lengths and subsequent molecular weights are inversely correlated to their polarity. Thereby, tricapric has a greater affinity for the columns' non-polar stationary phase than tricaprylic and will be the last to elute.

Observations of the SBE over the 9-day experimental period (Figure 5.4) displays significant changes overall. The most apparent occurring after the first 24 hours, with five new compounds of higher saturation appearing (i-v), indicated by their longer t_r. Though the number of synthesised compounds to be produced was unknown, elevated saturation levels were anticipated due to the substitution of caprylic/capric acid(s) with palmitic acid (C18:0). The potential TAGs synthesised in the reaction have been predicted (Table 5.3), which correlate with the chromatographic data in Figure 5.4 and are expected to elute in order of increasing molecular weight. An elution order that corresponds with increasing carbon number has previously been reported by Xu et al.[199] who used MCT oil and oleic acid as substrates in a PBR. The appearance of peak vi, which is assumed to be tripalmitin, would be an indication of significant acyl migration where 8:0 and/or 10:0 from *sn*-2 has relocated to *sn*-1/3, followed by an 18:0 migrating from *sn*-1/3 to *sn*-2: acylation of further C18:0 to the external position(s) continuing until the TAG was complete.

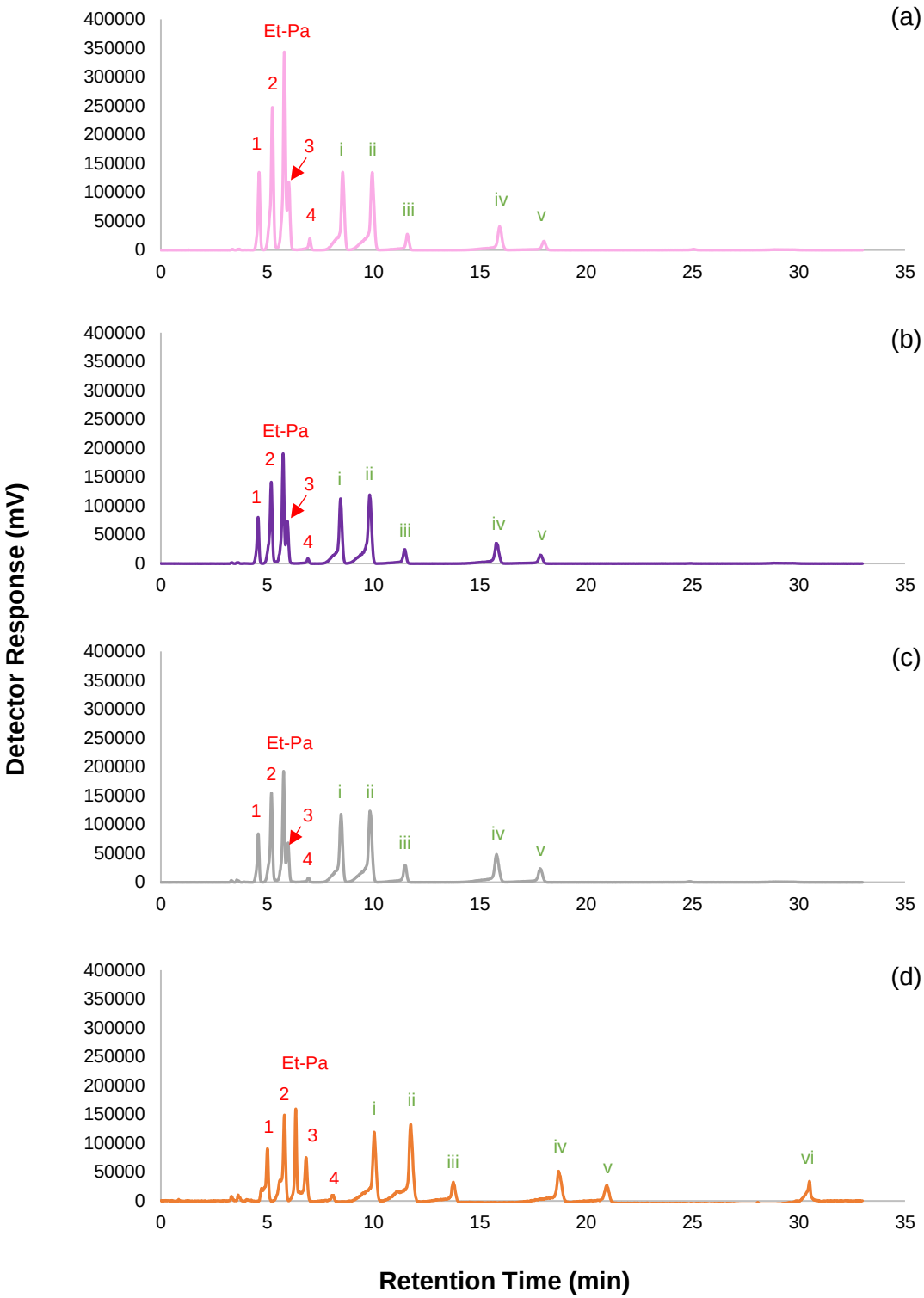

Figure 5.4 Aliquots of batch reaction mixture taken at various times; (a) 24 h, (b) 49 h, (c) 6 days and (d) 9 days. Peaks 1 – 4 refer to those initially identified in the MCT oil (Figure 5.3); Et-Pa has been labelled accordingly. Peaks identified with Roman numerals are those produced through the transesterification reaction. Analysis was conducted using a Waters Symmetry column using the method and equipment as described in section 2.2.1.

Table 5.3 Potential TAGs produced through transesterification in ascending order of molecular weight.

TAG	Molecular Formula	Molecular Weight ($g\ mol^{-1}$)
1-palmitin-2,3-dicaprylic/1,3-dicaprylic-2-palmitin	$C_{35}H_{66}O_6$	582.91
1-palmitin-2-caprylic-3-capric	$C_{37}H_{70}O_6$	610.96
1-palmitin-2,3-dicapric/1,3-dicapric-2-palmitin	$C_{39}H_{74}O_6$	639.02
1,3-dipalmitin-2-caprylic/1,2-dipalmitin-3-caprylic	$C_{43}H_{82}O_6$	695.12
1,3-dipalmitin-2-capric/1,2-dipalmitin-3-capric	$C_{45}H_{86}O_6$	723.18
Tripalmitin	$C_{51}H_{98}O_6$	807.34

Aside from the reduction in substrate concentrations between 24 and 48 hours (Figure 5.4), it appears that no further changes are occurring until 9 days. However, the AUC plot (Figure 5.5) shows subtle changes, particularly in new compound growth, helping to elucidate sample changes over time. The t_r shift observed in the 9-day spectra (Figure 5.4 (d)) may be an indication of alternative compounds than those predicted. Considering the extended reaction time and known acyl migration over long periods, this is a distinct possibility. However, t_r drifts have been observed with this instrument in other work and thus, the peaks have been tentatively assigned as in the other chromatograms.

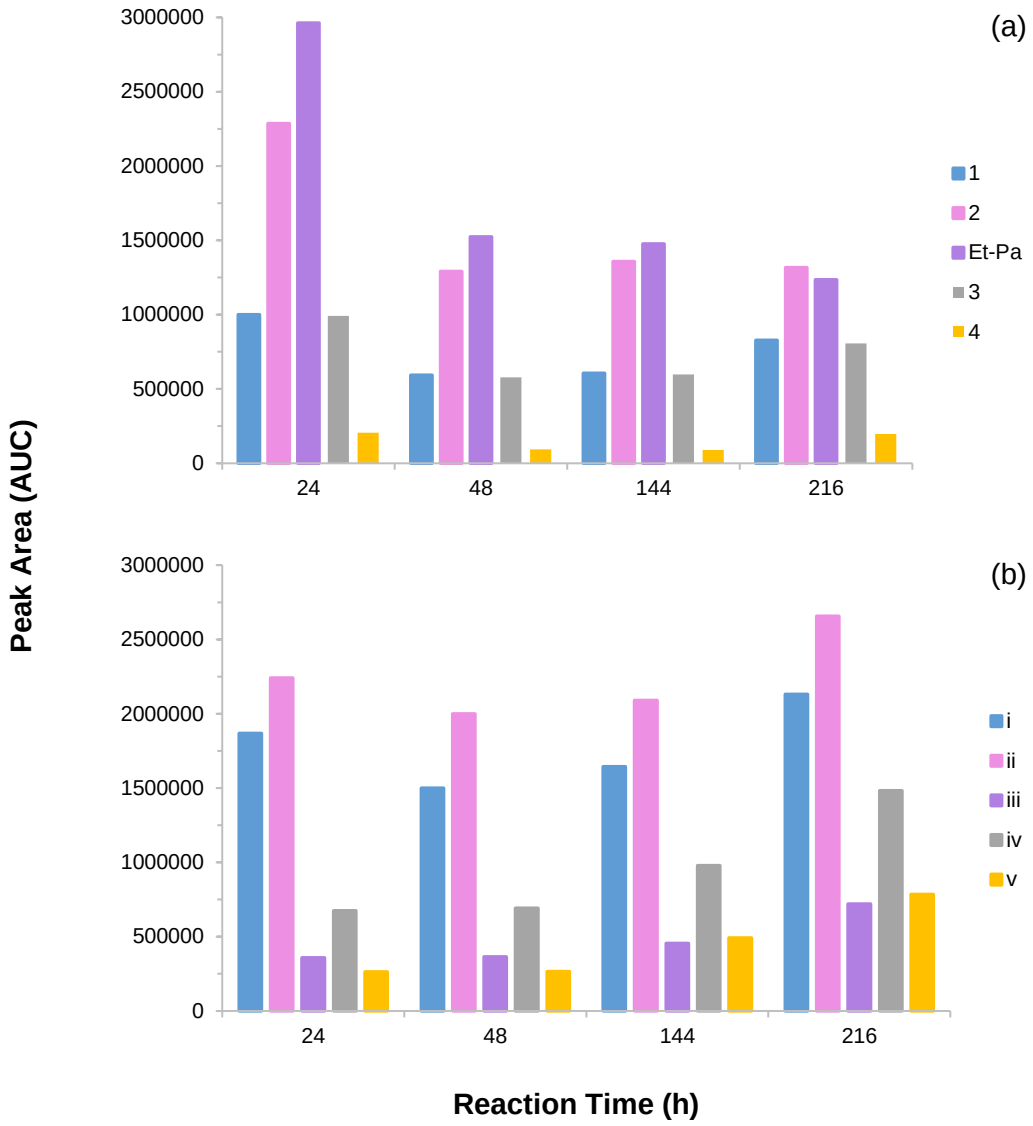

Figure 5.5 Changes in the SBE material over the reaction period of 9 days, (a) displaying a reduction in Et-Pa and potential TAGs of MCT oil; (b) a steady growth in the amount of synthesised compounds.

It is possible that the increase in AUC for some of the MCT oil peaks (1 – 4) is due to enzymatic acidolysis and/or interesterification as the compounds are repetitively exposed to lipase over the period: in addition, there is the acyl migration possibility as discussed[128, 129]. The observed increase for peaks i – v (Figure 5.5 (b)) providing evidence that the reaction can be driven towards the synthesis of new compounds when using ethyl esters as substrates; reinforced by the AUC reduction of Et-Pa.

5.1.3 Transesterification: continuous flow

To improve transesterification efficiency, a continuously recirculating system was trialled. Initially without temperature control of the CSTR (Figure 5.6), but the heating block was maintained at 50 ^{o}C to prevent column blockages by ensuring the substrates remained liquid during transportation.

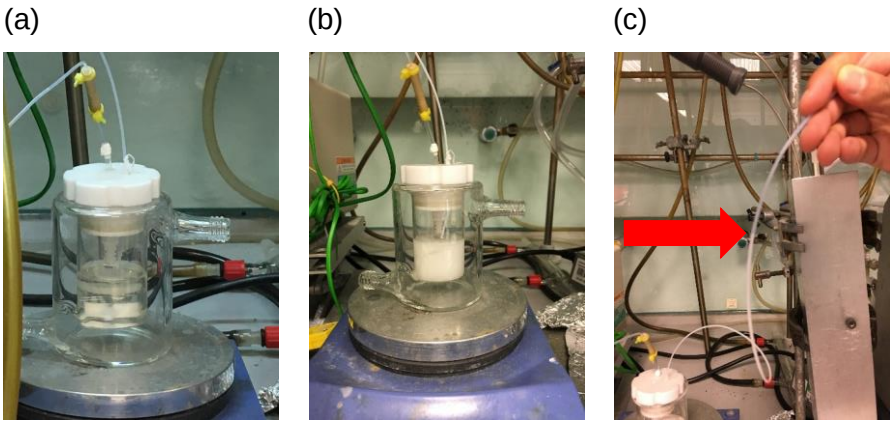

Figure 5.6 Images of initial continuous flow experiment at (a) onset showing an equal volume (11 mL each) of the MCT oil (20.66 mmol) and Et-Pa (33.13 mmol) in liquid form; (b) semi-crystalline solution after ca. 24 h reaction time; (c) solidification of product in column exit line, indicated by the block arrow.

Visually, it was evident that changes had occurred in the sample but solidification in the tubing caused the experimental run to be terminated. Nonetheless, HPLC analysis of the reaction product (Figure 5.7) showed that in the run time of ca. 24 hours, a similar profile to the SBE had been achieved. Indications of a further compound, labelled as vi, can be observed around 10 minutes where splitting of peak ii has occurred. The peak is assumed to be a DAG formed from one of the higher molecular weight TAGs.

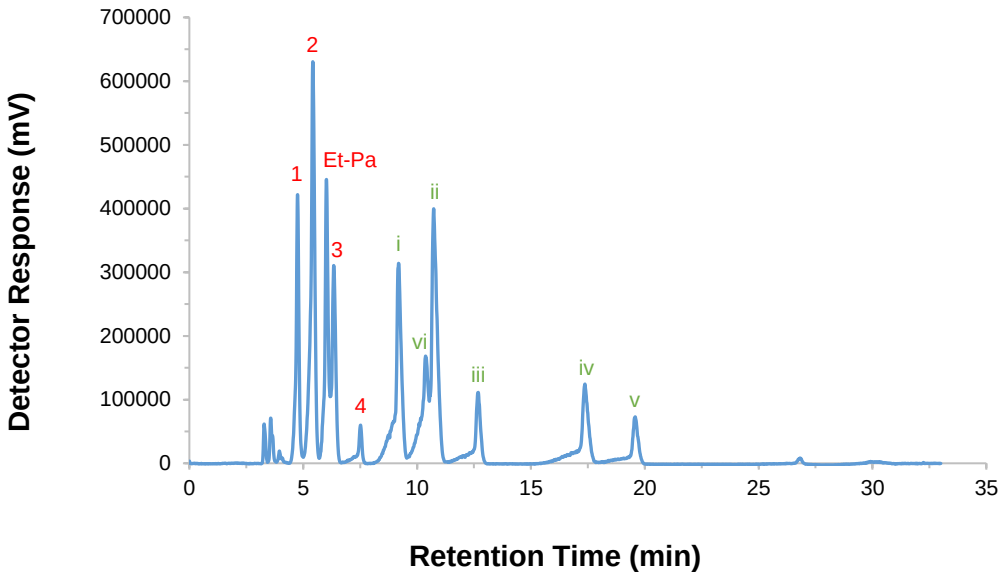

Figure 5.7 Product of transesterification in continuous flow system after ca. 24 h reaction time; prepared as a 1:10 dilution in DCM/ACN (3:7, v/v).

Successful results using MCT oil signified this could be substituted with trioleate (OOO). Alongside Et-Pa and Et-St, this was to be the starting material for production of enantiopure POSt. A preliminary experiment at ambient using Et-Pa and OOO was conducted (Figure 5.8).

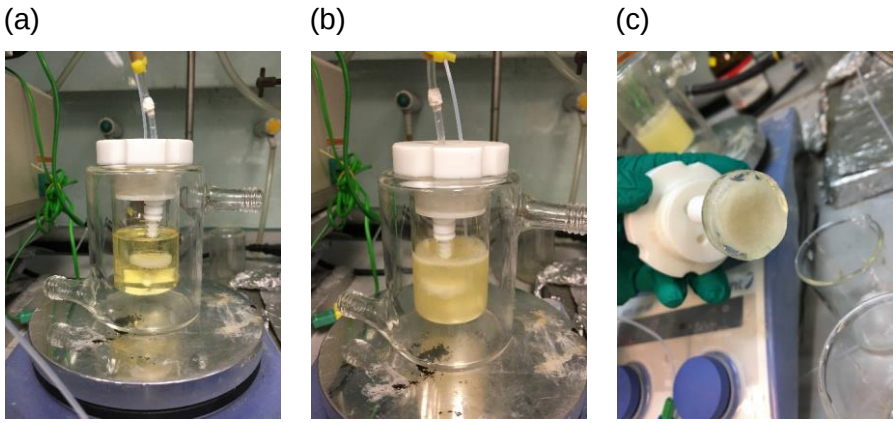

Figure 5.8 Trioleate (30.8 mmol) and Et-Pa (6.02 mmol) substrates at (a) the initial point of the ambient experiment and (b) after ca. 5 h, (c) displaying solidification around the outlet frit.

Following a relatively short period in the system, the experiment was stopped due to the inability of substrates to flow through the lines. Although there is a visual difference in the sample, HPLC analysis (Figure 5.9) confirmed no new compounds had been formed.

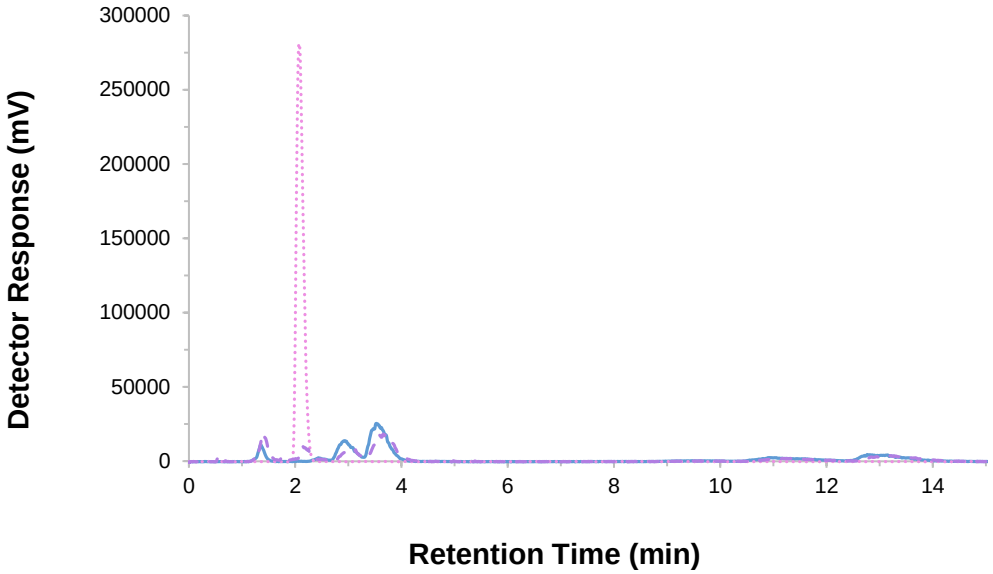

Figure 5.9 Transesterification substrates of OOO (blue solid) and Et-Pa (pink dotted) at 1:10 dilution in DCM/ACN (3:7, v/v) along with the product of ambient continuous flow experiment after 5 h (purple dashed); showing no evidence of TAG synthesis. HPLC analysis was performed over 33 min, but the baseline remained stable after 14 min.

A temperature control unit was attached to the CSTR (Figure 5.10 (a)) to maintain the bulk of the substrates/product in their liquid form and the experiment repeated.

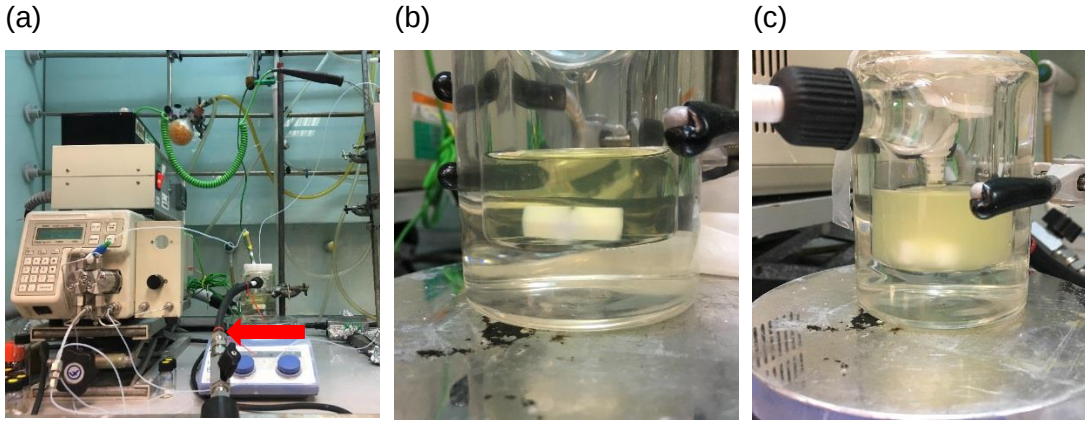

Figure 5.10 Set-up of continuous flow experiment using OOO (15.4 mmol) and Et-Pa (15.1 mmol) substrates with additional temperature control; (a) the black pipe attached to the CSTR indicated by the block arrow, leads to a Haake oil filled temperature controller set at 32 ^{o}C, which was sufficient to (b) maintain the substrates in the liquid phase for over 1 h prior to the experiment onset; (c) transesterification product after 4 h in the system.

Initial overheating of the heating block damaged the enzyme, which meant the column had to be emptied, cleaned and refilled. As a result, the sample remained in the CSTR for over an hour prior to experiment onset, where it remained liquid at 32 ^{o}C: an indication that the temperature was sufficient. On returning to the system after 4 hours under experimental conditions, high back pressure had caused the pump to fail and stopped the system flow. It is not clear as to how long the run was executed prior to pump failure, but a difference could be observed in the sample. Regardless of appearance, HPLC analysis showed no indication of additional compounds (data not shown).

Sustained complications with high back pressure in the pump and no reliable method to determine the enantiopurity/racemate of the product, led to the discontinuation of this synthesis technique. Enantiomeric detection is discussed in Chapter 3.

5.1.4 Chemoenzymatic synthesis of enantiopure TAGs

Method development was performed using the (*R*)-(+)-3-benzyloxy-1,2-propanediol ((*R*)-(+)) starting material according to the reaction scheme described in section 2.2.11. Acylation of vinyl palmitate (VP) to the *sn*-1 position was achieved in each of the six attempts; an example is presented in Figure 5.11.

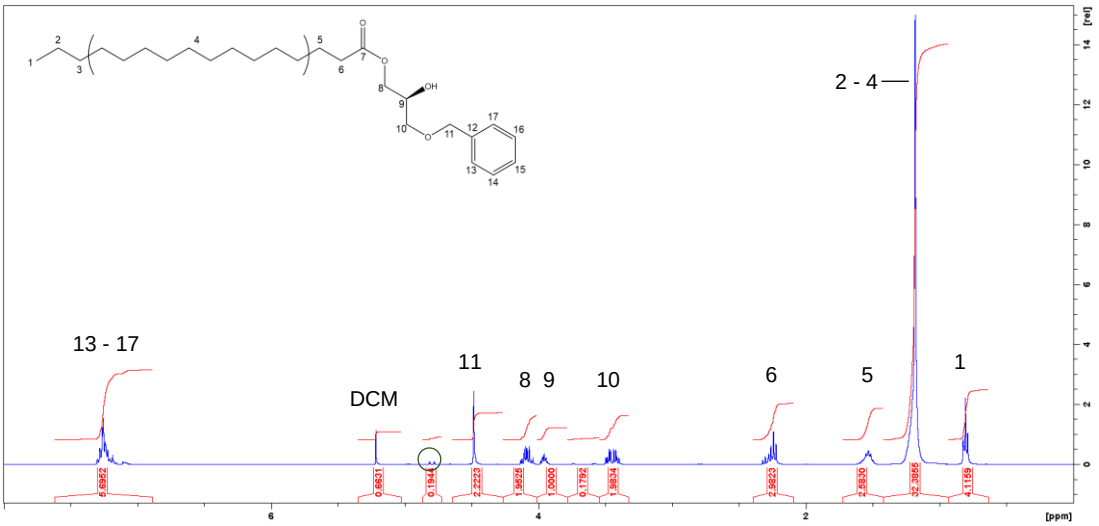

Figure 5.11 [1]H NMR following VP (1031 mg, 3.65 mmol) acylation to (R)-(+) (506.3 mg, 2.78 mmol). The encircled peaks at 4.82 – 4.78 ppm correspond with H-1 and H-2 of the VP starting material (see Appendix C.3.1 for assignment).

Integration values do not correlate with the expected for that structure, particularly around the H-1 to H-4 region, possibly indicating some palmitic acid. Evidence of VP (4.82 – 4.78 ppm) was expected due to it being the excess reactant, but specific assignment of the protons/impurities downfield has not been achieved. Purity of sample was not necessary at this stage, merely confirmation that acylation had been accomplished. Consequently, the sample is a mixture of starting materials and the acylated product ((*S*)-1, Figure 2.5): combined with residual solvent, accurate calculations of percent yield were not possible.

Using a 600 mL reaction vessel, the debenzylation stage proved to be difficult, with several attempts bringing inadequate results (Figure 5.12). Signals at 7.25 and 4.47 ppm, H-13 – H-17 and H-11 respectively, being indicative of the group to be removed.

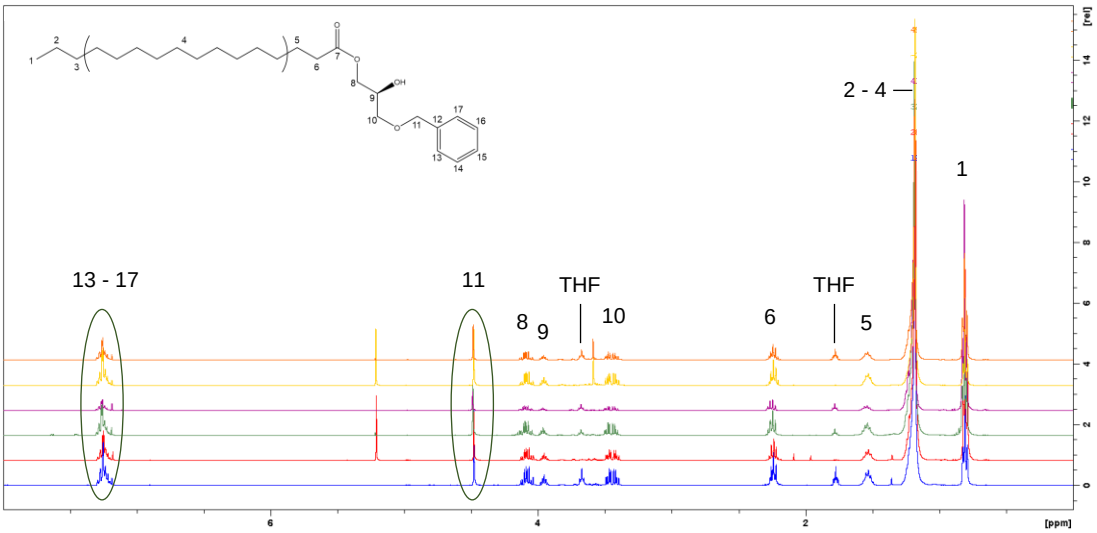

Figure 5.12 ^{1}H NMR spectra of six debenzylation attempts over three batches of reaction mixtures. Experiments were conducted in a 600 mL reaction vessel attached to the Parr reactor, using 200 mL total solvent (THF/hexane, 15:85 v/v).

Variable conditions were trialled; temperatures (room temperature to 40 ^{o}C), reaction times (2 – 20 hours) and Pd/C catalyst (30 – 60 mg; 5 wt.% wet and 10% powder), but none were able to affect the benzyl group. It was concluded that this was due to the molarity of the reaction material and catalyst, thus, reducing the amount of solvent would be essential. Instead of a 600 mL working volume Parr Hydrogenator vessel (requiring large amounts of materials), a much smaller 2 mL capacity stirred tank reactor (fReactor) was used[200, 201]. Small scale reactions were carried out using 0.5 – 1 mL solvent: substituting THF/hexane with DCM to avoid swelling of the Viton O-ring, caused by THF[202].

The amount of Pd loading on the catalyst is expressed as a percentage of dry weight. For each reaction the number of moles of Pd were calculated using Eq.(7) for the 10% dry powder and Eq.(8) for the 10% wet (substituting 0.05 for 0.1 for calculations corresponding with 5% wet Pd/C). Note that 50% of the wet Pd/C is water weight, which has been removed during the calculations.

$$n = \left(\frac{0.1 * W_c}{1000 * M_w}\right) \tag{7}$$

$$n = (\frac{0.1 * W_c}{1000 * M_w})/2 \quad (8)$$

where W_c is the weight of Pd/C in mg and M_w is the molecular weight of Pd (106.42 g mol^{-1}).

Initially, 5.5 mg Pd/C (10% wet; 2.58 µmol Pd) was used, which was not enough for successful debenzylation. Significantly increasing the catalyst to almost four-fold proved effective: a small peak indicating the benzyl group is present, yet ^{1}H NMR confirms a loss of >90% from the starting material (Figure 5.13). This is supported by COSY NMR (Figure 5.14) through the lack of coupling between the relevant protons.

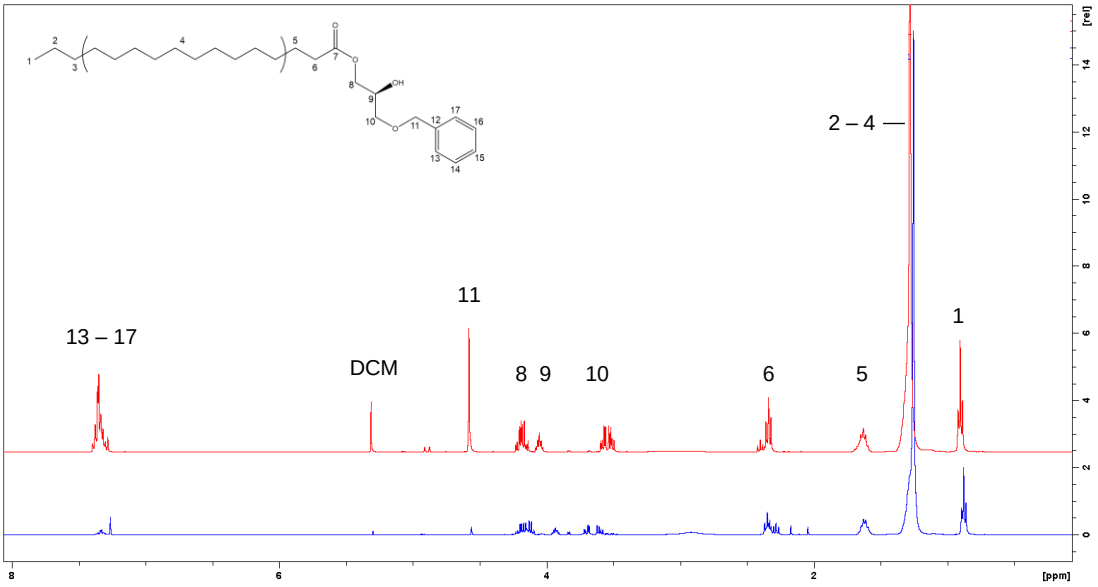

Figure 5.13 ^{1}H NMR spectra comparing 1-palmitoyl-3-O-benzyl-sn-glycerol ((S)-1; top) and the product of 1 h under hydrogenation at 9 bar in the fReactor using 20.2 mg Pd/C (10% wet; 9.5 µmol) ((S)-2; bottom).

(a)

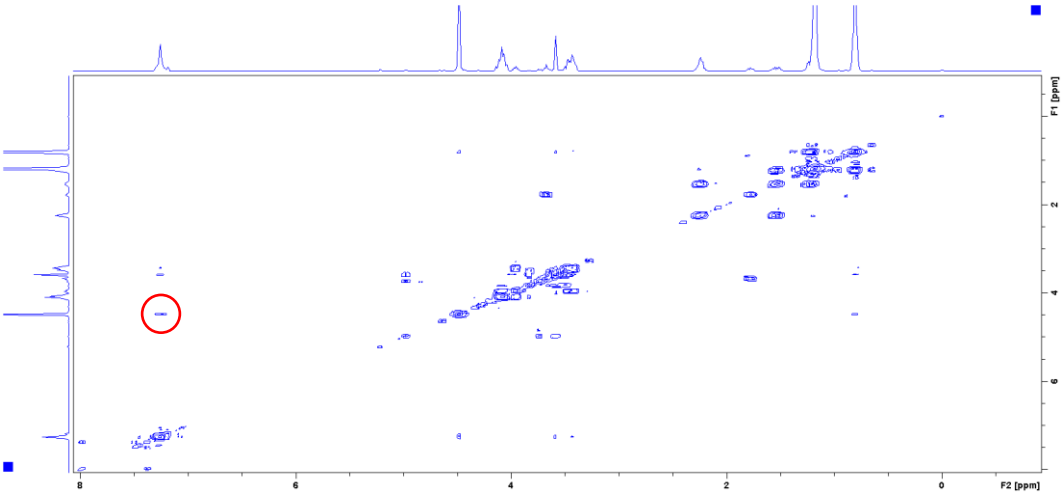

(b)

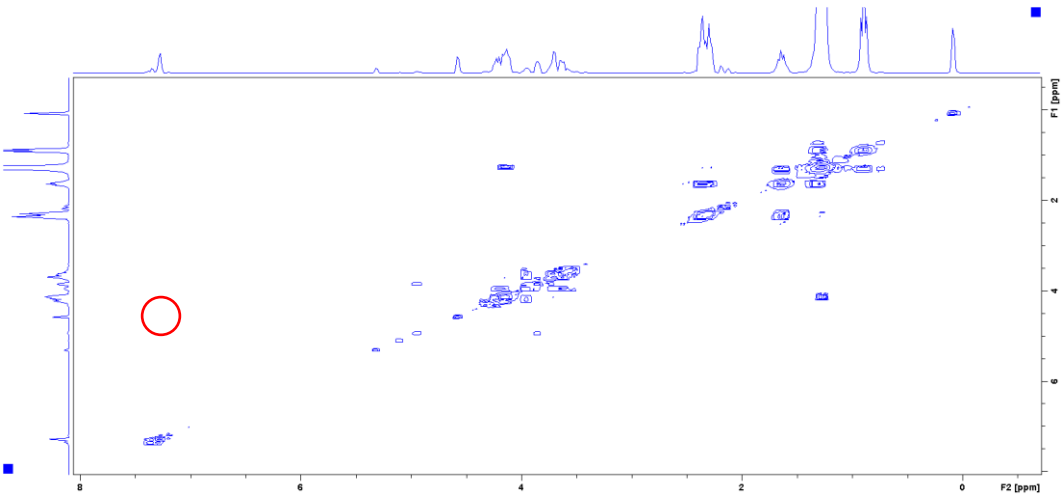

Figure 5.14 COSY NMR of reaction products following hydrogenation at (a) 5 bar in the 600 mL cylinder using 30.3 mg Pd/C (10% dry; 28.4 µmol) and (b) 9 bar in the 2 mL fReactor using 19.7 mg Pd/C (10% wet; 9.3 µmol). Circled portion in (a) displays coupling between the benzyl/CH_2 group protons, which is absent in (b).

By increasing the molarity of the catalyst, removal of the benzyl protecting group was repeated (Figure 5.15). However, recovery of (*S*)-2 (1-monopalmitin) was negligible in comparison to the amount of (*S*)-1 used in the reactions; hence the number of repeats to allow progression to the next stage. With an average of 13% yield, significant losses were endured. It was determined the product was being lost to the activated carbon and multiple washes with DCM had no effect. Switching to THF as the rinsing solvent increased the yield to 50%.

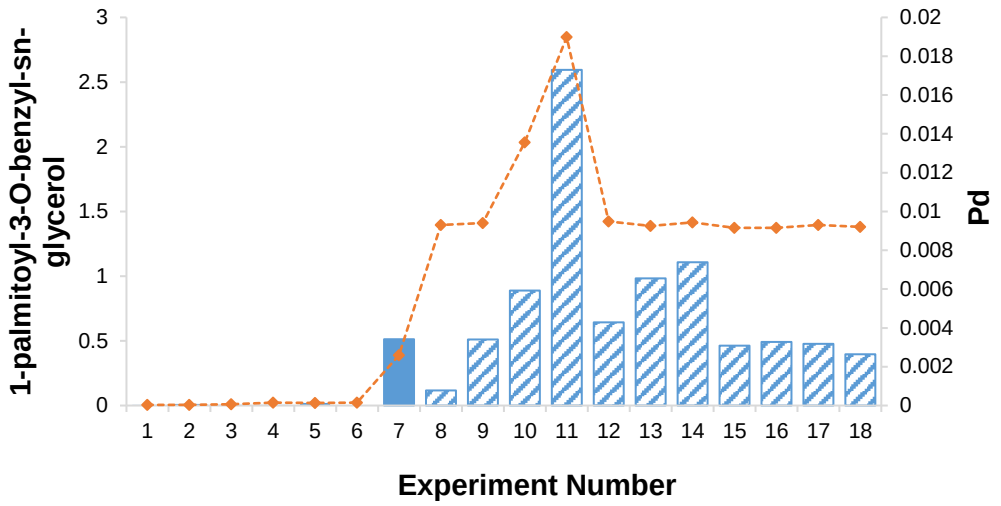

Figure 5.15 Comparison of reactant (bars) and catalyst (lined scatter) molar concentrations over the hydrogenation experiments. Experiments 1-6 were conducted in a 600 mL reaction vessel using 200 mL solvent (THF/Hexane (15:85 v/v); experiments 7-18 were performed in a 2 mL fReactor using 0.5 – 1 mL DCM; diagonally striped bars represent experiments where the removal of benzylic protons was successful.

Each of the successful debenzylation products were combined into three batches and recrystallisation from THF/hexane achieved. With all batches accounted for, the process was inefficient relative to recovery at ca. 31%, yet effective in removing impurities (Figure 5.16).

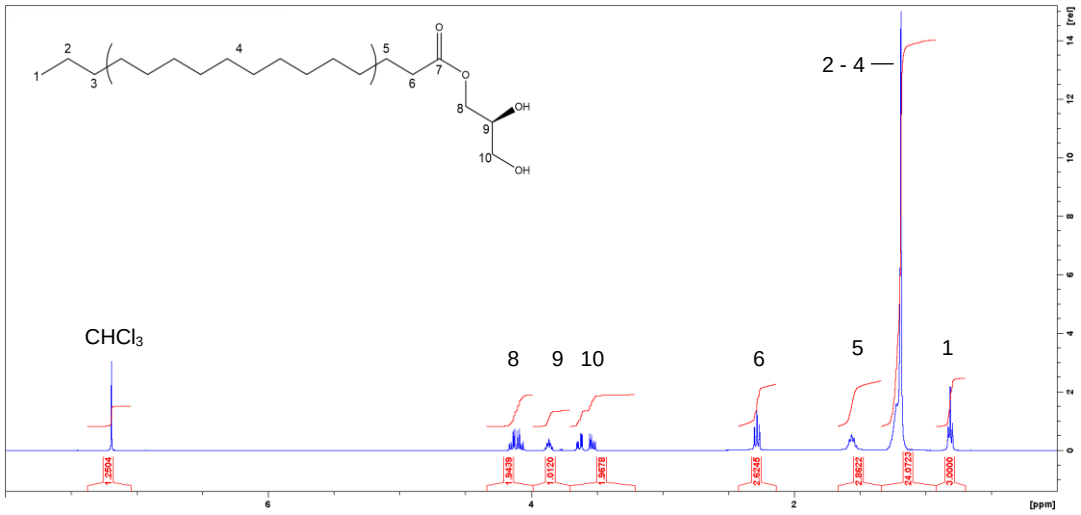

Figure 5.16 ^{1}H NMR spectra of 1-monopalmitin following purification using a two solvent system; see Appendix C.3.2 for integrations

Acylation of vinyl stearate proceeded as described in section 2.2.11 to give 1-palmitoyl-3-stearoyl-*sn*-glycerol ((*R*)-2) as a white solid in 64% yield following crystallisation from MeOH: see Appendix C.3.3 for NMR integrations.

Oleic acid was introduced to the *sn*-2 position of (*R*)-2 using EDAC as the coupling agent in the presence of DMAP. Liquid-liquid extraction using brine and hexane, followed by solvent removal in vacuo, afforded a white wax type product. ^{1}H (Figure 5.17) and COSY NMR (data not shown) confirmed the successful esterification.

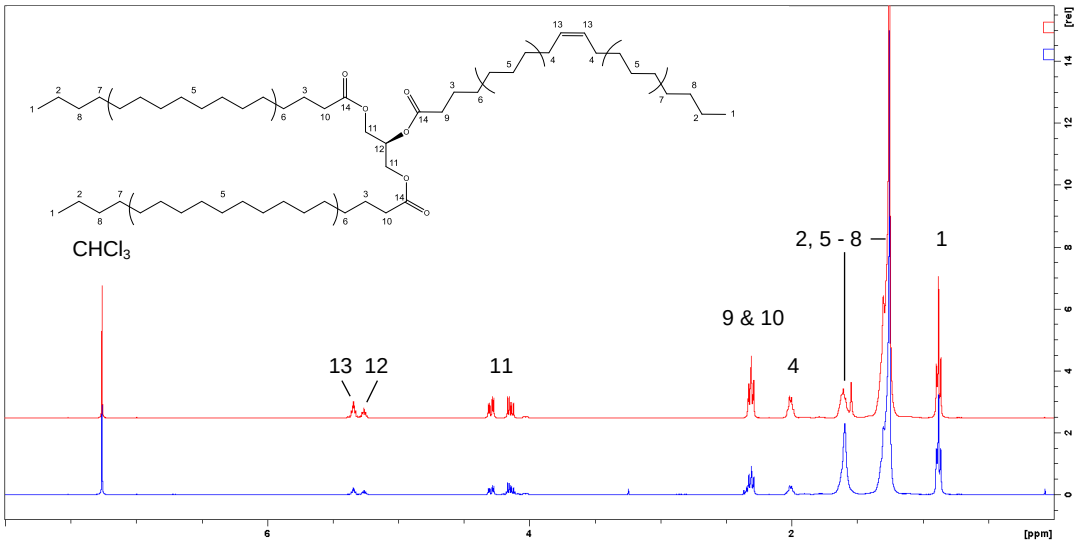

Figure 5.17 ^{1}H NMR spectra of the rac-POSt standard (top) and the final reaction product following chemical coupling of oleic acid to 1-palmitoyl-3-stearoyl-sn-glycerol (bottom).

Visually, the final reaction product displays a near identical spectra to its racemic standard counterpart. Integration values do not correspond with the expected for the product, but with ca. 12% molar excess of DAG, this was to be expected. Postulations that the product is enantiopure (*R*)-POSt can only be made from comparisons with spectra of the *rac*-POSt standard. Unprecedented circumstances resulting in a complete university shutdown (Covid-19) prevented any further experiments.

It must be pointed out that some analytical data for these samples is absent due to the aforementioned situation. Melting point, optical rotation and mass spectrometry for all; infra-red for oleic acid, MAG, DAG and the final product.

5.2 Discussion

In order to affect the enantiomeric ratio of POSt in CB, acquiring an enantiopure form of the TAG was necessary. These compounds are not readily available and were unfeasible to outsource for manufacture. As such, enantiomer TAG synthesis became a critical point of the project. The aim was to achieve this using natural materials, ruling out the use of solvents and heavy processing. Thus, in using transesterification a solvent free system was created.

MCT oil was chosen for method development due to its low viscosity and saturation levels, where it was anticipated to flow through the PBR without difficulty. With the appropriate enzymes it would be possible to sequentially introduce acyl groups to the MCT glycerol backbone(s); palmitic and stearic using an *sn*-1/3 specific lipase, followed by oleic using an *sn*-2 specific lipase[128, 203, 204]. However, once the method was clearly defined, using OOO as the starting material circumvents such complexity by requiring acylation of the primary groups only. Though the TAG composition of MCT oil was unknown and unable to be determined analytically, calculations of the hypothetical species correlated with the number of chromatographic peaks.

After 24 hours under magnetic dispersion it was apparent transesterification of MCT/Et-Pa had been successful by a further five peaks appearing in the chromatogram, as predicted (Table 5.3): an indication of lipase activity at both of the TAGs' primary positions. Only three additional peaks would be observed had just one of the primary groups been substituted. Following analysis of the aliquots extracted at additional time points of 48 hours, 6 and 9 days, it was apparent that the enzyme was still active. As this was an exploratory procedure, primarily to determine reactivity between substrates, the time to completion was unknown. Iwasaki et al.[62] found 71.1% of the Et-Pa substrate was consumed after 24 hours, yet in this work ca. 50% further reduction was observed in the AUC between 24 – 48 hours (Figure 5.5 (a)); an observation that would not have occurred had the reaction been stopped after one day. An ample amount of Et-Pa was residual at this point and thus, the reaction was allowed to continue to establish if further synthetic compounds could be attained. With the system running at an enzyme load of 8% compared to 10% reported in literature[107] and at lower temperature, it was conceived that a longer reaction may allow more of the Et-Pa to be incorporated into the TAG(s). However, it was clear that the batch process was uneconomical with a minimal reduction in AUC of MCT peaks between 24 hours and 9 days. During that period, the AUCs reduced by a total of 17.4, 42.4, 18.7 and 4.7% respectively for peaks 1 – 4. As previously mentioned, acyl migration in batch conditions is apparent[128] and under lengthy reactions, is a known side effect[132]. For this to occur there would have to be water present in the sample

for hydrolysis, which was not obvious in a solvent free system. However, taking the water content of the substrates into consideration, this reaction is a possibility. The analytical certificate for MCT oil states there to be 0.03%, but it is not known for Et-Pa. Though this is not expected to be high, when combined with that in MCT oil and moisture from the RBF[205], it may have been enough to at least induce hydrolysis, if not acyl migration[128]. The generated FFAs would subsequently be able to acylate to the *sn*-1/3 positions of the circulating DAGs, giving the impression of no change to the original TAGs when monitoring the AUC. Reactions of such length as reported in this thesis have not been identified elsewhere; however, as there was ample Et-PA remaining, observing the effect of allowing it to continue was desired, but there was no benefit to the extensive timeframe.

The continuously recirculating batch equipment produced similar results to the SB but maintaining movement of substrates was an issue due to crystallisation in the lines. The use of an infra-red lamp focused at the outlet port has been reported in literature[128] as a means to overcome blockages due to solidification; this being the concern with the ambient MCT/Et-Pa experiment. It is considered that the reaction product may have become too viscous to pass through the pores of the frit due to increased saturation; creating a bottleneck in the line that subsequently crystallised.

Transesterification using OOO/Et-Pa substrates at ambient, technically an undemanding reaction with the *sn*-1/3 lipase already in use, produced a different concern where flow restriction was due to the CSTR outlet frit, whereby the product was unable to leave the vessel. The blockage may have been created by Et-Pa, with a m.p. of 24 ^{o}C, crystallising out of solution at ambient[206], and growing around the frit. Though it had been 5 hours between experiment onset and returning to the vessel, the lack of apparent reactivity (Figure 5.9) is likely to be through an inefficient time in circulation. The addition of temperature control was anticipated to resolve this (Figure 5.10), but high back pressure in the pump caused it to cut out and stopped the circulation. In contrast to the ambient experiment, there appeared to be no solidification around the CSTR outlet frit, indicating that the problem stemmed from the

pump itself. However, several attempts at restarting the flow with the OOO/Et-Pa substrates were unsuccessful and subsequently, the trial was ceased. A simpler system would have been similar to that of Kim et al.[128] where a substrate combination of high oleic sunflower oil (HOSO) with a mixture of Et-Pa and Et-St was pumped directly into the PBR via a syringe wrapped with heating tape; thus removing the difficulties experienced with the CSTR frit and pump. However, such a system only allows the materials to be passed over the enzyme bed once, leaving a significant amount of residual starting material. The system used in this thesis was anticipated to remedy this by recirculating the materials until the product, being of increased saturation and m.p., crystallised out of solution in the CSTR and thus, able to be collected for further experiments.

Running in parallel to this was the experimental work to find a technique for determining the enantiomeric ratio of a TAG standard. As discussed in Chapter 3, this was not achieved. Without a reliable method of confirming the enantiopurity of a compound, the transesterification route of synthesis was no longer practical, and it was decided not to go further with development/optimisation of this method.

Chemoenzymatic synthesis using enantiomerically pure starting material alleviates concern as to which species is being formed due to the pre-defined spatial arrangement around the *sn*-2 position. Several groups have used 1,2- and/or 2,3-isopropylidene-*sn*-glycerol as starting materials for the preparation of enantiospecific TAGs[36, 65, 207]; however, acyl migration can occur during deprotection of the isopropylidene moiety, resulting in an undesirable mixture of 1- and 2-MAGs. Using benzyl as a blocking group at the *sn*-3 position of 1,2-isopropylidene-*sn*-glycerol, Kristinsson and Haraldsson[133] were able to avoid the issue of migration on removal of the isopropylidene moiety; distinctly advantageous where regiospecificity is necessary. In this thesis, the chiral antecedent (*R*)-(+)-3-benzyloxy-1,2-propanediol ((*R*)-(+); $[\alpha]_D^{20}$= 5.5°[208]) was used to circumvent the benzylation and successive removal of the isopropylidene protecting group of 2,3-isopropylidene-*sn*-glycerol. Successful acylation of vinyl palmitate to *sn*-1 using CAL B was achieved on six

occasions, with no acyl migration, as observed through ^{1}H and COSY NMR. Use of vinyl esters in the acylation stages ensured irreversibility of the reaction, producing acetaldehyde as the by-product[129, 209]. Palmitic and stearic acids used here would produce a water molecule, which has the potential to hydrolyse the newly formed bond and thus, regenerating the original compounds.

Removal of the benzyl protecting group under catalytic hydrogenolysis proved to be difficult with the standard Parr reactor equipment available. Using the 600 mL reaction vessel, the solvent volume was twice that used in literature[132, 133]; reducing the molar concentration of substrate and catalyst. Replicating the method unerringly using 30 mL THF and 70 mL hexane was unworkable due to the size of the vessel: the volume was not ample for the reactors stirrer and temperature probe to immerse in the mixture. Increasing the total volume to 200 mL by the addition of 100 mL hexane resolved this but as shown in Figure 5.12, the conditions were not optimal: hydrogenation at 5 bar for 3 hours saw a reduction of ca. 44% in the benzylic ring protons. The same sample was returned to the Parr reactor a further two times for longer periods, equating to ca. 23 hours under hydrogenation, where 81% overall reduction was achieved (starting material to end time). This was attempted two further times using freshly prepared 1-palmitoyl-3-O-benzyl-sn-glycerol each time, and as shown in Figure 5.12, a consistently similar level of benzyl reduction was reached. Kristinsson et al.[132] also found benzyl ether deprotection of groups with long-chain adducts to be difficult, to which their resolution was the use of perchloric acid as a promoter. Whilst the volume used was trivial, the debenzylation was successful and not expected to occur without it. However, the low yields of 56, 58 and 38% for 16:0, 20:0 and 22:0 respectively, did not inspire its use for this thesis: avoiding further hazardous materials was preferable.

It was determined that the low molarity of the benzyl ether and catalyst prevented them from binding. In a debenzylation study conducted by Yakukhnov and Ananikov[210], the lowest amount of Pd catalyst was reported to be 0.02 mol%, with 0.05 mol% deemed enough for full substrate conversion. The large vessel experiments conducted for this project had a significantly

lower amount. To achieve the minimum effective level, it would have been necessary to use 1 – 2 g of 10% Pd/C, depending on the dry or wet variety: an undesirable amount considering its pyrophoric nature. Reducing the reactor size increased the molarity and thus, encouraged an interaction between the components. However, the initial fReactor reaction used 0.02 mol% of Pd, which proved to be inadequate. Increasing this to 0.06 mol% for the second was successful and thus, subsequent reactions were maintained at similar concentrations. It may be possible to reduce the amount of catalyst and future work should look towards establishing the optimum catalyst/substrate molar ratio.

Early low yields were resigned to complications encountered during protocol optimisation. A quantity of BPR cartridges were releasing at pressures significantly below their reported maximum: 500 and 250 psi cartridges, 34 and 17 bar respectively, were opening during the nitrogen purge stage at pressures of no more than 5 bar. In doing this, substrate containing solvent was released into the fume hood, leaving the remaining quantity of starting material unknown; yet yield calculations could only be made with the known amount placed in the reactor. After resolving this, several experiments with particularly low yields ensued when it was subsequently concluded the product was becoming trapped within the activated carbon. This effect may have been exacerbated by the volatility of DCM. For several of the fReactor reactions, the amount of remaining solvent on completion was minimal, yet enough to maintain the Pd/C as a slurry. It was anticipated the solvent was evaporating through the exit point of the BPR, thus concentrating the substrate in and around the catalyst. Introducing a blanking nut to block the BPR outlet once pressure had been reached resolved this, as described in the method (2.2.11.2). As this is the first reported use of a fReactor for such a protocol, the difficulties experienced were unknown beforehand and should be taken under consideration for future work.

Recovery attempts of the MAG reaction product saw the volume of DCM for the catalyst/filter rinse increase from 5 mL to ca. 15 mL, to draw the substrate away from the carbon pores. A small increase in yield was attained, but

removal of the benzyl group had increased the MAGs polarity beyond the solubility capacity of DCM. Substituting THF as the rinsing solvent increased the yield from an average of 13% over seven experiments to 50% over three. This brought the yield to a similar level of that achieved by Kristinsson et al.[132] for the same 1-MAG; where 56% yield was reported with 16:0 esterified to *sn*-3. The publication states that the product precipitated following the reaction, which was subsequently dissolved in THF: precipitation was not observed in the fReactor, hence the lack of THF use initially. It must be noted that success with the fReactor was not dependent upon reaction time. On average, the experiments ran for ca. 90 minutes, but debenzylation was achieved in ca. 1 hour on four occasions. Therefore, in using the fReactor the reaction time was halved compared to that reported in literature[132]; a significant advantage when multiple repeats may be necessary.

A further consideration as to the low recovery rate was the use of filter paper over Celite for removal of the catalyst[132, 133]; chosen for the ease of disposal and ability to isolate used Pd/C for additional processing if required. The benefit of filter paper became pertinent when, following storage in hexane at 4 ^{o}C, additional rinsing of the catalyst with THF allowed more of the 1-MAG to be recovered. Furthermore, the potential of drying out the catalyst on the Celite pad under vacuum filtration was deemed an unnecessary hazard. However, it was observed that the THF filtrate appeared to pass slowly through the filter and the catalyst had congregated into a mass, which stuck to the paper and was unable to be extracted. It is possible that the mass encased some of the 1-MAG product within its core where the solvent could not reach to flush it away from the carbon: a potential reasoning for the slow filtration as the solvent was having to go around the catalyst, rather than through. It is recognised this probably would not have occurred with the porous structure of Celite and likely to have been easier for the product to be washed off the carbon. Future repetitions of this protocol would include adding the reaction product plus Pd/C to a volume of THF and stirring under magnetic dispersion prior to attempting filtration using Celite. In this sense, any product that has fixed itself to the carbon may dissolve in the THF and allow for greater product recovery.

After collating the successful debenzylation reaction products, recrystallisation in a two-solvent system using a minimal amount of THF and a four-fold volume of hexane progressed without incident, though the yield was low at 31%. However, ca. 5 mL of solvent was remaining from this stage following a hexane wash of the crystals. Removing the solvent under vacuo and repeating the recrystallisation would have likely increased the yield, yet this did not occur through time constraints.

Following a similar procedure to the initial acylation stage, vinyl stearate was successfully esterified to *sn*-3 of the purified 1-MAG to give asymmetric 1-palmitoyl-3-stearoyl-*sn*-glycerol. Though using an *sn*-1/3 specific lipase, confidence that the enzyme would not interact with palmitic acid at *sn*-1 was due to the reaction taking place in an anhydrous environment. With no water presence, there was no opportunity for hydrolysis to occur[118]: the reactions were performed under a stream of nitrogen. As such, the systematic addition of acyl groups was successful, with stearate acylation to *sn*-3 confirmed through ^{1}H and COSY NMR. Following recrystallisation from MeOH, proton integration values for the purified 1-palmitoyl-3-stearoyl-*sn*-glycerol, correlate with predicted for the DAG (Appendix C.3.3).

The final stage, chemical coupling of oleic acid to *sn*-2, proceeded in alignment with the method of Wang et al.[131]; a modification to the protocols used thus far[132, 133]. When considering the chain lengths of the alkyl groups, their synthesis showed a greater resemblance to the DAG here; where they coupled palmitic acid to the *sn*-2 of 1,3-dioleoyl-glycerol. The coupling agents remain the same, but differences in their molarity, and of the substrates. Following this method, the 1-palmitoyl-3-stearoyl-*sn*-glycerol was present as 1.1 mol equivalent to an equimolar ratio of oleic acid and EDAC; alongside 0.2 mol equivalent of DMAP. This appeared adequate for coupling to occur, producing what is assumed to be enantiopure (*R*)-POSt (Figure 5.17) from observations of the ^{1}H NMR spectra, which shows a convincing comparison with the racemic standard. Overcoming complications during the debenzylation stage was time-consuming and did not allow for the procedure to be repeated using (*S*)-(-) starting material, thus it was only possible to synthesise (*R*)-POSt.

Excess DAG in the reaction will be a contributory factor to the poor correlation between integration values of the racemic standard and synthesised (*R*)-POSt. However, it is possible that the coupling did not proceed to its optimum and the values also correspond with unreacted oleic. Working with equimolar substrates, previous literature[129] used EDAC and DMAP in 1.2 and 0.3 – 0.5 mol equivalents respectively, to attain optimal yields. It is recognised that using similar component ratios may have improved oleic coupling, thus reducing impurities in the final product. These impurities are not expected to be EDAC or DMAP due to their water solubility and the use of liquid-liquid extraction for their removal.

Unprecedented circumstances halted experimental work, meaning purification was not attained, nor could repeats be performed. Hence, the success of the reaction can only be postulated, along with the suggested steps for protocol optimisation.

5.3 Conclusions

Batch and continuous flow methods were trialled for the synthesis of enantiomerically pure POSt in a solvent free system. Both were successful during the development stages in the transesterification of Et-Pa to MCT oil TAGs, but instrument complications and no defined method for enantiomeric determination, established that an alternative protocol would be required.

Using chemoenzymatic methods, the synthesis of enantiopure (*R*)-POSt appears to have been achieved, which to the best of our knowledge, is the first study to have done so using the described conditions. Difficulties experienced in this work were also noted by Fodran et al.[211] citing Mori, who states that enantiomerically pure TAG synthesis continues to be a non-trivial matter in these current times. Despite this, the novel use of the fReactor proved to be an invaluable addition to the process but holds a disadvantage in the amount of product able to be generated. Nonetheless, the debenzylation consistency is a distinct motive for future development of the protocol to increase yields of small-scale reactions.

Chapter 6 General conclusions and future work

The course of this thesis sought to investigate three key parameters surrounding chirality in CB TAGs; elucidation of the enantiomeric ratio, the effect of stereochemistry on crystallisation and whether modifying the natural composition would alter the lipids' digestibility. Firstly, developing a method to validate or refute racemic POSt findings in CB[34, 53, 100] is relevant for comprehension as to whether this can be generalised amongst the species or selective to certain genus. The outcome of which being pertinent to the link between stereochemistry and polymorphism: the inclination for opposing TAG enantiomers to inhabit the same unit cell and crystallising in the most stable polymorph has not, to the best of our knowledge, been identified for POSt. Confirmation of this or any other chiral TAGs in CB is notable for not only furthering knowledge in the field, where research on the SUS type is currently lacking, but may be substantial information for commercial application. Should the enantiomers behave as recorded in previous literature[81, 87] where they are attracted to their opposites, then they may be the foundation to the lipids' polymorphism and manipulating their ratio could alter its crystallisation behaviour. Thus, opening the way for softer CBs to be used without increasing the saturation levels, as is currently required to improve functionality. Indeed, recent literature has reported POSt as being the dominant factor that controls the polymorphic behaviour in CB[212], yet an association with its stereochemistry has not been recognised: clarifying this would be a notable find.

The primary research focus was founded upon the belief that enzymes, being chiral, can only synthesise one enantiomer of a compound and thus the findings of a racemic mixture were inherently questioned. However, aside from the Kennedy pathway for the biosynthesis of TAGs (1.3.2.1), it is understood that a further route to TAG synthesis in seed oils gives rise to the formation of

both enantiomers via transacylation between DAGs[213]. This goes some way in explaining the finding of both enantiomers in one product, yet for this to effectively be the only process by which POSt is formulated in CB to produce racemate requires further clarification. Research conducted on the enantiomeric composition of CB is scarce and of those that report *rac*-POSt[34, 53, 100], two used stereospecific analysis procedures that do have the potential to elicit acyl migration. Takagi and Ando[53] refer to the minimal occurrence of this during their study, yet state that this did not affect the result. With a lack of studies for comparison this cannot be contested, however, it highlights the need for deeper investigation to the stereochemistry of CB. Fundamentally, the research in this thesis intended direct separation techniques to be used to remove the acyl migration potential, but the myriad of CSPs and mobile phases trialled unsuccessfully emphasise the difficulties of such an undertaking. The success of those that have resolved enantio-TAGs using polysaccharide based CSPs is postulated to be based on initial π-π interactions between double bonds of the *sn*-1/3 acyl chains and phenyl ring of the chiral selector; however, as recently stated by Scriba[214] the enantiorecognition mechanisms of CSPs are still not fully comprehended. Nonetheless, the fact that UUS or SSU type TAGs can be resolved where SUS types cannot, makes the interaction assumption plausible.

Although the chiral screen was extensive and unable to find the appropriate column, it is believed that under the correct conditions there will be one available for the separation of SUS type TAG enantiomers. The number of variables in chiral resolution using HPLC have not been exhausted and further investigations are warranted: the separation modes trialled in this thesis should act as a foundation, preventing future analytical studies from repeating those which are unsuitable. Considerations must be made to both the CSP and choice of mobile phase, where composition of the latter is suggested as modifying the chiral selector through altering intra- and intermolecular hydrogen bonds[214]. It is therefore possible that one of the columns already trialled may be suitable using different solvents, however, the cyclical β-cyclodextrin CSPs are of interest as a starting point for future trials due to their hydrophilic core. As with the polysaccharide-based columns, there are many

modifiers/derivatives but 3,5-dimethylphenylcarbamate has been used in several studies for TAG separation, as reviewed by Řezanka, Pádrová and Sigler[56], and it would be recommended that these be the first trialled. With no such study of SUS type enantio-TAGs currently identified, the non-trivial undertaking of recognising the appropriate conditions would open many an opportunity for future researchers. However, as a precursor to the task it would be advised to synthesise enantiopure TAGs as reference compounds to comprehend the elution order of each form. Although IR and MS analysis for (*R*)-POSt synthesised in this thesis could not be completed due to highly unprecedented circumstances (Covid-19), the ^{1}H NMR spectra for the final product was near identical to the *rac*-POSt standard, indicating the overall method was successful. It could thus be recommended as an approach with the addition of suspending the Pd/C catalyst in dry THF following pressure hydrogenation for dissolving any reaction product that may be trapped inside the carbon pores. Use of the fReactor for removal of the benzyl protecting group[200] was a novel approach to the problematic debenzylation, avoiding the use of perchloric acid which has been reported as an aid for the reaction in cases where it may not have occurred at all[132, 215].

The inability to source a suitable CSP prevented the collection of individual POSt enantiomer(s) from CB, which was a substantial obstacle. Their intended use was for the manipulation of the natural ratio to ascertain if there is an optimum that will enhance the crystallisation and polymorphic behaviour of CB. Synthesising enantiopure compounds therefore became a priority for proof of concept. The EU Directive[108] states that enzymatic rearrangement of fats within chocolate products is forbidden, yet there are no such statements with regards to the manipulation of enantiomeric content. Using (*R*) and/or (*S*)-POSt directly isolated from CB and returning it back to the lipid in relevant ratios could allow claims that the modified product is merely an extension of the lipids natural form. Where this could be substantial for CB is the premise that there will be strong heterochiral interactions between opposing enantiomers to form a racemic compound[216] in its most stable polymorph, that being β for POSt, which is the desired form for the chocolate industry. Research correlating stereochemistry and polymorphism thus far has done so

only on binary blends and the behaviour in a mixed TAG system is not known, which would be prominent information for the research area.

Derivatisation efforts using (*R*)-MTPA-Cl for diastereomeric conversion of a *rac*-POSt standard was unable to deliver the anticipated results, where it was expected to provide an easier analytical procedure than the lengthy stereospecific analysis. Though the NMR results show promise by presenting several peaks with a different δ ppm to the starting material, significant method development is needed for it to be practicable. As a minimum, purification and isolation stages should be incorporated as analysis of the reaction product without these produced a complex spectra that is difficult to interpret. It may be possible to circumvent this by using a method similar to that of Christie et al[217] where isolation of 1,3-, 1,2- and 2,3-DAGs was not necessary, but replace the (*S*)-(+)-1-(1-naphthyl) ethyl isocyanate CDA used in their work with Mosher's acid chloride. As the latter induces known behaviours in the NMR spectra, such as an upfield shift for glycerol protons, analysis using this technique would provide in-depth information on the structural arrangement using ^{19}F NMR to complement ^{1}H NMR. However, following the literature method as written first would be recommended prior to substituting the CDA to comprehend its viability and if the exchange is an improvement; though ^{19}F NMR could not be used for this analysis, which may not give as much structural information. It is recognised that replicating a stereospecific analysis procedure would have been beneficial in this thesis prior to the development of a new protocol, which would have allowed data to be compared; particularly that of Takagi and Ando[53] who used such a method to conclude POSt in CB as racemic. Method development is a large task to embark upon and could form a complete body of work in itself; an extra undertaking that was perhaps ambitious for this project considering all that was trying to be achieved.

Motivation for the study of CB digestibility was provided by the reported resistance to micellization of solid lipid components at body temperature, which is a prerequisite for lipolysis to occur[142]. Though CB has minimal SFC at 37 ^{o}C, it was not known whether the high melting TAGs affected its time dependence in the GIT. Additionally, understanding the lipids' behaviour in the

intestinal environment was necessary to compare its digestion profile with that of an enantiomerically modified product. Lipids that cannot be digested have the potential to elicit physical issues such as steatorrhea[136], which is an increase of faecal fat that can have highly undesirable side effects; thus, understanding the digestibility of CB is important to ensure any lipid modification does not significantly alter its biophysical behaviour.

Measuring droplet size distribution proved to be unachievable with the attempted analytical procedures, but it is recognised that omitting the oral and gastric phase may have inhibited bile in its role as a natural emulsifier. However, replicating these processes consecutively *in vitro* present difficulties as the lipid is likely to coalesce when transferring between reaction vessels, thus, negating any emulsifying action and not giving a true reflection of its *in vivo* behaviour. Nonetheless, under the *in vitro* digestion conditions of the pH stat, it was possible to analyse the extent of TAG lipolysis when comparing the initial melt temperatures of 37, 50 and 80 ^{o}C, which is the first study to have done so. With no difference between them regarding the amount of FFAs released, it can be concluded that the high melting TAGs do not affect the lipolytic process. However, at ca. 32%, the amount of FFA release appears low and is comparable to that of emulsions containing solid lipid particles that achieved 35%[143]: liquid lipid emulsions achieved 55%. It would therefore be suggested that further work be conducted to understand this behaviour and compare the effect of saturation and crystallinity by using alternative lipids.

In summary, the resolution of *rac*-POSt using direct separation techniques was unattainable using polysaccharide based CSPs, but it is anticipated that a β-cyclodextrin column may be the remedy to this. Until this can be resolved, further research using stereospecific analysis is required to verify or refute the scarce information on racemate in CB. Moreover, until a suitable chiral selector is sourced, the isolation of individual enantiomers will not be possible. In anticipation of the day a chiral selector and mobile phase is traced, research into the stereochemistry and polymorphism of SUS type TAGs should progress with synthetic enantiopure compounds to increase knowledge within the field. Using the method here established with the fReactor for the synthesis

of such materials, further studies should look to produce both enantiomeric forms of POSt for m.p. analysis of their binary blends which will aid in elucidating the enantiomeric composition of the isolated TAG from CB.

It is still considered that there is an optimum ratio of enantiomers that will enhance the lipids crystallisation behaviour to formulate a non-tempered ‘self-healing’ chocolate, where the product will be able to withstand climates of higher temperatures and fluctuations. Having established a method for the synthesis of enantiopure POSt reference standards, the developed protocol will allow future studies to produce such compounds and investigate the innovative theory offered. However, for now this will remain as one of the unanswerable questions of this PhD. The findings of this project have highlighted the difficulties of chirality as a research field. Though difficult, it is truly fascinating, and it is hoped that the work here presented will act as a foundation for further investigations to be conducted; resolving the curiosities that endure.

References

1. Beckett, S.T. *The Science of Chocolate.* Royal Society of Chemistry, 2008.
2. Vega, C. and Kwik-Uribe, C. Theobroma cacao - An Introduction to the Plant, Its Composition, Uses, and Health Benefts. In: Garti, N. and Widlak, N.R. eds. AOCS Press, 2012, pp.35-62.
3. Fold, N. Restructuring of the European chocolate industry and its impact on cocoa production in West Africa. *Journal of Economic Geography.* 2001, **1**(4), pp.405-420.
4. ReportLinker. *Global Chocolate Market By Product By Traditional Chocolate Type By Distribution Channel By Region, Industry Analysis and Forecast, 2020 - 2026.* [Online]. 2020. [Accessed 25th August 2020]. Available from: https://www.reportlinker.com/p05914545/Global-Chocolate-Market-By-Product-By-Traditional-Chocolate-Type-By-Distribution-Channel-By-Region-Industry-Analysis-and-Forecast.html?utm_source=GNW
5. Irigoyen, S. *Global Candy & Chocolate Manufacturing: Industry at a Glance.* [Online]. 2019. [Accessed 19th November 2020]. Available from: https://my.ibisworld.com/gl/en/industry/c1113-gl/industry-at-a-glance
6. Neo, P. *'All time high': No end to Asia's cocoa craze as Olam lists three factors driving market growth.* [Online]. 2019. [Accessed 24th August 2020]. Available from: https://www.foodnavigator-asia.com/Article/2019/05/17/All-time-high-No-end-to-Asia-s-cocoa-craze-as-Olam-lists-three-factors-driving-market-growth
7. CBI Ministry of Foreign Affairs. *What is the demand for cocoa on the European market?* [Online]. 2019. [Accessed 25th August 2020]. Available from: https://www.cbi.eu/market-information/cocoa/trade-statistics#:~:text=In%202017%2C%20the%20world%20average,kilos%20per%20capita%20per%20year.

8. WWF. *Bittersweet: chocolate's impact on the environment.* [Online]. 2017. [Accessed 5th December 2020]. Available from: https://www.worldwildlife.org/magazine/issues/spring-2017/articles/bittersweet-chocolate-s-impact-on-the-environment
9. Scott, M. *Climate & Chocolate.* [Online]. 2016. [Accessed 5th December 2020]. Available from: https://www.climate.gov/news-features/climate-and/climate-chocolate
10. International Cocoa Organization. *Production of Cocoa Beans.* [Leaflet]. 2020.
11. Afoakwa, E.O., Paterson, A. and Fowler, M. Factors influencing rheological and textural qualities in chocolate – a review. *Trends in Food Science & Technology.* 2007, **18**(6), pp.290-298.
12. International Cocoa Organization. *Growing Cocoa.* [Online]. [Accessed 5th December 2020]. Available from: https://www.icco.org/growing-cocoa/
13. Chaiseri, S. and Dimick, P.S. Lipid and hardness characteristics of cocoa butters from different geographic regions. *Journal of the American Oil Chemists' Society.* 1989, **66**(12), pp.1771-1776.
14. Talbot, G. Chocolate and Cocoa Butter - Structure and Composition. In: Garti, N. and Widlak, N.R. eds. *Cocoa Butter and Related Compounds*. AOCS Press, 2012, pp.1-33.
15. McClements, D.J. Emulsion Ingredients. In: *Food Emulsions: Principles, practices and techniques*. Boca Raton, Fl: CRC Press, 2016, pp.99-183.
16. Ziegleder, G. Flavour development in cocoa and chocolate. In: Beckett, S.T. ed. *Industrial Chocolate Manufacture and Use*. 4th ed., 2009, pp.169-191.
17. Vijayvergia, M. *How To Make Chocolate- A Sweet Satisfaction | Production Process With Flow Chart.* [Online]. 2016. [Accessed 16th July 2020]. Available from: https://discoverfoodtech.com/how-to-make-chocolate/
18. Talbot, G. Chocolate Temper. In: Beckett, S.T. ed. *Industrial Chocolate Manufacture and Use*. 4th ed., 2009, pp.261-275.

19. Ratnayake, W.M.N. and Galli, C. Fat and fatty acid terminology, methods of analysis and fat digestion and metabolism: a background review paper. *Annals of nutrition & metabolism.* 2009, **55**(1-3), pp.8-43.
20. Kolakowska, A. and Sikorski, Z.E. The Role of Lipids in Food Quality. In: Sikorski, Z.E. and Kolakowska, A. eds. CRC Press, 2002.
21. Shukla, V.K.S. Confectionery Lipids. In: Shahidi, F. ed. *Bailey's Industrial Oil and Fat Products*. 6th ed. Hoboken, NJ, USA: John Wiley & Sons Inc., 2005, pp.159-173.
22. Nichols, D.S. and Sanderson, K. The Nomenclature, Structure, and Properties of Food Lipids. In: *Chemical and Functional Properties of Food Lipids*. CRC Press, 2002.
23. Buscato, M.H.M., Grimaldi, R. and Kieckbusch, T.G. Cocoa butter symmetrical monounsaturated triacylglycerols: separation by solvent fractionation and application as crystallization modifier. *Journal of Food Science and Technology.* 2017, **54**(10), pp.3260-3267.
24. Himawan, C., Starov, V.M. and Stapley, A.G.F. Thermodynamic and kinetic aspects of fat crystallization. *Advances in Colloid and Interface Science.* 2006, **122**(1), pp.3-33.
25. Xu, X. Production of specific-structured triacylglycerols by lipase-catalyzed reactions: a review. *European Journal of Lipid Science and Technology.* 2000, **102**(4), pp.287-303.
26. Foubert, I., Vanrolleghem, P.A., Thas, O. and Dewettinck, K. Influence of Chemical Composition on the Isothermal Cocoa Butter Crystallization. *Journal of Food Science.* 2004, **69**(9), pp.E478-E487.
27. Weselake, R., Zou, J. and Taylor, D. *Plant Triacylglycerol Synthesis.* [Online]. [Accessed 20th June 2020]. Available from: https://lipidlibrary.aocs.org/chemistry/physics/plant-lipid/plant-triacylglycerol-synthesis#:~:text=Triacylglycerol%20is%20composed%20of%20three,2%20and%20sn%2D3%20positions.&text=Depending%20on%20the%20plant%20species,more%20forms%20of%20an%20enzyme.
28. Řezanka, T., Lukavský, J., Nedbalová, L. and Sigler, K. Production of structured triacylglycerols from microalgae. *Phytochemistry.* 2014, **104**, pp.95-104.

29. Kalpio, M., Nylund, M., Linderborg, K.M., Yang, B., Kristinsson, B., Haraldsson, G.G. and Kallio, H. Enantioselective chromatography in analysis of triacylglycerols common in edible fats and oils. *Food Chemistry.* 2015, **172**, pp.718-724.
30. Eliel, E.L., Wilen, S.H. and Doyle, M.P. *Basic organic stereochemistry.* New York, N.Y.: Wiley-Interscience, 2001.
31. Hardinger, S.A. *Illustrated Glossary of Organic Chemistry: Chiral.* [Online]. 2010-2017. [Accessed 25th August 2020]. Available from: http://www.chem.ucla.edu/~harding/IGOC/C/chiral.html
32. Singh, K., Shakya, P., Kumar, A., Alok, S. and Kamal, M. Stereochemistry and Its Role in Drug Design. *International Journal of Pharmaceutical Science Research.* 2014, **5**(11), pp.4644-4659.
33. Patel, E. *Naming Enantiomers by the R, S System.* [Online]. 2014. [Accessed 7th November 2018]. Available from: https://chem.libretexts.org/Textbook_Maps/Organic_Chemistry/Map%3A_Essential_Organic_Chemistry_(Bruice)/06%3A_Isomers_and_Stereochemistry/5.07%3A_Naming_Enantiomers_by_the_R%2CS_System
34. Schlenk, W. Synthesis and analysis of optically active triglycerides. *Journal of the American Oil Chemists Society.* 1965, **42**(11), pp.945-957.
35. Clark, J. *Plane Polarised Light.* [Online]. 2000. [Accessed 9th May 2016]. Available from: http://www.chemguide.co.uk/basicorg/isomerism/polarised.html#top
36. Řezanka, T. and Sigler, K. Separation of Enantiomeric Triacylglycerols by Chiral-Phase HPLC. *Lipids.* 2014, **49**(12), pp.1251-1260.
37. Maier, R. and Holman, R.T. Naturally Occurring Triglycerides Possessing Optical Activity in the Glycerol Moiety *. *Biochemistry.* 1964, **3**(2), pp.270-274.
38. Jandera, P. Stationary and mobile phases in hydrophilic interaction chromatography: a review. *Analytica Chimica Acta.* 2011, **692**(1-2), pp.1-25.

39. Waters. *HPLC Separation Modes.* [Online]. 2019. [Accessed 3rd April 2019]. Available from: http://www.waters.com/waters/en_US/HPLC-Separation-Modes/nav.htm?cid=10049076&locale=en_US

40. Clark, J. *High Performance Liquid Chomatography - HPLC.* [Online]. 2007. [Accessed 25th April 2016]. Available from: http://www.chemguide.co.uk/analysis/chromatography/hplc.html

41. Lísa, M. and Holcapek, M. Triacylglycerols profiling in plant oils important in food industry, dietetics and cosmetics using high-performance liquid chromatography-atmospheric pressure chemical ionization mass spectrometry. *Journal of chromatography. A.* 2008, **1198-1199**, pp.115-130.

42. Stolyhwo, A., Colin, H. and Guiochon, G. Analysis of Triglycerides in Oils and Fats by Liquid Chromatography with the Laser Light Scattering Detector. 1985, **57**, pp.1342-1354.

43. Roces, C., Kastner, E., Stone, P., Lowry, D., Perrie, Y., Roces, C.B., Kastner, E., Stone, P., Lowry, D. and Perrie, Y. Rapid Quantification and Validation of Lipid Concentrations within Liposomes. *Pharmaceutics.* 2016, **8**(3), pp.29-29.

44. Shimadzu. *ELSD-LTII.* [Online]. [Accessed 27th June 2019]. Available from: https://www.ssi.shimadzu.com/products/liquid-chromatography/elsd-ltii.html

45. McBride, B. *What are Evaporative Light-Scattering Detectors?* [Online]. 2017. [Accessed 4th June 2019]. Available from: https://www.peakscientific.com/blog/what-are-evaporative-light-scattering-detectors/

46. Buchgraber, M., Ulberth, F. and Anklam, E. Comparison of HPLC and GLC techniques for the determination of the triglyceride profile of cocoa butter. *Journal of Agricultural and Food Chemistry.* 2000, **48**(8), pp.3359-3363.

47. Christie, W.W. Detectors for high-performance liquid chromatography of lipids with special reference to evaporative light-scattering detection. *Advances in Lipid Methodology.* 1992, pp.239-271.

48. Byrdwell, W.C. Analysis of Lipids: Triacylglycerols, Phospholipids, Fatty Acids, and Others. *Bailey's Industrial Oil and Fat Products.* 2020, pp.1-43.
49. Murphy, R.C. and Axelsen, P.H. Mass spectrometric analysis of long-chain lipids. *Mass Spectrometry Reviews.* 2011, **30**(4), pp.579-599.
50. Byrdwell, W.C. Atmospheric pressure chemical ionization mass spectrometry for analysis of lipids. *Lipids.* 2001, **36**(4), pp.327-346.
51. The National High Magnetic Field Laboratory. *Atmospheric Pressure Chemical Ionization.* [Online]. 2015. [Accessed 11th June 2020]. Available from: https://nationalmaglab.org/user-facilities/icr/techniques/apci
52. ChemistryLibreTexts. *Diastereomers.* [Online]. 2019. [Accessed 24th July 2019]. Available from: https://chem.libretexts.org/Bookshelves/Organic_Chemistry/Supplemental_Modules_(Organic_Chemistry)/Chirality/Diastereomers
53. Takagi, T. and Ando, Y. Stereospecific analysis of monounsaturated triacylglycerols in cocoa butter. *Journal of the American Oil Chemists' Society.* 1995, **72**(10), pp.1203-1206.
54. Takagi, T. and Ando, Y. Stereospecific analysis of triacyl-sn-glycerols by chiral high-performance liquid chromatography. *Lipids.* 1991, **26**(7), pp.542-547.
55. Reusch, W. *Resolution of Racemates: Diastereomer Separation.* [Online]. 2013. [Accessed 4th June 2020]. Available from: https://www2.chemistry.msu.edu/faculty/reusch/VirtTxtJml/suppmnt4.htm
56. Řezanka, T., Pádrová, K. and Sigler, K. Regioisomeric and enantiomeric analysis of triacylglycerols. *Analytical Biochemistry.* 2016, **524**, pp.3-12.
57. Tang, M., Zhang, J., Zhuang, S. and Liu, W. *Development of chiral stationary phases for high-performance liquid chromatographic separation*. 2012, 39, pp.180-194. Available from: http://linkinghub.elsevier.com/retrieve/pii/S0165993612002002

58. Berthod, A. Chiral Recognition Mechanisms in Enantiomers Separations: A General View. *Chiral Recognition in Separation Methods, by Berthod, Alain, ISBN 978-3-642-12444-0. Springer-Verlag Berlin Heidelberg, 2010, p. 1.* 2010.
59. Wainer, I.W. CHROMATOGRAPHY: LIQUID | Mechanisms: Chiral. In: Wilson, I.D. ed. *Encyclopedia of Separation Science*. Oxford: Academic Press, 2000, pp.691-695.
60. Pryde, A. Chiral liquid chromatography: past and present. In: Lough, W.J. ed. *Chiral Liquid Chromatography*. Glasgow and London: Blackie and Son Ltd, 1989, pp.23 - 35.
61. Řezanka, T., Kolouchová, I., Nedbalová, L. and Sigler, K. Enantiomeric separation of triacylglycerols containing very long chain fatty acids. *Journal of Chromatography A.* 2018, **1557**, pp.9-19.
62. Iwasaki, Y., Yasui, M., Ishikawa, T., Irimescu, R., Hata, K. and Yamane, T. Optical resolution of asymmetric triacylglycerols by chiral-phase high-performance liquid chromatography. *Journal of Chromatography A.* 2001, **905**(1-2), pp.111-118.
63. Nagai, T., Mizobe, H., Otake, I., Ichioka, K., Kojima, K., Matsumoto, Y., Gotoh, N., Kuroda, I. and Wada, S. Enantiomeric separation of asymmetric triacylglycerol by recycle high-performance liquid chromatography with chiral column. *Journal of Chromatography A.* 2011, **1218**(20), pp.2880-2886.
64. Gunawardena, G. *Scalemic Mixture.* [Online]. 2019. [Accessed 14th April 2020]. Available from: https://chem.libretexts.org/Bookshelves/Ancillary_Materials/Reference/Organic_Chemistry_Glossary/Scalemic_Mixture
65. Lísa, M. and Holčapek, M. Characterization of Triacylglycerol Enantiomers Using Chiral HPLC/APCI-MS and Synthesis of Enantiomeric Triacylglycerols. *Analytical Chemistry.* 2013, **85**(3), pp.1852-1859.
66. Marangoni, A.G. and Wesdorp, L.H. Crystallography and Polymorphism. In: *Structure and Properties of Fat Crystal Networks*. 2nd ed. Boca Raton, FL: CRC Press, 2012, pp.1-26.

67. Mullin, J.W. Nucleation. In: *Crystallization*. 4th ed. Elsevier, 2001, pp.181-215.

68. Domingues, M.A.F., Ribeiro, A.P.B., Kieckbusch, T.G., Gioielli, L.A., Grimaldi, R., Cardoso, L.P. and Gonçalves, L.A.G. Advances in Lipids Crystallization Technology. In: Mastai, Y. ed. *Advanced Topics in Crystallization*. 2015, pp.105-132.

69. Marangoni, A.G. and Wesdorp, L.H. Nucleation and Crystalline Growth Kinetics. In: *Structure and Properties of Fat Crystal Networks*. 2nd ed. Boca Raton, FL: CRC Press, 2012, pp.27-100.

70. Ribeiro, A.P.B., Masuchi, M.H., Miyasaki, E.K., Domingues, M.A.F., Stroppa, V.L.Z., De Oliveira, G.M. and Kieckbusch, T.G. Crystallization modifiers in lipid systems. *Journal of Food Science and Technology.* 2015, **52**(7), pp.3925-3946.

71. Marangoni, A.G. Crystallization Kinetics. In: *Fat Crystal Networks*. New York: Marcel Dekker, 2004, pp.21-82.

72. Aquilano, D. and Sgualdino, G. Fundamental Aspects of Equilibrium and Crystallisation Kinetics. In: Garti, N. and Sato, K. eds. *Crystallization Processes in Fats and Lipid Systems*. Marcel Dekker Inc., 2001, pp.1-51.

73. McClements, D.J. Crystals and crystallization in oil-in-water emulsions: implications for emulsion-based delivery systems. *Advances in Colloid and Interface Science.* 2012, **174**, pp.1-30.

74. Encyclopaedia Britannica. *Polymorphism.* [Online]. 2016. [Accessed 4th May 2016]. Available from: http://www.britannica.com/science/polymorphism-crystals

75. Coultate, T.P. Lipids. In: *Food - The Chemistry of its Components*. 5th ed. Royal Society of Chemistry, 2009, pp.97-158.

76. Loisel, C., Keller, G., Lecq, G., Bourgaux, C. and Ollivon, M. Phase transitions and polymorphism of cocoa butter. *Journal of the American Oil Chemists' Society.* 1998, **75**(4), pp.425-439.

77. Narine, S.S. and Marangoni, A.G. Relating structure of fat crystal networks to mechanical properties. *Food Research International.* 1999, **32**(4), pp.227-248.

78. Sato, K. Crystallization behaviour of fats and lipids — a review. *Chemical Engineering Science.* 2001, **56**(7), pp.2255-2265.

79. Chemistry LibreTexts. *X-ray diffraction (XRD) basics and application.* [Online]. 2019. [Accessed 25th November 2019]. Available from: https://chem.libretexts.org/Courses/Franklin_and_Marshall_College/Introduction_to_Materials_Characterization_-_CHM_412_Collaborative_Text/Diffraction_Techniques/X-ray_diffraction_(XRD)_basics_and_application

80. Sögütoglu, L.-C., Steendam, R.R.E., Meekes, H., Vlieg, E. and Rutjes, F.P.J.T. Viedma ripening: a reliable crystallisation method to reach single chirality. *Chem. Soc. Rev.* 2015, **44**(19), pp.6723-6732.

81. Craven, R.J. and Lencki, R.W. Crystallization, Polymorphism, and Binary Phase Behavior of Model Enantiopure and Racemic Triacylglycerols. *Crystal Growth & Design.* 2011, **11**(5), pp.1723-1732.

82. Blackmond, D.G. The origin of biological homochirality. 2010, **2**, pp.a002147-a002147.

83. National Center for Biotechnology Information. *L(+)-Tartaric acid. PubChem Database. CID=44305.* [Online]. [Accessed 1st July 2020]. Available from: https://pubchem.ncbi.nlm.nih.gov/compound/444305

84. National Center for Biotechnology Information. *Tartaric acid. PubChem Database. CID=875.* [Online]. [Accessed 1st July 2020]. Available from: https://pubchem.ncbi.nlm.nih.gov/compound/875

85. Reusch, W. *Resolution of Racemates: Crystallization.* [Online]. 2013. [Accessed 4th June 2020]. Available from: https://www2.chemistry.msu.edu/faculty/reusch/VirtTxtJml/suppmnt4.htm

86. Craven, R.J. and Lencki, R.W. Symmetry, chirality and crystalline tendency: the polymorphism of triacylglycerols. *Food & Function.* 2012, **3**(3), pp.228-233.

87. Mizobe, H., Tanaka, T., Hatakeyama, N., Nagai, T., Ichioka, K., Hondoh, H., Ueno, S. and Sato, K. Structures and Binary Mixing Characteristics of Enantiomers of 1-Oleoyl-2,3-dipalmitoyl-sn-glycerol (S-OPP) and 1,2-Dipalmitoyl-3-oleoyl-sn-glycerol (R-PPO). *Journal of the American Oil Chemists' Society.* 2013, **90**(12), pp.1809-1817.

88. Sasaki, M., Ueno, S. and Sato, K. Polymorphism and Mixing Phase Behavior of Major Triacylglycerols of Cocoa Butter. In: Garti, N. and Widlak, N.R. eds. *Cocoa Butter and Related Compounds*. AOCS Press, 2012, pp.151-172.

89. Vereecken, J., Foubert, I., Smith, K.W., Sassano, G.J. and Dewettinck, K. Crystallization of model fat blends containing symmetric and asymmetric monounsaturated triacylglycerols. *European Journal of Lipid Science and Technology.* 2010, **112**(2), pp.233-245.

90. Yano, J., Ueno, S., Sato, K., Arishima, T., Sagi, N., Kaneko, F. and Kobayashi, M. FT-IR study of polymorphic transformations in SOS, POP, and POS. *The Journal of Physical Chemistry.* 1993, **97**(49), pp.12967-12973.

91. Arishima, T., Sagi, N., Mori, H. and Sato, K. Polymorphism of pos. I. occurrence and polymorphic transformation. *Journal of the American Oil Chemists Society.* 1991, **68**(10), pp.710-715.

92. Arishima, T. and Sato, K. Polymorphism of POP and SOS III. Solvent crystallization of β2 and β1 polymorphs. *Journal of the American Oil Chemists Society.* 1989, **66**(11), pp.1614-1617.

93. Padar, S., Mehrle, Y.E. and Windhab, E.J. Shear-Induced Crystal Formation and Transformation in Cocoa Butter. *Crystal Growth & Design.* 2009, **9**(9), pp.4023-4031.

94. Wille, R.L. and Lutton, E.S. Polymorphism of cocoa butter. *Journal of the American Oil Chemists Society.* 1966, **43**(8), pp.491-496.

95. Talbot, G. *Science and Technology of Enrobed and Filled Chocolate, Confectionery and Bakery Products.* Woodhead Publishing, 2009.

96. van Malssen, K., Langevelde, A., Peschar, R. and Schenk, H. Phase behavior and extended phase scheme of static cocoa butter investigated with real-time X-ray powder diffraction. *Journal of the American Oil Chemists' Society.* 1999, **76**(6), pp.669-676.

97. Timms, R.E. Phase behaviour of fats and their mixtures. *Progress in Lipid Research.* 1984, **23**(1), pp.1-38.

98. Beckett, S.T. *Physico-Chemical Aspects of Food Processing.* Springer Science & Business Media, 2012.

99. Lopes, D.G., Becker, K., Stehr, M., Lochmann, D., Haack, D., Zimmer, A. and Salar-Behzadi, S. Role of Lipid Blooming and Crystallite Size in the Performance of Highly Soluble Drug-Loaded Microcapsules. *Journal of Pharmaceutical Sciences.* 2015, **104**(12).

100. Sampugna, J. and Jensen, R.G. Stereospecific analysis of the major triglyceride species in the monounsaturated fraction of cocoa butter. *Lipids.* 1969, **4**(6), pp.444-449.

101. Chandler, I.C. and Quinlan, P.T. *Enzymic triglyceride conversion*. 1993.

102. Shin, J.-A., Akoh, C.C. and Lee, K.-T. Enzymatic interesterification of anhydrous butterfat with flaxseed oil and palm stearin to produce low-trans spreadable fat. *Food Chemistry.* 2010, **120**(1), pp.1-9.

103. Mu, H. and Porsgaard, T. The metabolism of structured triacylglycerols. *Progress in Lipid Research.* 2005, **44**(6), pp.430-448.

104. Ray, J., Nagy, Z.K., Smith, K.W., Bhaggan, K. and Stapley, A.G.F. Kinetic study of the acidolysis of high oleic sunflower oil with stearic–palmitic acid mixtures catalysed by immobilised Rhizopus oryzae lipase. *Biochemical Engineering Journal.* 2013, **73**, pp.17-28.

105. da Silva, R.C., Soares, D.F., Lourenço, M.B., Soares, F.A.S.M., da Silva, K.G., Gonçalves, M.I.A. and Gioielli, L.A. Structured lipids obtained by chemical interesterification of olive oil and palm stearin. *LWT - Food Science and Technology.* 2010, **43**(5), pp.752-758.

106. Marangoni, A.G. and Rousseau, D. Engineering triacylglycerols: The role of interesterification. *Trends in Food Science & Technology.* 1995, **6**(10), pp.329-335.

107. Kadivar, S., De Clercq, N., Van de Walle, D. and Dewettinck, K. Optimisation of enzymatic synthesis of cocoa butter equivalent from high oleic sunflower oil. *Journal of the Science of Food and Agriculture.* 2014, **94**(7), pp.1325-1331.

108. European Union. *Directive 2000/36/EC of the European Parliament and of the council of 23rd June 2000 relating to cocoa and chocolate products intended for human consumption.*, 2000.

109. Verstringe, S., De Clercq, N., Nguyen, T.M., Kadivar, S. and Dewettinck, K. Enzymatic and Other Modification Techniques to Produce Cocoa Butter Alternatives. In: Garti, N. and Widlak, N.R. eds. *Cocoa Butter and Related Compounds*. AOCS Press, 2012, pp.443-474.

110. Xavier Malcata, F., Reyes, H.R., Garcia, H.S., Hill, C.G. and Amundson, C.H. Immobilized lipase reactors for modification of fats and oils—A review. *Journal of the American Oil Chemists' Society.* 1990, **67**(12), pp.890-910.

111. Catalano, S., Wozniak, A. and Kaplan, K. *Packed Bed Reactors.* [Online]. [Accessed 5th January 2020]. Available from: http://encyclopedia.che.engin.umich.edu/Pages/Reactors/PBR/PBR.html

112. Xu, X., Guo, Z., Zhang, H., Vikbjerg, A.F. and Damstrup, M.L. Chemical and enzymatic interesterification of lipids for use in food. In: Gunstone, F.D. ed. *Modifying Lipids for Use in Foods*. Woodhead Publishing, 2006, pp.234 - 272.

113. Berry, S.E.E. Triacylglycerol structure and interesterification of palmitic and stearic acid-rich fats: an overview and implications for cardiovascular disease. *Nutrition research reviews.* 2009, **22**(1), pp.3-17.

114. Houde, A., Kademi, A. and Leblanc, D. Lipases and their industrial applications. *Applied biochemistry and biotechnology.* 2004, **118**(1), pp.155-170.

115. Willis, W.M. and Marangoni, A.G. Enzymatic Interesterification. In: Akoh, C.C. and Min, D.B. eds. CRC Press, 2008.

116. Osborn, H.T. and Akoh, C.C. Structured Lipids-Novel Fats with Medical, Nutraceutical, and Food Applications. *Comprehensive Reviews in Food Science and Food Safety.* 2002, **1**(3), pp.110-120.

117. Knothe, G., Kenar, J.A. and Gunstone, F.D. Chemical Properties. In: Gunstone, F.D.Harwood, J.L.Dijkstra, A.J. eds. *The Lipid Handbook* 3rd ed. Boca Raton, FL: CRC Press, 2007, pp.535 - 589.

118. Gandhi, N.N., Patil, N.S., Sawant, S.B., Joshi, J.B., Wangikar, P.P. and Mukesh, D. Lipase-Catalyzed Esterification. *Catalysis Reviews.* 2000, **42**(4), pp.439-480.

119. Schmid, U., Bornscheuer, U.T., Soumanou, M.M., McNeill, G.P. and Schmid, R.D. Highly selective synthesis of 1,3-oleoyl-2-palmitoylglycerol by lipase catalysis. *Biotechnology and Bioengineering.* 1999, **64**(6), pp.678-684.

120. Ortiz, C., Ferreira, M.L., Barbosa, O., Dos Santos, J.C.S., Rodrigues, R.C., Berenguer-Murcia, Á., Briand, L.E. and Fernandez-Lafuente, R. Novozym 435: the “perfect” lipase immobilized biocatalyst? *Catalysis Science & Technology.* 2019, **9**(10), pp.2380-2420.

121. Kadivar, S., De Clercq, N., Nusantoro, B.P., Le, T.T. and Dewettinck, K. Development of an offline bidimensional high-performance liquid chromatography method for analysis of stereospecific triacylglycerols in cocoa butter equivalents. *Journal of Agricultural and Food Chemistry.* 2013, **61**(33), pp.7896-7903.

122. Xu, X. Engineering of enzymatic reactions and reactors for lipid modification and synthesis. *European Journal of Lipid Science and Technology.* 2003, **105**(6), pp.289-304.

123. Mohamed, I.O. Lipase-catalyzed synthesis of cocoa butter equivalent from palm olein and saturated fatty acid distillate from palm oil physical refinery. *Applied biochemistry and biotechnology.* 2012, **168**(6), pp.1405-1415.

124. Kadivar, S., De Clercq, N., Danthine, S. and Dewettinck, K. Crystallization and polymorphic behavior of enzymatically produced sunflower oil based cocoa butter equivalents. *European Journal of Lipid Science and Technology.* 2016, **118**(10), pp.1521-1538.

125. Mohamed, I.O. Lipase-catalyzed acidolysis of palm mid fraction oil with palmitic and stearic fatty acid mixture for production of cocoa butter equivalent. *Applied biochemistry and biotechnology.* 2013, **171**(3), pp.655-666.

126. Çiftçi, O.N., Fadiloğlu, S., Kowalski, B. and Göğüş, F. Synthesis of cocoa butter triacylglycerols using a model acidolysis system. *Grasas y Aceites.* 2008, **59**(4), pp.316-320.

127. European Union. *Directive 2009/32/EC of the European Parliament and of the council of 23rd April 2009 on the approximation of the laws of the Member States on extraction solvents used in the production of foodstuffs and food ingredients.* 2009.

128. Kim, S., Kim, I.H., Akoh, C.C. and Kim, B.H. Enzymatic production of cocoa butter equivalents high in 1-palmitoyl-2-oleoyl-3-stearin in continuous packed bed reactors. *JAOCS, Journal of the American Oil Chemists' Society.* 2014, **91**(5), pp.747-757.

129. Halldorsson, A., Magnusson, C.D. and Haraldsson, G.G. Chemoenzymatic synthesis of structured triacylglycerols by highly regioselective acylation. *Tetrahedron.* 2003, **59**(46), pp.9101-9109.

130. Bornscheuer, U.T. and Yamane, T. Fatty acid vinyl esters as acylating agents: A new method for the enzymatic synthesis of monoacylglycerols. *Journal of the American Oil Chemists' Society.* 1995, **72**(2), pp.193-197.

131. Wang, X., Zou, W., Sun, X., Zhang, Y., Wei, L., Jin, Q. and Wang, X. Chemoenzymatic synthesis of 1,3-dioleoyl-2-palmitoylglycerol. *Biotechnology Letters.* 2015, **37**(3), pp.691-696.

132. Kristinsson, B., Linderborg, K.M., Kallio, H. and Haraldsson, G.G. Synthesis of enantiopure structured triacylglycerols. *Tetrahedron: Asymmetry.* 2014, **25**(2), pp.125-132.

133. Kristinsson, B. and Haraldsson, G.G. Chemoenzymatic synthesis of enantiopure structured triacylglycerols. *Synlett.* 2008, **2008**(14), pp.2178-2182.

134. Sarkar, A., Ye, A. and Singh, H. On the role of bile salts in the digestion of emulsified lipids. *Food Hydrocolloids.* 2016, **60**, pp.77-84.

135. Golding, M. and Wooster, T.J. The influence of emulsion structure and stability on lipid digestion. *Current Opinion in Colloid & Interface Science.* 2010, **15**(1-2), pp.90-101.

136. Wilde, P.J. and Chu, B.S. Interfacial & colloidal aspects of lipid digestion. *Advances in Colloid and Interface Science.* 2011, **165**(1), pp.14-22.

137. McClements, D.J., Decker, E.A. and Park, Y. Physicochemical and structural aspects of lipid digestion. In: McClements, D.J. ed. Woodhead Publishing, 2007, pp.483-503.
138. Maldonado-Valderrama, J., Wilde, P., Macierzanka, A. and Mackie, A. The role of bile salts in digestion. *Advances in Colloid and Interface Science.* 2011, **165**(1), pp.36-46.
139. Torcello-Gómez, A., Boudard, C. and Mackie, A.R. Calcium Alters the Interfacial Organization of Hydrolyzed Lipids during Intestinal Digestion. *Langmuir.* 2018, **34**(25), pp.7536-7544.
140. Joyce, P., Whitby, C.P. and Prestidge, C.A. Nanostructuring Biomaterials with Specific Activities towards Digestive Enzymes for Controlled Gastrointestinal Absorption of Lipophilic Bioactive Molecules. *Advances in Colloid and Interface Science.* 2016, **237**, pp.52-75.
141. Golding, M., Wooster, T.J., Day, L., Xu, M., Lundin, L., Keogh, J. and Clifton, P. Impact of gastric structuring on the lipolysis of emulsified lipids. *Soft Matter.* 2011, **7**(7), pp.3513-3513.
142. Berry, S.E.E. and Sanders, T.A.B. Influence of triacylglycerol structure of stearic acid-rich fats on postprandial lipaemia. *Proceedings of the Nutrition Society.* 2007, **64**(02), pp.205-212.
143. Bonnaire, L., Sandra, S., Helgason, T., Decker, E.A., Weiss, J. and McClements, D.J. Influence of Lipid Physical State on the in Vitro Digestibility of Emulsified Lipids. *Journal of Agricultural and Food Chemistry.* 2008, **56**(10), pp.3791-3797.
144. Christie, W.W. *The Chromatographic Resolution of Chiral Lipids.* [Online]. 1992. [Accessed 4th March 2019]. Available from: https://lipidlibrary.aocs.org/lipid-analysis/selected-topics-in-the-analysis-of-lipids/the-chromatographic-resolution-of-chiral-lipids
145. Zawirska-Wojtasiak, R. Chirality and the nature of food authenticity of aroma. *Acta Scientiarum Polonorum Technologia Alimentaria.* 2006, **5**(1), pp.21-36.
146. Shahkhalili, Y., Duruz, E. and Acheson, K. Digestibility of cocoa butter from chocolate in humans: a comparison with corn-oil. *European Journal of Clinical Nutrition.* 2000, **54**(2), pp.120-125.

147. Iwahashi, M. and Kasahara, Y. Dynamic molecular movements and aggregation structures of lipids in a liquid state. *Current Opinion in Colloid & Interface Science.* 2011, **16**(5), pp.359-366.

148. mbraun. *Solvent Purifiers.* [Online]. 2020. [Accessed 30th April 2020]. Available from: https://www.mbraun.com/en/products/solvent-purifiers.html

149. Torcello-Gómez, A. *Conversation with Louise Sim*, 2nd October, 2017.

150. Parr Instrument Company. Stirred Reactors and Pressure Vessels. **15**.

151. Ficara, E., Rozzi, A. and Cortelezzi, P. Theory of pH-stat titration. *Biotechnology and Bioengineering.* 2003, **82**(1), pp.28-37.

152. Minekus, M., Alminger, M., Alvito, P., Ballance, S., Bohn, T., Bourlieu, C., Carrière, F., Boutrou, R., Corredig, M., Dupont, D., Dufour, C., Egger, L., Golding, M., Karakaya, S., Kirkhus, B., Le Feunteun, S., Lesmes, U., Macierzanka, A., Mackie, A., Marze, S., McClements, D.J., Ménard, O., Recio, I., Santos, C.N., Singh, R.P., Vegarud, G.E., Wickham, M.S.J., Weitschies, W. and Brodkorb, A. A standardised static in vitro digestion method suitable for food – an international consensus. *Food Funct.* 2014, **5**(6), pp.1113-1124.

153. Holmes, M.J., Parker, N.G. and Povey, M.J.W. Temperature dependence of bulk viscosity in water using acoustic spectroscopy. *Journal of Physics: Conference Series.* 2011, **269**, p.012011.

154. Holčapek, M., Lísa, M., Jandera, P. and Kabátová, N. Quantitation of triacylglycerols in plant oils using HPLC with APCI-MS, evaporative light-scattering, and UV detection. *Journal of Separation Science.* 2005, **28**(12), pp.1315-1333.

155. Barth, H.G. *Chromatography Fundamentals, Part V: Theoretical Plates: Significance, Properties, and Uses.* [Online]. 2018. [Accessed 29th July 2020]. Available from: https://www.chromatographyonline.com/view/chromatography-fundamentals-part-v-theoretical-plates-significance-properties-and-uses

156. Rumble, J.R., ed.,. Permittivity (Dielectric Constant) of Liquids. *CRC Handbook of Chemistry and Physics.* [Online]. 100th Edition (Internet Version) ed. Boca Raton, FL.: CRC Press/Taylor & Francis, 2019. Available from: http://hbcponline.com/faces/contents/InteractiveTable.xhtml

157. The Pharmaceutics and Compounding Laboratory. *Factors Influencing the Solubility of Drugs: Solute and Solvent Structure/Polarity.* [Online]. 2020. [Accessed 11th March 2020]. Available from: https://pharmlabs.unc.edu/labs/solubility/structure.htm

158. Miller, K.J., Gal, J. and Ames, M.M. High-performance liquid chromatographic resolution of enantiomers of 1-phenyl-2-aminopropanes (amphetamines) with four chiral reagents. *Journal of Chromatography B: Biomedical Sciences and Applications.* 1984, **307**(C), pp.335-342.

159. Batista, A.N.L., Dos Santos Jr., F.M., Batista Jr., J.M. and Cass, Q.B. Enantiomeric Mixtures in Natural Product Chemistry: Separation and Absolute Configuration Assignment. *Molecules.* 2018, **23**(2), p.492.

160. Rocco, A., Aturki, Z. and Fanali, S. Chiral separations in food analysis. *TrAC Trends in Analytical Chemistry.* 2013, **52**, pp.206-225.

161. Wei, Q., Su, H., Gao, D. and Wang, S. HPLC with cellulose Tris (3,5-DimethylPhenylcarbamate) chiral stationary phase: Influence of coating times and coating amount on chiral discrimination. *Chirality.* 2019, **31**(3), pp.164-173.

162. Nagai, T., Matsumoto, Y., Jiang, Y., Ishikawa, K., Wakatabe, T., Mizobe, H., Yoshinaga, K., Kojima, K., Kuroda, I., Saito, T., Beppu, F. and Gotoh, N. Actual Ratios of Triacylglycerol Positional Isomers and Enantiomers Comprising Saturated Fatty Acids and Highly Unsaturated Fatty Acids in Fishes and Marine Mammals. *Journal of Oleo Science J. Oleo Sci.* 2013, **62**(12), pp.1009-1015.

163. Scriba, G.K.E. *Chiral recognition mechanisms in analytical separation sciences*. 2012, 75, pp.815-838. Available from: http://link.springer.com/10.1007/s10337-012-2261-1

164. Ali, I., Kumerer, K. and Aboul-Enein, H.Y. Mechanistic Principles in Chiral Separations Using Liquid Chromatography and Capillary Electrophoresis. *Chromatographia.* 2006, **63**(7), pp.295-307.

165. Sigma-Aldrich. Chiral Chromatography. [Online]. [Accessed 25th July 2019]. Available from: https://mz-at.de/fileadmin/user_upload/Brochures/supelco-3-chiral.pdf

166. Azzi, J., Danjou, P.-E., Landy, D., Ruellan, S., Auezova, L., Greige-Gerges, H. and Fourmentin, S. The effect of cyclodextrin complexation on the solubility and photostability of nerolidol as pure compound and as main constituent of cabreuva essential oil. *Beilstein Journal of Organic Chemistry.* 2017, **13**, pp.835-844.

167. Sadeghpour, A., Parada, M.L., Vieira, J., Povey, M. and Rappolt, M. Global Small-Angle X-ray Scattering Data Analysis of Triacylglycerols in the Molten State (Part I). *The Journal of Physical Chemistry B.* 2018, **122**(45), pp.10320-10329.

168. Sahin, N., Akoh, C.C. and Karaali, A. Lipase-catalyzed acidolysis of tripalmitin with hazelnut oil fatty acids and stearic acid to produce human milk fat substitutes. *Journal of Agricultural and Food Chemistry.* 2005, **53**(14), pp.5779-5783.

169. Sun, C., Wei, W., Su, H., Zou, X. and Wang, X. Evaluation of sn-2 fatty acid composition in commercial infant formulas on the Chinese market: A comparative study based on fat source and stage. *Food Chemistry.* 2018, **242**, pp.29-36.

170. Rupiani, S. *Email to Louise Sim*, 9th May 2019,

171. Hoye, T.R., Jeffrey, C.S. and Shao, F. Mosher ester analysis for the determination of absolute configuration of stereogenic (Chiral) carbinol carbons. *Nature Protocols.* 2007, **2**(10), pp.2451-2458.

172. Mori, K. Pheromone synthesis. Part 253: Synthesis of the racemates and enantiomers of triglycerides of male Drosophila fruit flies with special emphasis on the preparation of enantiomerically pure 1-monoglycerides. *Tetrahedron.* 2012, **68**(40), pp.8441-8449.

173. Sonnet, P.E. and Dudley, R.L. Stereospecific synthesis of selected triglycerides: comments on acyl migration and analysis of configuration. *Chemistry and Physics of Lipids.* 1994, **72**(2), pp.185-191.

174. Meyer, S., Berrut, S., Goodenough, T.I.J., Rajendram, V.S., Pinfield, V.J. and Povey, M.J.W. A comparative study of ultrasound and laser light diffraction techniques for particle size determination in dairy beverages. *Measurement Science and Technology.* 2006, **17**(2), pp.289-297.

175. Anton Paar. *Viscosity of Water.* [Online]. 2019. [Accessed 29th October 2019]. Available from: https://wiki.anton-paar.com/uk-en/water/

176. Armand, M., Borel, P., Ythier, P., Dutot, G., Melin, C., Senft, M., Lafont, H. and Lairon, D. Effects of droplet size, triacylglycerol composition, and calcium on the hydrolysis of complex emulsions by pancreatic lipase: an in vitro study. *The Journal of Nutritional Biochemistry.* 1992, **3**(7), pp.333-341.

177. Borel, P., Armand, M., Ythier, P., Dutot, G., Melin, C., Senft, M., Lafont, H. and Lairon, D. Hydrolysis of emulsions with different triglycerides and droplet sizes by gastric lipase in vitro. Effect on pancreatic lipase activity. *The Journal of Nutritional Biochemistry.* 1994, **5**(3), pp.124-133.

178. Helbig, A., Silletti, E., Timmerman, E., Hamer, R.J. and Gruppen, H. In vitro study of intestinal lipolysis using pH-stat and gas chromatography. *Food Hydrocolloids.* 2012, **28**(1), pp.10-19.

179. Singh, H., Ye, A. and Horne, D. Structuring food emulsions in the gastrointestinal tract to modify lipid digestion. *Progress in Lipid Research.* 2009, **48**(2), pp.92-100.

180. Ehrlein, H. and Schemann, M. Gastrointestinal motility. *Technische Universität München: Munich.* 2005, pp.1-26.

181. Doran, P.M. *Bioprocess engineering principles.* Second ed. Amsterdam: Elsevier/Academic Press, 2013.

182. O'Driscoll, A. *Selecting an Impeller for Your Overhead Stirrer.* [Online]. 2019. [Accessed 2nd October 2019]. Available from: https://stirrers.net/blogs/blog/selecting-an-impeller-for-your-overhead-stirrer

183. Chen, J., Gaikwad, V., Holmes, M., Murray, B., Povey, M., Wang, Y. and Zhang, Y. Development of a simple model device for in vitro gastric digestion investigation. *Food & Function.* 2011, **2**(3-4), pp.174-182.

184. Smith, K.W. Confectionery Fats. In: Garti, N. and Widlak, N.R. eds. AOCS Press, 2012, pp.475-495.

185. Smith, K.W., Bhaggan, K. and Talbot, G. Phase behavior of symmetrical monounsaturated triacylglycerols. *European Journal of Lipid Science and Technology.* 2013, **115**(8), pp.838-846.

186. National Center for Biotechnology Information. *2-[Bis-(2-hydroxy-ethyl)-amino]-2-hydroxymethyl-propane-1,3-diol. PubChem Compound Summary for CID 81462.* [Online]. [Accessed 16th December 2020]. Available from: https://pubchem.ncbi.nlm.nih.gov/compound/81462

187. Mat, D.J.L., Le Feunteun, S., Michon, C. and Souchon, I. In vitro digestion of foods using pH-stat and the INFOGEST protocol: Impact of matrix structure on digestion kinetics of macronutrients, proteins and lipids. *Food Research International.* 2016, **88**, pp.226-233.

188. Andreska, J. *Condition for $NaHCO_3$ to react to form CO_2 with organic acids.* [Online]. 2015. [Accessed 26th April 2020]. Available from: https://chemistry.stackexchange.com/a/33014

189. Loerting, T. and Bernard, J. Aqueous Carbonic Acid (H_2CO_3). *ChemPhysChem.* 2010, **11**(11), pp.2305-2309.

190. National Center for Biotechnology Information. *Sodium bicarbonate. PubChem Database. CID=516892.* [Online]. [Accessed 28th April 2020]. Available from: https://pubchem.ncbi.nlm.nih.gov/compound/Sodium-bicarbonate

191. European Commission - Joint Research Centre. *Certified Reference Material IRMM-801.*

192. Coultate, T. Melting and Crystallisation. In: *Food - The Chemistry of its Components (6th Edition)*. Royal Society of Chemistry, 2016, pp.147-153.

193. Lide, D.R. ed. *CRC Handbook of Chemistry and Physics, 1992-1993 : A Ready-Reference Book of Chemical and Physical Data.* 73 ed. Boca Raton (Florida): CRC Press, 1992.

194. Gass, J., Vora, H., Hofmann, A.F., Gray, G.M. and Khosla, C. Enhancement of Dietary Protein Digestion by Conjugated Bile Acids. *Gastroenterology.* 2007, **133**(1), pp.16-23.

195. Ayala-Bribiesca, E., Turgeon, S.L. and Britten, M. Effect of calcium on fatty acid bioaccessibility during in vitro digestion of Cheddar-type cheeses prepared with different milk fat fractions. *Journal of dairy science.* 2017, **100**(4), pp.2454-2470.

196. Baggaley, A. ed. *Human Body.* London: Dorling Kindersley Limited, 2001.

197. Chromatography Today. *What is Peak Fronting?* [Online]. 2014. [Accessed 9th March 2020]. Available from: https://www.chromatographytoday.com/news/columns-lc/37/breaking-news/what-is-peak-fronting/31490

198. AAK. *Analytical Certificate: Akomed R (MCT).* 2018.

199. Xu, X., Mu, H., Høy, C.E. and Adler-Nissen, J. Production of specifically structured lipids by enzymatic interesterification in a pilot enzyme bed reactor: process optimization by response surface methodology. *European Journal of Lipid Science and Technology.* 1999, **101**(6), pp.207-214.

200. Guan, F., Kapur, N., Sim, L., Taylor, C.J., Wen, J., Zhang, X. and Blacker, A.J. A universal reactor platform for batch and flow: application to homogeneous and heterogeneous hydrogenation. *Reaction Chemistry & Engineering.* 2020.

201. Chapman, M.R., Kwan, M.H.T., King, G., Jolley, K.E., Hussain, M., Hussain, S., Salama, I.E., González Niño, C., Thompson, L.A., Bayana, M.E., Clayton, A.D., Nguyen, B.N., Turner, N.J., Kapur, N. and Blacker, A.J. Simple and Versatile Laboratory Scale CSTR for Multiphasic Continuous-Flow Chemistry and Long Residence Times. *Organic Process Research & Development.* 2017, **21**(9), pp.1294-1301.

202. ERIKS. *VITON® Fluorelastomers: An overview.* [Leaflet]. 2000.

203. Sánchez, D.A., Tonetto, G.M. and Ferreira, M.L. Screening of Lipases with Unusual High Activity in the sn-2 Esterification of 1,3-Dicaprin under Mild Operating Conditions. *Journal of Agricultural and Food Chemistry.* 2017, **65**(24), pp.5010-5017.

204. Xiong, D., Zhang, H., Xie, Y., Tang, N., Berenjian, A. and Song, Y. Conversion of Mutton Fat to Cocoa Butter Equivalent by Increasing the Unsaturated Fatty Acids at the Sn-2 Position of Triacylglycerol Through Fermentation by Yarrowia Lipolytica. *American Journal of Biochemistry and Biotechnology.* 2015, **11**(2), pp.57-65.

205. Nichols, L. *Drying Glassware.* [Online]. 2019. [Accessed 25th May 2020]. Available from: https://chem.libretexts.org/Bookshelves/Organic_Chemistry/Book%3A_Organic_Chemistry_Lab_Techniques_(Nichols)/01%3A_General_Techniques/1.01%3A_Glassware_and_Equipment/1.1.0F%3A_1.1F%3A_Drying_Glassware

206. National Center for Biotechnology Information. *Ethyl palmitate. PubChem Database. CID=12366.* [Online]. [Accessed 12th December 2019]. Available from: https://pubchem.ncbi.nlm.nih.gov/compound/Ethyl-palmitate

207. Rezanka, T., Nedbalova, L. and Sigler, K. Enantiomeric separation of triacylglycerols containing polyunsaturated fatty acids with 18 carbon atoms. *Journal of Chromatography A.* 2016, **1467**, pp.261-269.

208. Tokyo Chemical Industry UK Ltd. *(R)-(+)-3-Benzyloxy-1,2-propanediol.* [Online]. [Accessed 2nd June 2020]. Available from: https://www.tcichemicals.com/GB/en/p/B2141#docomentsSectionPDP

209. Hidalgo, A.M., Sánchez, A., Gómez, J.L., Gómez, E., Gómez, M. and Murcia, M.D. Kinetic Study of the Enzymatic Synthesis of 2-Phenylethyl Acetate in Discontinuous Tank Reactor. *Industrial & Engineering Chemistry Research.* 2018, **57**(33), pp.11280-11287.

210. Yakukhnov, S.A. and Ananikov, V.P. Catalytic Transfer Hydrodebenzylation with Low Palladium Loading. *Advanced Synthesis & Catalysis.* 2019, **361**(20), pp.4781-4789.

211. Fodran, P., Das, N.J.L.C., Eisink, N.N.H.M., Welleman, I.M., Kloek, W. and Minnaard, A.J. An efficient catalytic three-step synthesis of enantiopure triacylglycerols. *European Journal of Lipid Science and Technology.* 2016, **118**(11), pp.1768-1774.

212. Ghazani, S.M. and Marangoni, A.G. The Triclinic Polymorphism of Cocoa Butter Is Dictated by Its Major Molecular Species, 1-Palmitoyl, 2-Oleoyl, 3-Stearoyl Glycerol (POS). *Crystal Growth and Design.* 2019, **19**(1), pp.90-97.

213. Christie, W.W. *Triacylglycerols: 2. Biosynthesis and Metabolism.* [Online]. 2019. [Accessed 6th January 2020]. Available from: https://www.lipidmaps.org/resources/lipidweb/index.php?page=lipids/simple/tag2/index.htm

214. Scriba, G.K.E. Chiral recognition in separation sciences. Part I: Polysaccharide and cyclodextrin selectors. *TrAC Trends in Analytical Chemistry.* 2019, **120**, p.115639.

215. Haraldsson, G. *Email to Louise Sim*, 19th October 2019.

216. Blackmond, D.G. The Origin of Biological Homochirality. *Cold Spring Harbor perspectives in biology.* 2019, **11**(3).

217. Christie, W.W., Nikolova-Damyanova, B., Laakso, P. and Herslof, B. Stereospecific analysis of triacyl-sn-glycerols via resolution of diastereomeric diacylglycerol derivatives by high-performance liquid chromatography on silica. *Journal of the American Oil Chemists Society.* 1991, **68**(10), pp.695-701.

Appendix A Supporting information for Chapter 3

A.1 Calibration curves of POP, POSt and StOSt

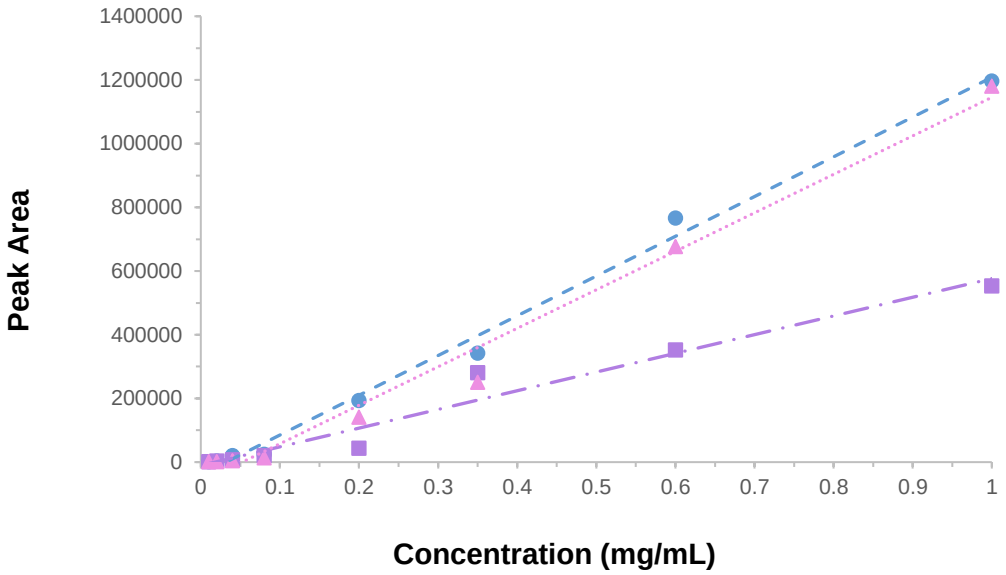

Figure A.1 Peak area as a function of injected concentration of POP (blue circles), POSt (purple squares) and StOSt (pink triangles). Injection volume was 20 µL.

A.2 Potential diastereomeric derivatives of a rac-POSt standard

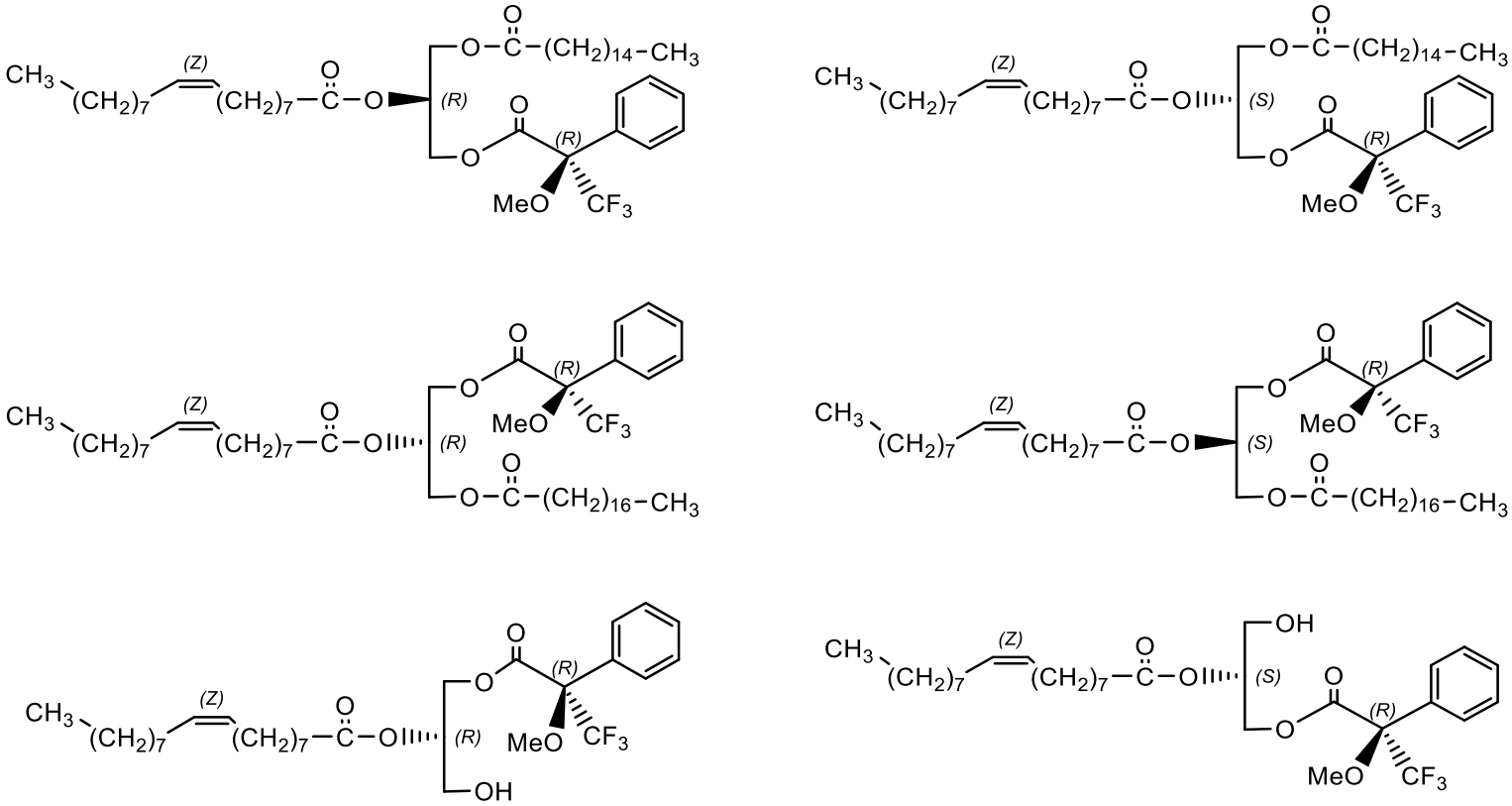

Figure A.2 Potential diastereomers formed following the derivatisation of rac-POSt with (R)-(+)-MTPA-Cl CDA. A further possible structure not shown is one where the CDA is present at both primary positions of the glycerol, leaving oleic acid at sn-2.

A.3 Derivatisation NMR spectra

A.3.1 POSt derivatisation experiment following solubility trials

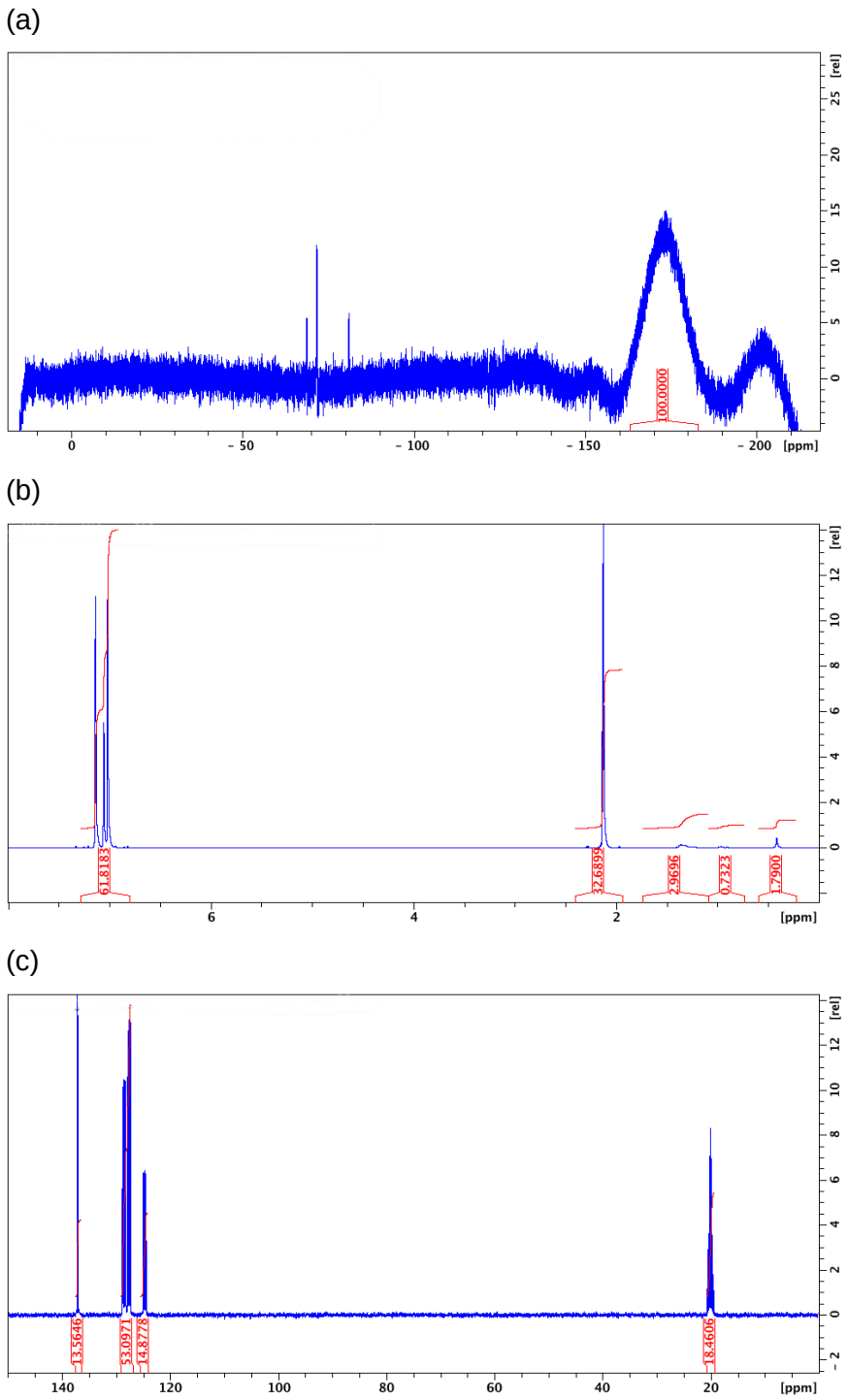

Figure A.3 Derivatisation product dissolved in Tol-D8 following various solvent trials showing (a) ^{19}F, (b) ^{1}H and (c) ^{13}C spectra.

A.3.2 Derivatisation experiment: conducted and analysed same day

(a)

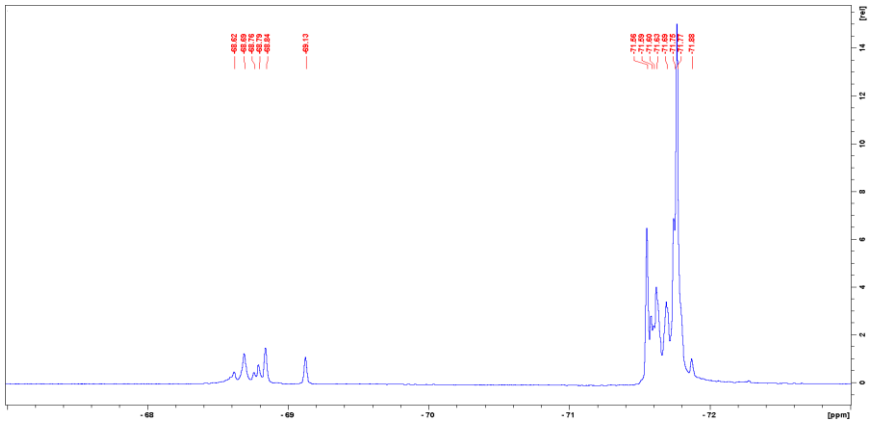

(b)

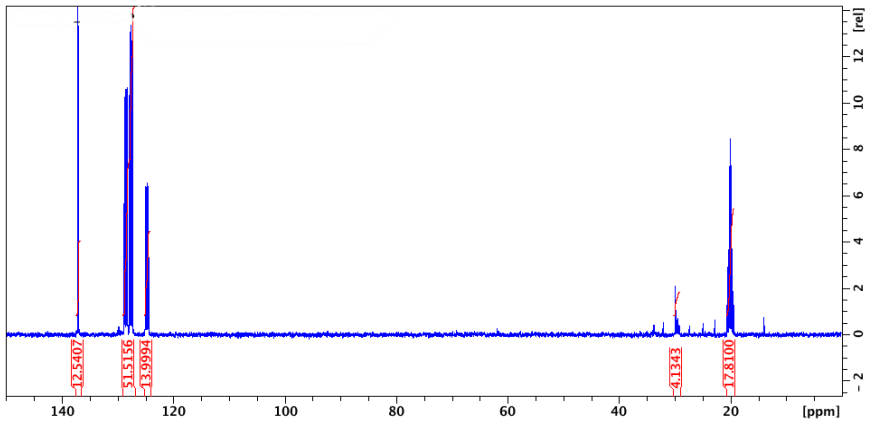

Figure A.4 Derivatisation was performed and sample analysed on the same day where (a) shows the result from ^{19}F analysis and (b) ^{13}C NMR. The reaction product was suspended in 0.6 mL Tol-D8.

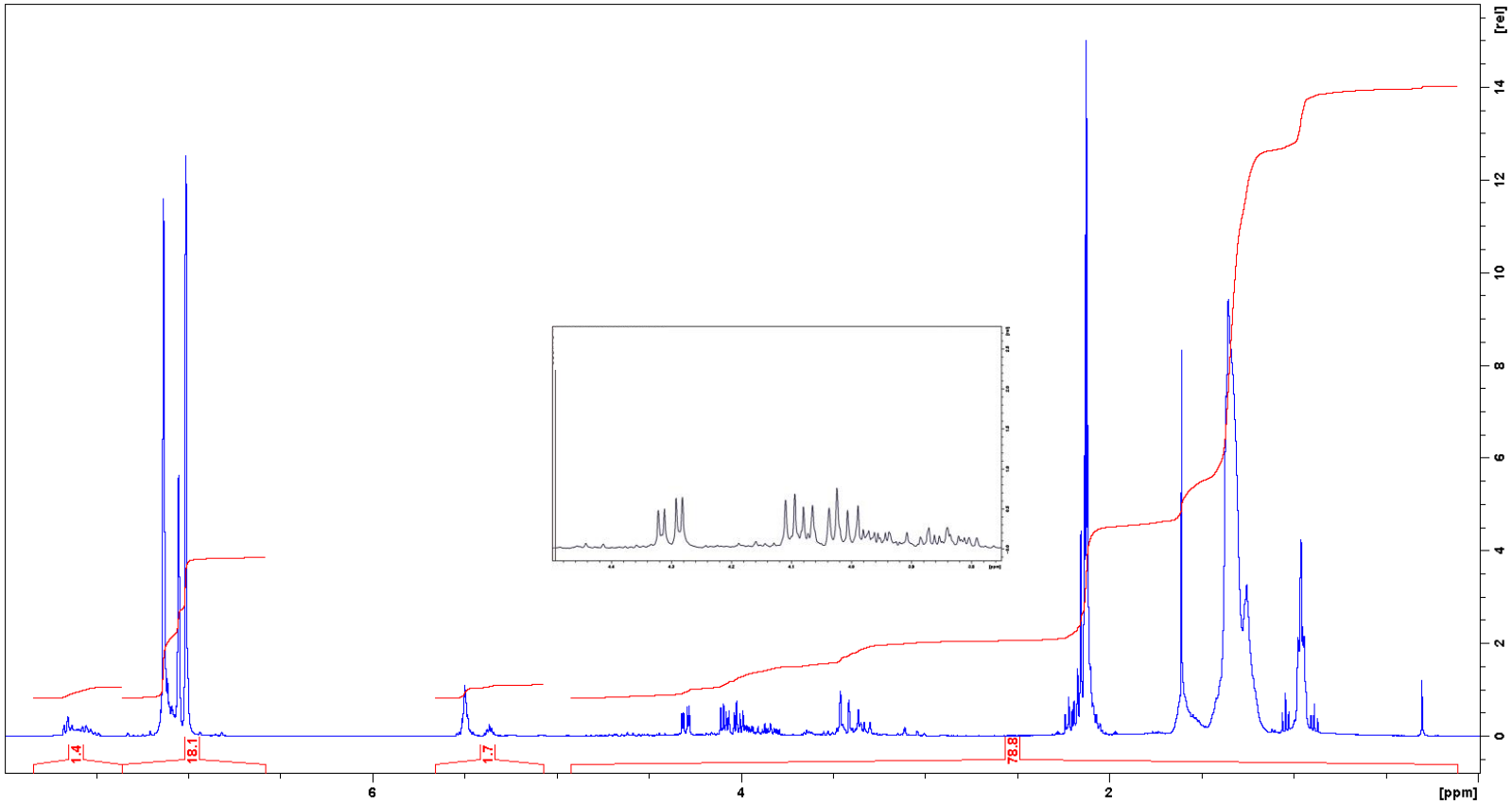

Figure A.5 ^{1}H NMR spectra of the derivatisation product created and analysed on the same day. Insert shows the area corresponding with CH_2 groups of the glycerol; peaks to the left-hand side are as expected, but the right-hand peaks show an upfield shift, alongside additional peaks that may relate to diastereomeric compounds of rac-POSt.

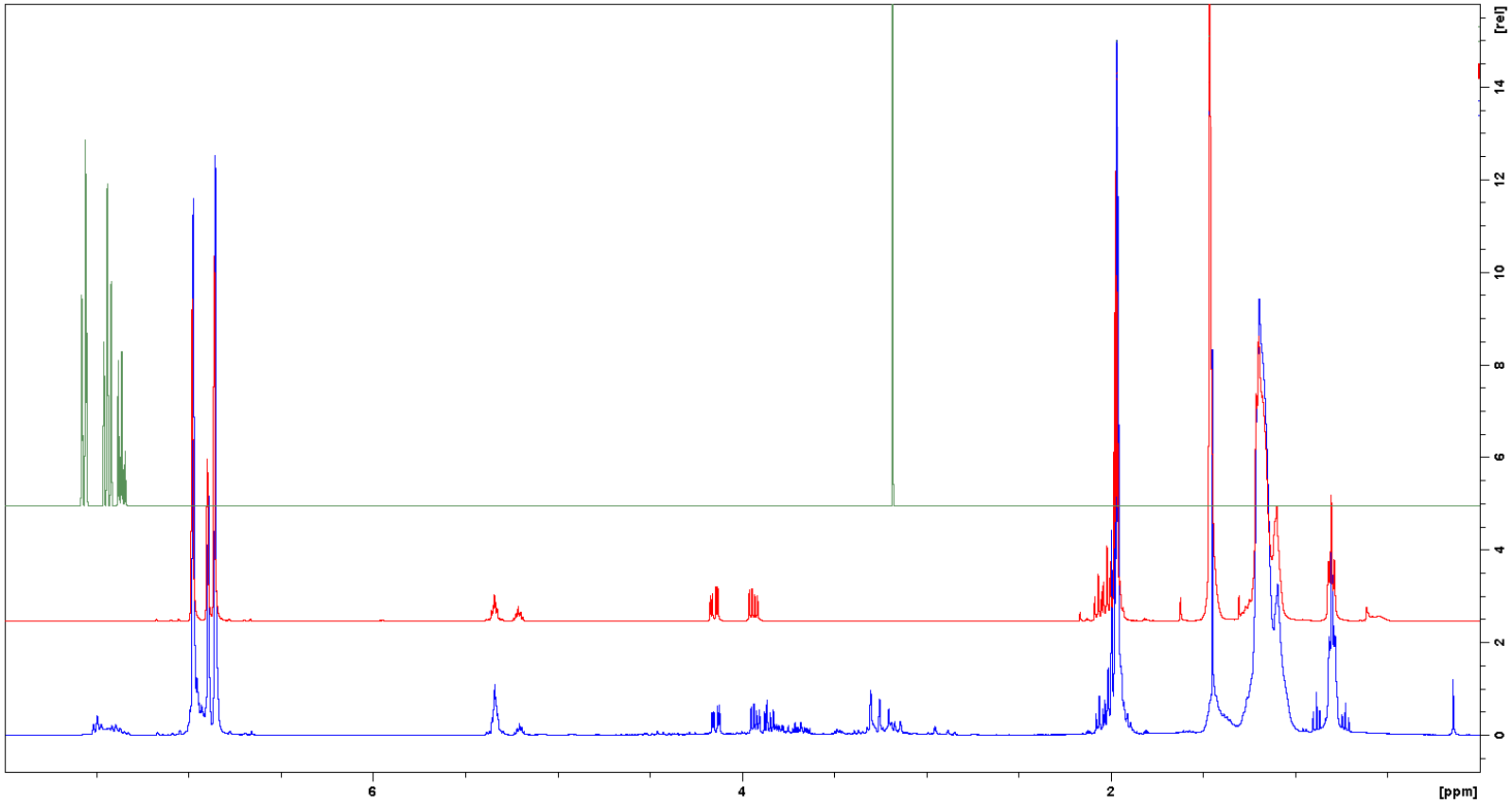

Figure A.6 ^{1}H NMR spectra comparing the same-day derivatisation product (bottom; blue), rac-POSt standard (middle; red) and a predicted spectra for (R)-(-)-MTPA-Cl (top; green): analytical data unavailable for the latter. Differences in the glycerol protons, as highlighted in Figure A.5, can be seen between the same-day product and the rac-POSt standard, along with three sets of triplets for the product at 1.0 – 0.9 ppm where the methyl group is observed in the standard; an indication that diastereomeric derivatives of the standard may have been achieved.

Appendix B Supporting information for Chapter 4

B.1 Differential scanning calorimetry: melting thermograms of CB and CBA

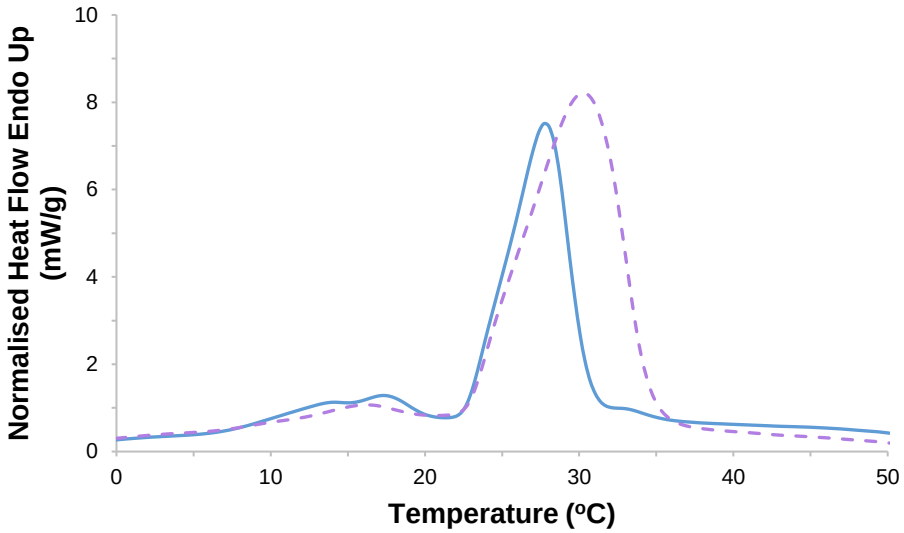

Figure B.1 Melting thermograms of CB (1.357 mg) (blue solid) and the CBA (1.326 mg) (purple dashed) indicating the most stable β_V polymorph following a temperability program. The β_V m.p. for CB at 28.7 °C appears lower than expected, but it is akin with the findings of van Malssen et al.[96]. The peak maximum for one of their samples in the β phase being 29.4 °C.

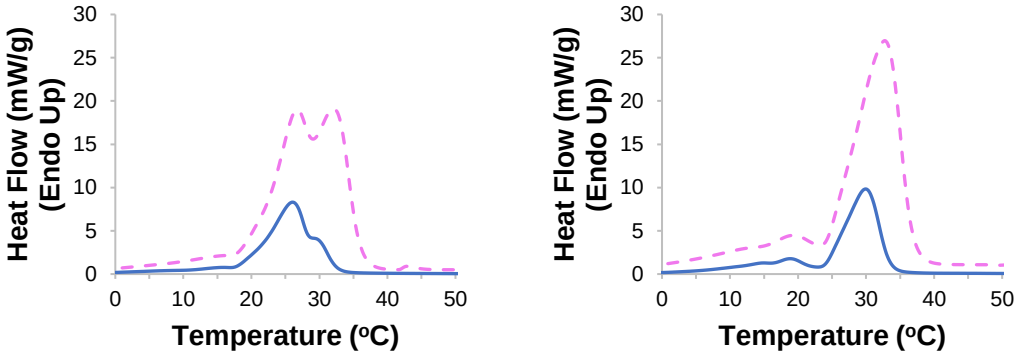

Figure B.2 Polymorphic transformation of CB (blue solid; 1.5 mg) and the CBA (pink dashed; 2 mg) from mixed alpha and beta (left) to predominantly beta phase (right). Determination of m.p. for both fats are higher in these examples than Figure B.1 and closer to what is expected for the polymorphs of CB.

Appendix C Supporting information for Chapter 5

C.1 Analytical method development: transesterification

C.1.1 Stage one to three of method development: optimisation of HPLC conditions

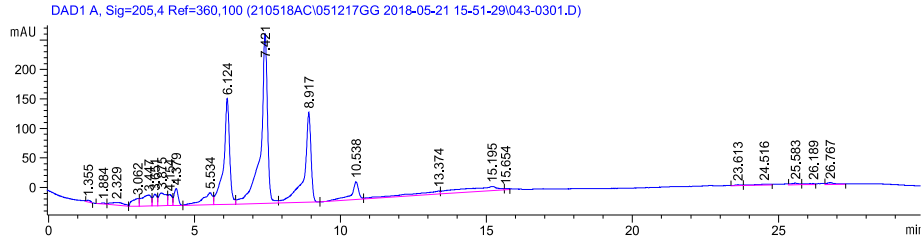

Figure C.1 Stage one: MCT oil in MeOH (1:10 dilution) analysed with the Waters Symmetry C18 (4.6 mm X 250 mm, 5 µm) column over 30 minutes using the Agilent 1100 series HPLC with diode array detector set to 205 nm.

(a)

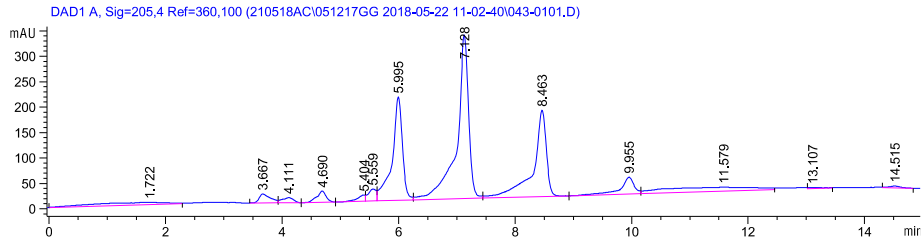

(b)

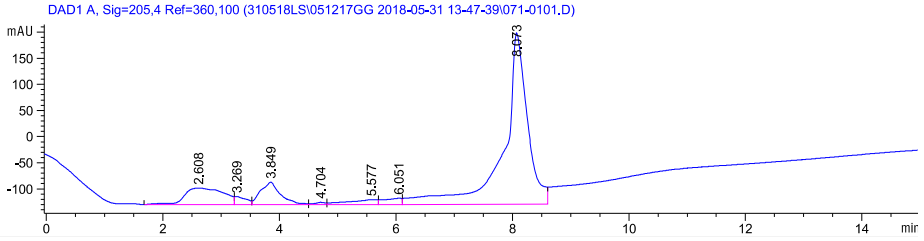

Figure C.2 Stage two: transesterification starting materials analysed as 1:10 dilutions where (a) is MCT oil in MeOH and (b) Et-Pa in MeOH. Samples were analysed under the same conditions as in stage one, but with a reduced run time of 15 minutes.

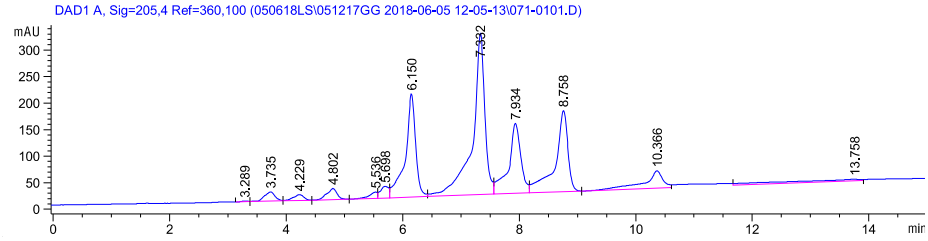

Figure C.3 Stage three: Et-Pa (0.33 mmol) and MCT oil (0.38 mmol) in MeOH analysed over 15 minutes under the conditions described for stage two.

C.2 NMR integrations of starting materials: chemoenzymatic synthesis

C.2.1 (R)-(+)- 3-Benzyloxy-1,2-propanediol

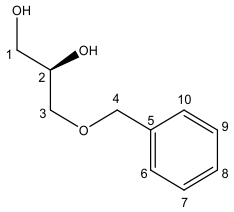

δ_H in ppm (400 MHz, $CDCl_3$); δ 7.40 – 7.30 (m, 5H, H6 – H10), 4.57 (s, 2H, H-4), 3.91 (tt, *J* = 5.8 and 4.0 Hz, 1H, H-2), 3.68 (ddd, *J* = 31.4, 11.5 and 4.7 Hz, 2H, H-3), 3.58 (ddd, *J* = 15.6, 10.5 and 5.2 Hz, 2H, H-1), 2.84 – 2.42 (brd, 2H, OH groups); δ_c in ppm (100 MHz, $CDCl_3$); 137.7 (C-5), 128.5 (C-7 and C-9), 127.9 (C-8), 127.8 (C-6 and C-10), 73.6 (C-4), 71.8 (C-2), 70.7 (C-3), 64.0 (C-1); IR v_{max}/cm^{-1}; 3362, 2922, 2864, 1603.

C.2.2 Vinyl palmitate

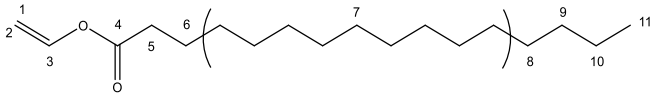

δ_H in ppm (400 MHz, $CDCl_3$); δ 7.31 (dd, *J* = 14.0 and 6.3 Hz, 1H, H-3), 4.89 (dd, *J* = 14.0 and 1.6 Hz, 1H, H-1), 4.58 (dd, *J* = 6.3 and 1.6 Hz, 1H, H-2), 2.40 (t, *J* = 7.5 Hz, 2H, H-5), 1.68 (quint, *J* = 7.4 Hz, 2H, H-6), 1.32 – 1.28 (m, 24H, CH_2 groups, H-7, H-8, H-9, H-10), 0.90 (t, *J* = 6.8 Hz, 3H, H-11); δ_C in ppm (100 MHz, $CDCl_3$); 170.9 (C-4), 141.2 (C-3), 97.4 (C-1, C-2), 33.9 (C-5), 31.9 (C-9), 29.7 – 29 (C-7, C-8), 24.6 (C-6), 22.7 (C-10), 14.1 (C-11); IR v_{max}/cm^{-1}; 2918, 2850, 1753, 1645.

C.2.3 Vinyl stearate

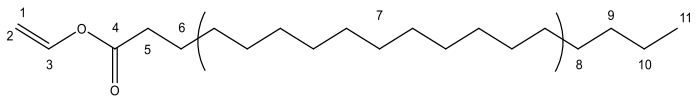

δ_H in ppm (400 MHz, $CDCl_3$); δ 7.31 (dd, *J* = 14.0 and 6.3 Hz, 1H, H-3), 4.89 (dd, *J* = 14.0 and 1.5 Hz, 1H, H-1), 4.57 (dd, *J* = 6.3 and 1.5 Hz, 1H, H-2), 2.40 (t, *J* = 7.5 Hz, 2H, H-5), 1.67 (quint, *J* = 7.3 Hz, 2H, H-6), 1.32 – 1.28 (m, 28H, H-7, H-8, H-9, H-10), 0.90 (t, *J* = 6.8 Hz, 3H, H-11); δ_C in ppm (100 MHz, $CDCl_3$); 170.8 (C-4), 141.2 (C-3), 97.3 (C-1, C-2), 33.9 (C-5), 31.9 (C-9), 29.7 – 29.1 (C-7, C-8), 24.6 (C-6), 22.7 (C-10), 14.1 (C-11); IR v_{max}/cm^{-1}; 2954, 2915, 2847, 2017, 1749.

C.2.4 Oleic acid

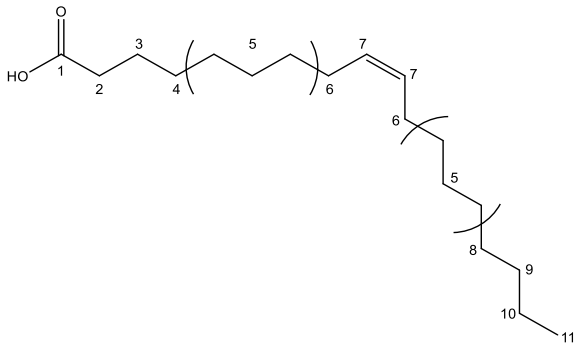

δ_H in ppm (400 MHz, $CDCl_3$); δ 5.41 – 5.33 (m, 2H, H-7), 2.37 (t, *J* = 7.5 Hz, 2H, H-2), 2.04 (q, *J* = 5.9 Hz, 4H, H-6), 1.66 (quint, *J* = 7.2 Hz, 2H, H-3), 1.34 – 1.29 (m, 20H, H-4, H-5, H-8, H-9 and H-10), 0.91 (t, *J* = 6.7 Hz, 3H, H-11); δ_C in ppm (100 MHz, CDCl3); 180.5 (C-1), 130.0 and 129.7 (C-7), 34.1 (C-2), 31.9 (C-9), 29.7 (C-8), 29.5 (C-4), 29.3 and 29.1 (C-5), 27.2 and 27.1 (C-6), 24.7 (C-3), 22.7 (C-10), 14.1 (C-11).

C.3 NMR integrations of reaction products: chemoenzymatic synthesis

C.3.1 1-palmitin-3-O-benzyl-glycerol

Product was impure: the method did not require purification for this intermediate stage. Therefore, the spectra have been interpreted in alignment with values suggested by predictive ^{1}H NMR software.

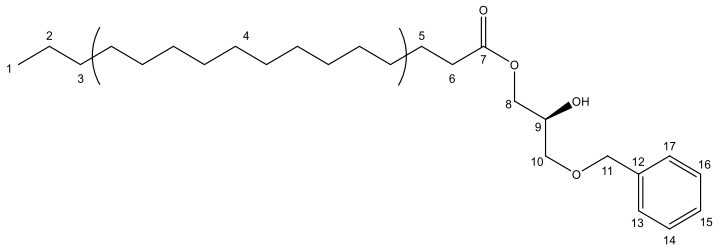

δH in ppm (400 MHz, CDCl3); δ 7.39 – 7.28 (m, 5H, H-13 – H-17), 4.58 (s, 2H, H-11), 4.18 (ddd, J = 20.4, 11.5 and 5.3 Hz, 2H, H-8), 4.08 – 4.03 (m, 1H, H-9), 3.54 (ddd, J = 24.1, 9.6 and 5.2 Hz, 2H, H-10), 2.34 (t, J = 7.6 Hz, 2H, H-6), 1.66 – 1.59 (m, 2H, H-5), 1.32 – 1.28 (m, 24H, H-2, H-3, H-4), 0.90 (t, J = 6.8 Hz, 3H, H-1); δc in ppm (100 MHz, CDCl3); 174 (C-7), 137.7 (C-12), 128.5 (C-14 and C-16), 127.9 (C-15), 127.8 (C-13 and C-17), 73.5 (C-11), 70.9 (C-9 or C-10), 68.0 (C-9 or C-10), 65.4 (C-8), 34.2 (C-6), 32.0 (C-3), 29.7 – 29.3 (C-4), 24.9 (C-5), 22.7 (C-2), 14.1 (C-1).

C.3.2 Purified 1-monopalmitin

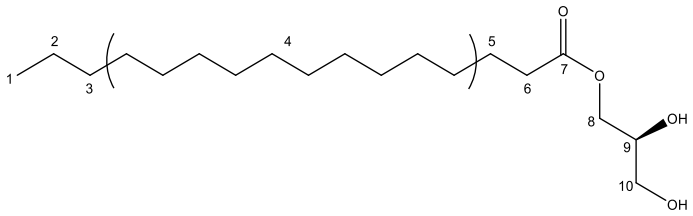

δ_H in ppm (400 MHz, $CDCl_3$); δ 4.11 (ddd, *J* = 25.0, 11.7 and 5.4 Hz, 2H, H-8), 3.89 – 3.84 (m, 1H, H-9), 3.58 (ddd, *J* = 39.1, 11.4 and 4.9 Hz, 2H, H-10), 2.28 (t, *J* = 7.6 Hz, 2H, H-6), 1.56 (quint, *J* = 7.2 Hz, 2H, H-5), 1.22 – 1.19 (m, 24H, H-2, H-3, H-4), 0.81 (t, *J* = 6.8, 3H, H-1); δ_c in ppm (100 MHz, $CDCl_3$); ~172.9 expected (no signal for C=O – sample size too small), 70.3 (C-9), 65.2 (C-8 or C-10), 63.3 (C-8 or C-10), 34.2 (C-6), 31.9 (C-3), 29.7 – 29.1 (C-4).

C.3.3 Purified 1-palmitoyl-3-stearoyl-*sn*-glycerol

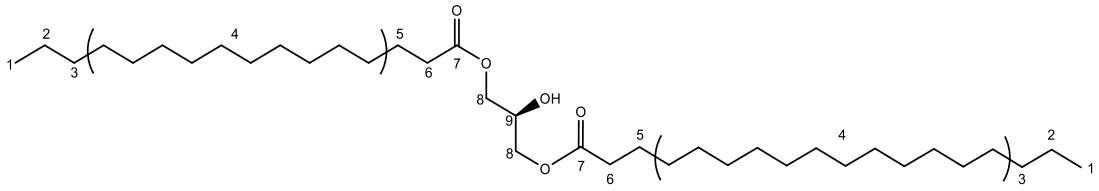

δ_H in ppm (400 MHz, $CDCl_3$); δ 4.19 – 4.11 (m, 5H, H-8 and H-9), 2.41 (brs, 1H, OH group), 2.34 (t, *J* = 6.8 Hz, 4H, H-6), 1.63 (brs, 4H, H-5), 1.29 – 1.25 (m, 52H, H-2, H-3, H-4), 0.88 (m, 6H, H-1); δ_c in ppm (100 MHz, $CDCl_3$); 173.9 (C-7), 67.3 (C-9), 63.9 (C-8), 32.9 (C-6), 30.8 (C-3), 28.6 – 27.9 (C-4), 23.8 (C-5), 21.6 (C-2), 12.9 (C-1).

C.3.4 Final reaction product: (*R*)-1-palmitoyl-2-oleoyl-3-stearoyl-*sn*-glycerol

Product was impure: university shutdown dictated purification could not be attained. Consequently, the spectra has been interpreted in alignment with values determined by the reference standard.

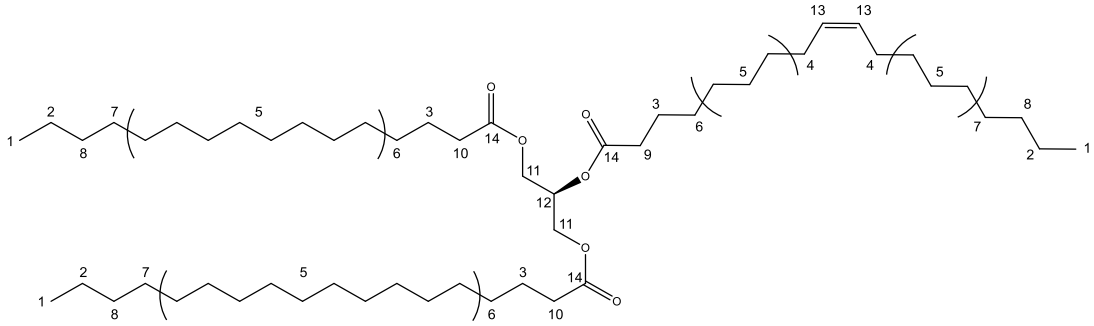

δ_H in ppm (400 MHz, $CDCl_3$); δ 5.29 – 5.26 (m, 2H, H-13), 5.19 (quint, *J* = 5.1 Hz, 1H, H-12), 4.15 (ddd, *J* = 59.5, 11.9 and 5.2 Hz, 4H, H-11), 2.24 (dt, *J* = 7.5 Hz, 6H, H-9, H-10), 1.94 (quint, *J* = 6.3 Hz, 4H, H-4), 1.57 – 1.53 (m, 6H, H-3), 1.23 – 1.18 (m, 72H, H-2, H-5, H-6, H-7, H-8), 0.81 (t, *J* = 6.7 Hz, 9H, H-1); sample size too small for ^{13}C NMR spectra to be acquired.

C.3.5 Reference standard: 1-palmitoyl-2-oleoyl-3-stearoyl-*rac*-glycerol

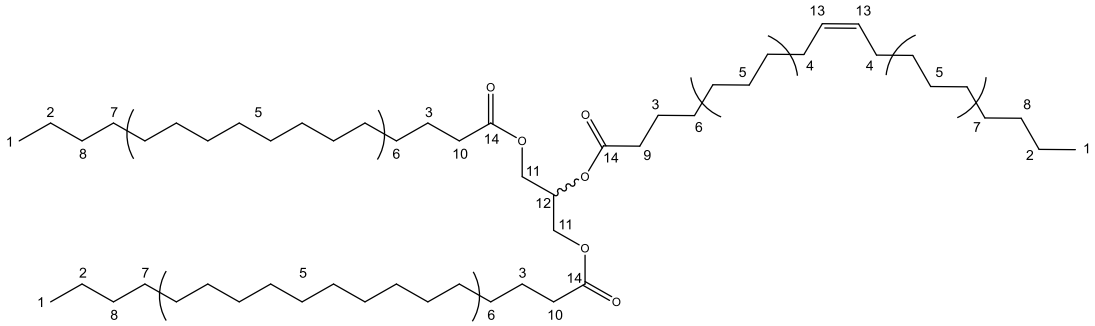

δ_H in ppm (400 MHz, $CDCl_3$); δ 5.29 – 5.26 (m, 2H, H-13), 5.19 (quint, *J* = 5.1 Hz, 1H, H-12), 4.15 (ddd, *J* = 59.9, 11.9 and 5.1 Hz, 4H, H-11), 2.4 (dt, *J* = 7.5 Hz, 6H, H-9, H-10), 1.94 (quint, *J* = 6.1 Hz, 4H, H-4), 1.55 – 1.48 (m, 8H, H-3), 1.23 – 1.18 (m, 72H, H-2, H-5, H-6, H-7, H-8), 0.81 (t, *J* = 6.8 Hz, 9H, H-1);δ_c in ppm (100 MHz, $CDCl_3$); 173.3 (C-14), 130.0 – 129.7 (C-13), 68.8 (C-12), 62.1 (C-11), 34.2 (C-9), 34.0 (C-10), 31.9 (C-8), 29.7 – 29.1 (C-5, C-6, C-7), 27.2 (C-4), 24.8 (C-3), 22.7 (C-2), 14.1 (C-1).